Elucidating the function of WAC in macroautophagy through investigating the WAC-GM130 interaction

Justin Joachim

University College London

and

The Francis Crick Institute, London Research Institute

PhD Supervisor: Sharon A. Tooze

A thesis submitted for the degree of

Doctor of Philosophy

University College London

September 2015

Declaration

I Justin Francis Joachim confirm that the work presented in this thesis is my own. Where information has been derived from other sources, I confirm that this has been indicated in the thesis.

Abstract

Macroautophagy, hereafter called autophagy, is an intracellular degradation pathway that functions to degrade bulk material and recycle macromolecules to maintain cell homeostasis. Autophagy has a protective role and is also implicated in disease processes such as cancer, neurodegeneration and pathogen clearance. Autophagy is characterised by the formation of a double-membrane structure in response to stress insults such as amino acid starvation, which encapsulates cargo to form an enlarged vesicle called an autophagosome. The autophagosome fuses with the lysosome for degradation of the contents. Although the core protein machinery of autophagy has been known for some time, the regulation of this process is not fully understood.

WAC was previously identified as a novel positive regulator of starvation-induced autophagy. However the mechanism by which WAC regulates autophagy is completely unknown. It is known that WAC performs functions both in the nucleus and on the Golgi. In order to elucidate the function of WAC in autophagy, I performed a study of WAC function by a combination of microarray transcriptomic analysis and immunoprecipitation coupled with mass spectrometry to identify genes regulated by WAC and novel WAC interaction partners, respectively. WAC is not a potent regulator of autophagy gene expression. However, I identified GM130, a negative regulator of autophagy, as a novel WAC interaction partner. I show here that WAC promotes ULK1 activation whereas GM130 inhibits the early autophagy stages. GM130 is the receptor for WAC on the Golgi and binds WAC directly. This interaction is mediated by the C-terminal regions of both proteins which contain predicted coiled-coil domains. WAC and GM130 both interact with the autophagy protein GABARAP, indirectly and directly respectively. WAC regulates a novel centrosomally-localised pool of GABARAP, GABARAP binding to GM130 and GABARAP localisation to the Golgi. This centrosomal pool of GABARAP, is able to translocate to autophagic structures during starvation. In addition I describe a GABARAP mediated activation of the ULK1 complex. Through the WAC-GM130-GABARAP interplay, I propose that WAC promotes a centrosome to autophagosome GABARAP trafficking step that may in addition maintain ULK1 activation during starvation-induced autophagy.

Acknowledgements

Firstly and foremost, I would like to thank my supervisor Sharon Tooze for her never-ending support and encouragement that has been instrumental for my development during my PhD. I am extremely privileged to have had such a brilliant mentor and scientist during the past four years.

I would like to thank my examiners, Ian Ganley and Martin Lowe for reading my thesis and traveling, and I look forward to our discussion.

I thank the invaluable Francis Crick Institute core facilities. I especially thank Bram Snidjers and David Frith at the proteomics facility and Probir Chakravarty in the bioinformatics and biostatistics service. In addition, I thank Brenda for making things run smoothly on our floor.

I thank Mark Petalcorin at the Francis Crick Institute who helped me understand BAC technology and answered my questions.

Thank you to my thesis committee members, Helen Walden, Peter Parker and Jesper Svejstrup for their useful suggestions and input.

Thank you to funding bodies who have enabled me to present my work at meetings and conferences, CRUK, BACR and the Biochemical society.

To my fellow PhD students, the CRUK softball team and friends around the institute thank you for making the past four years a lot of fun too.

To all the past and present members of the SPW lab thank you for making my time here so wonderful, it's great to be surrounded by such funny and intelligent people and friends. I thank all of you for your time, sharing of ideas, knowledge and materials. Thank you to Nicole for your work on WAC. Thank you to Harold for all the help with revisions and also to Minoo, who has always given me lots of ideas for my project. Thank you to Martina for the many late evening discussions and intelligent ideas. Thank you to Chris for helping me to settle in when I had lots of questions and for putting up with your messy neighbour. Thank you to Delphine for looking out for me and to Tim, Eyal and Hannah for being genuinely caring and funny.

Thank you to all my friends and family for all your love and support. Thank you to Jack for trying to solve scientific problems with a philosopher's brain. Thank you to my mum and stepdad Steven who have always encouraged me. I would not be here without their inspiration and support. Finally, I would like to thank Magda

for her constant support, especially when moving house whilst writing up, and for making my days better.

Table of Contents

Table of figures

List of tables

Abbreviations

AKAP450	A-kinase anchor protein 450 kDa
AMBRA1	Activating molecule in BECN1-regulated autophagy protein 1
AMPK	5’ adenosine monophosphate-activated protein kinase
Atg	Autophagy related
ATP	Adenosine triphosphate
BAC	Bacterial artificial chromosome
BafA	Bafilomycin A1
BAR	Bin/Amphiphysin/Rvs
BATS	Barkor/Atg14L autophagosome targeting sequence
CC	Coiled-coil
CDK	Cyclin-dependent kinase
CMA	Chaperone-mediated autophagy
CRISPR	Clustered regularly interspaced short palindromic repeats
CTD	C-terminal domain
Deptor	DEP Domain Containing mTOR-Interacting Protein
DFCP1	Double FYVE-containing protein 1
DMEM	Dulbecco’s modified Eagle’s Medium
DMSO	Dimethyl sulfoxide
DUB	Deubiquitinase
EBSS	Earle’s balanced salt solution
ECD	Evolutionarily conserved domain
ECL	Ehanced chemiluminescence
ER	Endoplasmic reticulum
ERGIC	ER-Golgi intermediate compartment
FACS	Fluorescence activated cell sorting
FBS	Fetal bovine serum
FDR	False discovery rate
FIP200	FAK family kinase-interacting protein of 200 KDa
FLAP	Flag localisation and affinity purification
GABARAP	GABA receptor-associated protein
GAP	GTPase activating protein

GAPR-1	Golgi-associated plant pathogenesis-related protein 1
GATE-16	Golgi-associated ATPase enhancer of 16kDa
GEF	GTPase exchange factor
GFP	Green fluorescent protein
GM130	Golgi matrix protein of 130 kDa
GMAP-210	Golgi-associated microtubule-binding protein 210
GRASP65	Golgi reassembly-stacking protein of 65 kDa
GST	Glutathione S-Transferase
GTP	Guanosine-5'-triphosphate
H2B	Histone H2B
HA	Haemagglutinin
HEK293A	Human embryonic kidney 293A cells
HeLa	Henrietta Lacks
HOPS	Homotypic fusion and protein sorting
HRP	Horseradish peroxidase
Hsc70	Heat shock cognate 70 protein
iBAQ	intensity based absolute quantification
LAMP-2A	Lysosome-associated membrane protein type 2A
LC3	Microtubule-associated protein 1 light chain 3
LIR	LC3-interaction region
MEF	Mouse embryonic fibroblast
MHC	Major histocompatibility complex
miRNA	micro RNA
MTMR	Myotubularin-related protein 3
mTOR	Mechanistic target of rapamycin
NDP52	Nuclear domain protein 52
NES	Nuclear export signal
NLS	Nuclear localisation signal
NSF	N-ethylmaleimide-sensitive factor
PAGE	Polyacrylamide gel electrophoresis
PAS	Phagophore assembly site
PBS	Phosphate buffered saline
PCR	Polymerase chain reaction

PE	Phosphatidylethanolamine
PI3P	Phosphatidylinositol 3-phosphate
PI4P	Phosphatidylinositol 4-phosphate
PLEKMH1	Pleckstrin homology domain-containing family M member 1
PP2A	Protein Phosphatase 2A
Pras40	Proline-rich AKT1 substrate 1
PRMT5	Protein arginine N-methyltransferase 5
qRT-PCR	Quantitative polymerase chain reaction
RAG	Ras-related GTP-binding protein
Raptor	Regulatory associated protein of mTOR complex
Rheb	Ras homologue enriched in brain
RINT-1	RAD50-interacting protein 1
RISC	RNA-induced silencing complex
RNAP	RNA polymerase II
RNF20	RING finger protein 20
RNF40	RING finger protein 40
RPE-1	Retinal pigment epithelium
Rubicon	Run domain Beclin-1 interacting and cysteine-rich containing protein
SC35	Splicing component, 35 kDa
SDM	Site directed mutagenesis
SDS	Sodium dodecyl sulphate
SEM	Standard error of the mean
shRNA	Short hairpin RNA
siRNA	Small interfering RNA
SNAP-29	Synaptosomal-associated protein 29
SNARE	Soluble N-ethylmaleimide-sensitive factor attachment protein receptor
SNRP70	U1 small nuclear ribonucleoprotein 70 kDa
SOEing	Splicing by overlap extension
STK36	Serine/threonine-protein kinase 36
Stx17	Syntaxin 17
TECPR1	Tectonin beta-propeller repeat-containing protein 1

TFEB	Transcription factor EB
TGN	Trans Golgi network
TIP60	60 kDa Tat-interactive protein
TPX2	Targeting protein for Xklp2
TRAF6	TNF receptor-associated factor 6
Ub	Ubiquitin
ULK	Uncoordinated 51-like kinase
UPS	Ubiquitin proteasome system
UVRAG	UV radiation resistance-associated gene protein
VAMP	Vesicle-associated membrane protein
V-ATPase	Vacuolar-type H^+-ATPase
VCIP135	Valosin-containing protein p97/p47 complex-interacting protein p135
VCP	Valosin-containing protein
VMP1	Vacuole membrane protein 1
Vps34	Vacuolar protein sorting-associated protein 34
WAC	WW domain-containing adaptor protein with coiled-coil
WIPI	WD repeat domain phosphoinositide-interacting
WT	Wild type
YFP	Yellow fluorescent protein
ZIPK	Zipper-interacting protein kinase
ZKSCAN3	Zinc finger protein with KRAB and SCAN domains 3

Chapter 1. Introduction

1.1 Autophagy introduction

1.1.1 The three forms of autophagy

Autophagy is an evolutionarily conserved membrane trafficking pathway that functions as an intracellular recycling pathway. Autophagy can be divided into three forms known as macroautophagy, microautophagy and chaperone-mediated autophagy (Mizushima and Komatsu, 2011) (Figure 1.1). This thesis focuses on the regulation of macroautophagy. These three forms of autophagy have in common the delivery of cargo to the lysosome for degradation. Microautophagy involves the invagination of the lysosomal membrane to capture cytoplasmic cargo in a non-selective manner. This results in the formation of an intralumenal vesicle in the lysosome. The resultant vesicle and its contents are degraded by lysosomal proteases. There are other, selective forms of microautophagy such as piecemeal microautophagy of the nucleus in yeast, where invaginations of the vacuole take a part of the nucleus for degradation (Krick et al., 2009). During chaperone-mediated autophagy (Cuervo and Wong, 2014), proteins containing a pentapeptide motif related to the KFERQ sequence are selectively targeted to the lysosome via binding to the chaperone heat shock cognate protein of 70 kDa (hsc70), and delivery to the lysosomal membrane by binding to lysosome-associated membrane protein type 2A (LAMP-2A) on the outer membrane. This promotes the oligomerisation of LAMP-2A monomers. The targeted protein is unfolded and this is likely mediated by hsc70 at the lysosomal membrane. Multimeric LAMP-2A then functions to translocate the unfolded peptide chain into the lysosomal lumen for degradation.

Macroautophagy involves the *de novo* formation of a large vesicle that sequesters cargo, known as an autophagosome, followed by terminal fusion of the vesicle to the lysosome for content degradation. Macroautophagy, hereafter called autophagy, can be a non-selective process or a selective one and this has been reviewed extensively (Behrends and Fulda, 2012, Johansen and Lamark, 2011, Okamoto, 2014, Stolz et al., 2014, Svenning and Johansen, 2013, Rogov et al., 2014). During selective autophagy, cargoes are specifically targeted for

encapsulation into the autophagosome by autophagy receptors, which bind to both the cargo and to proteins attached to the autophagosome membrane. Thus autophagy receptors function to bridge the autophagosome to the cargo. Such cargo could be bacterial pathogens, protein aggregates, mitochondria and the endoplasmic reticulum (ER) (Khaminets et al., 2015) as well as others. The focus of my study has been on non-selective autophagy and from now on I use the term autophagy to refer to non-selective macroautophagy. It should be mentioned though that the discovery of increasing numbers of autophagy receptors on a wide range of cargo, has led some to believe that non-selective autophagy does not exist and rather that autophagy is a highly specific process. However for the purposes of my discussion, I use the term non-selective autophagy to refer to the common autophagy pathway that employs the basic core machinery, not biased to any one particular cargo.

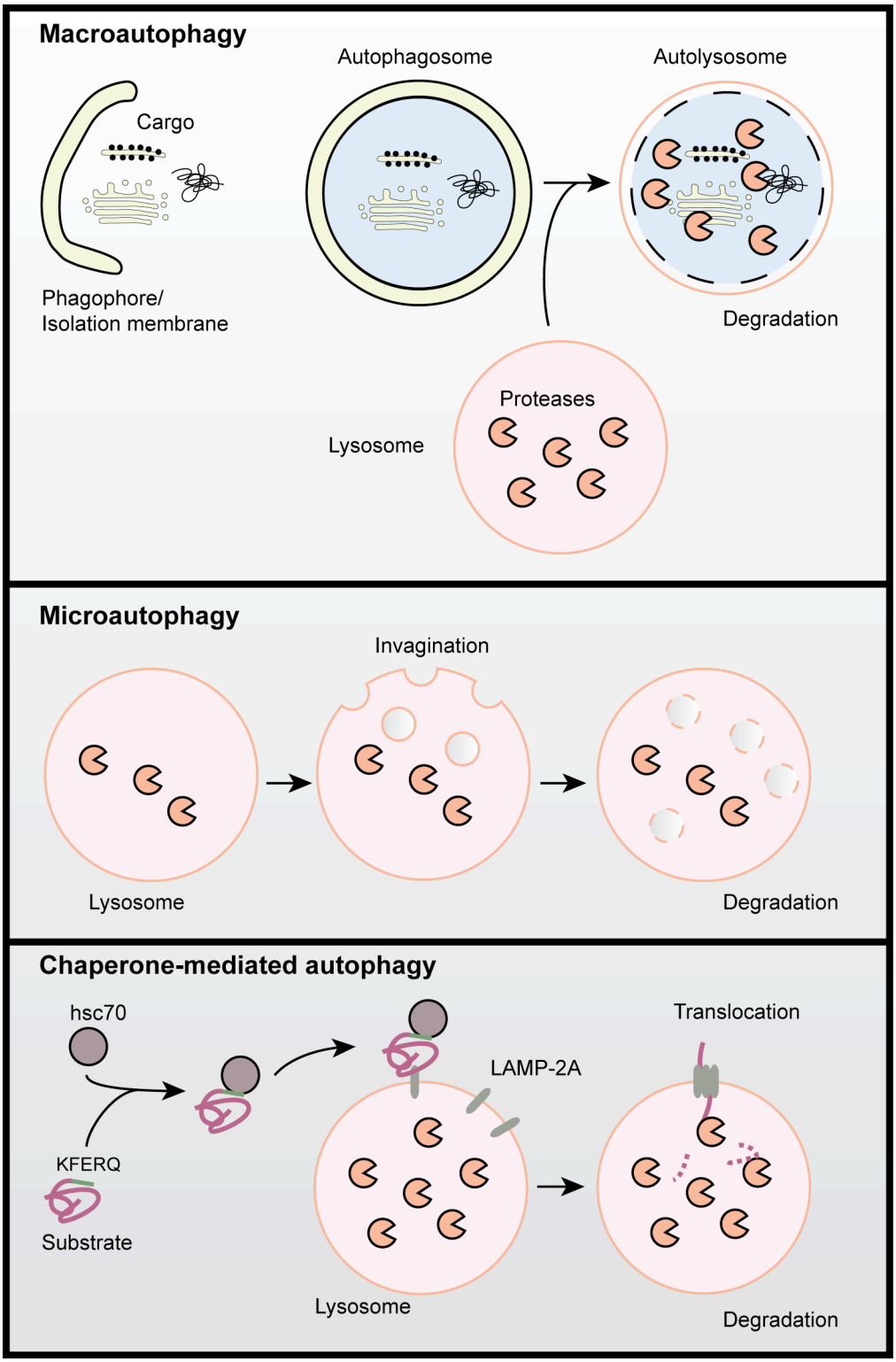

Figure 1.1 All roads lead to the lysosome - the three major forms of autophagy

All three forms of the autophagy result in the degradation of cargo in the lysosome and the recycling of macromolecule products, which can be used for biosynthetic and metabolic pathways.

1.1.2 Proteasomal and lysosomal degradation

There are two main forms of intracellular protein degradation in the cell, namely the proteasomal and the lysosomal pathways. In the proteasomal pathway (Finley, 2009), individual proteins are targeted to the proteasome, a large (>2.5 MDa) multi-subunit protein complex that assumes a barrel-like structure. The core of the proteasome is a 28-subunit particle (also known as the 20S particle) that has protease activity. The core particle consists of four rings of seven subunits that are stacked on top of each other. Unfolded peptide chains are threaded into the barrel core of the proteasome where they are accessed by proteases, resulting in the degradation of the protein and the release of peptides but not free amino acids. These peptides can be used for antigen presentation in the adaptive immune response. The unfolding and translocation of the protein requires ATP hydrolysis. The targeting of proteins to the proteasome is tightly regulated by the attachment of a small 8.5 kDa protein called Ubiquitin, to lysine residues on the target protein. Ubiquitin is attached to the target protein through its C-terminus. Ubiquitin molecules themselves can be attached together to form polyubiquitin chains. These chains can have different linkages, dictated by the positions of the lysines on the ubiquitin molecule itself. Together this system of tagging, targeting and degradation is called the ubiquitin-proteasome system (UPS). Molecules known as E1 (ubiquitin-activating enzymes), E2 (ubiquitin-conjugating enzymes) and E3 (ubiquitin ligases) act to ubiquitinate the target protein. The specificity of the system is directed by the E3 ligases, which is a much more diverse family than the E1 and E2 proteins. The ubiquitinated substrate docks onto the proteasome at the 19-subunit regulatory particle (also known as the 19S particle) that controls substrate entry into the proteasome, through a variety of ubiquitin receptors. The 19S regulatory particle sits on the entrance of the 20S core particle. Ubiquitinated substrates can also be recognised by proteasome-associated subunits that are not integral to the proteasome, but contain ubiquitin-associated domains. The substrate is then threaded into the core particle, driven by a set of six ATPases that form a ring complex in the regulatory particle. Covalently attached ubiquitin moieties can be removed by the action of deubiquitinases (DUBs). Proteins can also be targeted to the proteasome for degradation independently of ubiquitin, although most known cases of proteasomal degradation involve ubiquitination. Although a well-known

function of ubiquitin post-translational modifications is in protein turnover and stability, monoubiquitination and different chain linkages of polyubiquitin can direct different functions. For example, ubiquitination can direct protein sorting in membrane trafficking pathways, kinase activation and is used as an epigenetic modification (Komander and Rape, 2012). Although the UPS directs specificity, the problem remains that only one protein molecule can be processed by a proteasome at any one time. Autophagy, on the other hand, functions to efficiently dispatch much larger substrates, such as a malfunctioning mitochondrion for example.

Proteins are also delivered to the lysosome for degradation by various autophagic mechanisms as discussed above. In addition, the endocytic pathway can function to degrade extracellular molecules and cell surface receptors via membrane trafficking from the plasma membrane to the lysosome. Autophagy solves the problem of the degradation of large structures, such as organelles or protein aggregates. In addition autophagy tends to degrade long-lived proteins, whereas shorter lived proteins are degraded by the proteasome (Finley, 2009). Autophagy is conserved in eukaryotes, from yeast to human. In the presence of an adequate nutrient supply there is a low level of continuous autophagy, which I refer to as basal autophagy. However, autophagy is in general considered a stress response, as withdrawal of nutrients is a potent inducer of autophagosome formation. In yeast nitrogen starvation and in mammalian cells amino acid starvation are potent inducers of autophagosome formation (Mizushima, 2007). In the Tooze lab we use amino acid starvation of HEK293A cells to study autophagy. This is achieved by washing cells from growth medium into EBSS medium, which is devoid of amino acids but also of serum. Withdrawal of amino acids is thought to be a more potent inducer of autophagy than withdrawal of serum *in vitro* (Mizushima et al., 2010). HEK293A cells provide a useful model for studying autophagy, as autophagy can be switched readily from an off to an on position by starvation, whereas some cell lines have high levels of basal autophagy to start with, making interpretation of autophagic flux sometimes difficult (Klionsky et al., 2012). In addition, HEK293A cells grow rapidly and are easy to transfect for DNA overexpression or siRNA knockdown studies. It is worth noting that amino acid withdrawal is not the only inducer of autophagy, but hypoxia, glucose starvation,

serum starvation, ammonia, pathogen invasion and mitochondrial dysfunction, as well as other signals, induce autophagy (Kroemer et al., 2010).

Autophagy is implicated in a range of pathogenic and physiological process, such as neurodegeneration, immunity, cancer and exercise, as has been reviewed in (Cuervo and Wong, 2014). For example autophagy is involved in the removal of α-Synuclein (Webb et al., 2003) and mutant huntingtin protein aggregates (Martin et al., 2015), which are implicated in Parkinson's disease and Huntingtin's disease respectively. In cancer, autophagy provides a dual role. Autophagy is thought to protect from tumourigenesis perhaps by maintaining mitochondrial function and reducing the formation of reactive oxygen species (Takamura et al., 2011). The autophagy gene Beclin 1 is also a tumour suppressor gene (Liang et al., 1999, Yue et al., 2003). However, autophagy is also used by cancer cells to survive and autophagy may allow cancer cells to overcome insults such as nutrient deprivation or chemotoxicity.

1.1.3 Autophagy is a membrane remodelling process

The initiation of autophagy results in the *de novo* formation of an organelle called an autophagosome. The autophagosome is a large double membrane vesicle that can be between 0.5-1.5 μm in diameter in mammalian cells (Mizushima et al., 2002). Thus is it much larger than other membrane trafficking vesicles, such as COPI coated vesicles which are typically around 50-70 nm (excluding coat) in diameter (Bednarek et al., 1995). The contents of an autophagosome are identical to the surrounding cytoplasm, and autophagosomal membranes stain heavily with osmium and thus can be distinguished from other organelles by electron microscopy (Lamb et al., 2013). Indeed, autophagy was originally discovered more than half a century ago by transmission electron microscopy, and for some time this was the only method to study autophagosome biogenesis (Eskelinen et al., 2011). Autophagosomes form within minutes of starvation (Kochl et al., 2006) and in mammalian cells multiple autophagosomes form and are seen throughout the cytoplasm. The formation of the autophagosome takes place through the elongation of unclosed membranes which finally fuse to form the closed autophagosome. The unclosed autophagosomal membrane is known as the

isolation membrane or the phagophore. Clearly the formation of this organelle, the autophagosome, represents a significant and dynamic membrane remodelling step that the cell has to rapidly undergo in response to stress stimuli. The autophagosome is thought to acquire its membrane from pre-existing membrane compartments or by lipid synthesis activity localised to other compartments. Many membranes have been proposed to contribute to the forming autophagosome (Figure 1.3), such as the ER-Golgi intermediate compartment (ERGIC) (Ge et al., 2014, Ge et al., 2013), the nuclear envelope (English et al., 2009), the ER (Hayashi-Nishino et al., 2009, Yla-Anttila et al., 2009), mitochondria (Hailey et al., 2010), ER-mitochondria contact sites (Hamasaki et al., 2013), the plasma membrane (Ravikumar et al., 2010), recycling endosomes (Longatti et al., 2012, Knaevelsrud et al., 2013), Golgi (Geng et al., 2010, Yamamoto et al., 1990, Ohashi and Munro, 2010, van der Vaart et al., 2010, Biazik et al., 2015) and the Atg9 compartment (Orsi et al., 2012, Mari et al., 2010, Yamamoto et al., 2012). This has recently been reviewed (Lamb et al., 2013). It could be that the source of the membrane contributing to the forming autophagosome varies according to cell type or nutrient stimulus, however this remains to be demonstrated.

Perhaps the best characterised proposed source of autophagosome membrane is the ER. Autophagosomes can form at phosphatidylinositol-3-phosphate (PI3P) enriched, Ω-shaped subdomains of the endoplasmic reticulum (ER) known as omegasomes (Axe et al., 2008) (Figure 1.2). The PI3P-binding protein Double FYVE Containing Protein 1 (DFCP1) is used to mark omegasomes. DFCP1 also colocalises with early autophagy proteins such as WIPI2 (Polson et al., 2010). Direct connections between the ER and the phagophore have been observed (Hayashi-Nishino et al., 2009, Yla-Anttila et al., 2009) and the phagophore is often in close proximity to the ER membrane, at a distance that may allow lipid transfer (Biazik et al., 2015). The ER is the membrane compartment that makes the most frequent contacts with phagophores. These conclusions have been reached by the use of electron microscopy and tomography. The phagophore has been observed cradled between two sheets of ER, in a structure that resembles, or is identical to, the omegasome. Conceptually, it would make sense if the ER was the primary membrane source of the forming autophagosome, as it has a much larger surface area then the plasma membrane of the cell (Alberts, 2002). In addition to a possible role in membrane supply, proteins involved in autophagy

such as Atg14L, VMP1 and ULK1 are resident on the ER (Matsunaga et al., 2010, Itakura and Mizushima, 2010). Moreover, the localisation of Atg14L to the ER is required for autophagy. In addition to being present at the ER, the ULK complex also associates with omegasomes and appears to dissociate prior to closure of the autophagosome (Karanasios et al., 2013). A summary of the autophagy proteins and their functions will be provided later.

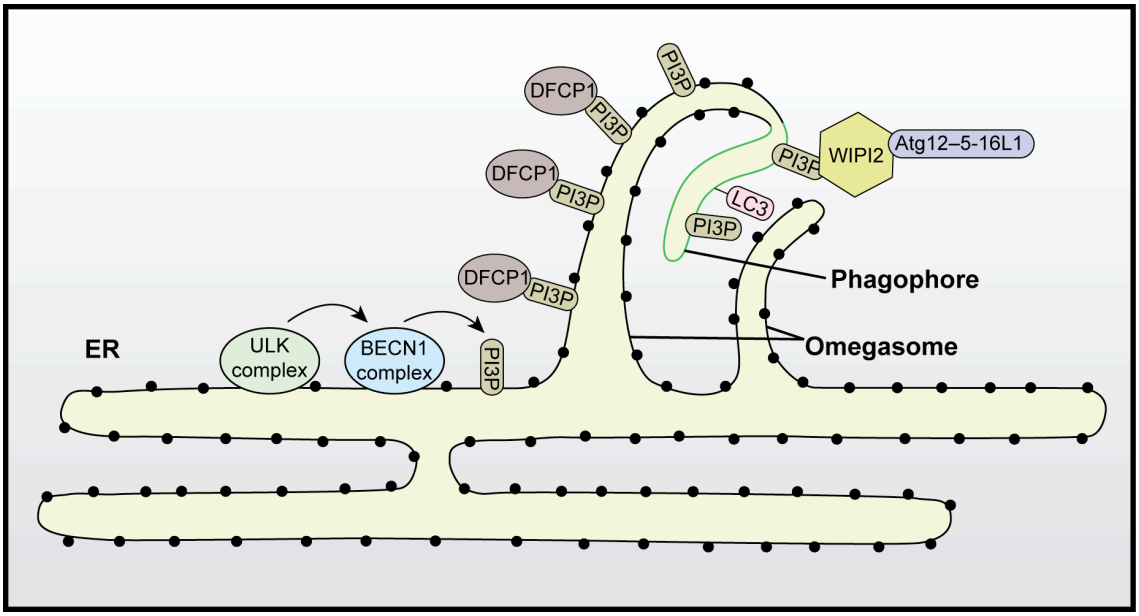

Figure 1.2 The omegasome model of the phagophore assembly site (PAS) in mammalian cells

In yeast autophagosomal proteins are recruited to a single site for autophagosome biogenesis, known as the phagophore assembly site (PAS). In contrast, in mammals autophagosomes form throughout the cytoplasm. The current best candidate for an analogous PAS in mammalian cells is the omegasome.

Membrane contact sites have also been observed between the phagophore and other organelles such as the Golgi and mitochondria (Biazik et al., 2015) (Figure 1.3). Markers of the outer mitochondrial membrane have been observed on autophagosomes too, suggesting that the mitochondrial membrane can contribute to autophagosome biogenesis (Hailey et al., 2010). The mitochondria could be a site of autophagy regulation, as autophagy regulating proteins such as Ambra1, BCL-2 and Beclin 1 localise to mitochondria (Pattingre et al., 2005, Strappazzon et al., 2011). The contribution of the ER or mitochondria as membrane sources for the autophagosome could be linked rather than competing models for organelle

biogenesis. This is because ER-mitochondria contact sites are also thought to be sites of autophagosome formation (Hamasaki et al., 2013). ER-mitochondria contact sites are the best characterised organelle contact sites, and they provide functions such as lipid synthesis and Ca^{2+} transfer (Rowland and Voeltz, 2012). These contact sites are characterised by apposition of two membranes that are in close proximity to one-another (10-30 nm apart) but are not fused, suggesting tethering of two organelles together. The contact sites also appear to be stable structures. Atg14L and Atg5, proteins that mark the early stages of autophagosome formation, were shown to localise to the ER-mitochondria contact site upon starvation. Furthermore, disruption of ER-mitochondria contact sites impairs starvation-induced autophagy (Hailey et al., 2010, Hamasaki et al., 2013).

The Golgi complex is also likely involved in autophagy modulation through the regulation of autophagy proteins and by direct membrane contribution to the autophagosome. A minority of phagophores or autophagosomes were found to make contacts with the Golgi complex, defined as membranes within 20 nm distance of each other (Biazik et al., 2015). The Golgi also acts as a hub for autophagy proteins under basal conditions, such as Beclin 1, GATE-16, Atg9, Atg16, GABARAP and LC3 (Sagiv et al., 2000, Guo et al., 2012, Itoh et al., 2008, Shoji-Kawata et al., 2013, Kittler et al., 2001, Young et al., 2006). For example, Beclin 1 is tethered to the Golgi via binding to GAPR-1/GLIPR2 (Shoji-Kawata et al., 2013). Introduction of a peptide from Beclin 1 that binds to GAPR-1, or knockdown of GAPR-1, results in the relocalisation of Beclin 1 to autophagosomes and induces autophagy. In addition, Golgi localised Rab proteins are known to control autophagy. Rabs are a family of small GTPases that regulate membrane trafficking steps and are thought to confer membrane compartment identity. Rab1 is localised to the Golgi and is involved in secretion (Moyer et al., 2001). However, Rab1 is also required for omegasome (Huang et al., 2011) (Mochizuki et al., 2013) and autophagosome formation (Zoppino et al., 2010). Rab33b, a Golgi localised protein thought to be involved in retrograde trafficking (Zheng et al., 1998) (Valsdottir et al., 2001), is also involved in autophagy. Rab33b interacts with Atg16L1 (Itoh et al., 2008) and expression of a piece of Atg16L1 that binds Rab33b inhibits autophagosome formation, suggesting that this interaction regulates autophagy. In addition, Rab33b is also thought to be involved in autophagosome maturation mediated by its proposed regulator OATL1 (Itoh et al., 2011). Coiled-coil Golgi

tethering proteins, known as golgins, have also been implicated in autophagy. GM130/GOLGA2, a cis-Golgi protein (Nakamura et al., 1995), is thought to be a negative regulator of autophagosome formation (Chang et al., 2012). In addition, the trans-Golgi protein p230/golgin-245 is a positive regulator of autophagosome formation (Sohda et al., 2015). The role of the plasma membrane, recycling endosomes and plasma membrane will not be discussed here for brevity, and has been recently reviewed in (Lamb et al., 2013).

Under starvation conditions the forming autophagosomes capture cargo in a non-specific fashion, which could include for example cytosol, Golgi stacks, mitochondria and ER. The enclosed autophagosome then undergoes a maturation process whereby it fuses with endosomes forming an amphisome. Proteins involved in the secretory pathway, such as the COPI coatomer, which are also involved in maintaining endosome function, are also involved in autophagosome maturation (Razi et al., 2009). The amphisome can terminally fuse with the lysosome forming the autolysosome. Additionally the autophagosome can fuse with lysosomes without fusing to endosomes beforehand. These fusion events are regulated by soluble N-ethylmaleimide-sensitive factor attachment protein receptor (SNARE) proteins. For example syntaxin 17 (Stx17) is found on the outer surface of fully formed but not immature autophagosomes, and interacts with SNAP-29 and VAMP8 on the endosome/lysosome to mediate fusion (Itakura et al., 2012). SNAREs can also function in autophagosome formation, for example VAMP3 is thought to mediate the fusion of the autophagosome precursor membranes (Puri et al., 2013). Other membrane trafficking proteins direct the vesicle tethering and fusion events of maturation, such as Rab7 (Gutierrez et al., 2004) and the HOPS complex (McEwan et al., 2015). As my project has focused on the regulation of autophagosome formation, an exhaustive description of the players in autophagosome maturation will not be provided here. After fusion with the lysosome, the contents of the autophagosome are degraded by proteases and this includes the degradation of the inner autophagosomal membrane but not the outer membrane. The resultant macromolecules exit the lysosome via membrane permeases. These macromolecules are then available for use in biosynthetic and metabolic pathways. Thus, in its most basic (non-selective) physiological function, autophagy functions as a recycling process.

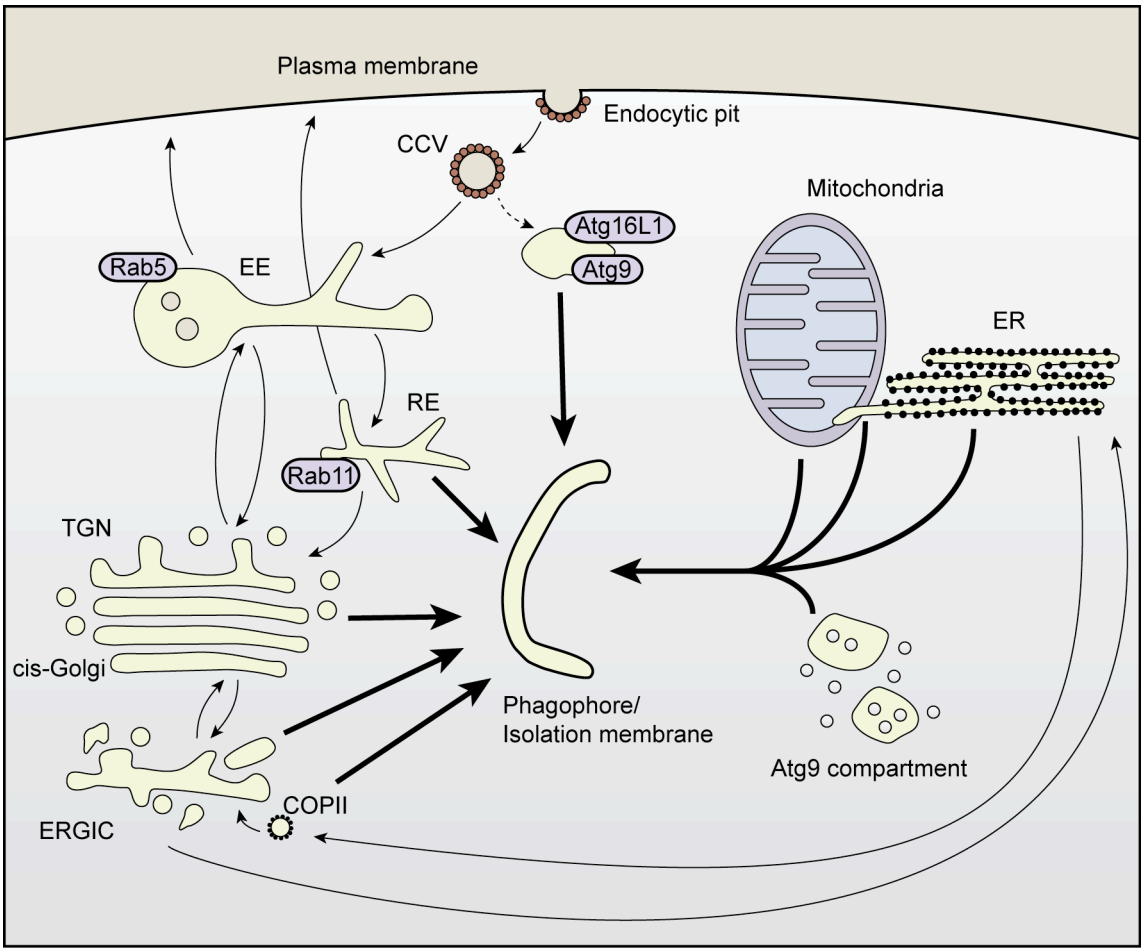

Figure 1.3 Membrane sources for autophagosome biogenesis

There is extensive cross-talk between the secretory pathway and endosomal system and the autophagosome formation pathway. In addition, and not depicted here, autophagy functions in the non-conventional secretion of cytosolic proteins (Ponpuak et al., 2015). Early endosomes (EE) are marked by Rab5. Recycling endosomes (RE) are marked by Rab11. Atg9 may traffic to forming autophagosomes from the highly tubulovesicular Atg9 compartment and/or Atg9 may be endocytosed from the plasma membrane into clathrin coated vesicles (CCVs), in a pathway that forms Atg16L1 and Atg9 positive autophagosome precursor membranes. COPII coat is thought to be involved in the budding of ERGIC membranes as an autophagic membrane source.

1.2 Autophagy machinery and signalling

The core genes involved in autophagy were discovered in genetic screens in yeast in the early 1990s (Tsukada and Ohsumi, 1993, Thumm et al., 1994, Harding et al., 1995). These genes are known as autophagy-related (Atg) genes in yeast. Their mammalian homologues often, but not always, have alternative names. These Atg genes encode for the core protein machinery that drives formation of the autophagosome. Since the discovery of the Atg genes, there has been an increase in our knowledge of how this machinery is regulated through the discovery of binding partners, a variety of post-translational modifications and other processes that direct the activity of the core autophagy machinery (Boya et al., 2013). This increase in our knowledge has been facilitated by the development of tools to study autophagy, such as marker proteins that can be used to study autophagosome formation by western blot or immunofluorescence in mammalian cells (Kabeya et al., 2000). A PubMed search for publications (Figure 1.4) focusing on autophagy shows the striking progression of the field, especially in the last decade, and highlights the growing interest in autophagy research. My work investigates the regulation of autophagy in human cells and thus I will focus on the mammalian autophagy system. Although some of the mammalian autophagy genes have sequence and/or functional orthologues in yeast, some of the critical mammalian autophagy proteins do not have identified equivalents in yeast.

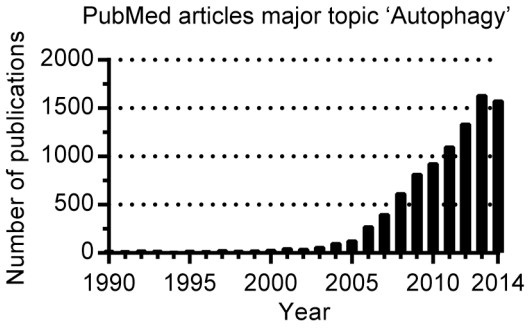

Figure 1.4 Autophagy publications per year, PubMed

In the past decade there has been a greater than 10-fold increase in the number of autophagy papers.

1.2.1 mTORC1

In mammals, under nutrient replete conditions autophagy is kept in the off state by the kinase, mechanistic target of rapamycin complex 1 (mTORC1). mTORC1 is a master regulator of cell growth and of autophagy and integrates multiple input signals; for example from growth factor and amino acid availability (Laplante and Sabatini, 2012). In the presence of nutrients mTORC1 functions to drive cell growth by promoting biosynthetic pathways such as protein synthesis and repress the catabolic autophagy pathway. mTORC1 is a serine/threonine kinase complex containing: mTOR, Raptor, mLST8 (GβL), Pras40, Deptor and Tti1/Tel2 (Laplante and Sabatini, 2012). The Raptor subunit functions to regulate substrate binding to mTORC1. mTOR also exists in a separate complex known as mTORC2, which also contains the Deptor, mLST8 (GβL) and Tti1/Tel2 subunits in addition to the mTORC2 unique subunits of mSin1, protor1/2 and Rictor. The Rictor subunit regulates the substrate binding of mTORC2. mTORC1 is thought to be more critical for the regulation of macroautophagy and will be discussed here, however mTORC2 has been implicated in chaperone-mediated autophagy (Arias et al., 2015). The presence of amino acids maintains mTORC1 in the active state and amino acids are especially important for mTORC1 activity, as re-feeding starved cells with growth factors in the absence of amino acids fails to activate the kinase (Wang et al., 1998, Hara et al., 1998). The current view, reviewed by (Jewell et al., 2013), of how amino acids activate mTORC1 begins with a signal to the vacuolar H^+-ATPase (v-ATPase) on the lysosome (Figure 1.5). The v-ATPase controls the guanine nucleotide exchange factor (GEF) activity of the Ragulator complex, which functions as a GEF for the RAG small GTPase complex. The presence of amino acids results in the formation of an active RAG complex. mTORC1 binds to the RAG complex and is recruited to the lysosome, where it is possibly kept in an active state by the action of the RHEB GTPase. Other signals, such as growth factor signalling and energy status, signal to mTORC1 via different routes.

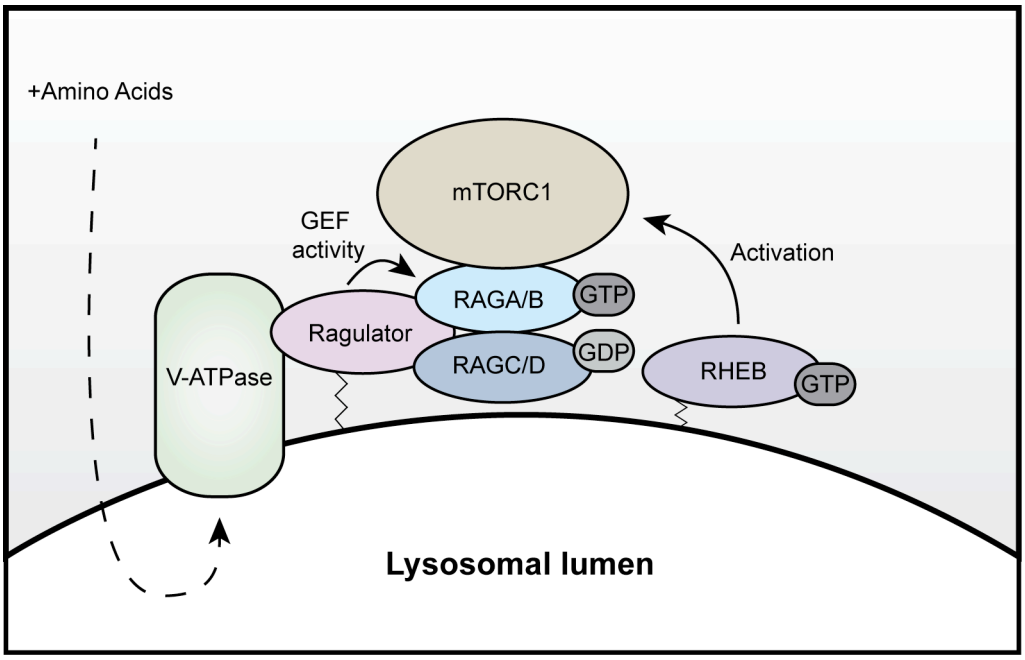

Figure 1.5 'Inside-out' signalling of amino acids from the lysosomal lumen to activate mTORC1

The Ragulator complex is a pentameric complex of p18, p14, MP1, C7orf59 and HBXIP. p18 is tethered to the membrane by myristoylation and palmitoylation, mediating the lysosomal localisation of the Ragulator complex and the RAG GTPases. There are four RAG GTPase proteins in humans and the RAGs form heterodimers, RAGA or RAGB dimerises with RAGC or RAGD, with four possible complexes being formed.

1.2.2 The ULK complex

Active mTORC1 binds, phosphorylates and inhibits the action of the uncoordinated 51-like kinase (ULK) complex and therefore autophagy (Ganley et al., 2009, Hosokawa et al., 2009a, Jung et al., 2009) (Figure 1.6). mTORC1 also inhibits autophagy in an indirect fashion, through the phosphorylation of the transcription factor TFEB, to repress the expression of lysosomal biogenesis genes (Martina et al., 2012, Roczniak-Ferguson et al., 2012, Settembre et al., 2012). The ULK complex can be considered the autophagy initiating kinase and is a serine/threonine kinase. The ULK complex consists of the proteins ULK1 or ULK2, FIP200, Atg13 and Atg101, and the complex is thought to be stable under basal or starvation conditions (Mercer et al., 2009, Hara et al., 2008, Chan et al., 2009, Ganley et al., 2009, Hosokawa et al., 2009b, Hosokawa et al., 2009a, Jung et al., 2009). Moreover, members of the complex appear to stabilise one another. In the

presence of nutrients mTORC1 phosphorylates ULK1 and Atg13. The phosphorylation of ULK1 by mTORC1 on Ser757 antagonises the pro-autophagic interaction between ULK1 and AMPK (Kim et al., 2011). The yeast orthologue of ULK is Atg1 and in humans there are 5 proteins orthologous to Atg1, known as ULK1-4 and STK36/fused (Chan and Tooze, 2009). Of these orthologues ULK1 and ULK2 are the most similar to yeast Atg1. ULK1 was the first human Atg1 homologue to be characterised and it was shown in HEK293A cells and cerebellar granule neurons that ULK1 alone but not ULK2 is required for autophagy (Chan et al., 2007, Lee and Tournier, 2011). However ULK1 and ULK2 have a redundant pro-autophagy function in MEFs (Lee and Tournier, 2011, McAlpine et al., 2013). Out of the five Atg1 homologues in humans, ULK1 is the best characterised. Upon starvation, mTORC1 is deactivated, ULK1 is released from Raptor, and the inhibitory phosphorylation on ULK1 is reduced and ULK1 relocalises to autophagic membranes (Chan et al., 2009). The PP2A-B55α phosphatase complex dephosphorylates ULK1 upon starvation (Wong et al., 2015). Active ULK1 is autophosphorylated and phosphorylates its complex members Atg13 and FIP200. Atg13 purified from *E. coli* was able to bind to the lipids phosphatidic acid, PI3P and PI4P, via a short motif near its N-terminus (Karanasios et al., 2013). Mutation of this lipid association motif reduced the number of starvation-induced puncta that GFP-Atg13 was able to form. Thus it is plausible that Atg13 could promote targeting of the ULK complex to membranes. Another nutrient sensing kinase, AMP-activated kinase (AMPK), also regulates (activates) ULK1 in response to glucose starvation (Kim et al., 2011). Aspects of regulation of and by the ULK complex have been reviewed in more detail (Wirth et al., 2013, Wong et al., 2013). Active ULK1 is thought to exert its function by phosphorylating substrates such as Ambra1 (Di Bartolomeo et al., 2010) and Beclin 1 (Russell et al., 2013). Upon starvation ULK1 phosphorylates Ser14 on Beclin 1 to promote the lipid kinase activity of the Vps34-containing Beclin1 complex, which catalyses the next signalling stage in autophagosome formation.

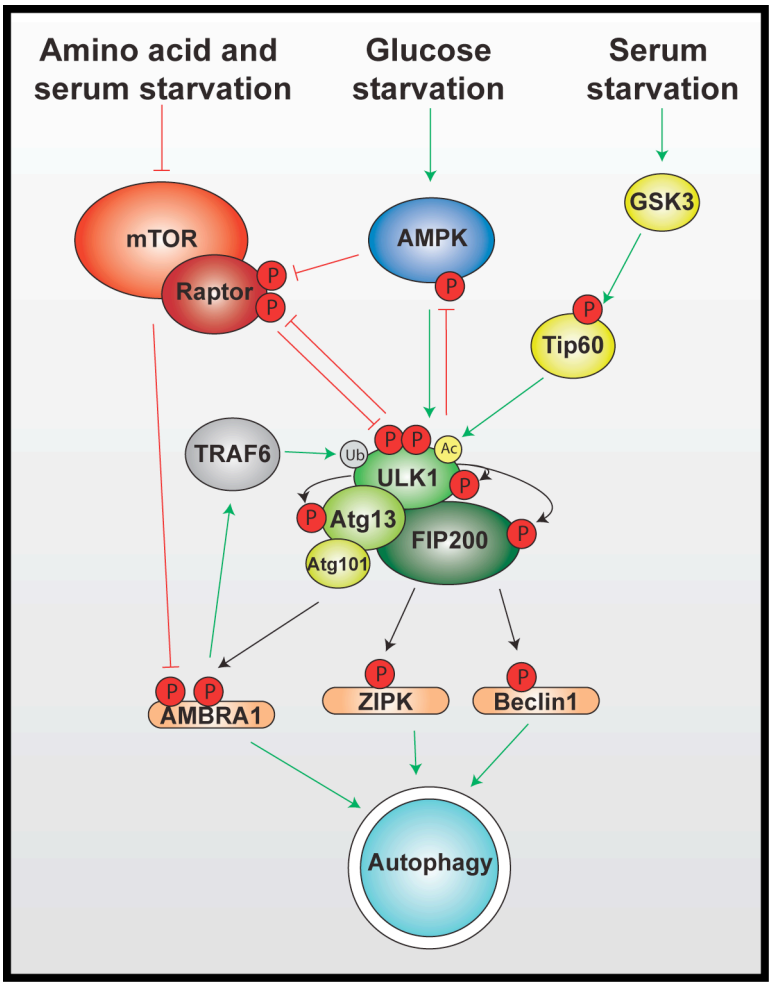

Figure 1.6 Aspects of regulation of and by the ULK1 complex

The mTORC1 complex is depicted with only the mTOR and Raptor subunits, for clarity. In addition to the mechanisms discussed in the text, ULK1 is also activated upon serum starvation through acetylation (Ac) by Tip60 (Lin et al., 2012). mTOR also phosphorylates and inhibits the Beclin 1 regulator Ambra1, whereas Ambra1 promotes the TRAF6-mediated activating K63-linked ubiquitination of ULK1 (Nazio et al., 2013). ZIPK promotes autophagy and is phosphorylated upon ULK1 overexpression and interacts with ULK1 (Tang et al., 2011). Other aspects of ULK regulation are discussed in section 1.2.5 and also reviewed in (Wong et al., 2013).

1.2.3 The Beclin 1 complex

The Beclin 1 complex performs the next major signalling function in the stages of autophagy initiation (Figure 1.7). The core Beclin 1 complex consists of the members Beclin1, p150 and Vps34, and there are additional more transient or unstable interactors such as the positive autophagy regulator Ambra1 and the negative regulator Rubicon (Funderburk et al., 2010, Simonsen and Tooze, 2009, Kang et al., 2011, Wirth et al., 2013). Vps34 is the class III lipid kinase that catalyses the conversion of phosphatidylinositol (PI) to phosphatidylinositol 3-phosphate (PI3P) on membranes, and thus the Beclin 1 complex functions to create a pool of PI3P at the omegasome and phagophore. The p150 subunit is N-terminally myristoylated and anchors the complex to membranes. The core Beclin 1 complex can associate with different proteins to form mutually exclusive and functionally different complexes with Atg14L (also known as Barkor) and UVRAG (Liang et al., 2006, Itakura et al., 2008, Sun et al., 2008, Zhong et al., 2009, Matsunaga et al., 2009). The Atg14L-containing Beclin 1 complex is required for autophagosome formation and Atg14L targets the Beclin 1 complex to the ER and the Omegasome (Matsunaga et al., 2010). The C-terminal region of Atg14L contains an amphipathic α-helix within its BATS (Barkor autophagosome targeting sequence) domain that targets the protein to autophagosomes (Fan et al., 2011). Moreover, through this region Atg14L can preferentially bind directly to highly curved membranes (possibly equivalent to early autophagic structures) enriched for PI3P, and it is thought that Atg14L can sense and maintain membrane curvature. Thus, the Atg14L-containing Beclin 1 complex may function in a reinforcing manner, to create and maintain PI3P enriched curved membranes. In addition to Atg14L, Beclin 1 can interact with membranes via the evolutionarily conserved domain (ECD) of Beclin 1, which contains an aromatic finger (a surface loop with aromatic residues at the tip) required for the function of Beclin 1 autophagosome biogenesis (Huang et al., 2012).

The Beclin 1 core complex can also interact with UVRAG, exclusive of the Beclin 1-Atg14L complex, and UVRAG promotes the activity of the Beclin 1 complex. Both UVRAG and Atg14L have coiled-coil domains and compete for

Beclin 1 binding to the coiled-coil domain of Beclin 1. The UVRAG-containing Beclin 1 complex has been implicated in both autophagosome formation and maturation (Liang et al., 2006, Itakura et al., 2008, Sun et al., 2008, Matsunaga et al., 2009, Zhong et al., 2009). However the role of UVRAG in autophagosome formation is controversial, as knockdown of UVRAG did not reduce autophagosome formation in a study by (Itakura et al., 2008). In addition, UVRAG localises to the ER and binds PI3P and the localisation of UVRAG to the ER is dependent on PI3P (He et al., 2013). This ER-localised UVRAG regulates COPI retrograde trafficking to the ER, and Golgi maintenance, through an interaction with an ER-tethering complex containing RINT-1. However, the UVRAG-RINT-1 complex dissociates upon autophagy induction and UVRAG interacts with the Bif-1 containing Beclin 1 complex to mobilise the Atg9 compartment and promote autophagosome formation. Thus, this demonstrates another intersection between the secretory pathway and autophagy. The Beclin 1 complex is regulated by interactions with other proteins, post-translational modifications and transcriptional and translational control mechanisms, see reviews (Wirth et al., 2013, Kang et al., 2011, Wirawan et al., 2012).

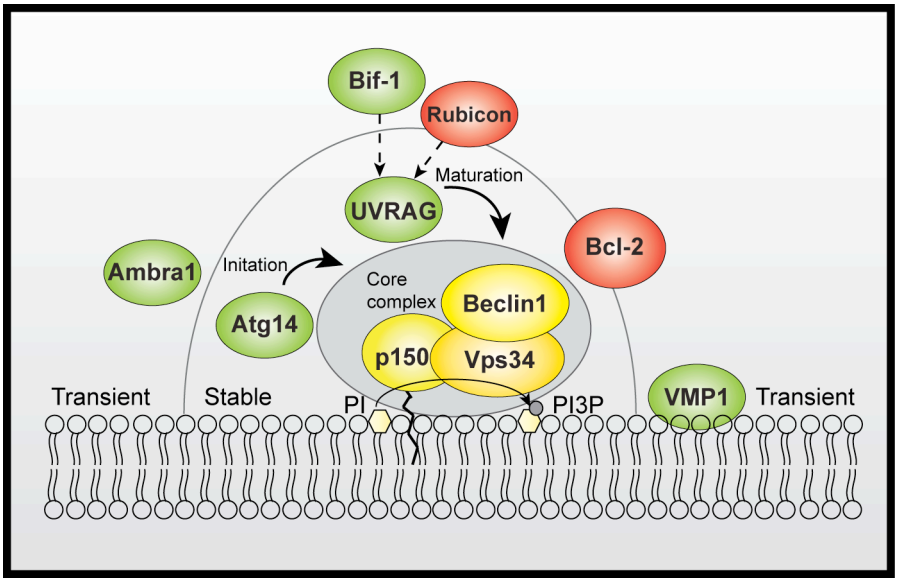

Figure 1.7 The Beclin 1 complex and subcomplexes

The core complex is shown in yellow. Stable interactors with the core complex are shown in the semi-circle and more transient or unstable interactors are shown outside of the circle. Positive regulators are shown in green and negative regulators shown in red. UVRAG directly interacts with the BAR domain-containing protein Bif-1, which can bind membranes and induce curvature (Takahashi et al., 2007). This interaction is thought may be important in starvation-induced Atg9 trafficking (Takahashi et al., 2011). Bcl-2 binds to the BH3 domain of Beclin 1 to inhibit binding of Beclin 1 to Vps34 and autophagy (Pattingre et al., 2005). Bcl-2 binding to Beclin 1 can be disrupted by binding to the transmembrane protein VMP1 (Molejon et al., 2013). Figure adapted from Wirth et al. (Wirth et al., 2013).

1.2.4 PI3P effectors, Atg9 and the ubiquitin-like conjugation systems

The spatially and temporally restricted pool of PI3P formed at autophagosome formation sites by the Beclin 1 complex upon starvation functions to recruit PI3P binding proteins that act as autophagy effectors. Such proteins include DFCP1 (Axe et al., 2008) and the WIPI proteins (Proikas-Cezanne et al., 2004, Polson et al., 2010, Dooley et al., 2014). DFCP1 localises to the ER and Golgi and upon amino acid starvation relocalises to PI3P-positive omegasomes but is not incorporated into the autophagosome. However, the exact function of DFCP1 in autophagy is unknown, as siRNA depletion of DFCP1 does not inhibit autophagy (Axe et al., 2008). WIPI2 also binds to the autophagosomal pool of PI3P formed upon starvation and depletion of WIPI2 results in reduced autophagosome formation (as assessed by LC3 lipidation and spot formation) and an accumulation

of DFCP1-positive omegasomes. Thus WIPI2 functions in the progression of omegasomes to autophagosomes. The function of WIPI2 is to recruit a complex of Atg12–5-16L1 to drive LC3 lipidation. The pool of autophagosomal PI3P is removed by PI3P phosphatases such as MTMR14 (Jumpy) (Vergne et al., 2009) and MTMR3 (Taguchi-Atarashi et al., 2010), which negatively regulate autophagy.

The transmembrane protein Atg9 has an important function in the very early stages of autophagosome formation and promotes the formation of DFCP1-positive structures and autophagosomes (Orsi et al., 2012). Atg9-positive structures have been observed making dynamic contacts with forming autophagosomes but it is thought that mammalian Atg9 itself does not become incorporated into the autophagosomal membrane. It is likely that Atg9 functions in the expansion of the phagophore. Atg9 resides on endosomes and recycling endosomes but also on a morphologically distinct membrane compartment comprised of tubulated and vesicular membranes radiating from vacuolar structures. This compartment exists under basal and starvation conditions. Atg9 is also found on the trans-Golgi network (TGN) under basal conditions and redistributes to peripheral endosomal membranes upon autophagy induction (Young et al., 2006). This trafficking of Atg9 requires ULK1 and PI3 kinase activity. Atg9 also resides on the plasma membrane (Puri et al., 2013, Popovic and Dikic, 2014), and the endocytosis of Atg9 is thought to contribute to the formation of autophagosome precursor membranes. The mobilisation of Atg9-positive membranes is hypothesised to function in the delivery of lipids or regulators to the forming autophagosome upon starvation, however the precise molecular role of mammalian Atg9 in autophagosome biogenesis remains to be elucidated.

There are two ubiquitin-like conjugation systems involved in the closure of the autophagosome (Figure 1.8), reviewed in (Mizushima et al., 2011). The first system of reactions results in the formation of the constitutive Atg12–Atg5-Atg16L1 complex. The second system results in the formation of lipidated Atg8. Atg12 is a small ubiquitin-like protein that becomes covalently attached to the Atg5 protein. The protein Atg10 acts as the E2-like enzyme in this reaction and Atg7 acts as the E1-like enzyme. Atg12 is activated by Atg7 and transferred to Atg10 prior to conjugation to Atg5, to form the Atg12–Atg5 conjugate (Mizushima et al., 1998). Atg7 is also the E1-like enzyme for the generation of lipidated Atg8. Atg16L1 non-covalently associates non-covalently with Atg5 forming the Atg12–Atg5-Atg16L1

complex (Mizushima et al., 2003). The Atg12–5-16L1 complex resides (mostly) on the outer surface of the phagophore and dissociates from the membrane soon after autophagosome completion or just before (Mizushima et al., 2001).

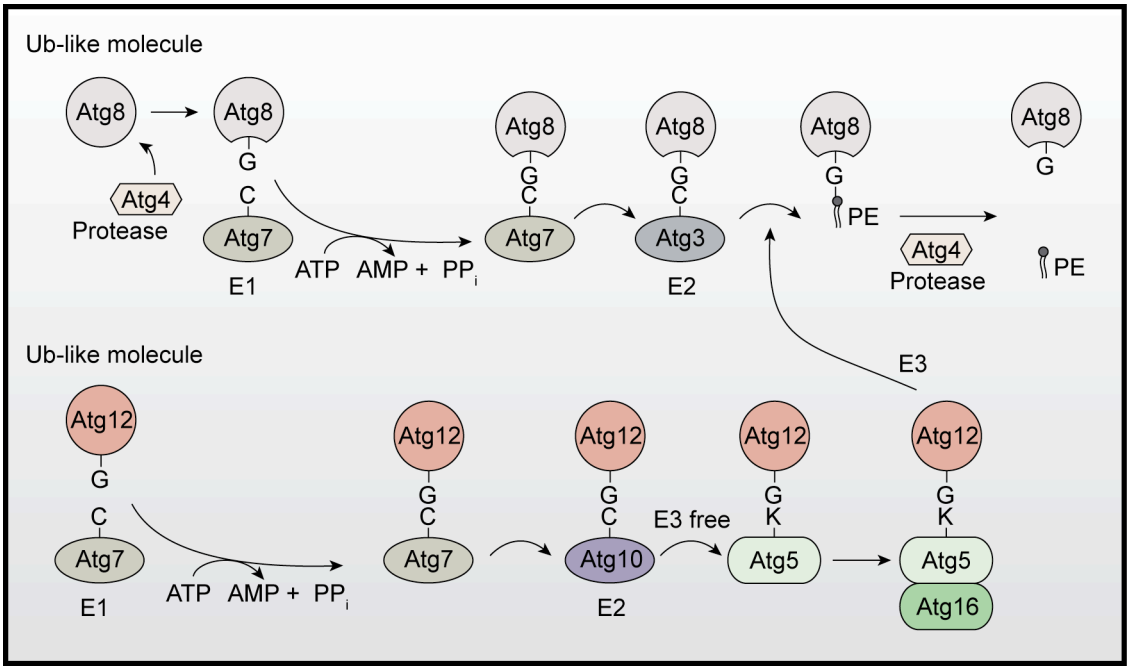

Figure 1.8 The two ubiquitin-like conjugation systems operating in autophagy
Illustrated here is the yeast conjugation system, as was originally elucidated. However Atg8 could be substituted with LC3s or GABARAPs and Atg16 and be substituted with Atg16L1 for the analogous mammalian system. Atg10 can mediate the formation of the Atg12-5 conjugate without an E3-like enzyme (Yamaguchi et al., 2012).

The Atg12–5-16L1 complex acts as an E3-like enzyme for the generation of lipidated Atg8, with Atg3 providing the E2-like function in the Atg8 conjugation system (Hanada et al., 2007). Atg3 promotes the lipidation of Atg8 proteins at highly curved membranes and this function, mediated by an N-terminal amphipathic helix, may have evolved to sense the highly curved cup-shaped structure of the phagophore (Nath et al., 2014). The ubiquitin-like protein Atg8 is translated as a pro-protein that becomes cleaved by Atg4 at the C-terminus to expose a glycine residue (Kirisako et al., 2000). Unlike yeast which has only one Atg8 protein in mammals there are multiple Atg8 homologues that have different names, which are discussed later, however the mechanism of their processing and subsequent conjugation is thought to be the same (Kabeya et al., 2004). This cleaved form of the Atg8 protein is cytosolic and is known as the “I” form. The C-

terminal glycine of the cleaved Atg8 protein is attached to the lipid phosphatidylethanolamine (PE) to anchor the Atg8s to the phagophore membrane. This lipidated form is known as the “II” form. LC3B is the best known Atg8 homologue in mammalian cells and is routinely used as a marker for autophagy. LC3B is often abbreviated simply to LC3. The LC3-II form (lipidated) migrates faster by SDS-PAGE than the LC3-I (cytosolic) form and thus the initiation of autophagy by starvation can be monitored by western blotting (Klionsky et al., 2012).

When autophagy is initiated, LC3 becomes lipidated, but also becomes degraded in the lysosome. This is because LC3 is attached to both the concave and convex surfaces of the phagophore membrane (unlike the Atg12–5-16L1 complex) and is also on fully formed autophagosomes (Kirisako et al., 1999) (Figure 1.9). Thus the LC3 on the inner (concave) membrane is terminally delivered to the lysosomal lumen. Atg4 acts as a deconjugating enzyme to cleave and release LC3 from PE on the autophagosome membrane after formation. One function of the Atg8s is to promote the elongation and final closure of the autophagosomes (Weidberg et al., 2010), likely mediated through the activity of the Atg8s in membrane tethering and fusion (Weidberg et al., 2011). It has been shown with purified yeast proteins that the Atg12–5-16 complex along with Atg8-PE forms a scaffold structure on the outer (convex) surface of the phagophore and that Atg8 interacts with Atg12 to facilitate this cage-like structure (Kaufmann et al., 2014). Formation of this scaffold is important for progression of autophagy, however on the concave surface Atg8 functions to bind cargo receptor proteins for capturing cargo (Behrends and Fulda, 2012, Johansen and Lamark, 2011, Okamoto, 2014, Stolz et al., 2014, Svenning and Johansen, 2013, Rogov et al., 2014). Thus it appears that Atg8 could have distinct spatially controlled functions on the same membrane structure, in phagophore expansion and cargo capture. Whether this scaffold occurs in mammalian cells remains to be elucidated.

As mentioned the Atg8s function in binding cargo receptors to recruit substrates for degradation. One such cargo receptor that binds the Atg8s directly is p62 (Pankiv et al., 2007, Bjorkoy et al., 2005), which is also known as sequestosome-1. p62 contains an LC3-interacting region (LIR), which is a short motif that facilitates the direct interaction with Atg8s. In addition to binding Atg8s, p62 functions to bind ubiquitinated protein aggregates and thus facilitates the

clearance of protein aggregates by autophagy (aggrephagy). Because p62 is bound to and encapsulated by the autophagosome, it is also degraded upon starvation. Because of this, degradation of p62 is routinely monitored by western blotting as a late stage readout of autophagic flux (Klionsky et al., 2012).

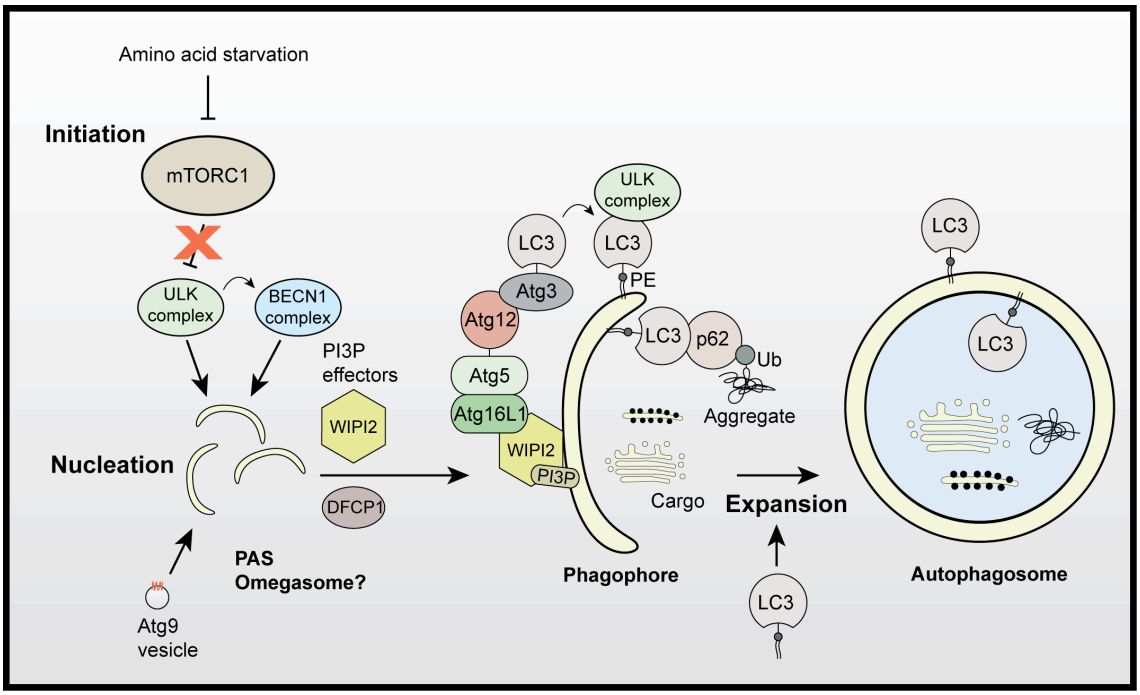

Figure 1.9 The mammalian machinery of autophagosome formation

Autophagosome formation can be divided into 3 stages: initiation, nucleation and expansion. Initiation is the transmission of the nutrient status signal to the membrane where phagophore membranes are generated (nucleation). The membranes must grow in size (expansion) to form the cargo-capturing autophagosome.

1.2.5 Non-hierarchical autophagy

Autophagy is usually described as a hierarchical sequence of signal transduction and protein recruitment events, as I have done above. However in recent years this view has been modified somewhat, as it is apparent now that autophagy is a complicated network of protein interactions and feedback/forward mechanisms (Behrends et al., 2010). The autophagy proteins I have described here are involved in the starvation-induced autophagy pathway, however autophagy can occur in certain settings without these core proteins, this form of autophagy is known as non-canonical autophagy (Codogno et al., 2012). For

example ammonia induces autophagy in ULK1 and ULK2 double knockout MEFs, suggesting that the canonical initiating signals of autophagy can be bypassed in some way (Cheong et al., 2011).

I will highlight some examples of how autophagy is not a simple hierarchical pathway. The non-hierarchical autophagy I describe here is canonical in the sense that it requires the core autophagy components. ULK1 promotes the phosphorylation of the Raptor subunit of the mTORC1 complex and reduces the binding of substrates to Raptor (Dunlop et al., 2011) and inhibits mTOR function (Jung et al., 2011) (Figure 1.6). In addition ULK1 can also phosphorylate and inhibit AMPK (Loffler et al., 2011). Thus ULK1 can feedback to two major upstream regulators of its function. The ULK complex is thought of as the autophagy initiating kinase that acts at very early stages. However, it is also known that maximal and stable recruitment of the ULK complex requires PI3P (Karanasios et al., 2013), which is formed downstream of ULK1 activation. Thus PI3P functions as a signal to enforce ULK maintenance at the phagophore. Atg14L, which is part of the early acting Beclin 1 lipid kinase complex, binds to the SNARE syntaxin 17 and promotes tethering and fusion of autophagosome membranes to later compartments (Diao et al., 2015). In addition, the Atg12–5 conjugate is also implicated in later maturation stages. The Atg12–5 conjugate forms a complex with TECPR1, which is separate from the Atg12–5-16L1 complex, that promotes the fusion of autophagosomes with lysosomes (Chen et al., 2012). Thus, an emerging theme is that an individual autophagy protein may regulate the pathway at different points and indeed provide different functions at different stages. An additional worthwhile consideration is that autophagy proteins have functions outside of autophagy; for example Atg7 binds the tumour suppressor protein p53 to regulate the transcription of the p21 cell cycle arrest gene (Lee et al., 2012). The non-autophagic functions of the Atg proteins have been recently reviewed (Subramani and Malhotra, 2013). Conceptually this makes sense as the autophagy proteins are already translated and at adequate supply to facilitate the rapid formation of autophagosomes upon starvation. Thus during basal conditions when autophagy levels are low, it would be sensible to have dual functions of the autophagy proteins. However, I think the question remains as to what these proteins are doing in the basal state. For example, the majority of the WIPI2 and ULK1 proteins are not on membranes by subcellular fractionation (Chan et al., 2009) (Polson et al., 2010), and there is no significant

recruitment to a crude membrane extract during starvation. Presumably the membrane localised populations of the proteins are involved in autophagy, so one may ask what is the function of the remaining population?

Since the discovery of the autophagy machinery proteins, there has been a great increase in our understanding of the regulation of these proteins. The literature on autophagy regulation is vast and autophagy proteins can be regulated by: protein binding partners, control of subcellular localisation, stabilisation from proteasomal degradation, post-translational modifications such as acetylation, ubiquitination and phosphorylation (Kroemer et al., 2010) (Xie et al., 2015). The expression of autophagy genes is also regulated by transcription factors, epigenetic control and translational control through miRNAs (Fullgrabe et al., 2014). However, our understanding of the regulation of autophagy is still in its growing stages.

1.3 WAC

WW domain-containing adapter protein with coiled-coil (WAC) is a recently discovered positive regulator of starvation-induced autophagy (McKnight et al., 2012). As described, the core protein machinery of autophagosome formation has been known for some time, however how this process is regulated is still to be uncovered. To this end a previous PhD student in the lab, Nicole McKnight, carried out a genome-wide screen (McKnight et al., 2012) to uncover novel regulators of amino acid starvation-induced autophagy. WAC was a main candidate for a novel positive regulator of autophagy whose function in autophagy was unknown. It has been shown that WAC is a positive regulator of autophagy in HEK293A cells and in HeLa cells (McKnight et al., 2012) and Nicole McKnight, ("A Genome-wide Screen for Starvation-induced Autophagy Identifies New Modulators of Autophagy", 2010). In HEK293 cells stably expressing GFP-LC3B, WAC was required for maximal puncta (autophagosome) formation under conditions of EBSS starvation and leupeptin treatment to block lysosomal protein degradation. In HEK293A cells, WAC is required for efficient endogenous LC3 lipidation as determined by depleting WAC, EBSS starving cells and simultaneously treating with the vacuolar ATPase inhibitor bafilomycin A1 (BafA) (Yamamoto et al., 1998). BafA and leupeptin prevent the degradation of LC3 covalently linked to the inner autophagosomal membrane. Thus, during treatment with BafA or leupeptin it is possible to assay solely for the formation of LC3-II (lipidated LC3) and exclude degradation of LC3 (Klionsky et al., 2012). This phenotype was observed with multiple siRNA sequences targeting WAC, suggesting that it was not an off-target effect of any one siRNA. In addition, in basal and starvation conditions, knockdown of WAC results in the accumulation of the autophagy substrate p62, suggesting a defect in p62 degradation by autophagy. These data suggest that basal autophagy, as well as starvation-induced autophagy, is regulated by WAC. Upon starvation in EBSS, some p62 degradation was observed in WAC knockdown cells. This suggests that WAC is not absolutely required for autophagy, but is rather a regulatory protein. It is also possible that a WAC knockout, such as generation of a CRISPR cell line, would exhibit a more enhanced phenotype. WAC depletion also attenuated LC3

lipidation in HeLa cells, this was evidenced by an observed decrease in the LC3-II/LC3-I ratio (Nicole McKnight, “A Genome-wide Screen for Starvation-induced Autophagy Identifies New Modulators of Autophagy”, 2010). As HeLa cells have a high level of basal LC3-II in our hands (data not shown), it may be more informative to measure changes in LC3-I in addition to LC3-II rather than LC3-II/Actin (Nicole McKnight, “A Genome-wide Screen for Starvation-induced Autophagy Identifies New Modulators of Autophagy”, 2010). Myc-WAC was also shown to interact with GFP-Beclin 1 (McKnight et al., 2012) and was found as a low confidence interactor of FLAG-HA-Beclin 1 in the autophagy network (Behrends et al., 2010). In addition to WAC’s role in promoting autophagy, WAC may negatively regulate proteasomal degradation (McKnight et al., 2012). Using Ub^{G76V}-YFP, a reporter of proteasomal degradation (Dantuma et al., 2000), after depletion of WAC less Ub^{G76V}-YFP was found, and this was rescued with the proteasomal inhibitor MG132, suggesting that the UPS was enhanced upon WAC depletion.

WAC is implicated in pathologies and is expressed in a wide range of tissues (Totsukawa et al., 2011). For example, WAC is mutated in acute myeloid leukaemia after relapse but not in the primary cancer (Ding et al., 2012), mutations in WAC could be involved in intellectual disability (Hamdan et al., 2014) and WAC nonsense or frameshift mutations are thought to result in neurocognitive phenotypes and facial dysmorphism (DeSanto et al., 2015). WAC was first cloned and expressed over a decade ago and in humans there are four WAC isoforms that are generated by alternative splicing (Xu and Arnaout, 2002). Isoform 1 of WAC is the best characterised and the longest WAC isoform of 647 amino acids, encoded by 14 exons on chromosome 10 (Ensembl). WAC contains a predicted WW domain towards its N-terminus, and a predicted coiled-coil (CC) domain at its C-terminus. See Figure 4.9c for the primary structure of WAC human isoform 1, discussed in greater detail in Chapter 4. Both of these WAC domains mediate protein-protein interactions (Zhang and Yu, 2011). There are no other known domains in the protein. The WW and CC domains of WAC are conserved to *Drosophila*, however there is no known WAC homologue in yeast. The rest of the WAC protein is not well conserved, although between mouse and human WAC there is 95% similarity at the amino acid level of the full length protein (Xu and Arnaout, 2002). In flies, the homologous sequences of the WW and CC domains of WAC are encoded by a polypeptide chain (protein name CG8949) that also contains sequences

homologous to SNRP70, a component of the spliceosome. However in mammals, WAC orthologues exist as separate peptide chains to SNRP70. This suggests that evolutionarily, WAC may have functioned in splicing but has since diverged in function. The WW domain of WAC comprises of 2 tryptophan (W) residues separated by 23 amino acids (inclusive). WW domains are protein interaction domains, which usually bind to proline rich regions (PPXY, PPLP and PGM motifs) (Chen and Sudol, 1995) (Bedford et al., 1998) (Chan et al., 1996) or to phosphorylated serine or threonine residues (Lu et al., 1999). The WW domain of WAC has been shown to bind proline motifs directly, suggesting that it is a functional WW domain (Kato et al., 2004). The WW domain in WAC is characterised by the presence of a triple tyrosine (YYY) motif, which is an element found in the WW domains of some spliceosomal proteins. When WAC was first expressed (Xu and Arnaout, 2002), immunofluorescence showed that the tagged form of the protein formed nuclear speckles that colocalised with the splicing factor SC35. Thus it was hypothesised that WAC functioned in splicing. However, to date there has been no functional evidence of this. In my hands overexpressed WAC does form structures that resemble nuclear speckles, however this only occurs in cells expressing high levels of WAC, and does not reflect the localisation of the endogenous protein (data not shown). The earliest paper on WAC (Xu and Arnaout, 2002) also provided evidence that WAC is phosphorylated on tyrosine residues. Indeed, numerous phosphorylation sites have since been discovered on WAC by mass spectrometry (www.phosphosite.org).

WAC was later shown to perform a function in the nucleus (Zhang and Yu, 2011) (Figure 1.10). WAC promotes monoubiquitination of histone 2B (H2B) at lysine 120. This epigenetic mark is associated with regions of active transcription and is enriched downstream of the transcription start site (Bonnet et al., 2014). WAC, via its WW domain, binds to RNA polymerase II (RNAP) and binds to the phosphorylated C-terminal domain (CTD) of RNAP when phosphorylated at the serine 2 position of the heptads in the CTD. This modification is associated with the coding regions of genes and is promoted by CDK9 (Komarnitsky et al., 2000, Pirngruber et al., 2009). At the same time as binding RNAP, WAC is thought to act as an adaptor by binding to and activating, an E3 ligase complex of RNF20/40. This interaction occurs through the CC domain of WAC, with the CC domains of RNF20/40. WAC also indirectly interacts with the E2 enzyme RAD6. Thus WAC

recruits the RNF20/40 E3 ligase complex to RNAP, to promote the ubiquitination of histones in front of the processing polymerase. Through this mechanism of H2B ubiquitination, WAC promotes the expression of p53 target genes such as p21.This mechanism was shown to be important for the protective response of cell cycle arrest after DNA damage. Normally this checkpoint would ensure arrest of DNA replication to allow DNA repair. However in WAC knockdown cells exposed to ionising radiation, the expression of p21 was impaired leading to the continuation of DNA replication instead of arrest. The complex of WAC/RNF20/40 was shown to exist in nuclear extracts and the interactions are direct. Moreover this complex remains associated during size-exclusion chromatography and is predicted to occur as a heterohexameric complex with a 2:2:2 stoichiometry. In addition to WAC's role in the DNA damage response, WAC and H2B monoubiquitination are involved in the differentiation of human mesenchymal stem cells into osteoblast or adipocyte lineages (Karpiuk et al., 2012).

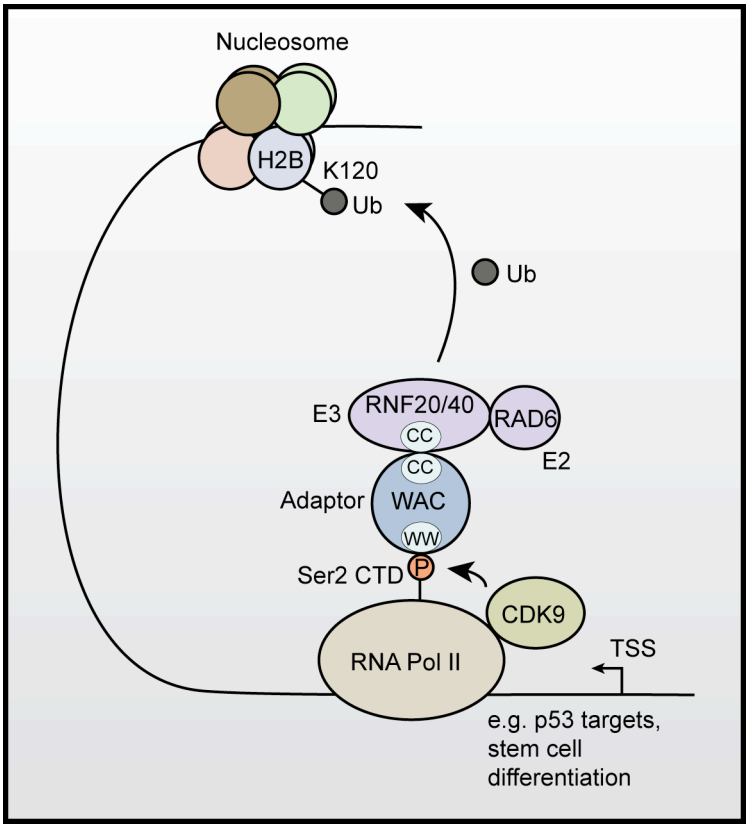

Figure 1.10 The function of WAC in the nucleus

See main text for details. Transcription start site, TSS.

WAC was also found in purified rat liver Golgi membranes, where it was stably associated after 1M KCl washes (Totsukawa et al., 2011). This is similar to the Golgi matrix protein GM130 (Nakamura et al., 1995) and WAC also colocalises with GM130 in HeLa cells (Totsukawa et al., 2011). On the Golgi, WAC interacts directly with the deubiquitinase (DUB) VCIP135 and stimulates its DUB activity (Figure 1.11). VCIP135 interacts with valosin-containing protein (VCP) also known as p97 and Cdc48 in yeast, and through VCIP135, WAC and VCP interact indirectly. This interaction of WAC with VCIP135 and its stimulation of VCIP135 DUB activity function in the reformation of Golgi cisternae post-mitosis. During mitosis the Golgi vesiculates, through the phosphorylation-mediated inhibition of factors such as GM130 by cell cycle regulated kinases, and the disassembly of tethering complexes (Nakamura et al., 1997, Lowe et al., 1998, Wang et al., 2003, Corda et al., 2012). Knockdown of WAC resulted in the fragmentation of the Golgi complex by immunofluorescence and by electron microscopy, where there was a reduction in cisternal structures and an increase in tubules and vesicles around the Golgi. Although WAC may anchor VCIP135 to the Golgi, the factor that anchors WAC to the Golgi is unknown. Thus WAC appears to have at least 2 functions, one in the nucleus in epigenetic regulation and one on the Golgi in membrane biogenesis, and WAC interacts with both E3 ligases and deubiquitinases.

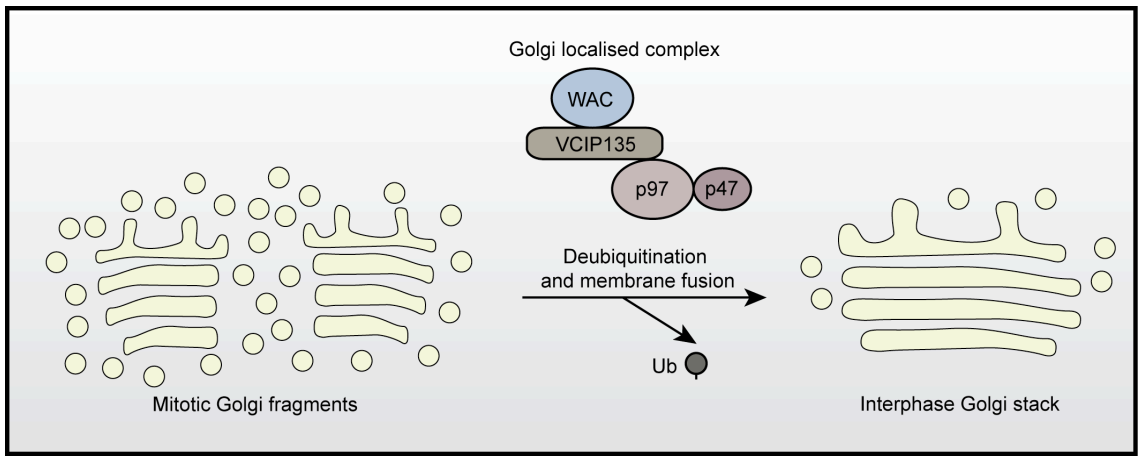

Figure 1.11 The function of WAC on the Golgi complex

See main text for details. Golgi membrane fusion is facilitated by ATPases such as NSF and p97. p97 forms distinct complexes with p37 or p47 (shown here). The p97/47 mechanism of membrane fusion is thought to be specific for Golgi reformation at mitosis and mediated by the syntaxin 5 SNARE but not by the p115 or GM130 tethers.

1.4 GM130

GM130 was first characterised around two decades ago and was shown to be a Golgi matrix protein localised mostly to the cis-Golgi with a predicted extended rod-like structure and extensive coiled-coil regions (Nakamura et al., 1995). GM130 can also cycle between the Golgi complex and the ERGIC and is part of a family of extended coiled-coil Golgi proteins known as golgins (Wong and Munro, 2014, Marra et al., 2001). GM130 may be involved in disease; for example GM130 is downregulated in breast and colorectal cancer and depletion of GM130 in breast cancer cells increases their migration speeds and invasiveness (Baschieri et al., 2015, Baschieri et al., 2014). In addition the bacterial toxin EspG, found in pathogenic strains of *E. coli*, binds to GM130 and induces the fragmentation of the Golgi (Clements et al., 2011). GM130 was isolated from rat liver Golgi extracts and remained associated with Golgi matrix after 1 M KCl washes and is 130 kDa in size (Nakamura et al., 1995). GM130 has a homologue in *Drosophila* and a functional homologue in yeast, Bug1 (Behnia et al., 2007). GM130 has 4 or 6 major coiled-coil domains, depending on the bioinformatic prediction tool used, and forms a parallel homotetramer (Ishida et al., 2015). GM130 has also been observed as a hexamer (Hu et al., 2015). A schematic of the primary structure of GM130 is provided in Figure 4.11c. GM130 also contains a functional nuclear localisation signal towards its N-terminus (Wei et al., 2015). At its N-terminus GM130 binds to the coiled-coil tethering factor p115 and during mitosis GM130 is phosphorylated on Ser25 by the kinase CDK1/Cdc2 (Nakamura et al., 1997, Lowe et al., 1998). The phosphorylation of GM130 is associated with the dissociation of the p115 and GM130 interaction and this is thought to facilitate the COPI mediated disassembly of the Golgi complex at mitosis (Nakamura et al., 1997, Lowe et al., 1998). However, Ser25 phosphorylation of GM130 may not be the only mechanism for mitotic Golgi fragmentation (Sundaramoorthy et al., 2010). In addition N-terminal arginine residues in GM130 are targeted for methylation by the methyltransferase PRMT5 (Zhou et al., 2010), and this appears important for the integrity of the Golgi. p115 is thought to bridge the interaction between GM130 on the Golgi and Giantin, a large ~400 kDa protein enriched on COPI vesicles (Lesa et al., 2000, Seemann et al., 2000, Sonnichsen et al., 1998). However, this view has been challenged by the observation that p115 binds GM130 or Giantin individually but not

simultaneously (Linstedt et al., 2000). The GM130-p115 interaction can be disrupted by microinjection of a GM130 peptide corresponding to the interaction region (Seemann et al., 2000), this results in vesiculation around the Golgi complex suggesting that the GM130-p115 interaction promotes vesicle tethering and fusion with Golgi membranes (Figure 1.12b). However, the role of the GM130-p115 interaction in maintaining Golgi structure is controversial, as it was reported that inhibition of GM130-p115 binding, by microinjection of anti-GM130 antibodies, has no detectable effect on Golgi structure (Puthenveedu and Linstedt, 2001). In addition, it was reported that the GM130-GRASP65 interaction (Figure 1.12d), and the GM130 mediated regulation of ER-to-Golgi carriers (Figure 1.12c) are important in regulating Golgi ribbon formation (Puthenveedu et al., 2006) (Marra et al., 2007). The complicated nature of GM130's role in the maintenance of the Golgi is highlighted by the use of hamster cells (ldlG) with no detectable GM130, where the role of GM130 in Golgi morphology is apparent only at certain temperatures (Vasile et al., 2003). In addition to its proposed role in maintaining Golgi structure, GM130 also regulates anterograde ER-Golgi traffic (Alvarez et al., 2001) although may not be absolutely required for forward secretion (Marra et al., 2007) (Puthenveedu et al., 2006). This likely because of redundancy between the golgins, and GM130 has recently been shown to function in a redundant manner with the golgin GMAP-210 in ER to Golgi trafficking (Roboti et al., 2015). The role of GM130 in regulating protein glycosylation is also controversial (Marra et al., 2007) (Puthenveedu et al., 2006). In support of GM130's role in forward trafficking, GM130 interacts with Rab1b-GTP independently of p115 forming an effector complex that is thought to promote COPII vesicle tethering and fusion at the cis-Golgi (Weide et al., 2001, Moyer et al., 2001). In addition, mitochondrially targeted GM130 has been shown to capture ER-derived carriers (Wong and Munro, 2014). GM130 also interacts with another small Rab GTPase Rab33b in its active (GTP bound) state, although the exact function of this interaction is unknown (Valsdottir et al., 2001). Interestingly, as discussed earlier, Rab1 and Rab33b are both implicated in the regulation of autophagosome formation. At its C-terminus GM130 binds to the Golgi protein GRASP65 and this interaction is required for the localisation of both proteins to the Golgi (Barr et al., 1998) (Figure 1.12b). The anchoring of GM130 to the Golgi complex is thought to be mediated by N-myristoylation of GRASP65 (Barr et al., 1997). The zinc finger integral membrane protein ZFPL1 and the SNARE protein

syntaxin 5 also interact with the C-terminal region of GM130 (Chiu et al., 2008, Diao et al., 2008) (Figure 1.12a). The interaction of GM130-syntaxin 5 is inhibited by the binding of p115 to the N-terminus of GM130. It is thought that GM130 may function to spatiotemporally coordinate vesicle tethering and subsequent SNARE-mediated fusion events.

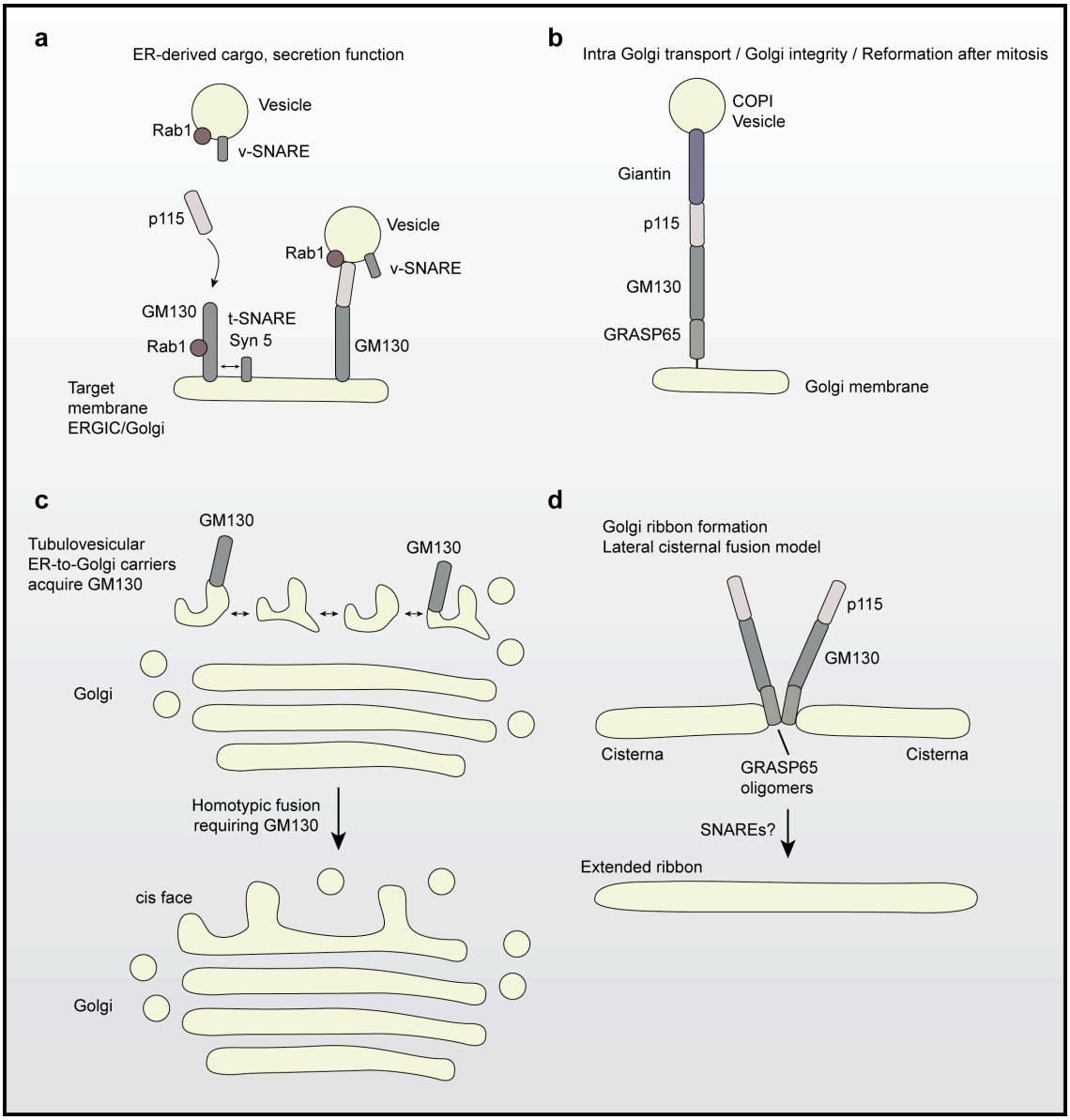

Figure 1.12 Functions of GM130 in Golgi biogenesis and membrane trafficking

(a) GM130 has a role in anterograde trafficking. p115 can bind Rab1b and could allow the capture of vesicles by GM130, possibly inducing a conformational change in GM130 to allow SNARE mediated fusions to occur after the release of syntaxin 5 (Diao et al., 2008). For explanation of the other models see main text.

In addition to its role in membrane dynamics GM130 performs multiple other functions that have been discovered more recently. For example GM130 regulates signalling by maintaining the activity of the Rho family GTPase Cdc42. GM130 interacts with Tuba, a GEF for Cdc42, and promotes Cdc42 activation at the Golgi (Kodani et al., 2009). This axis of Cdc42 and GM130 is thought to function in centrosomal organisation and function in interphase cells (Kodani and Sutterlin, 2008b, Kodani et al., 2009). Furthermore, GM130 binds to an inhibitor of Cdc42, RasGRF (Baschieri et al., 2014). Depletion of GM130 releases RasGRF resulting in the inhibition of the Golgi pool of Cdc42 and dysregulation of cell polarity. GM130 also regulates signalling by binding to and activating the YSK1 kinase, whose function is required for Golgi organisation, cell migration and invasion (Preisinger et al., 2004).

GM130 is also connected with microtubule dynamics. GM130 interacts with AKAP450, a centrosomal gamma-tubulin interacting protein, and both GM130 and AKAP450 are involved in nucleating microtubules from the cis-face of the Golgi (Rivero et al., 2009, Hurtado et al., 2011). As mentioned GM130 regulates centrosome organisation but GM130 also controls mitotic and meiotic spindle formation and the localisation of spindle pole proteins (Kodani and Sutterlin, 2008b, Zhang et al., 2011, Wei et al., 2015). Upon mitosis, the phosphorylation of GM130 by CDK1 to remove p115 binding is thought to allow importin α binding to the NLS of GM130, this then releases the microtubule nucleating factor TPX2 from importin α and TPX2 can then nucleate microtubules (Wei et al., 2015). GM130 additionally captures the nascent microtubules directly (Wei et al., 2015). This mechanism is thought to function in accurate Golgi segregation during mitosis. Finally, GM130 appears to be a negative regulator of autophagy (Chang et al., 2012). This will be discussed in more depth in Chapter 5.

1.5 GABARAP and the Atg8 family

In yeast there is only one Atg8 protein, however in humans Atg8 has diverged into different orthologues (Shpilka et al., 2011). There are also multiple Atg4 genes in mammals, perhaps to direct specified processing of the different mammalian Atg8s. These mammalian Atg8s (mAtg8s) are split into three subfamilies based on their sequence similarity to one another. The Atg8 family of proteins are structurally similar ubiquitin-like proteins (Ubiquitin-like by structure not sequence), consisting of 2 N-terminal α-helices and a ubiquitin-like core. However, the family members vary at their N-terminus. There is the LC3 subfamily, comprised of LC3A (2 isoforms by alternative splicing), LC3B, LC3B2 and LC3C, the GABARAP subfamily comprised of GABARAP and GABARAPL1, and the GATE-16 subfamily containing GABARAPL2 only, which is also known as GATE-16. Sometimes the three GABARAP genes from two subfamilies are grouped together and called the GABARAPs. LC3B is usually used as a readout of autophagy, because of the development of tools to study this particular mAtg8 (Kabeya et al., 2000). The mAtg8s can make protein-protein interactions that are LIR independent or LIR dependent (e.g. p62). The LIR motif has the core sequence (W/F/Y)XX(L/I/V), and often has acidic residues preceding the first hydrophobic residue (Alemu et al., 2012). As mentioned earlier, the mAtg8s may also have a direct role in membrane tethering or fusion events, in addition to binding LIR-containing cargo receptors. In recent years there has been a great increase in the number of proteins known to bind the mAtg8s, many of which bind several different family members (Wild et al., 2014). Moreover, some of the mAtg8s interact with one another. A few questions arise from this. What are the roles of the individual family members and what is the extent of redundancy versus specialism? Why are there so many mAtg8-interacting proteins and how is this selectivity regulated?

There are examples of specific regulation/function of the mAtg8s and also of redundancy. The different mAtg8s have some difference in tissue expression (reviewed in (Shpilka et al., 2011)), which could be indicative of specialised functions. Moreover there are differences in expression levels of the mAtg8s, with GABARAP being the most abundantly expressed in the LNCaP prostate cancer cell

line (Szalai et al., 2015). Depletion of individual mAtg8 family members only has a partial inhibitory effect on autophagy, which could suggest redundancy of the family members (Weidberg et al., 2010). However, knockdown of the GABARAP proteins together, resulted in the accumulation of large unclosed phagophore membranes by electron microscopy (Weidberg et al., 2010). In contrast depletion of the LC3 proteins together resulted in the accumulation of small phagophore structures. Depletion of the GABARAPs or the LC3s resulted in the accumulation of Atg5 and Atg12 puncta, suggesting a stalling of autophagosome biogenesis after recruitment of the Atg12-5-16L1 complex. These data suggest that the GABARAPs could function in the final elongation and closure stages of the phagophore whereas the LC3 subfamily may have a role in early phagophore elongation. Other examples of specific function include LC3C, which is involved in antibacterial autophagy of *Salmonella* via binding the LIR-containing adaptor protein NDP52 (von Muhlinen et al., 2013). In addition, LC3B appears to be more crucial for the incorporation of p62 into the autophagosome than the GABARAPs (Maruyama et al., 2014, Shvets et al., 2011). One study concluded that the GABARAP proteins were crucial for bulk (non-selective) autophagy but the LC3s were dispensable (Szalai et al., 2015). However, despite evidence of specificity, the specific functions of the mAtg8s is largely unknown.

I shall focus on an introduction of the GABARAP member of the Atg8 family, as this been a significant portion of my work. $GABA_A$ receptor associated protein (GABARAP) was identified as a 17 kDa interactor with $GABA_A$ receptors, which are receptors that mediate inhibitory neurotransmission (Wang et al., 1999). GABARAP facilitates the trafficking of $GABA_A$ receptors to the plasma membrane (Leil et al., 2004) and also ER-to-Golgi trafficking of N-cadherin/β-catenin complexes (Nakamura et al., 2008). Another indication that GABARAP could be involved in membrane trafficking events, is that GABARAP was found enriched on the Golgi and to interact with N-ethylmaleimide-sensitive factor (NSF), which is an ATPase that mediates membrane fusion events (Kittler et al., 2001). In addition, GABARAP binds directly to tubulin and this is mediated by the N-terminal region of GABARAP through ionic interactions (Wang and Olsen, 2000). The crystal structure of GABARAP shows that it can oligomerise with itself in a head-to-tail manner and can adopt different conformations (Coyle et al., 2002). The role of GABARAP in

membrane trafficking events is incompletely understood and recent work has been focused more on the role of GABARAP in autophagy.

In addition to the function of GABARAP in phagophore closure and binding cargo receptors, GABARAP also interacts with the ULK complex (Okazaki et al., 2000, Alemu et al., 2012, Kraft et al., 2012). ULK complex members, ULK1, ULK2, Atg13 and FIP200, all have LIR motifs and bind GABARAP preferentially over LC3B (Alemu et al., 2012). The implication of this binding preference is currently unknown. ULK1 with its LIR mutated, formed fewer punctate structures upon starvation than wild-type ULK1. Hence, the presence of LIR motifs in the ULK complex is thought to facilitate the recruitment of ULK to the phagophore. In addition, overexpression of LIR mutant ULK1 causes the accumulation of WIPI2 puncta, compared with wild-type ULK1. This suggests that immature autophagic structures accumulate in the absence of a functional ULK1 LIR. Thus it was hypothesised that the ULK1 complex somehow aids the function of the Atg8s in autophagosome formation. It could also be possible that GABARAP may regulate ULK1 activity through its interaction, although this remains to be demonstrated.

GABARAP may also regulate autophagy, or be regulated, by binding to positive regulators such as MAPK15/ERK8 (Colecchia et al., 2012) and folliculin (FLCN) (Dunlop et al., 2014) or the negative regulator Bcl-2 (Ma et al., 2013). In addition GABARAP can function as a signalling scaffold. The interaction of GABARAP with an E3 ligase complex continuing CUL3, KBTBD6 and KBTBD7 was required for substrate ubiquitination (Genau et al., 2015). GABARAP likely mediates selective cargo recognition for autophagy. For example, the LIR-containing protein ALFY, which interacts with p62 and is involved in aggrephagy, selectively binds GABARAPs (and also LC3C) and this allows the clearance of a subset of p62 structures by autophagy (Lystad et al., 2014). Also, the interaction of GABARAP with the LIR-containing mitochondrial E3 ligase Mulan may be involved in mitophagy (Ambivero et al., 2014). Recently GABARAPs have been implicated in the later stages of autophagosome maturation. Both LC3s and GABARAPs interact directly with PLEKHM1, which forms a complex with the HOPs complex to regulate autophagosome-lysosome fusion (McEwan et al., 2015). Additionally, GABARAPs recruit the PI4 kinase PI4KIIα to autophagosomes from the Golgi region, in order to generate a pool of PI4P which promotes autophagosome-lysosome fusion (Wang et al., 2015).

1.6 Aims

WAC is a positive regulator of autophagosome formation as judged by different readouts in HEK293A and HeLa cells: LC3 lipidation, GFP-LC3 spot formation and p62 degradation. This suggests that WAC affects autophagy at the stage of LC3 attachment to the phagophore or even earlier. However the mechanism of WAC's effect on autophagy is completely unknown. One clue is a proposed interaction of overexpressed WAC with Beclin 1 although this will have to be further investigated. There are two known functions of WAC, one in the nucleus and one centred on the Golgi. As the Golgi may act as a direct membrane source for phagophore formation/expansion and harbours autophagy regulatory proteins, WAC's function at the Golgi is a good candidate for its role in autophagy. On the other hand, nuclear regulation of autophagy has been become more apparent recently, and the communication between the nucleus and cytoplasm certainly has a role in autophagy regulation. I aim to elucidate the mechanism by which WAC promotes autophagosome formation, by conducting an investigation into the novel functions of WAC in the nucleus and cytoplasm, exploring gene regulation and the identification of novel WAC binding partners.

Chapter 2. Materials & Methods

2.1 Cell culture and transfection

2.1.1 Cell culture

Dishes, flasks and multiwell plates for cell culture were procured from Corning, and Dulbecco's Modified Eagle Medium (DMEM) and fetal bovine serum (FBS) from Sigma. The following solutions were produced by Cell Services at the Francis Crick Institute, London: Earle's Balanced Salt Solution (EBSS) (5.56 mM D-glucose, 123.08 mM NaCl, 5.37 mM KCl, 1.82 mM $CaCl_2$, 0.81 mM $MgSO_4$, 0.99 mM Na_2HPO_4, 13.10 mM $NaHCO_3$), Phosphate buffered saline (PBSA) (137 mM NaCl, 3.4 mM KCl, 10 mM Na_2HPO_4, 1.8 mM KH_2PO_4, pH 7.2), trypsin (0.25% trypsin, 137 mM NaCl, 0.7 mM Na_2HPO_4, 5.6 mM D-glucose, 25 mM Tris-HCl pH 7.7, 5.1 mM KCl, 42 µM Phenol Red, 0.25 mM penicillin, 172 µM streptomycin) and versene (0.02% (w/v) EDTA in PBSA).

HEK293A cells were obtained from Cell Services, the Francis Crick Institute. MEFs used were from (McAlpine et al., 2013). RPE-1 cells were from Laurent Sansregret, the Francis Crick Institute. HeLa cells were obtained from Eeva-Liisa Eskelinen University of Helsinki, Helsinki, Finland. HCT116 and U2OS cells were a kind gift from Kevin Ryan, The Beatson Institute, Cancer Research UK, Glasgow. HEK293 Flp-In T-Rex GFP-GABARAP cells were a kind gift from Anne Simonsen, (University of Oslo, Norway). All cell lines in were maintained in DMEM supplemented with 10% FBS and 4.8 mM L-glutamine (full medium) under humidified conditions at 37 ºC in 10% CO_2, unless otherwise specified here. Stably expressing WAC-FLAP HeLa cell line is maintained under 400 µg/mL geneticin (Life Technologies). HEK293 Flp-In T-Rex GFP-GABARAP cells were maintained in full medium + 200 µg/ml Hygromycin B + 5 µg/ml Blasticidin and induced for 24 hr with 1 µg/ml tetracycline in full medium to express GFP-GABARAP after which cells were processed for immunofluorescence (Chapter 2.4.1).

Cells were grown to 80-90% confluency and were passaged by washing once in versene before incubation in trypsin to detach cells. For maintenance, detached cells were split in a 1:10 dilution. Cells were maintained until a passage number of 20, after which they were discarded. Cells were frozen in a mixture of

90% FBS with 10% DMSO. For freezing, trypsinised cells from a confluent T150 flask were centrifuged (1000 rpm, 3 minutes, room temperature) and resuspended in 4 mL of 90% FBS with 10% DMSO mixture. Aliquots of 1 mL were frozen in liquid nitrogen. When thawing, aliquots were resuspended in T75 flasks.

To induce autophagy by starvation, cells were washed 3 times with Earle's balanced salt solution (EBSS) and incubated in EBSS for two hours, unless otherwise stated. 'Basal' or 'fed' cells were maintained in growth medium as above. Where indicated, cells were treated with: 100 nM Bafilomycin A1 (Calbiochem), 100 nM Wortmannin (Calbiochem), 10 µg/ml Brefeldin A (Sigma), 100 nM Torin1 (Cayman Chemical), 50 µM Nocodazole (Sigma), 10 µM MG132 (Calbiochem), 100 nM MitoTracker Red CMXRos (Thermo Fisher), 50 µM 5,6-Dichlorobenzimidazole 1-β-D-ribofuranoside (DRB, Calbiochem) for 4 hours, or 20 ng/ml Leptomycin B (Sigma) for the specified time. To minimise detachment of HEK293A cells, 0.1 mg/mL poly-D-lysine (Sigma) was used to coat the wells of multiwell plates or glass coverslips when cells were cultured in/on these. Poly-D-lysine coating was not required for other cell lines, or for HEK293A cells in dishes or flasks.

2.1.2 Transfection

All siRNA was used at a final concentration of 37.5 nM or at a combined concentration of 37.5 nM when multiple siRNAs were pooled together. However for knockdown of GABARAP for immunofluorescence (see Chapter 2.1.2.4) concentrations were different.

Note that in transfection protocols 'forward' transfection refers to transfection the day after cells have been seeded, whereas 'reverse' transfection refers to a cell suspension that is added to pre-plated transfection complexes.

2.1.2.1 siRNA and plasmid DNA transfection

Lipofectamine 2000 (Life Technologies) was used for plasmid transfections of cells that were plated to be 80% confluent on the day of transfection. For transfection of plasmid DNA; for example for immunoprecipitation studies, 10 cm plates were seeded with 2 X 10^6 cells the day before Lipofectamine 2000

transfection. Cell numbers for smaller dish sizes were scaled according to the ratio of the surface area. The following was the reaction mixture for transfecting a 10 cm dish. Mixes for differently sized dishes were scaled according to surface area ratios. Mix 'A' was formed of 12 µL of Lipofectamine 2000 in 500 µL OptiMem. Mix 'B' is formed of 1 µg of plasmid DNA in 500 µL of Optimem. Mixes A and B were incubated separately at room temperature for 5 minutes before mixing and further incubating for 20 minutes at room temperature. Cells were incubated in the transfection mixture for at least 4 hours after aspirating the full medium they were grown in, adding 4 mL of OptiMem, and adding the 1 mL transfection mixture dropwise on top, (but not longer than 8 hours) before replacing the mix with fresh full medium. Cells were analysed 24 hours after plasmid DNA transfection. Where indicated pcDNA 3.1 (+) was used as an empty vector control.

For siRNA knockdown studies, cells were transfected by a reverse transfection protocol using Lipofectamine 2000, usually in 24-well plates as follows. For one well in a 24-well plate: Mix 'A' was formed of 1.25 µL of Lipofectamine 2000 in 50 µL OptiMem. Mix 'B' is formed of 0.93 µL of siRNA (20 µM stock) in 50 µL of Optimem. Mixes A and B were incubated separately at room temperature for 5 minutes before mixing and further incubating for 20 minutes at room temperature. The combined mix of 100 µL volume was added on to the poly-D-lysine coated well and 400 µL of a single-cell suspension (1.75 X 10^5 cells / mL in full medium or for HeLa cells, 3.5 X 10^5 cells / mL in full medium) was added on top and mixed. This mixture was incubated for 48 hr before changing the medium with fresh full medium and incubation for another 24 hr. Cells were analysed after 78 hr total knockdown. For siRNA transfections in other plates or dishes, the mixes and cell numbers were scaled according to surface area.

2.1.2.2 Generation of HeLa WAC-FLAP stable cell line

HeLa cell line stably expressing WAC-FLAP was established by transient transfection with a BAC (CTD-2309I17) containing the human WAC gene, obtained from Life Technologies. The WAC BAC was modified by homologous recombination to contain a C-terminal FLAP tag (Poser et al., 2008). Please refer to Chapter 4.2.2 for a more detailed explanation of the procedure. Transfection of

HeLa cells was carried out with Effectene (Qiagen) according to the method in (Poser et al., 2008). After transfection cells were selected with Geneticin (Life Technologies) at 800 µg/ml and surviving pools cloned by single-cell FACs sorting into 96-well plates for EGFP expression before being maintained in the presence of Geneticin (Life Technologies) at 400 µg/ml in full medium after colonies had grown.

FACS sorting was performed by Andy Filby at the Francis Crick Institute. Geneticin stable pools of transfected HeLa cells were trypsinised and passed through a cell strainer cap into a 5 mL falcon tube to reduce clogging of the FACS sorter, into full medium containing 1% FBS only. Polystyrene tubes were used for sample intake but polypropylene tubes were used for collection to reduce static effects. Collection medium was full medium supplemented with penicillin and streptomycin. Please refer to Chapter 4.2.2 for more details.

2.1.2.3 Rescue experiments

Knockdown and rescue experiments for Immunofluorescence were performed by transfection with siRNA on day 1 as above. On day 2, the transfection medium was changed for fresh full medium and incubated for around 1 hr before splitting the cells onto poly-D-lysine glass coverslips. The cells were left to adhere and on day 3 they were transfected with siRNA-resistant plasmid DNA. Rescue assay was carried out 24 hr after DNA transfection.

For rescue of autophagy with GFP-WAC and analysis by immunoblot, siRNA reverse transfection with Lipofectamine 2000 was performed on day 1 and on day 3 plasmid siRNA-resistant plasmid DNA transfection was carried out with Lipofectamine 3000 (Life Technologies) according to the manufacturer's instructions.

2.1.2.4 GABARAP knockdown and RNAi for immunoprecipitation studies

For RNAi of GABARAP for immunofluorescence, cells were transfected with siRNA reverse transfection on day 1 and with siRNA forward transfection on day 2 of the procedure with two different siRNA duplexes with a combined concentration of 75 nM. For RNAi studies for immunoprecipitation. Cells were transfected in 10

cm dishes by siRNA reverse transfection on day 1 and by siRNA forward transfection on day 3 of the procedure, using 37.5 nM siRNA each time.

2.1.2.5 siRNA duplexes

siRNA was reconstituted in 1X siRNA buffer (Thermo Scientific) (60 mM KCl, 6 mM HEPES pH 7.5, 0.2 mM $MgCl_2$).

Table 2.1 siRNAs used in this thesis

Target Gene	siRNA	Target sequence	Supplier
(RISC-free control)	D-001220-01	N/A	Dharmacon
ULK1	D-005049-04	UGUAGGUGUUUAAGAAUUG	Dharmacon
WAC	D-013325-02 (for MEFs)	UAAGCACACCUCAAACUAA	Dharmacon
WAC	D-013325-03	GAGACAAACCCGUAUCACA	Dharmacon
WAC	D-013325-04	CGAUCCACGUGUUCAUUAA	Dharmacon
GM130	D-017282-01	GGACAAUGCUGCUACUCUA	Dharmacon
GM130	D-017282-03	GAAUAUCAGCAGAGGAAUA	Dharmacon
RNF40	D-006913-01	GAGAUGCGCCACCUGAUUA	Dharmacon
RNF40	D-006913-02	GAUGCCAACUUUAAGCUAA	Dharmacon
RNF40	D-006913-03	GAUCAAGGCCAACCAGAUU	Dharmacon
RNF40	D-006913-04	CAACGAGUCUCUGCAAGUG	Dharmacon
RNF20	D-007027-01	CCAAUGAAAUCAAGUCUAA	Dharmacon
RNF20	D-007027-02	UAAGGAAACUCCAGAAUAU	Dharmacon
RNF20	D-007027-03	GCAAAUGUCCCAAGUGUAA	Dharmacon
RNF20	D-007027-04	AGAAGAAGCUACAUGAUUU	Dharmacon
GABARAP	D-012368-02	GGUCAGUUCUACUUCUUGA	Dharmacon
GABARAP	D-012368-03	GAAGCGAAUUCAUCUCCGA	Dharmacon
LC3B	D-012846-01		Dharmacon
GABARAPL1	D-014715-02		Dharmacon

Target Gene	siRNA	Target sequence	Supplier
GATE-16	D-006853-03	GUACUUGGUUCCAUCUGAU	Dharmacon

Unless otherwise specified, the siRNAs used for WAC, GM130 and GABARAP were -03, -01 and -02 respectively.

2.2 Microarray and qRT-PCR

2.2.1 Microarray

Whole-genome gene expression analysis was performed by the Genome Centre at Barts and the London School of Medicine and Dentistry, Queen Mary University of London (London, UK) using the Illumina human HT-12 v4 beadchip. All gene expression data will be available through the GEO repository (http://www.ncbi.nlm.nih.gov/geo/) via accession number GSE66475.

HEK293A cells were treated with RISC free, WAC, RNF40 or RNF20 siRNA pools (WAC-03 and 04; RNF40-01 and 02; RNF20-01, 02, 03 and 04) in triplicate and maintained in full medium, as described above. RNA was extracted using the RNeasy kit (Qiagen) and purity was assessed by NanoDrop spectrophotometer.

The RNA was then sent on dry ice to the Genome centre (see above) where RNA integrity was confirmed by Agilent Bioanalyser. At this point I no longer processed the samples. RNA labelling was performed using the Ambion Total Prep Kit (Life Technologies). Briefly, total RNA is converted to double-stranded cDNA by reverse transcription followed by an *in vitro* transcription reaction to create biotin labelled cRNA. The cRNA is then hybridised to the bead array which consists of immobilised beads conjugated to 50-mer gene specific probes. The Bead chip is washed and blocked and streptavidin-Cy3 is added to bind to the biotin labelled cRNA and the chip is visualised and a fluorescence intensities quantified.

The resultant data was analysed by Probir Chakravarty in the bioinformatics and statistics service (Francis Crick Institute). The following is a protocol provided by Probir. Gene expression data was analysed using Bioconductor 2.2 (http://bioconductor.org) running on R2.7.1 (http://www.R-project.org). Normalised probe set expression measures were calculated using log2 transformation and quantile normalization using the Lumi package (Du et al., 2008). All groups

contained three independent samples except for RNF40, which had two independent samples after removal of one replicate for quality control.
To determine significant differences of expression in the three groups: siWAC, siRNF20 and siRNF40 relative to RISC free, a moderated Student's t-test was computed on a gene-by-gene basis using the empirical Bayes statistics in the Limma package (Ritchie et al., 2015). The resultant p-values were adjusted for multiple testing using the False Discovery Rate (FDR) Benjamini and Hochberg method, where any probe sets that exhibited a FDR of less than 0.05 were called differentially expressed. No fold change thresholds were applied.
Differential genes from three comparisons were intersected to identify common genes (Figure 3.8 and Table 7.3). The common genes (319) were further subdivided into two groups: those whose FC difference relative to RISC free were down regulated in all comparisons (183) and those whose FC difference relative to RISC free were up regulated in all comparisons (118). 18 genes were differentially regulated between knockdown of the 3 proteins and subtracted from our analysis. Differentially expressed genes (301) were analysed for enrichment of pathways, biological processes and transcription factor targets using gene sets from Metacore Pathway analysis tool (Thomson Reuters) using a hypergeometric distribution to determine enriched gene set using all genes on the Illumina array as the background. Pathways or processes that showed a FDR of less than 0.05 were called as enriched.

2.2.2 qRT-PCR

HEK293A cells were treated with the indicated siRNA and maintained in full medium. Total RNA was isolated using the RNeasy kit (Qiagen), the RNA was eluted in 30µL RNAase-free water and the RNA concentration was measured using a NanoDrop spectrophotometer (Thermo Scientific). All RNA was stored at -80ºC. cDNA synthesis was performed on 1 µg of RNA per sample with SuperScript II reverse transcriptase and Oligo dT (Life Technologies). qRT-PCR was performed using the Fast SYBR Green Master Mix (Applied Biosystems, 4385612) in a 20 µL reaction (2.5 µL cDNA, 10 µL Fast SYBR Green master mix and 2.4 µL of 2.5 µM forward and reverse primer mix, made to 20 µL with dH_2O). PCR products were detected by the 7500 FAST Real-Time PCR System (Applied Biosystems). The

cycle threshold (CT) values corresponding to target mRNA were normalised to that of GAPDH mRNA.

Table 2.2 qRT-PCR primers used in this thesis

All primers were purchased from Sigma.

Target name	Forward primer (5' - 3')	Reverse primer (5' - 3')
BEX2	AATGTTGTTTTTGACCCAGTTTG	CATCTTTCCATGCAATAGGTAAAAC
C12ORF5	GGAAGAGTGCCCTGTGTTTA	TCCGCTTCTTTCAGGATTAGTT
CARD10	ACTACCCCGAACACTTCACG	GTCATCAAGAATTGGGTCAGG
DENND5B	CCAAAAACCTCCTCGAAATG	TCGTGACCAATCTGAACAGTG
DUSP3	CTTCATTGACCAGGCTTTGG	GGGGAGCGGCTATAACCTT
FAM69A	GGTTTTTGTTGGAAGCTGGAT	CAATAACTCCAGTCTTGTACTTGTCAC
FHL1	GAAGTGTGCTGGATGCAAGA	AGCAGTAGTCGTGCCAGGAT
GABARAP	GCG AGA AGA TCC GAA AGA AA	GAT CAG AAG GCA CCA GGT ATT T
GABARAPL1	TGG GCC AAC TGT ATG AGG A	CTA CCC CCA AGT CCA GGT G
GAPDH	GAC CAC TTT GTC AAG CTC ATT TC	CTC TCT TCC TCT TGT GCT CTT G
GATE-16	CCG TCG TTG TTG TTG TGC T	CTC CAC GCA TCT GTG TTC C
HLA-E	CTGGGATCATGGTAGATGGAAC	GGACACGGAAGTGTGGAAATA
HSPA1A	CCACCATTGAGGAGGTAGATTAG	CAGGAAATTGAGAACTGACAAACA
LC3B	GAG GAT CTT TAG GCC TGA G	TTC TCA CAC AGC CCG TTT AC
LITAF	GGCATGAATCCTCCTTCGTATTA	AGGACAACACATTTGGATAGGG
MBTPS1	GCTACAAGCCACAGGCAAGT	GCCACATGTAGGGACACTCA
NFKB1	CTGGCAGCTCTTCTCAAAGC	TCCAGGTCATAGAGAGGCTCA
p53	TTGCACCTACCTCACAGAGTGCAT	AGAAACTACCAACCCACCGACCAA
RAPGEF5	CCAGTATGCAGAAGAGGATCTG	CGAGGGATTTGGAGATGACTAAG
RCAN3	GTGATCTGCCTACCTCACTTT	TGGTCATCATAGATGGTGAAGAG
RNF20	CAGTTGAAAGCACACTTGGATG	GACTAACCTCATCTCGCTCAATAA
RNF40	AAC AAC GGC AGG CTT GTG AAG ATG	ATC GGA GAA GGG CTT CCA CAG TTT
SAMD9	ATCACACATGGACCAGCTATT	TTACTGGGCTTTCCCATCTTAG
Sestrin-2	ACAAGTGTTGTGGCCTTCCTGAAC	ATGGGTGAATGGCAAGTAGGAGGT
SH3PXD2A	AACCCCTCCAAGCACTACG	TGCTGTACCTCCGGTAGATAGTC
SLC30A7	CAAGATCTCGGGCTGGTTTAG	TCCAGATGCCGTAGAGTAGTT
SYK	ATGTGGGAAGCATTCTCCTATG	CATCCGCTCTCCTTTCTCTAAC
TMEM237	TCCACCTTTACACACCTTCTTC	CACCACGAGATTCACCACAA
UFC1	CAGCGACTGAAGGAGGAATATC	CACCGAGTTCCTTCCTTGTT
VAMP2	CTGCTATGCAATAGTCCCTCTC	GAGTGAGGAGGAAAGAGGAAAG
VAMP3	TGTGGGCAATCGGGATTACTGTT	GAACAGCAGTTTTGAGTTCCGC
WAC	CCTCAAACTAACACAGTCCCTATC	TGACACTGGTCCTTGCTTAAC
ZSWIM5	CACAGCCCAGACTCCTTATC	TTATTCGCTGTAGGTGGCTATC

2.3 Biochemical methods

2.3.1 Antibodies

Table 2.3 Primary antibodies used in this thesis

Antigen	Species	Antibody	Supplier	Dilution	Notes
Actin	Rabbit	ab8227	Abcam	WB 1:1000	
Atg13	Rabbit	STO281	CRUK	WB 1:500	(Chan et al., 2009)
Atg13 pSer318	Rabbit	600-401-C49	Rockland	WB 1:500	Run gel in MOPS
Atg9	Rabbit	STO218	CRUK	WB 1:1000*	Heat samples to 65^{o}C
Atg9	Hamster	14F2		IF 1:1000	(Young et al., 2006) Heat samples to 65^{o}C
Beta COP	Mouse	M3A5, G2279	Sigma	IF 1:500	Saponin method overnight
Beta Tubulin	Rabbit	ab6046	Abcam	IF 1:1000	Methanol method
Beta' COP	Rabbit		F. Wieland	WB 1:1000	
Centrin3	Mouse	ab54531	Abcam	IF 1:500	Methanol method
ERGIC-53	Mouse	ALX-804-602-C100	Enzo Life Sciences	IF 1:100	Triton method Sapnonin method for only juxtanuclear
FLAG	Mouse	M2	Sigma	WB 1:2000	
GABARAP	Sheep	Ab62114	Abcam	IF 1:500	Methanol method, Stained centrosomal GABARAP but not autophagosomal
GABARAP	Rabbit	AP1821a	Abgent	WB 1:250 IF 1:250	Methanol method, Good spots after starvation
Gamma-tubulin	Mouse	GTU-88, T6557	Sigma	IF 1:5000	Methanol method
GFP	Mouse	11814460001	Roche	WB 1:1000	Only antibody that detects WAC-FLAP in lysate as low levels
GFP	Mouse	3E1	CRUK	WB 1:4000-1:20,000 IF 1:250-1:1000	Saponin method for WAC-FLAP on Golgi
GFP	Rabbit	sc-8334	Santa Cruz	WB 1:100	

Antigen	Species	Antibody	Supplier	Dilution	Notes
GM130	Mouse	610822	BD	IF 1:250 WB 1:200	Methanol or saponin method
GM130	Rabbit	ab52649	Abcam	WB 1:1000	Monoclonal
H2B	Mouse	ab52484	Abcam	WB 1µg/ml final	
HA	Mouse	HA.11	Covance	WB 1:1000	
HA	Rat	3F10, 11867423001	Roche	IF 1:1000	Methanol method
HA	Rabbit	PRB-101P	Covance	WB 1:1000	
Lamin B	Mouse	LN43	CRUK	WB 1:500	
LC3B	Rabbit	ab48394	Abcam	IF 1:2000 WB 1:1000	Methanol method
Myc	Mouse	9E10	CRUK	WB 1:500 IF: 1:200	Methanol method
p230/ GOLGA4	Mouse	611280	BD	IF 1:500	Saponin method
p53	Mouse	SC-126	Santa Cruz	WB 1:1000	
p62	Mouse	H00008878-M01	Abnova	WB 1:250	Incubate overnight Detects murine p62
p62	Mouse	610832	BD	WB 1:500	Incubate overnight
p62 C-terminus	Guinea Pig	GP62-C	Progen	IF 1:300	Methanol method
RNF40	Rabbit	A300-718A	Bethyl Labs	WB 1:500	
S6	Rabbit	2217	Cell signalling	WB 1:1000	Monoclonal
S6 pSer240/244	Rabbit	2215	Cell Signalling	WB 1:4000	Dilute according to datasheet instructions
SOD1	Rabbit	Ab16831	Abcam	WB 1:2000	Overnight incubation
TGN46	Sheep	AHP500G	Serotec	IF 1:500	Methanol or saponin methods
Ubiquitin	Mouse	FK2 D058-3	MBL	IF 1:500	Methanol method
Ubiquityl-Histone H2B	Mouse	Clone 56	Millipore	WB 1:4000	
ULK1	Rabbit	sc-33182	Santa Cruz	WB 1:250	Incubate overnight
ULK1 pSer757	Rabbit	6888	Cell signalling	WB 1:1000	Dilute according to datasheet instructions, TBS not PBS
VAMP3	Rabbit	V31 & V32	Andrew Peden	WB 1:200	

Antigen	Species	Antibody	Supplier	Dilution	Notes
WAC	Rabbit		Hisao Kondo	WB 1:1000* IF 1:500	(Totsukawa et al., 2011) Saponin method, detects nuclear and Golgi WAC
WAC	Rabbit	STO296	CRUK Tooze Lab	WB 1:1000* IF 1:3000	Affinity purified at 1.8 mg/ml, triton method detects nuclear WAC
WIPI2	Rabbit	STO280	CRUK	IF 1:250* WB 1:250	(Polson et al., 2010) Use whole serum for western blot
WIPI2	Mouse	2A2	Dundee Cell Products	IF 1:4000 WB 1:1000	

*, affinity purified antibody

Table 2.4 Secondary antibodies used in this thesis

Antigen	Conjugated to	Supplier	Dilution
Rabbit IgG TrueBlot	HRP	Rockland	WB 1:2000
Rabbit IgG	HRP	GE Healthcare	WB 1:4000
Mouse IgG	HRP	GE Healthcare	WB 1:4000
Hamster IgG	HRP	GE Healthcare	WB 1:4000
Rabbit IgG	Alexa Fluor 488	Life Technologies	IF 1:1000
Rabbit IgG	Alexa Fluor 555	Life Technologies	IF 1:1000
Rabbit IgG	Alexa Fluor 647	Life Technologies	IF 1:1000
Mouse IgG	Alexa Fluor 350	Life Technologies	IF 1:1000
Mouse IgG	Alexa Fluor 488	Life Technologies	IF 1:1000
Mouse IgG	Alexa Fluor 555	Life Technologies	IF 1:1000
Mouse IgG	Alexa Fluor 647	Life Technologies	IF 1:1000
Guinea pig IgG	Alexa Fluor 555	Life Technologies	IF 1:1000
Guinea pig IgG	FITC	Santa Cruz	IF 1:1000
Rat IgG	Alexa Fluor 488	Life Technologies	IF 1:1000
Rat IgG	Alexa Fluor 633	Life Technologies	IF 1:1000
Sheep IgG	Alexa Fluor 488	Life Technologies	IF 1:1000

Antigen	Conjugated to	Supplier	Dilution
Sheep IgG	Alexa Fluor 647	Life Technologies	IF 1:1000
Hamster	Cy3	Jackson ImmunoResearch	IF 1:1000

2.3.2 Cell lysis for western blot

For cell lysis before immunoprecipitation see Chapter 2.3.6. For analysis of knockdown, expression, or autophagic readouts such as LC3 lipidation, cells were washed 3 x PBSA, liquid aspirated and then cells lysed in ice cold TNTE buffer (20 mM Tris, pH 7.4, 150 mM NaCl, 0.5% w/v Triton X-100, 5 mM EDTA) containing 1 X EDTA-free Complete Protease Inhibitor cocktail (Roche) and 1x PhosSTOP (Roche) on ice. Cells that were incubated in EBSS prior to lysis were not washed in PBSA before lysis, to reduce detachment (HEK293A cells only). 80 µL of lysis buffer was used for a single well of a 24-well plate, and volumes were adjusted for other sized plates or dishes based on the ratio of their surface areas. Cells were washed multiple times with the lysis buffer by pipetting up and down whilst scraping with the pipette tip. The lysis buffer from each well was then transferred to a clean 1.5 mL Eppendorf tube and centrifuged at maximum speed (13,200 rpm) for 15 minutes to pellet the nuclei. The clarified lysate was transferred to clean 1.5 mL Eppendorf tubes and 5X SDS sample buffer (15% SDS (w/v), 213.5 mM Tris-HCl pH 6.8, 50% glycerol (w/v), 16% β-mercaptoethanol, bromophenol blue) was added to a final concentration of 1X. Samples were heated at 100 ºC for 10 minutes (or 65^{o}C for detection of Atg9) before loading onto SDS-PAGE gels for electrophoresis and protein transfer (see below).

For investigating histone modifications, 5X SDS sample buffer was added to 1X to the insoluble pellet, which was then subjected to sonication and benzonase nuclease treatment (100U/ml added to sample in SDS sample buffer for 5 minutes at room temperature) to solubilise the sample, followed by boiling as above.

2.3.3 SDS-PAGE and protein transfer

SDS-PAGE was carried out with precast NuPAGE 4-12% Bis-Tris mini or midi protein gels from Life Technologies. SDS-PAGE Gels were electrophoresed at 200 V in MOPS (Life technologies, 20 X stock: 50 mM MOPS, 50 mM Tris Base, 0.1% SDS, 1 mM EDTA, pH 7.7) or MES (Life technologies, 20 X stock: 50 mM MES, 50 mM Tris Base, 0.1% SDS, 1 mM EDTA, pH 7.3) until the blue dye front reached the bottom of the gel (the time taken was approximately 50 minutes). MOPs was generally used for the running buffer, however for the analysis of LC3 lipidation, or for analysis of Atg13 phosphorylation at Ser318, samples were run in MES buffer. This is to improve the separation of the LC3-I and –II forms and to improve the separation of p-Atg13 Ser318 from a non-specific band.

Proteins were transferred to PDVF (polyvinylidene fluoride) membrane (Millipore) using wet transfer (GENIE® electrophoretic transfer, Idea Scientific Company). PDVF membrane was soaked in methanol before washing in transfer buffer (0.2% methanol, 150 mM glycine, 20 mM tris base). Thick blot paper (Sigma), transfer sponges and SDS-PAGE gels were also soaked in transfer buffer, prior to assembly of the transfer unit. Proteins were transferred at 27 V for 1 hour 30 min. Protein transfer to the PVDF membrane was visualised and assessed using Ponceau S stain (Sigma). The PVDF membrane was incubated in Ponceau S stain for ≥ 10 minutes with rocking at room temperature. Surplus dye was removed by repeated washes with water. The Ponceau S stained membrane was scanned and either dried by washes into Methanol and air drying for processing later, or processed for continuation of the Western blot protocol as below.

2.3.4 Western blotting and detection

If dried, PDVF membranes were soaked in methanol followed by washing in PBSA. The following incubation times are all at room temperature with rocking (unless otherwise declared). PVDF membranes were incubated in 5% powdered milk (w/v) (Marvel) in PBSA for 30 min, for blocking. Following blocking, membranes were incubated for 1-2 hours in primary antibodies diluted (as indicated in Table 2.3) in 5% milk (w/v) in PBSA for polyclonal antibodies or diluted in PBSA for monoclonal antibodies, unless otherwise specified in Table 2.3. Where

noted that an antibody was used overnight, this incubation was at 4 ºC. For western blotting of co-immunoprecipitated GM130 after immunoprecipitating WAC for example, GM130 primary antibody was diluted with SignalBoost Immunoreaction Enhancer Kit (Merck Millipore, 407207) and blots were developed with Luminata Crescendo Western HRP substrate (Merck Millipore). This technique was used to amplify weak signals in general. After incubation in primary antibody, the membrane was washed 5 times quickly in 0.05% Tween 20 in PBSA (PBST), followed by 3 x 5 minute washes in PBST. Membranes were then incubated in HRP-conjugated secondary antibodies (see Table 2.4) for 1-2 hours in 5% milk (w/v) in PBSA before washing in PBST as before, but with an additional 5 minute wash. Following washing, membranes were transferred to a clean glass plate and covered in ECL (Amersham, GE healthcare) for 1 min before exposing to film (Amersham Hyperfilm ECL, GE healthcare). For difficult to detect signals, membranes were covered with Luminata Crescendo Western HRP substrate (Merck Millipore) for between 2-5 minutes. Exposure times varied between western blots.

For re-probing the same membrane, membranes were incubated in Restore™ Plus Western Blot Stripping Buffer (Thermo Scientific) for 15 minutes. Membranes were subsequently washed in PBSA 7 times quickly and three times for 5 minutes before blocking in 5% milk (w/v) in PBSA for 30 minutes and then continuing with primary and secondary antibody incubations and washes as above.

To reduce cross reactivity of secondary antibodies with denatured immunoglobulin chains in immunoprecipitation experiments, TrueBlot® from Rockland was used as a secondary antibody at 1:2000, to detect native conformations of immunoglobulins only. This was used when proteins of interest ran close to the immunoglobulin heavy chain. TrueBlot antibodies cross-react with protein G and A, and to counter this, when proteins ran close to protein G the TrueBlot secondary was diluted in EasyBlocker (GeneTex) following the manufacturer's instructions.

2.3.5 Crude subcellular fractionation

9 x 10^6 HEK293A cells were plated in a 15cm dish per sample the day prior to the extraction for assessing endogenous proteins. For overexpressed proteins 1.5 x 10^6 cells were plated in a 10cm dish per sample for DNA transfection the next day and extraction 24 hours following transfection (see Chapter 2.1.2). On the day of extraction, for 10cm dishes (scaled accordingly for surface area in different sized dishes) cells were washed 1 x with 5 mL HB buffer (20 mM HEPES-KOH pH 7.5, 10 mM KCl, 2.5 mM MgOAc, 1mM EDTA) and then scraped into 10 mL HB buffer. Cell suspensions were pelleted by centrifugation at 1,000 rpm for 5 min at 4^{o}C in 15 mL falcon tubes. The supernatant was discarded and the cell pellet was resuspended in 500 µL HB2 buffer (20 mM HEPES-KOH pH 7.5, 10 mM KCl, 2.5 mM MgOAc, 1mM EDTA, 250 mM sucrose, 1mM DTT, 1 X PhosSTOP (Roche) and 1 X complete protease inhibitors (Roche)). Cell suspension was left for 20 minutes on ice with occasional gentle mixing and then cells were homogenised by passing through a 27 gauge ½ inch needle (Becton, Dickinson and Company) 12-14 times using a 1 mL syringe. Cell breakage was monitored with a light microscope and Trypan Blue staining. The nuclear pellet and intact whole cells were pelleted by centrifugation at 5,000 rpm for 5 minutes at 4^{o}C in a microfuge. The post-nuclear supernatant (PNS1) was taken and pellet kept aside. The centrifugation was repeated with PNS1 to yield PNS2. The pellet after this spin was discarded. A sample of PNS2 was set aside for analysis and the remainder was taken for a second spin in a 1.5 mL Beckman Coulter ultracentrifuge tube at 112,500 x g for 1 hour at 4^{o}C in a benchtop ultracentrifuge. The resultant supernatant produces the true cytosol and the crude membrane fraction is contained in the pellet fraction. 5 X SDS sample buffer (15% SDS (w/v), 213.5 mM Tris-HCl pH 6.8, 50% glycerol (w/v), 16% β-mercaptoethanol, bromophenol blue) was added to the membrane pellet at a final of 2 X in 50 µL volume, to produce a 10 X concentrated membrane sample relative to the cytosol and nuclear fractions. 5 X SDS sample buffer was added to 1 X to the cytosolic fraction. To solubilise the nuclear pellet, 500 µL of 1 X SDS sample buffer was added to the pellet and the pellet was passed through a needle and syringe followed by sonication and benzonase nuclease treatment to digest the DNA (100U/ml benzonase added to sample in SDS sample buffer for 5 minutes at room temperature). The samples

were heated to 65^{o}C for 10 mins to denature proteins and processed by Western blotting as above.

2.3.6 Immunoprecipitation

For immunoprecipitation of endogenous proteins, 4 x 10^6 cells were seeded in 10 cm dishes for immunoprecipitation the next day and for immunoprecipitation of overexpressed proteins, cells were transfected as described in Chapter 2.1.2.1 prior to immunoprecipitation the next day. For extraction, cells were washed twice in PBSA (unless cells were staved in EBSS) and then lysed in 1mL ice cold TNTE buffer (20 mM Tris, pH 7.4, 150 mM NaCl, 0.5% w/v Triton X-100, 5 mM EDTA) containing 1 X EDTA-free Complete Protease Inhibitor cocktail (Roche) and 1x PhosSTOP (Roche) on ice. Once lysed, cells were centrifuged at 13,200 rpm for 10 minutes at 4ºC to pellet insoluble material.

For each immunoprecipitation, 60 µL of a 50% slurry of protein G sepharose beads (Sigma) was washed four times in 1 mL of PBSA in a 1.5 mL Eppendorf tube with pelleting by centrifugation, aspirated and resuspended in PBSA to restore a 50% slurry. The clarified lysate was incubated with 30 µL of the washed beads with rotation at 4^{o}C for 1 hour to pre-clear the lysate. After pre-clear 40 µL of pre-cleared lysate was taken for the 'input' lysate sample. The remaining 30 µL of beads were subsequently resuspended in 700 µL of PBSA with 0.1% Triton X-100 and incubated with 5 µg of the relevant antibody for 45 minutes with rotation at 4^{o}C, followed by washing twice in 1 mL of PBS before the pre-cleared clarified cell lysate was added. Immunoprecipitation mixes were rotated for 1 hr 30 min at 4 ºC and were subsequently washed three times in 1 mL of TNTE buffer without PhosSTOP (Roche). After removal of the final wash, beads were resuspended and boiled in 30 µL of 2 X SDS sample buffer before analysis by western blot.

For GFP-Trap (ChromoTek) immunoprecipitation, 5 µL of GFP-Trap beads were washed 2 x PBSA with 0.1% Triton X-100. Cells were lysed as for protein G immunoprecipitations above. Cleared lysates were pre-cleared with rotation at 4^{o}C for 1 hour with 5 µL blocked agarose beads (ChromoTek). Blocked agarose beads were washed as per GFP-Trap beads prior to the addition of clarified lysate for pre-clear. After pre-clear 40 µL of pre-cleared lysate was taken for the 'input' lysate

sample. The remaining lysate was added to the 5 µL of GFP-Trap beads, which were used for each immunoprecipitation. GFP-tagged proteins were immunoprecipitated 1 hr 30 min by rotating at 4 ºC.

For the immunoprecipitation of FLAG-tagged proteins, 20 µL agarose slurry of FLAG M2 Affinity Gel (Sigma) was used for each immunoprecipitation. The slurry was washed the same way as the GFP-Trap beads before adding the FLAG-tagged clarified cell lysates (with no pre-clear) and rotating at 4 ºC for one hour 30 minutes. GFP-Trap and FLAG M2 immunoprecipitations were all washed three times in TNTE lysis buffer without PhosSTOP (Roche) before adding 30 µL of 2 X SDS buffer and boiling at 100ºC for 10 minutes.

2.3.7 Immunoprecipitation from mixed lysates

This method refers to Figure 4.11b. I found that the expression levels of tagged proteins could be very variable, after co-transfection of multiple plasmids. Therefore, in experiments involving co-immunoprecipitation of overexpressed proteins, proteins were expressed in separate 10 cm dishes before mixing cell lysates to try and even out protein levels. Briefly, cells were lysed as detailed for immunoprecipitations (Chapter 2.3.6) and clarified lysate was obtained. HA-GM130 pieces were expressed in separate dishes to GFP-WAC full length or GFP-WAC ΔCC Figure 4.11b. Each dish was lysed in 500 µL TNTE buffer. After clearing the lysates, ~500 µL of lysate containing GFP-WAC was mixed with ~500 µL of lysate containing HA-GM130 pieces. The clarified lysates were then used for pre-clearing and 40 µL of 'input' sample was taken after pre-clear. Pre-cleared cell lysates were then used for immunoprecipitation.

2.3.8 Normalising variable levels of overexpressed proteins for immunoprecipitation

Some constructs expressed at variable levels to others, making experimental interpretation difficult. For example, EGFP expresses much more readily then EGFP-WAC, even though they are both from the same base vector pEGFP C2. In these instances one of two methods was used. This was done on an

empirical basis after a working knowledge of the relative expression levels of different constructs was gained. During the transfection procedure, the amount of plasmid transfected would be reduced or increased relative to the others. However all samples would be transfected with the same total amount of DNA, with the remaining portion made up of empty vector DNA (pcDNA 3.1 (+)). In other cases the DNA ratios were not altered. Instead, after immunoprecipitation a small sample of the immunoprecipitation would be assessed by SDS-PAGE to judge the relative levels of the immunoprecipitated overexpressed proteins. Then a second final gel would be ran with different amounts of each sample to normalise for the amount of immunoprecipitated protein. The inputs were not altered in this procedure and a background binding control is always included, enabling interpretation of the experiment.

2.3.9 Mass spectrometry to identify novel WAC interactors

HEK293A or HeLa WAC-FLAP cells, maintained in full medium, were washed 3 times in PBSA and lysed in TNTE buffer (20 mM Tris-HCl pH 7.4, 150 mM NaCl, 5 mM EDTA, 0.5 % Triton X-100, 1x Complete protease inhibitor (Roche), 1x PhosSTOP (Roche)) and the lysate clarified by centrifugation (16,100 x g, 15 min). Lysates from HeLa WAC-FLAP cells were incubated with GFP-TRAP® beads at 4^{o}C for 2 hr. Lysates from HEK293A cells were incubated with Rabbit anti-WAC (5 µg) bound to protein G sepharose (Sigma) at 4^{o}C for 2 hr. Pelleted beads were washed 3 times with TNTE buffer and eluted with 2x SDS sample buffer at 100^{o}C for 10 min. Care was taken to use fresh tips, tubes and sample buffer and to regularly change gloves and wear a clean lab coat, to prevent contamination of the immunoprecipitation samples.

Eluted proteins were separated by SDS-PAGE. SDS-PAGE was performed using a clean gel tank (under a laminar-flow hood) and sterile MOPS running buffer made up in Milli-Q deionised water. The SDS-PAGE gel was run as usual, until the dye front exited the gel, and the gel was stained using GelCode Blue Stain Reagent (Thermo Scientific), a colloidal Coomassie based dye. 8 bands covering the entire lane were excised for each sample lane. Each of the 8 bands was cut into ~1mm^3 pieces and placed into a 96-well plate with 100 µL HPLC-grade water, before being sent to the proteomics facility at the Francis Crick Institute.

The following is a protocol provided by the Proteomics facility at the Francis Crick Institute, for processing samples by mass spectrometry. This work was performed by Bram Snijders and David Frith. In-gel trypsin digestion was performed using a Perkin Elmer Janus liquid handling system. Lyophilized peptide samples were dissolved in 15 µL of 0.1 % Trifluoroacetic acid (TFA) and subjected to LC-MS analysis using a LTQ-Orbitrap instrument for data acquisition. Raw spectra were processed using the MaxQuant/Andromeda bioinformatics suite (Cox and Mann, 2008) and further analyzed in Perseus software. Data was searched against a UniProt fasta database containing human sequences and intensity based absolute quantification (iBAQ) (Schwanhausser et al., 2011) was used for label free quantification. WAC, WAC-FLAP and control IPs (beads and lysate) were analyzed to screen for novel WAC interactors and filtered as follows. Only proteins that received iBAQ values in both experiments and not in the control IPs were considered candidates. The original dataset contained 1536 protein identifications and using the filter criteria the list was reduced to 20 candidates that were enriched in the WAC & WAC-FLAP pull-downs vs control conditions.

2.3.10 Recombinant protein expression, purification and *in vitro* binding

Human GST-WAC fusion proteins were cloned into pGEX-4T-2 and expressed in *E. coli* BL21-CodonPlus(DE3)-RIL (Agilent) cells in LB medium. Human GST-GABARAP pGEX-5X-1 was a gift from Zvulun Elazar (Weizmann Institute of Science, Israel). Expression was induced by addition of 1 mM IPTG at OD_{600} = 0.6 and cells were incubated at 37°C for 4 hr. For analytical purposes, cells were pelleted and lysed directly in 5X SDS sample buffer (15% SDS (w/v), 213.5 mM Tris-HCl pH 6.8, 50% glycerol (w/v), 16% β-mercaptoethanol, bromophenol blue) diluted to 1X, by sonication followed by boiling at 100^{o}C for 10 minutes. Alternatively, harvested cells were lysed using sonication on ice in a lysis buffer (PBSA + 1 % Triton X-100, supplemented with 1 x Complete protease inhibitor (Roche)) and the clarified supernatant after centrifugation was subsequently applied to Glutathione Sepharose 4B beads (GE Healthcare). The pellet after sonication was sometimes kept to analyse protein solubility. The beads were incubated with the lysate for 1 hour at 4^{o}C with rotation. After 5 washes with (PBSA

+ 1 % Triton X-100 + 500 mM NaCl supplemented with 1 x Complete protease inhibitor (Roche)), fusion protein-bound beads were used directly in GST pulldown assays or GST proteins were eluted and concentrations measured as described below.

Purified untagged human GABARAP was a gift from Stephane Mouilleron, Francis Crick Institute, London, UK. GST-GABARAP purification was performed by Harold Jefferies, Tooze Lab, Francis Crick Institute.

Strep-Tag II-GM130 (Rat) was cloned into pcDNA 3.1(+) and co-expressed in HEK293A cells with the Ebola virus protein HA-VP35 to boost protein expression (Gantke et al., 2013). Cells were lysed in TNTE buffer (20 mM Tris-HCl pH 7.4, 150 mM NaCl, 5 mM EDTA, 0.5 % Triton X-100, 1x Complete protease inhibitor (Roche), 1x PhosSTOP (Roche)). After clarification of lysates, lysates were incubated with magnetic Strep-Tactin beads (Qiagen) for 1 hr before 5x washes in stringent conditions (20 mM Tris-HCl pH 7.4, 1 M NaCl, 5 mM EDTA, 1 % Triton X-100, 1x Complete protease inhibitor (Roche), 1x PhosSTOP (Roche)). Beads were incubated with elution buffer (TNTE + 10mM Biotin) for 15 mins on ice to elute Strep-Tag II-GM130. Purity of eluted protein was assessed by SDS-PAGE and colloidal coomassie staining. The yield of purified Strep-Tag II-GM130 was low and not directly measured, instead amounts were added by volume rather than µg for binding experiments.

For *in vitro* binding, soluble Strep-Tag II-GM130 was incubated with immobilized GST (20 µg), GST-GABARAP (20 µg), GST-WAC or GST-WAC ΔCC on glutathione beads for 2 hr at 4^{o}C in TNTE buffer (GST-WAC) or 1.5 hr at 4^{o}C in TNTE buffer supplemented with 10% (v/v) glycerol and 0.1% (w/v) BSA (GST and GST-GABARAP). Beads were then washed 3 x with TNTE before SDS-PAGE and western blotting.

2.3.11 Measuring GST fusion protein concentration

To measure the protein amounts (for GST and GST-GABARAP, performed by Harold Jefferies), GST-proteins were eluted off glutathione beads using elution buffer (10 mM reduced glutathione, 50 mM Tris-HCl pH 8, 0.1% Triton X-100, 150 mM NaCl) at 4^{o}C, by gravity flow of beads packed in a column. The eluate was

then dialysed overnight into PBSA using Slide-A-Lyzer™ dialysis cassettes (Thermo Fisher). The dialysed eluted GST protein was measured using Bio-Rad protein assay dye solution (Bio-Rad). Serial dilutions of an IgG standard (Bio-rad) in same buffer as sample were made up to 800 µL with dH_2O and added to 200 µL of dye solution for the production of a standard curve. The protein content of samples was determined by making up small volume of the sample to 800 µL with dH_2O, as for the standard IgG, and adding 200 µL of dye solution. Both the protein sample mixes and the standard mixes were vortexed and incubated at room temperature for 15-60 minutes before measuring the absorbance at 595 nm using a spectrometer.

2.4 Imaging methods

2.4.1 Immunofluorescence labeling and confocal and epifluorescence microscopy

8 X 10^4 cells were plated onto glass coverslips (The Francis Crick Institute) in 12-well plates (these were coated in poly-D-lysine for HEK293A cells) for immunofluorescence (IF), the day before fixation. If cells were plated onto coverslips for DNA transfection the next day, 1 X 10^5 cells were used because of Lipofectamine 2000 toxicity. All subsequent steps and solutions are at room temperature, unless otherwise stated. Cells were fixed in 3% paraformaldehyde (Agar Scientific) in PBS supplemented with 0.01 mM $MgCl_2$ and 0.01 mM $CaCl_2$ for 20 minutes. Typically, cells were then washed twice in PBSA before permeabilisation with either 0.1 % saponin in PBS for 20 min (WAC & βCOP), 0.2 % Triton X-100 in PBS for 3 min (ERGIC-53) or room temperature methanol for 5 min (WIPI2 & GABARAP & other antibodies, see Table 2.3). Coverslips were then washed twice in PBSA and blocked for 20 minutes in 5 % BSA fraction V in PBS (Roche) after methanol permeabilisation, with 0.2 % gelatin in PBS after Triton X-100 permeabilisation or with 0.1 % saponin + 1 % BSA + 0.2 % gelatin in PBS for 20 min after saponin permeabilisation. Coverslips were incubated with primary antibody diluted as indicated in Table 2.3, in 1 % BSA in PBS or 0.2 % gelatin in PBS for 1 hr at room temperature. For WAC and βCOP staining, coverslips were incubated with primary antibody + 0.1 % saponin, 1 % BSA and 0.2 % gelatin in

PBS overnight at 4^{o}C. Coverslips were inverted onto 100 µL drops of primary antibody mix and incubated in a humidified chamber for 1 hour. Coverslips were washed once in the same solution as the primary antibody was diluted in and incubated with secondary antibody diluted (see Table 2.4) in the same buffer as primary for between 30 minutes to 1 hour. If used, Hoechst (Sigma) was added to the diluted secondary antibody solution at 5 µg/ml final concentration. Finally, coverslips were washed twice with PBSA and once with water. Coverslips were then mounted onto glass microscope slides (Thermo Scientific) with 10 µL of Mowiol 4-88 (CalBiochem). LC3 and WIPI2 puncta formation and centrosomal GABARAP intensity was quantified by Imaris image analysis software (Chapter 2.6.1).

Confocal images were taken with a Zeiss LSM510 laser-scanning microscope with a 63X, 1.4 NA, oil-immersion objective (Carl Zeiss MicroImaging, Inc). Epifluorescence images were taken on a Nikon epifluorescence microscope (Nikon Eclipse E1000), using either a 60X or 100X oil-immersion objective both 1.4 NA. Separate fluorescence channels on the epifluorescence microscope are displayed as grayscale images. To obtain colour images, the separate channels were false-coloured in Adobe Photoshop and superimposed on each other to create a merge channel. Confocal images were taken with a slice thickness of 1 µm (normally for spot counting) or 2 µm (Atg9 staining). Laser settings were kept constant for imaging each condition of an experiment for comparison (e.g. spot counting, centrosomal signal intensity). Images were processed using Zeiss LSM 510 software V4.2 and to obtain scale bars and to perform line scans.

2.4.2 Live cell imaging and photoconversion

Live cell imaging was performed on HEK293A cells transiently expressing EosFP-GABARAP. Alternatively, cells were treated with WAC siRNA for 48 hr prior to transfection with EosFP-GABARAP and imaging 24 hr later. Cells were plated onto poly-D-lysine coated glass bottom gridded 35 mm MatTek dishes. 1.7 x 10^5 cells were plated the day prior to an imaging experiment. Cells were washed 3 times into EBSS and maintained at 37^{o}C with 10% CO_2 during imaging with a Nikon Eclipse Ti microscope swept field confocal system. The imaging chamber

was brought to temperature overnight before each experiment. Photoconversion was performed with pulses of 405 nm light. Images were processed, and data analyzed, using the Fiji distribution of ImageJ. Where indicated, cells were pretreated with 50 μM Nocodazole (Sigma) in full medium for 2 hr before incubation with EBSS + 50 μM Nocodazole followed by imaging. During each experiment day the photoactivation laser would be tested on a few cells expressing EosFP-GABARAP as I found the same laser setting couldn't be used between sessions. This was to ensure I was able to photoconvert only a small area of choice, but also to have enough laser power to get a strong red signal after photoconversion. When I found a cell of choice to film (usually exhibiting an enlarged ring-like GABARAP structure), the position on the glass bottom grid was noted, the medium was changed into EBSS with washing 3 times with EBSS. This required me to remove the dish. The cell was located again and image acquisition was commenced. After a few seconds to minutes, photoactivation was performed. Usually 5-12 minutes had passed from the beginning of starvation to the moment of photoactivation.

After time-lapse microscopy (usually 25 minutes filming), cells were immediately fixed in 3% paraformaldehyde and processed for confocal microscopy as detailed in Chapter 2.4.1. Photoconverted cells were located using gridded MatTek dishes. During 4-colour imaging (Figure 5.18c), 405 nm illumination was carried out only after acquisition of the other fluorophore signals, in order to prevent artefactual photoconversion. Note: caution must be taken as even fixed samples can be photoconverted (data not shown).

2.5 Molecular biology methods

2.5.1 PCR

Polymerase chain reaction (PCR) was typically performed using the KOD hot start DNA polymerase kit (Novagen).

PCR mix:

10X Buffer for KOD Hot Start DNA Polymerase - 5 µL

10X PCR_x enhancer solution (Life Technologies, not included in kit) - 5 µL

25 mM $MgSO_4$ - 3 µL

dNTPs (2 mM each) - 5 µL

Forward primer (10 µM from Sigma) - 1.5 µL

Reverse primer (10 µM from Sigma) - 1.5 µL

Template plasmid - 10 ng

KOD Hot Start Polymerase 1 µL

dH_2O to 50 µL

PCR cycle:

Segment	**Cycles**	**Temperature (ºC)**	**Time**
1	1	95	2 min
2	30	95	20 sec
		55	10 sec
		70	25 s/kb
3	1	4	∞

A small amount of the complete PCR reaction was assayed by DNA agarose gel electrophoresis (Chapter 2.5.2). PCR products were purified using the QIAquick PCR purification Kit (Qiagen) (spin column purification) according to the manufacturer's instructions, if a single PCR product was yielded. PCR products were purified by DNA agarose gel electrophoresis (Chapter 2.3.2) using the QIAquick Gel Extraction Kit if there were multiple PCR products produced in the reaction, according to the manufacturer's instructions. When spin column purifying, PCR products were eluted in 30 µL elution buffer (Qiagen).

When performing the PCR SOEing (splicing by overlap extension) method (Ho et al., 1989). The product of the two separate PCR reactions were mixed in equimolar ratios and used as both the template and primer for a second PCR reaction to generate a single PCR product containing both original sequences fused together. This was enabled by designing PCR primers/products with overhangs homologous to one another. Please see Chapter 4.4.3 for a further explanation.

2.5.2 DNA agarose gel electrophoresis

Usually 0.8% agarose (w/v) (Invitrogen) was dissolved in 1 X Tris-borate-EDTA (TBE) buffer (Cell services, The Francis Crick Institute) by heating using a microwave. For analysis of smaller DNA fragments (<500 bp) 2% agarose (w/v) gels were used. One drop of 0.625 mg/mL ethidium bromide (Amresco) was added per 50-100 mL of molten agarose and the mixture was poured into a mould with well comb to set. DNA was added to 5X DNA loading buffer (Qiagen) to a final of 1 X, mixed, and loaded into wells. HyperLadder^{TM}1kb (Bioline) was used as a size ladder marker. For smaller DNA fragments <500 kb HyperLadder^{TM} 100bp marker (Bioline) was used as a size ladder. DNA bands were imaged using a UV irradiator (GeneFlash, SynGene BioImaging). If required, DNA bands were excised quickly using a clean scalpel, while visualised using a UV lamp, and purified using QIAquick Gel Extraction Kit (Qiagen) according to the manufacturer's instructions. DNA was eluted from the column using 30 µL elution buffer (Qiagen) and incubating at room temperature for 4 minutes before eluting.

2.5.3 DNA digestion with restriction enzymes

Plasmid DNA and PCR products were digested using the required restriction enzymes from New England Biolabs (NEB) according to the manufacturer's instructions.

Generally, the following mix was used in a 1.5 mL Eppendorf:
DNA (µg as required)
10X NEB buffer (1 µL)
BSA 100 µg/ml final (if required)
Restriction enzyme (0.5 µL)
Nuclease-free water to 50 µL

Restriction digest reactions were incubated for at least 30 minutes at 37^{o}C in a water bath. If double digestions were required, the best compromise was

chosen in terms of NEBuffer. Double digestions were used to prevent re-ligation of the cut empty vector during DNA ligation.

2.5.4 Ligation

DNA fragments were ligated using T4 DNA Ligase (NEB) according to the manufacturer's instructions.

Ligation mix:

10X T4 DNA Ligase Buffer 1 µL
Vector DNA 10 ng
Insert DNA 60 ng
T4 DNA Ligase 1 µL
Nuclease-free water to 10 µL

Ligations were incubated at 16 ºC overnight in a 1.5mL Eppendorf in a water bath. A vector to insert ratio of 1:6 is shown above. 10ng of vector was used per ligation reaction, with the amount (ng) of insert determined by the formula: 6(insert length bp/vector length bp) x ng of vector. If ligations were unsuccessful a higher insert-to-vector ratio was tried.

2.5.5 In-Fusion cloning

Alternatively to 'cut and paste' cloning above. Cloning was performed using the In-Fusion® HD Cloning Kit (Clontech), a ligation free cloning method, according to the manufacturer's instructions. I found this yielded a higher efficiency than ligation cloning. In brief, this method utilises the propriety In-Fusion enzyme. 15bp overhangs are introduced to each end of the desired insert fragment (linear PCR product) by PCR. These overhangs are homologues to the cut ends of the linearised vector at both the 5' and 3' (sticky or blunt) ends. The PCR products and cut vectors are prepared as above, then they are mixed in an In-Fusion cloning reaction with the following components:

2 µL 5X In-Fusion HD Enzyme Premix
X µL Linearised vector (as per kit instructions)
X µL Purified PCR fragment (as per kit instructions)
dH_2O to 10 µL

The reaction is incubated for 15 minutes at 50°C and then placed on ice. 2.5 µL of the mixture is then transformed into Stellar Competent Cells provided with the kit, using the heat shock transformation method as detailed in Chapter 2.5.8 for DH5α *E. coli*.

2.5.6 BAC recombineering

Please refer to Chapter 4.2.1 for more details. The CFLAP tag was amplified from the R6Kamp-FLAP plasmid from Tony Hyman (Max Planck Institute or Molecular Cell Biology and Genetics, Dresden, Germany). 50bp overhangs at the 5' and 3' ends of the PCR product were designed to straddle to the WAC STOP codon of human WAC isoform 1 contained in the WAC-BAC (CTD-2309I17 was purchased from Life Technologies). These homology arms were designed using the mitocheck BAC finder tool (http://www.mitocheck.org/cgi-bin/BACfinder). pSC101-BAD-gbaAtet (for Red/ET recombination) was purchased from Gene Bridges. The recombination of the CFLAP tag into the WAC-BAC was carried out using a previously described method (Poser et al., 2008) and the Quick & Easy BAC Modification Kit from Gene Bridges. This is as specified in the kit however there are some factors worth noting, which are different to handling plasmid DNA. The BAC is a very large DNA fragment prone to shearing and breaking. Thus when handling BACs especially, they should never be vortexed and freezing should be avoided. Storage at 4°C in a Tris-EDTA buffer is sufficient for stability in my experience. BAC DNA is also too large to purify using the Qiagen Spin Miniprep kit. Specialised kits for purifying BAC DNA are available commercially. However, for maxi prep of large amount of BAC DNA I used a phenol-chloroform extraction method as described in detail here (Ciotta et al., 2011). For mini prep of smaller amount of BAC DNA for screening, I also used the detailed method (Ciotta et al.,

2011). Briefly this uses the buffers from the QIAprep spin miniprep kit (Qiagen) to resuspend and lyse the bacteria and for neutralisation, followed by clarification and isopropanol precipitation of the BAC DNA. The BAC DNA is pelleted by centrifugation without using any columns. Insertion of the CFLAP TAG into the WAC-BAC was verified by sequencing, not by restriction digest. Sequencing directly from the BAC was problematic and unsuccessful for me. Therefore, I had to PCR amplify the region of the CFLAP tag insertion and sequenced the linear PCR product (see Chapter 2.5.12). Electroporation of the recombination plasmid or the linear PCR product (FLAP tag) into *E. coli* was performed according to the Quick & Easy BAC Modification Kit from Gene Bridges using a Bio-Rad *E. coli* Pulser, in chilled 1 mm cuvettes at 1350 V, 10 µF.

2.5.7 Site-directed mutagenesis

For site-directed mutagenesis (SDM) QuikChange Multi Site-Directed Mutagenesis Kit (Agilent Technologies) was used according to the manufacturer's instructions. Multiple primers can be used in a single reaction to generate mutations, so long as the primers do not overlap. Briefly, primers were designed to incorporate single or multiple base pair changes according to the manufacturer's guidelines (see Table 2.5). These primers were used for production of circular PCR products using an enzyme mix containing high fidelity PfuTurbo DNA polymerase and nick-sealing 'components'. See below for PCR mix and cycle. Following PCR, the template (un-mutated) plasmid was degraded by incubation with Dpn I for 1 hour at 37^{o}C, and the remaining DNA mix was used to transform XL10-GOLD ultracompetent cells (see Chapter 2.5.8). The obtained colonies were used for miniprep plasmid DNA purification, verification by sequencing and then used for maxiprep DNA production.

Site-directed mutagenesis PCR mix:

Note, half of the manufacturer's recommended volumes work well. Half reactions are shown below:

Reagent	Amount
10X QuikChange Multi reaction buffer	1.25 µL
QuikSolution	0.38 µL
Template DNA	50 ng
Mutagenic primer(s)	50 ng each
dNTP mix	0.5 µL
QuikChange Multi enzyme blend	0.5 µL
dH_2O	Make up to 12.5 µL

PCR cycle:

Segment	Cycles	Temperature (ºC)	Time
1	1	95	1 min
2	30	95	1 min
		55	1 min
		65	2 min/kb
3	1	4	∞

2.5.8 Bacterial transformation

Chemically competent DH5α *E. coli* (Life Technologies), stored at -80 ºC, were thawed on ice. 50 µL of DH5α was used per transformation. DNA added to and gently mixed with the bacteria, before incubation for 30 minutes on ice. For transformation of ligation products, 10 µl of ligation mixture was added to the bacteria, and for transformation of plasmid for the preparation of maxiprep DNA, 0.5 µg of DNA was added to the bacteria. Following incubation on ice, the bacteria were heat shocked at 42 ºC for 45 seconds in a water bath before incubating on ice for 2 minutes. 250 µL of SOC (2% trypton (w/v), 0.5% yeast extract (w/v), 10.0 mM NaCl, 2.7 mM KCl, 21.0 mM $MgCl_2$, 20.8 mM $MgSO_4$, 20 mM D-glucose, The Francis Crick Institute) was added to the bacteria and the bacteria were recovered by incubating at 37 ºC in a. Eppendorf ThermoMixer for 45 minutes to 1 hour. Bacteria were plated onto LB-agar plates (1% Bacto-Tryptone (w/v), 0.5% yeast extract, 1.7 M NaCl, 1.5% agar, The Francis Crick Institute) containing the appropriate antibiotic (either ampicillin at 100 µg/µL or kanamycin at 50 µg/µL). For transformation of ligation products, the whole 250 µL of recovered bacteria was

plated, whereas 50 µL of plasmid transformation was plated for maxiprep. Bacteria were incubated overnight at 37 ºC to allow the formation of colonies.

XL10-Gold Ultracompetent Cells (Agilent) were used for transformation of site-directed mutagenesis (SDM) products. The transformation protocol for these bacteria is the same as for DH5α, except that prior to transformation 1 µL of β-Mercaptoethanol (provided in kit) is gently mixed with the chilled bacteria by tapping, and the mixture incubated on ice for 10 minutes before addition of DNA. 2.5 µL of SDM reaction was used for each transformation. Bacteria on plates supplemented with the appropriate antibiotic were incubated overnight to allow colonies to form.

2.5.9 Purification of plasmid DNA

Colonies from bacterial plates were picked over a flame and inoculated into 5 mL LB starter culture (1% Bacto-Tryptone (w/v), 0.5% yeast extract, 1.7 M NaCl, The Francis Crick Institute) supplemented with the appropriate antibiotic. These cultures were grown in a shaking incubator at 37 ºC overnight. Bacteria were pelleted at 4000 rpm for 4 minutes at 4ºC and the supernatant discarded. When a large number of minipreps were being processed the miniprep service at the Francis Crick Institute equipment park was used. For small numbers of minipreps, QIAprep Spin Miniprep Kit (Qiagen) was used according to the manufacturer's instructions. DNA was eluted in 50 µL EB buffer. Miniprep DNA was then subjected to restriction digest as specified above and reaction products were analysed by agarose gel electrophoresis as described above. Plasmids harbouring inserts of the correct size (when cloning) were taken forward to sequencing verification as below. For SDM, plasmids were taken for sequencing without restriction digest.

For the production of larger quantities of plasmids (after sequence verification), maxipreps were performed using the Qiagen Plasmid Maxi Kit. Colonies from bacterial plates were picked over a flame and inoculated into 5 mL LB starter culture supplemented with the appropriate antibiotic. These cultures were grown in a shaking incubator at 37 ºC overnight. The next morning, these 5 mL starter cultures were added to 200 mL of LB medium with added antibiotic and incubated for 24 hours while swirling at 37 ºC. Bacterial cultures were pelleted at

6000 rpm for 30 minutes at 4 ºC and the supernatant discarded. Qiagen Plasmid Maxi Kit was then used according to the manufacturer's instructions for purification of plasmid DNA. After precipitation and washing, DNA was dissolved in 500 µL TE (Tris-EDTA) buffer. The concentration of DNA was subsequently measured using a spectrophotometer (NanoDrop, Thermo Scientific) and the DNA made up to 1 µg/µL with TE. Aliquots were stored at -20 ºC for long-term storage, or at 4 ºC if the aliquot was in regular use.

2.5.10 Primers

All primers were purchased from Sigma.

Table 2.5 Primers used in this thesis

Primer Name	Sequence (5' - 3')	Used for:	To make:
EcoRVNtermMycWAC Forward	TAGAGATATCACCACCATGGAGCAAAAGCTCATTTCTGAGGAAGATCTCAATGGTGTAATGTATGCGAGGAAA	Ligation Cloning	Myc-WAC constructs from WAC start
WAC BamHI Reverse	TCTAGGATCCTCACACCATGAAGGAATT	Ligation Cloning	WAC constructs from WAC Stop
EcoRVNtermMycWAC aa320 For	TAGAGATATCACCACCATGGAGCAAAAGCTCATTTCTGAGGAAGATCTCAATGGTACAACTCCTTCCACGTCT	Ligation Cloning	Myc-WAC 320-
WAC BamHI rev aa490	TCTAGGATCCTCACACTGGTCCTTGCTTAACTA	Ligation Cloning	Myc-WAC 320-490
EcoRVNtermMycWAC For aa542	TAGAGATATCACCACCATGGAGCAAAAGCTCATTTCTGAGGAAGATCTCAATGGTGTTGTACCACAGAATTCTTCTGC	Ligation Cloning	Myc-WAC 542-647
WAC BamHI Rev aa319	TCTAGGATCCTCAGCAAGAATGTGATACGGG	Ligation Cloning	Myc-WAC 1-319
EcoRVNtermMycWAC aa163 For	TAGAGATATCACCACCATGGAGCAAAAGCTCATTTCTGAGGAAGATCTCAATGGTTGGCTTGAAAGAGAACAGAG	Ligation Cloning	Myc-WAC 163-647
WAC BamHI rev aa610	TCTAGGATCCTCAAGATCTTAAATTTTTTAATTCAGTACAAAT	Ligation Cloning	Myc-WAC 1-610
In Fusion pEGFP-C2, XhoI, WAC Iso1 Forward	GGACTCAGATCTCGAGCATGGTAATGTATGCGAGGAAACAG	In Fusion cloning	EGFP-WAC constructs from WAC Stop
In Fusion pEGFP-C2, Sal I, WAC Iso1 Reverse	CCGCGGTACCGTCGACTTCACACCATGAAGGAATTCTG	In Fusion cloning	EGFP-WAC constructs from WAC start
In Fusion pEGFP-C2, Sal I, 610aa Rev STOP	CCGCGGTACCGTCGACTTCAAGATCTTAAATTTTTTAATTCAGTACAAAT	In Fusion cloning	EGFP-WAC 1-610
In Fusion pEGFP-C2, XhoI, 163aa For	GGACTCAGATCTCGAGCTGGCTTGAAAGAGAACAGAG	In Fusion cloning	EGFP-WAC 163-647
In Fusion pEGFP-C2, Sal1, 319aa Rev	CCGCGGTACCGTCGACTTCAGCAAGAATGTGATACGGG	In Fusion cloning	EGFP-WAC 1-319
In Fusion pEGFP-C2, Xho1, 320aa For	GGACTCAGATCTCGAGCACAACTCCTTCCACGTCT	In Fusion cloning	EGFP-WAC 320-647
In Fusion pEGFP-C2, XhoI, 611 For	GGACTCAGATCTCGAGCTTAGTCCGAGTATGTGAAATTCAAG	In Fusion cloning	EGFP-WAC 611-647
In Fusion pEGFP-C2, Sal I, 630 Reverse	CCGCGGTACCGTCGACTTCATCTCAAAAATAGTATCCTTTGCTCT	In Fusion cloning	EGFP-WAC 1-630
In Fusion pEGFP-C2, Sal I, 620 Reverse	CCGCGGTACCGTCGACTTCAAGTTGCTTGAATTTCACATACTCG	In Fusion cloning	EGFP-WAC 1-620

Primer Name	Sequence (5' - 3')	Used for:	To make:
In Fusion pEGFP-C2, XhoI, 580aa For	GGACTCAGATCTCGAGCGAGAAGCAGGCATCAAGATTAC	In Fusion cloning	EGFP-WAC 580-647
-612-618 for	TGTACTGAATTAAAAAATTTAAGATCTTTAGCAACTTTGCGAGAGCAAAGG	PCR SOEing	WAC aa619-647 Fragment, SOE with below
-612-618 rev	CCTTTGCTCTCGCAAAGTTGCTAAAGATCTTAAATTTTTTAATTCAGTACA	PCR SOEing	WAC aa1-611 fragment, SOE with above
5'p for aa621 inverse	(P)TTGCGAGAGCAAAGGATACTA	Inverse PCR	EGFP-WAC Δ611-620
5'p Rev aa610 inverse	(P)AGATCTTAAATTTTTTAATTCAGTACAAAT	Inverse PCR	EGFP-WAC Δ611-620
pcDNA 3.1 + NheI infu Strep tag For aa13	ACCCAAGCTGGCTAGCGCCACCATGTGGTCCCACCCCCAGTTCGAGAAGGGCGGCATGTCGGAAGAAACCAGGC	In Fusion cloning	Strep-tag II-GM130
pcDNA 3.1 + XhoI infu Stop Rev aa998	GCCCTCTAGACTCGAGTTATATAACCATGATTTTCACCTCGTCG	In Fusion cloning	Strep-tag II-GM130
In Fusion pGEX 4T2, SmaI, WAC Iso1 Forward	ATCCCCGGAATTCCCGGGATGGTAATGTATGCGAGGAAACAG	In Fusion cloning	GST-WAC
In Fusion pGEX 4T2, NotI, WAC Iso1 Reverse	AGTCACGATGCGGCCGCTCACACCATGAAGGAATTCTG	In Fusion cloning	GST-WAC 1-647
In Fusion pGEX 4T2, NotI, WAC Iso1 Reverse aa610	AGTCACGATGCGGCCGCTCAAGATCTTAAATTTTTTAATTCAGTACAAAT	In Fusion cloning	GST-WAC 1-610
NheI In Fu EosFP For Kozak	ACCCAAGCTGGCTAGCGCCACCATGAGTGCGATTAAGCCAGACATG	PCR SOEing, In Fusion	EosFP-GABARAP
In Fu EosFP REV 5xGly linker	GCCTCCTCCACCACCTCGTCTGGCATTGTCAGGC	PCR SOEing, In Fusion	EosFP-GABARAP
In Fu huGABARAP For 5xGly linker	GGTGGTGGAGGAGGCAAGTTCGTGTACAAAGAAGAGCATC	PCR SOEing, In Fusion	EosFP-GABARAP
In Fu huGABARAP REV STOP XhoI	GCCCTCTAGACTCGAGTCACAGACCGTAGACACTTTCGT	PCR SOEing, In Fusion	EosFP-GABARAP
WAC SDM Primer 1	GAAAAGAATCTACATCAGGTGATAAACCCGTATCACATTC	SDM	Silent mutations To make WAC (Q9BTA9-1) resistant to WAC-03 siRNA
WAC SDM Primer 2	CTACATCAGGTGATAAGCCGGTATCGCATTCTTGCACAACTCCTTC	SDM	Silent mutations To make WAC (Q9BTA9-1) resistant to WAC-03 siRNA
WAC SDM I626S L629S	TTGCGAGAGCAAAGGAGCCTATTTTCGAGACAACAAATTAAG	SDM	Mutations of hydrophobic ‘a’ and ‘d’ positions in WAC CC domain to remove RNF40 binding
GABARAP SDM primer	GACGAAAGTGTCTACGCTCTGTGAAGCTGCTCG	SDM	To make human GABARAP G116A mutation

(p), 5’ phosphorylated primer

2.5.11 Plasmids

All Myc-WAC and EGFP-WAC constructs are resistant to WAC-03 siRNA by site-directed mutagenesis (see Chapter 2.5.7).

Table 2.6 Plasmids used in this thesis

Name	Insert	Vector	Resistance	Source
pEGFP-C2	GFP	pEGFP-C2	Kanamycin	Clontech
pcDNA3.1 (+)	Empty	pcDNA3.1 (+)	Ampicillin	
Myc-WAC	Human WAC isoform 1 full length (1-647)	pcDNA3.1 (-)	Ampicillin	N. McKnight
Myc-WAC ΔCC	WAC aa1-610	pcDNA3.1 (-)	Ampicillin	J. Joachim
Myc-WAC ΔN	WAC aa163-647	pcDNA3.1 (-)	Ampicillin	J. Joachim
Myc-WAC NT	WAC aa1-319	pcDNA3.1 (-)	Ampicillin	J. Joachim
Myc-WAC CT	WAC aa320-647	pcDNA3.1 (-)	Ampicillin	J. Joachim
Myc-WAC 320-490	WAC aa320-490	pcDNA3.1 (-)	Ampicillin	J. Joachim
Myc-WAC 542-647	WAC aa542-647	pcDNA3.1 (-)	Ampicillin	J. Joachim
GFP-WAC	Human WAC isoform 1 full length (1-647)	pEGFP-C2	Kanamycin	J. Joachim
GFP-WAC ISLS	WAC I626S & L629S double mutation	pEGFP-C2	Kanamycin	J. Joachim
GFP-WAC ΔCC	WAC aa1-610	pEGFP-C2	Kanamycin	J. Joachim
GFP-WAC 1-620	WAC aa1-620	pEGFP-C2	Kanamycin	J. Joachim
GFP-WAC 1-630	WAC aa1-630	pEGFP-C2	Kanamycin	J. Joachim
GFP-WAC 611-647	WAC aa611-647	pEGFP-C2	Kanamycin	J. Joachim
GFP-WAC Δ611-620	WAC with aa611-620 deleted inclusive	pEGFP-C2	Kanamycin	J. Joachim
GFP-WAC Δ612-618	WAC with aa612-618 deleted inclusive	pEGFP-C2	Kanamycin	J. Joachim
GFP-WAC 580-647	WAC aa580-647	pEGFP-C2	Kanamycin	J. Joachim
GFP-WAC ΔN	WAC aa163-647	pEGFP-C2	Kanamycin	J. Joachim
GFP-WAC NT	WAC aa1-319	pEGFP-C2	Kanamycin	J. Joachim
GFP-WAC CT	WAC aa320-647	pEGFP-C2	Kanamycin	J. Joachim
GST-WAC	Human WAC isoform 1 full length (1-647)	pGEX-4T-2	Ampicillin	J. Joachim
GST-WAC ΔCC	WAC aa1-610	pGEX-4T-2	Ampicillin	J. Joachim
GST-GABARAP	Human GABARAP	pGEX-5X-1	Ampicillin	Z. Elazar
GST	GST	pGEX-4T-2	Ampicillin	GE life sciences
pSC101-BAD-gbaAtet	Red/ET recombinases	pSC101-BAD-gbaAtet	Tetracycline	Gene Bridges

Name	Insert	Vector	Resistance	Source
R6Kamp-FLAP	C-terminal FLAP	R6Kamp-FLAP	Ampicillin	T. Hyman
WAC-BAC	Human WAC gene 14 exons and promoter	pBAC	Chloramphenicol	Life Technologies
3xHA-GM130	Rat GM130	pcDNA3.1 (+)	Ampicillin	J. Seemann
Strep-tag II-GM130	Rat GM130	pcDNA3.1 (+)	Ampicillin	J. Joachim
HA-GM130 aa383-1002	Human GM130 isoform 1 aa381-1002	pSV-SPORT	Ampicillin	A. Barnekow
HA-GM130 aa446-1002	Human GM130 aa446-1002	pSV-SPORT	Ampicillin	A. Barnekow
HA-GM130 aa692-1002	Human GM130 aa692-1002	pSV-SPORT	Ampicillin	A. Barnekow
HA-GM130 aa774-1002	Human GM130 aa774-1002	pSV-SPORT	Ampicillin	A. Barnekow
GM130-ΔCterm-HA-MAO	Rat GM130 aa1-879 and MAO-A TMD aa481-528	pcDNA3.1 (+)	Ampicillin	S. Munro
GFP-LC3A	Human LC3A	pDEST-EGFP	Ampicillin	T. Johansen
GFP-LC3B	Human LC3B	pDEST-EGFP	Ampicillin	T. Johansen
GFP-LC3C	Human LC3C	pDEST-EGFP	Ampicillin	T. Johansen
GFP-GABARAP	Human GABARAP	pDEST-EGFP	Ampicillin	T. Johansen
GFP-GABARAP G116A	GABARAP G116A mutation	pDEST-EGFP	Ampicillin	H. Jefferies
Myc-GABARAP	Human GABARAP	pDEST	Ampicillin	T. Johansen
Myc-GABARAP	GABARAP G116A mutation	pDEST	Ampicillin	H. Jefferies
GFP-GABARAPL1	Human GABARAPL1	pDEST-EGFP	Ampicillin	T. Johansen
GFP-GATE-16	Human GATE-16	pDEST-EGFP	Ampicillin	T. Johansen
mCherry-GFP-p62	Human p62	pDEST-CMV	Ampicillin	T. Johansen
EosFP-GABARAP	Human GABARAP	pcDNA3.1 (+)	Ampicillin	J. Joachim
Atg13-FLAG	Atg13	pcDNA3.1 (-)	Ampicillin	N. McKnight
HA-ULK1 WT	Full length human ULK1	pcDNA3.1 (+)	Ampicillin	A. Longatti
HA-ULK1 ΔLIR	ULK1 D356A, F357A, P361A triple mutant	pcDNA3.1 (+)	Ampicillin	F. McAlpine
HA-ULK1 ΔLIR/KI	ULK1 K46I, D356A, F357A, P361A quadruple mutant	pcDNA3.1 (+)	Ampicillin	F. McAlpine

2.5.12 Sequencing

Sequencing was performed with BigDye Terminator v3.1 (BDT) (The Francis Crick Institute) sequencing reactions.

Reaction mix:
BDT Mix (provided by the equipment park, The Francis Crick Institute) 8 µL
Sequencing primer 1 µL of 3.2 pmol / µL
Plasmid DNA 200 ng or linear PCR product (>2000bp, 40-100 ng, 1000-2000bp 10-40 ng)
Made to 20 µL final volume in dH_2O

Sequencing reaction PCR cycle:

Segment	Cycles	Temperature (ºC)	Time
1	1	96	3 min
2	25	96	10 sec
		50	5 sec
		60	4 min
3	1	4	∞

Sequencing reactions were cleaned up using the DyeEx 2.0 Spin Kit (Qiagen) according to the manufacturer's instructions. Cleaned reactions were dried using a vacuum centrifuge at 45^{o}C for 20 minutes. Sequencing was performed using capillary sequencing on an Applied Biosystems 3730Xl DNA analyser by The Francis Crick Institute equipment park. DNA sequences were analysed and aligned using MegAlign (DNASTAR) software.

2.6 Data analysis

2.6.1 Imaris image analysis software

LC3 and WIPI2 puncta and centrosomal GABARAP intensity was quantified using Imaris 7 X64 software (Bitplane). The thresholds for detection limits based on the size and intensity of puncta, were set manually by comparing puncta detection in starved (+ Bafilomycin) vs fed cells. The same image analysis settings were used for each condition of an experiment for comparability. Cells were counted manually, or a mask was created in Imaris to measure cell area. For quantification purposes, the enlarged GABARAP positive structure was designated as centrosomal GABARAP.

2.6.2 ImageJ densitometry

ImageJ (National Institute of Health) was used for quantification of western blots by measuring the density of film exposure. Microsoft excel was used to tabulate and normalise the data and statistics were performed as below. Live cell imaging data was analysed by image J, regions of interest were designated on movies to obtain intensity over time data. The Maximum intensity projection function was used to flatten Z-stacks (where indicated) and individual projections combined into a time-lapse.

2.6.3 Statistical analysis

Statistical analysis was performed using GraphPad Prism 6 software as indicated in figure legends. Asterisk(s) indicate significance: *, $p \leq 0.05$, **, $p \leq 0.01$, ***, $p \leq 0.001$, ****, $p \leq 0.0001$. Data shown is the mean of the indicated number of experiments. Error bars display the standard error of the mean (SEM) for 3 or more experiments or the standard deviation (SD) for less than 3 experiments.

Chapter 3. Analysis of WAC nuclear function

3.1 Introduction and aim

3.1.1 Introduction

WAC performs functions on the Golgi and in the nucleus (Totsukawa et al., 2011, Zhang and Yu, 2011), as well as promoting starvation-induced autophagy (McKnight et al., 2012). It is not known whether WAC's nuclear function is related to its role in autophagy regulation. In the nucleus WAC promotes monoubiquitination of histone 2B (H2B) at lysine 120, an epigenetic modification that is associated with maintenance of active transcription (Bonnet et al., 2014). I hypothesised that WAC may control autophagy gene regulation via its epigenetic function rather than its Golgi localised function. In this manner WAC may be a potent regulator of autophagy gene transcription in a similar way to TFEB and ZKSCAN3 (Martina et al., 2012, Roczniak-Ferguson et al., 2012, Settembre et al., 2011, Chauhan et al., 2013). ZKSCAN3 functions as a transcriptional repressor of autophagy gene expression such as LC3B and WIPI2 as well as a repressor of lysosomal biogenesis genes. Upon nutrient starvation or Torin 1 treatment, which both stimulate autophagy, ZKSCAN3 relocalises from the nucleus to the cytoplasm. On the other hand, transcriptional factor EB (TFEB) functions as an activator of autophagic and lysosomal gene expression. Under nutrient rich conditions TFEB is phosphorylated by kinases such as mTOR, binds 14-3-3 proteins and is retained in the cytoplasm. Upon starvation, TFEB is dephosphorylated and it translocates to the cell nucleus.

3.1.2 Aim

In order to understand more about WAC's role in the nucleus I began by cloning a series of truncations of the WAC protein, to understand how WAC localises to the nucleus versus cytoplasm. These truncations were designed to remove the highly conserved WW or CC domains of WAC, separate the two halves of WAC or to isolate folded regions of the WAC protein. A full explanation of the rationale behind these truncations is given is (Chapter 4.4.2) and a map of the

truncations is shown in Figure 3.1. I next investigated WAC's effects on the regulation of autophagy gene transcription by knockdown experiments coupled with qRT-PCR. A more comprehensive, unbiased analysis of WAC's effect on transcription was gleaned by transcriptome-wide microarray analysis of WAC knockdown samples as well as knockdown of the entire WAC/RNF20/RNF40 complex. After bioinformatic analysis of the datasets hits were validated by qRT-PCR experiments. Finally I began investigating the role of the interaction between WAC and RNF20/40 in epigenetic modification.

3.2 Analysis of WAC nuclear localisation

3.2.1 Amino acids 1-162 are required for WAC nuclear retention whereas aa320-647 direct membrane association

WAC has no canonical nuclear localisation signal (data not shown) and it is unknown which domain(s) of the WAC protein direct its residency in the nucleus. WAC binds RNA polymerase II (RNAP) via its WW domain and also RNF20/40 via its coiled-coil (CC) domain. As RNAP and RNF20/40 are both nuclear proteins, both the WW and CC domains of WAC are candidates for nuclear localisation. I cloned a series of WAC truncations to determine the region of WAC that controls its subcellular localisation (Figure 3.1). Full length Myc-WAC human isoform 1, aa1-647, localised primarily to the nucleus in most cells, and was also detected in the cytoplasm occasionally (Figure 3.2a). Myc-WAC was excluded from regions of the nucleus, which could be nucleoli. This was confirmed by subcellular fractionation, whereby most of Myc-WAC was found in the nuclear pellet whereas a small amount was found associating with membranes (Figure 3.2b). WAC's association with membranes has been shown before by subcellular fractionation (Totsukawa et al., 2011). Removal of the CC domain of WAC (aa1-610) resulted in a similar localisation to the full-length protein (Figure 3.2a). However, removal of a large section of the N-terminus of WAC, aa163-647, including the WW domain of WAC, resulted in accumulation of WAC in the cytoplasm, although WAC was still able to localise to the nucleus. This suggests that the first 162 amino acids of WAC are required for its nuclear retention. In support of this, the N-terminal half of WAC aa1-319, was primarily localised to the nucleus and sometimes to the cytoplasm,

similarly to the full-length protein. In contrast the C-terminal half of WAC localised primarily to punctate structures in the cytoplasm, reminiscent of membranous structures, and also to a minor extent in the nucleus. This was confirmed by subcellular fractionation (Figure 3.2b), whereby the C-terminal half of WAC was enriched on membranes compared with the full-length protein. The final two pieces of the WAC protein cloned were two regions that are predicted to be folded (Figure 4.8). WAC aa320-490 was found in the nucleus and in the cytoplasm as was aa542-647. However aa542-647 exhibited a more cytosolic localisation than aa320-647, which associates with membranes. Taken together, these data suggest that the first 162aa of WAC are required for concentration in the nucleus, perhaps by interaction with RNAP. Whereas the C-terminal half of WAC directs its association with membranes, perhaps including the Golgi.

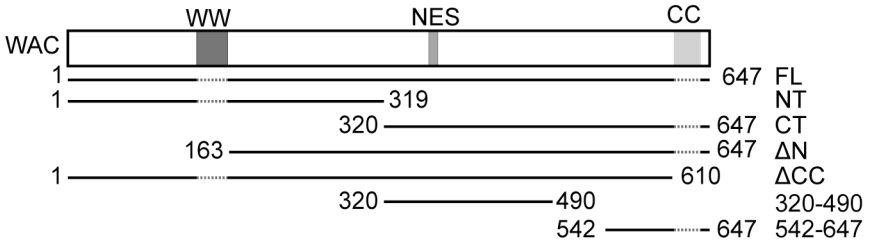

Figure 3.1 Schematic showing human Myc-WAC isoform 1 truncation constructs

Primary structure map of Myc-WAC isoform 1 constructs used for localisation studies. The conserved WW domain and coiled-coil (CC) domains are shown boxed as well as the putative nuclear export signal (NES). The dashed lines indicate the positions of WW or CC domains in the constructs.

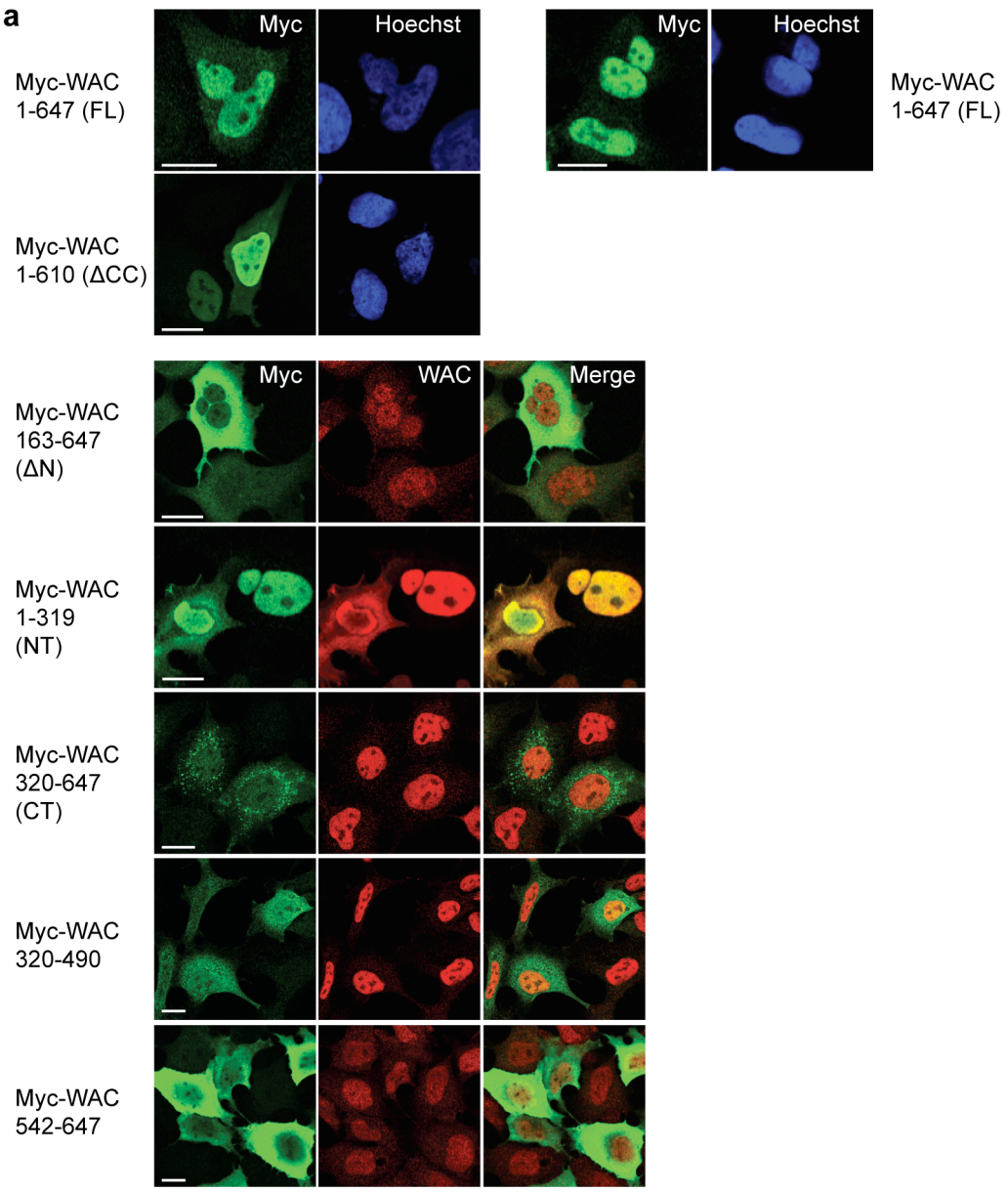
a
Myc
Hoechst
Myc-WAC
1-647 (FL)
Myc-WAC
1-610 (ΔCC)
WAC
Merge
Myc-WAC
163-647
(ΔN)
Myc-WAC
1-319
(NT)
Myc-WAC
320-647
(CT)
Myc-WAC
320-490
Myc-WAC
542-647
b
Myc-WAC (FL)
Myc-WAC (CT)
1X
10X
NP
PNS
Cyt
Mem
Mw
kDa
Atg9
Myc
Lamin B
SOD1
76
102
38
24

Figure 3.2 WAC nuclear versus membrane localisation is encoded by different amino acid regions

(a) HEK293A cells expressing the indicated construct were analysed by confocal microscopy. Scale bars 20 μm. Experiment was performed once for aa320-490 and aa542-647 fragments and three times for other truncations. For interpreting WAC staining, WAC antibody epitope is within the first 163 amino acids of WAC. **(b)** HEK293A cells expressing the indicated construct were subjected to subcellular fractionation followed by western blotting. Experiment was performed once.

3.3 Investigating the role of WAC in transcriptional regulation

3.3.1 WAC depletion reduces LC3B mRNA levels and p53 mRNA and protein levels

I next wanted to understand if WAC controls the transcription of autophagy genes and began by analysing mRNA levels of mAtg8 proteins after WAC knockdown, under basal or starvation conditions. WAC knockdown was confirmed by western blot (Figure 3.3a). qRT-PCR revealed that LC3B mRNA levels were modestly reduced after WAC knockdown under both basal and starvation conditions (Figure 3.3b). There was little effect of WAC knockdown on GABARAP mRNA levels under basal conditions however a reduction was observed during starvation. Unlike LC3B, GATE-16 (GABARAPL2), was barely affected by WAC knockdown. These data suggest that WAC may be a regulator of LC3B mRNA expression but not of Atg8 mRNA expression as a whole; further repeat experiments are necessary to confirm this (see Figure 3.6).

WAC is known to regulate target genes of the p53 transcription factor (Zhang and Yu, 2011). Furthermore, RNF20 regulates p53 gene expression (Shema et al., 2008). Thus it is also possible that WAC regulates p53 gene expression itself. Indeed WAC depletion reduced p53 transcript levels as well as reduced p53 protein expression levels (Figure 3.3b, c and d). p53 is also known as a regulator of autophagy; in the nucleus p53 is promotes the expression of genes that positively regulate autophagy such as TSC2, DRAM, and AMPK subunits, whereas in the cytoplasm it appears to repress autophagy (Maiuri et al., 2010). One of the targets of p53 that promotes autophagy is sestrin-2, which promotes autophagy by activating AMP-activated protein kinase (AMPK) to phosphorylate

and activate TSC2 and thereby inhibit mTOR (Budanov and Karin, 2008). Sestrin2 also inhibits mTOR in an AMPK-independent fashion (Parmigiani et al., 2014). However, in contrast to the reduction of p53 mRNA levels after WAC knockdown, only small changes in sestrin2 transcript levels were detected (Figure 3.3b). Thus it is unlikely that changes in Sestrin2 expression explains WAC's effect on autophagy. It could be that a greater reduction in p53 levels is required to see effects on Sestrin2.

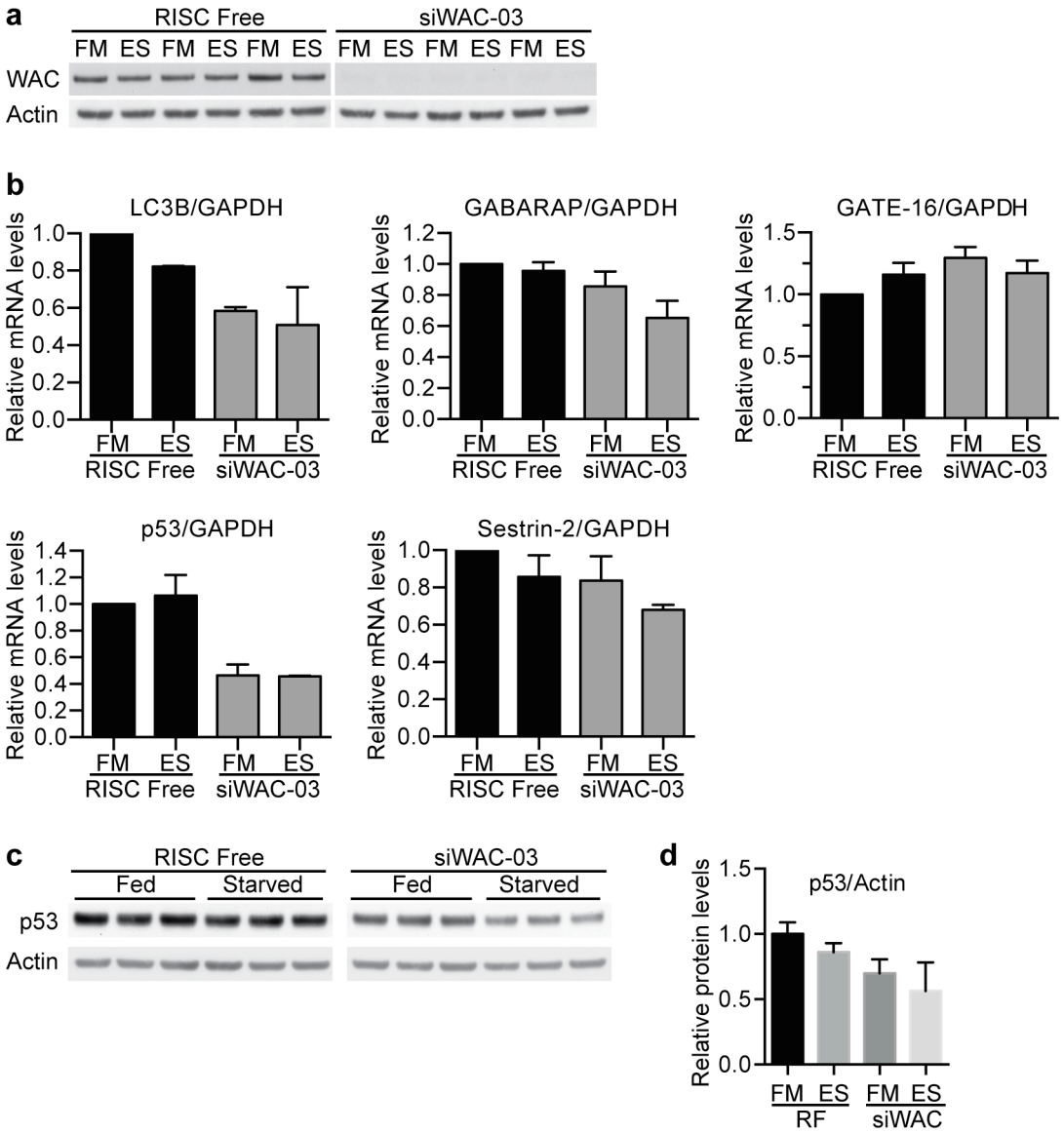

Figure 3.3 WAC depletion affects LC3B mRNA and p53 mRNA and protein expression

(a) HEK293A cells were treated with the indicated siRNA for 72 hours followed by incubation in full medium (FM) or EBSS (ES) for 2 hours prior to analysis by immunoblot. **(b)** Triplicate samples set up the same day as **(a)** were taken for qRT-PCR analysis of the indicated genes. Mean ± SD. **(a and b)** were performed once. **(c)** HEK293A cells were treated with the indicated siRNA for 72 hours followed by incubation in full medium (Fed) or EBSS (Starved) for 2 hours prior to analysis by immunoblot. **(d)** Quantification of **(c)** from 2 independent experiments. Mean ± SD.

3.3.2 RNF40 knockdown does not reduce LC3B mRNA levels or affect autophagy flux

In the nucleus WAC functions as a heterohexameric complex with the E3 ligases RNF20 and RNF40 with a 2:2:2 stoichiometry and each of these complex members is required for H2B monoubiquitination at lysine 120 (Zhang and Yu, 2011). Thus, genes regulated by WAC should also be regulated by RNF20 and RNF40, according to the canonical model of WAC nuclear function. Efficient knockdown of RNF40 mRNA was obtained with 4 different siRNA duplexes (Figure 3.4). To my surprise, although depletion of WAC again modestly reduced LC3B mRNA levels, RNF40 knockdown did not. There may even be an increase of LC3B transcript levels upon RNF40 depletion, although this was not observed with every siRNA duplex. This suggests that there may be genes that are regulated specifically by WAC independently of RNF20/40, and perhaps independently of WAC's function in H2B monoubiquitination. Of course it is also possible that the reduction of LC3B transcript upon WAC knockdown is an off-target effect of the WAC-03 siRNA and future studies should aim to rescue this effect. Again there was a reduction of p53 mRNA levels after WAC knockdown and there was a small reduction of p53 transcript after knockdown with all 4 RNF40 siRNAs (Figure 3.4). This suggests that WAC and RNF40 both regulate p53 transcription, and therefore one may predict that the WAC/RNF20/40 complex as a whole controls p53 expression.

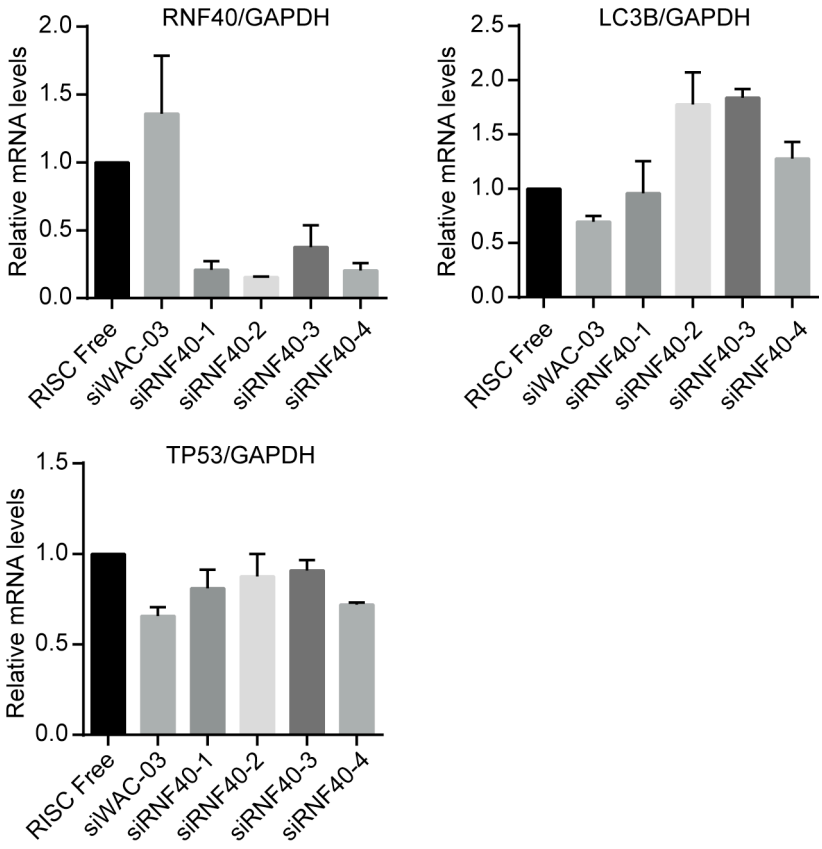

Figure 3.4 Depletion of RNF40 may affect p53 mRNA expression

(a) HEK293A cells were treated with the indicated siRNA for 72 hours followed by analysis by qRT-PCR for the indicated gene targets. Mean ± SD biological duplicates. Experiment was performed once.

I next wanted to investigate if knockdown of RNF40 affected autophagic flux. Knockdown of WAC reduced LC3 lipidation under conditions of starvation and Bafilomycin A1 treatment (Figure 3.5) as expected (McKnight et al., 2012). Moreover, ULK1 activity, as measured by phosphorylation by ULK1 on its complex member Atg13 at Serine 318 (Joo et al., 2011) was slightly reduced after WAC knockdown (Figure 3.5 and see also Figure 5.5a), further suggesting that autophagy flux is reduced after WAC knockdown. Depletion of RNF40 showed no reduction in LC3 lipidation and ULK1 activity. Efficacy of RNF40 siRNAs was assessed in a separate experiment (Figure 3.4). As expected, depletion of RNF40 reduced WAC protein levels, as the complex members stabilised one another (Karpiuk et al., 2012, Zhang and Yu, 2011). The effects of WAC on autophagy flux and different stages of the pathway are studied in greater detail in Chapter 5.

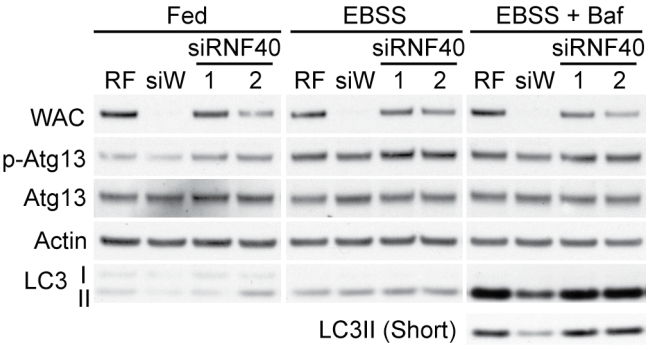

Figure 3.5 Knockdown of RNF40 did not affect autophagy flux

HEK293A cells were treated with the indicated siRNA for 72 hours followed by incubation for 2 hours in full medium (Fed), EBSS or EBSS + BafA and then immunoblot. Experiment was performed once. Shorter film exposure of LC3II, LC3II (Short).

3.3.3 Design and optimisation of siRNA knockdown for transcriptomic analysis

The data presented so far suggests that WAC modestly regulates the expression of at least 2 genes involved in autophagy: LC3B and p53. However, many proteins directly participate as members of the autophagic machinery and many other proteins functions as regulators of the autophagic process (Chapter 1). I next decided to take an unbiased approach to analyse WAC's effects on autophagy gene expression by performing a transcriptome-wide microarray analysis. This has obvious throughput advantages versus qRT-PCR. It is worth noting that qRT-PCR arrays targeting a set of genes involved in autophagy are available (e.g. Qiagen, 84 gene array) and although these offer a cost advantage versus a microarray the resultant dataset is limited.

To prepare RNA samples for microarray analysis I designed the following experiment to optimise the sample preparation (Figure 3.6). HEK293A cells were subjected to knockdown by reverse transfection method as usual (see Materials and Methods), however this was done in 6-well plates as opposed to my normal knockdown in 24-well plates. Using a larger plate size allows enough RNA material to be available for qRT-PCR hit validation after microarray analysis within the same samples. 3 independent experiments were carried out with cells treated with RISC Free or WAC siRNAs for 72 hours with a 2 hour incubation in starvation medium

(EBSS) or full medium prior to RNA extraction. RNA quality (purity and degradation) was assessed as discussed in the Materials and Methods. After this, I assessed knockdown efficacy by qRT-PCR, and assessed changes in genes previously shown to be affected by WAC knockdown. As expected WAC knockdown resulted in significant reductions in LC3B and p53 mRNA levels, whereas no effect on the GAPDH 'housekeeping' gene was observed. One concern I had was that I was only able to achieve a ~70% knockdown in WAC mRNA levels, whereas before at the protein level (Figure 3.3a) I obtained a more impressive knockdown. For the purposes of the microarray submission I wanted to ensure that I provided samples with the best possible WAC knockdown, in order to reduce false negatives from the analysis. With this in mind I decided to repeat the knockdowns and also to redesign the experiment as explained below.

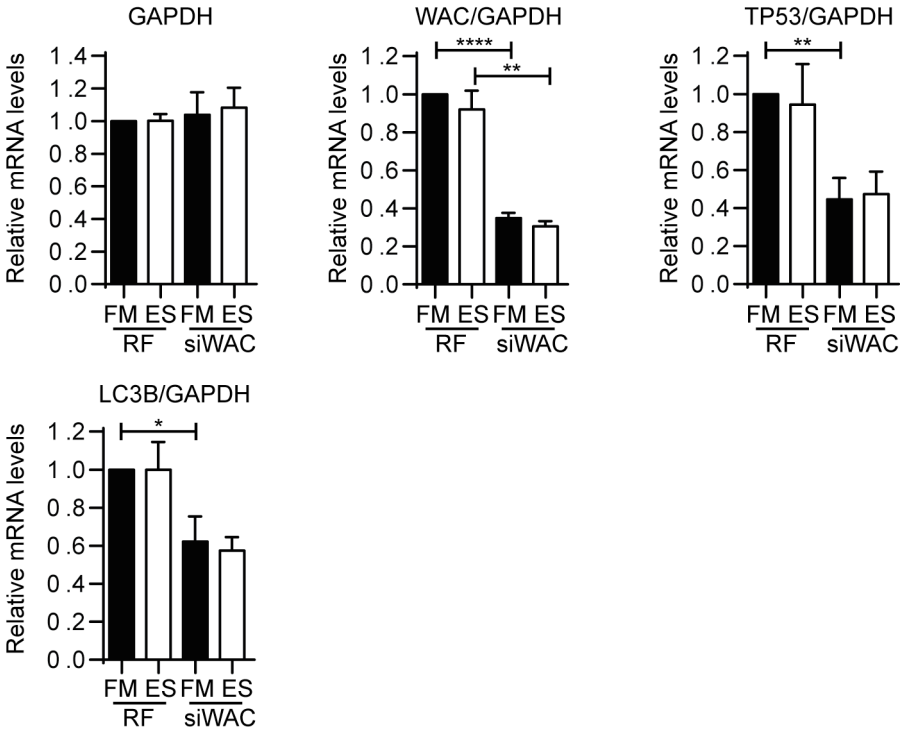

Figure 3.6 Optimisation of WAC depleted samples for microarray analysis

HEK293A cells were treated with the indicated siRNA for 72 hours followed by analysis by qRT-PCR for the indicated gene targets. Mean ± SEM 3 independent experiments. Unpaired Student's t test, *, $p \leq 0.05$.

HEK293A cells were treated with siRNAs, this time in 24-well format (Figure 3.7), as I have previously done (Figure 3.3a). The experiment was designed for samples to be hybridised to an Illumina HT-12 v4 BeadArray. This array consists of 50mer probes on immobilised beads that probe to exon regions. Some genes are covered by multiple probes, which improves the confidence of expression changes. However, some genes are only covered by a single probe sequence. The advantage of this system is that it is cheaper than competing technologies whilst still providing transcriptome-wide data. Furthermore, we have bioinformatic processes (e.g. scripts) in place at the Francis Crick Institute that allow the rapid analysis of the resultant dataset. Other options for analysing transcriptomic changes include exome arrays and RNA-seq technology. These methods have the advantage of being able to detect changes in individual isoform expression and splicing.

The Illumina chip that holds the BeadArray has space for 12 samples to be hybridised and thus my experiment was designed with the submission of 12 samples in mind. I designed the experiment with triplicate samples from the same experiment, with RISC Free, WAC, RNF20 and RNF40 siRNA treatments making up the 12 samples (Figure 3.7). This meant I could not do a comparison of basal versus starvation conditions. However, I reasoned that WAC affects basal autophagy as p62 accumulates upon WAC knockdown under basal conditions (McKnight et al., 2012). The advantage of including RNF20/40 knockdowns as well as WAC, meant that I could investigate genes regulated by the entire complex, as well as genes regulated by WAC independently perhaps by a non-canonical mechanism. By using biological replicates from the same experiment, rather than separate experiments, I could reduce sample variability to reduce the possibility of false negatives in the microarray, especially when dealing with modest gene changes. Reproducibility of hits could then be further confirmed during the validation stage.

The final alteration to experimental design was to use pools of siRNAs against WAC, RNF20 or RNF40 rather than individual duplexes (Figure 3.7). This should in theory dilute any off-target effects whilst maintaining the on-target effects. As can be seen in Figure 3.7 knockdown of WAC with 2 different siRNAs (3+4) resulted in >85% knockdown of WAC message. This was a good improvement over

the knockdown previously achieved in the 6-well format (Figure 3.6). This could be due to the scalability of the reverse transfection knockdown protocol or perhaps the aliquot/batch of siRNA used. A good knockdown of RNF40 was also achieved using a pool of 2 siRNAs (1+2) (Figure 3.7) which individually work well (Figure 3.4). Four individual RNF20 siRNAs and a pool of all four produced a robust depletion of RNF20 message. Triplicate RNA samples of the pooled siRNA treatments for WAC, RNF20, RNF40 as well as RISC free, were submitted to the Genome Centre at Barts and The London School of Medicine and Dentistry, London. Samples were processed as briefly described in the Materials and Methods.

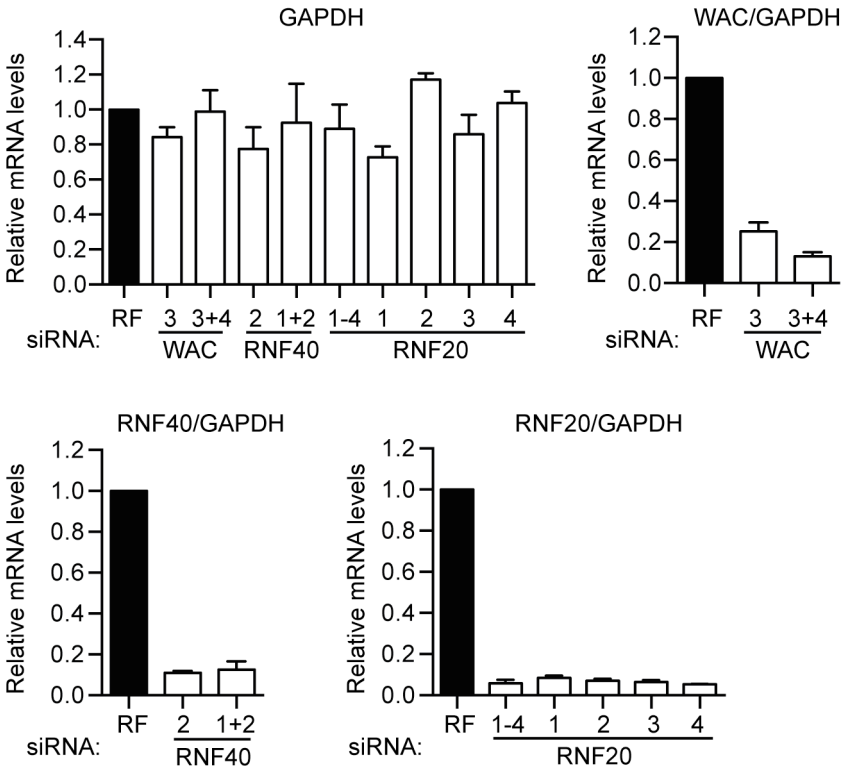

Figure 3.7 Preparation of knockdown samples for Illumina BeadArray™ analysis

HEK293A cells were treated with the specified siRNA or siRNA pools for 72 hours followed by analysis by qRT-PCR for the indicated gene targets. Mean ± SD biological triplicates from one experiment. The following samples were used in Illumina BeadArray™ analysis: RISC Free (RF) siRNA and siRNA pools of WAC (siRNAs 3+4), RNF40 (siRNAs 1+2) and RNF20 (siRNAs 1-4).

3.3.4 WAC regulates gene expression independently and as part of the WAC/RNF20/40 complex

The microarray data was analysed by Probir Chakravarty in the Bioinformatics service at the Francis Crick Institute after discussions about how best to probe the dataset. An explanation of the analysis is provided in the Materials and Methods. Knockdown of WAC significantly affected (up or downregulated) the mRNA expression levels of 1,925 genes versus the RISC Free control (Figure 3.8). It is worth noting that the numbers displayed (Figure 3.8) show genes that are significantly affected ($p \leq 0.05$) however no cut-off for fold change has been applied, therefore mild effects are also displayed.

Out of the 1,925 genes regulated by WAC knockdown, 961 were uniquely affected by WAC knockdown alone (Figure 3.8 and Table 7.1). Some of these will likely be due to off-target effects but some are likely to be genuinely regulated by WAC. These genes are listed in Table 7.1 and ranked by fold change, negative to positive order. The most decreased gene after WAC knockdown was reassuringly WAC. It is worthwhile to note that this change was around -3.7 fold, whereas by qRT-PCR I was able to detect a stronger decrease of WAC from the same samples (Figure 3.7). This may be due to some difference between the two techniques. The majority of significantly affected genes showed modest changes, with a change in either direction of < 1.5 fold (Table 7.1). Out of these 961 genes uniquely regulated by WAC, 551 were downregulated after WAC knockdown, whereas 410 were upregulated. The up and downregulated genes were separated and taken for gene set enrichment analysis. Specifically, I was looking for biological pathways which were, as a whole, significantly affected by WAC knockdown. Importantly, autophagy, membrane trafficking and lysosomal pathways were included in this analysis. In the 410 genes upregulated after WAC knockdown, no biological pathways were significantly affected. However, in the 551 genes downregulated by WAC knockdown, pathways involved in the immune response and in inflammation were significantly enriched (Table 7.2). Autophagy was not a significantly affected pathway. Of note, genes involved in MHC class I antigen presentation were downregulated upon WAC knockdown (Table 7.2); these were the HLA genes and

beta-2 microglobulin (B2M) (Table 7.1), which are components of the MHC class I complex (Neefjes et al., 2011).

Some genes involved in autophagy were regulated by WAC knockdown alone. However, there was no consistent trend of up or down regulation. For example WIPI1, VAMP3 and LC3B were downregulated upon WAC depletion, whereas VMP1 and WIPI2 were upregulated. It was good to see that LC3B came out as specifically regulated by WAC as predicted by my qRT-PCR data (Figure 3.4 and Figure 3.6). The unpredictable effects on autophagy genes highlights the importance of statistical analysis of the dataset rather than hand-picking favourite genes. Nonetheless, it was still possible that WAC modulates autophagy by affecting the expression of a cluster of genes that regulate autophagy, that are not well known autophagy proteins. With this in mind the 551 genes downregulated specifically by WAC knockdown were cross-referenced with Nicole McKnight's genome-wide screen for novel autophagy regulators (Table 7.1) (McKnight et al., 2012). Genes that were downregulated after WAC knockdown, and in the top quarter of the genome-wide screen, i.e. those that had a tendency to decrease GFP-LC3 spot formation after knockdown, were given a 'Yes' value in Table 7.1. This was used for a further validation of the microarray results, which will be described in Chapter 3.3.5.

Interestingly, 319 genes were commonly affected by knockdown of WAC, RNF20 or RNF40 versus RISC free control (Figure 3.8 and Table 7.3). Of these 319 genes, 18 were differentially regulated by knockdown of WAC, RNF20 or RNF40 (highlighted red in Table 7.3). For example the target may be increased in knockdown of WAC and RNF20 but be decreased in knockdown of RNF40. Reassuringly, 301 out of the 319 genes moved in the same direction (up or downregulated) upon knockdown of the 3 complex members (shown in black in Table 7.3). These 301 genes likely provide a high-confidence list of transcripts regulated by the WAC/RNF20/40 complex as a whole. It is unlikely that these common genes are due to an off-target effect of any one siRNA. Whether these genes are directly regulated by the WAC/RNF20/40 complex, or are secondary effects of knockdown of the complex, would need to be determined by another technique such as chromatin immunoprecipitation followed by DNA sequencing (ChIP-seq).

Of these 301 genes, 183 were downregulated after knockdown and 118 were upregulated. These groups were taken for pathway analysis. Genes involved in mitosis were significantly downregulated (data not shown). However, no other pathways were significantly affected. To gain more information from the gene lists, they were taken for transcription factor pathway analysis. This was to ascertain whether genes that are controlled by particular transcription factors were significantly enriched in the 118 up (Table 7.4) or 183 downregulated (Table 7.5) gene lists. This analysis has its limitations, for example c-Myc targets were both significantly enriched in the up and downregulated gene lists. Some target groups appeared specific though. For example, genes regulated by SMAD proteins were significantly upregulated after knockdown of WAC/RNF20/40. Whereas targets of the Glucocorticoid receptor alpha were significantly decreased. It was reassuring to see that p53 target genes and p53 itself, were significantly reduced after knockdown of WAC/RNF20/40 as expected (Table 7.3 and Table 7.5).

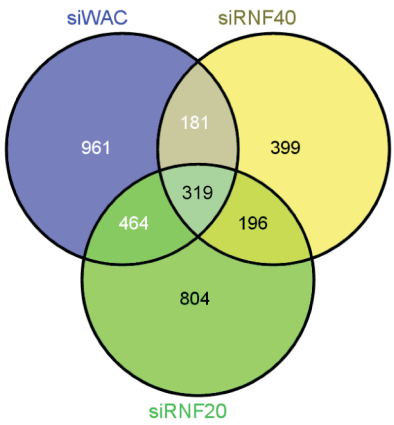

Figure 3.8 Number of genes significantly up or down regulated upon depletion of WAC, RNF20 or RNF40

Venn diagram showing genes that are significantly ($p \leq 0.05$) affected (either upregulated or downregulated) upon knockdown of WAC (blue), RNF20 (green) or RNF40 (yellow) for 72 hr versus the RISC free control in HEK293A cells. 1,925, 1,095 and 1,783 genes were significantly affected (either upregulated or downregulated) upon depletion of WAC, RNF40 or RNF20 respectively. 319 genes were commonly affected by knockdown of WAC, RNF20 or RNF40. For more information, (including direction of regulation, fold change and p-values) about genes uniquely affected by WAC knockdown (961 genes) and those commonly affected by knockdown of WAC, RNF20 or RNF40 (319 genes) see Table 7.1 and Table 7.3 respectively.

3.3.5 Validation of microarray data

As mentioned above, it was still possible that WAC modulates autophagy by affecting the expression of autophagy regulating genes that are not well characterised. Furthermore, a subset of autophagy regulating genes, rather than the pathway in general may be affected. Thus, I began validating hits from the microarray dataset by qRT-PCR. I focused on the 551 genes uniquely downregulated after WAC knockdown (Table 7.1). This is because RNF40 knockdown did not affect autophagic flux (Figure 3.5). The first gene I investigated was VAMP3, which was one of the most potently downregulated genes (-1.9 fold versus RISC free) after WAC knockdown and it is involved in autophagosome formation (Puri et al., 2013). Puri et al. showed VAMP3 is involved in the fusion of Atg16L1 and Atg9 membrane carriers which may form precursor membranes for autophagosome formation. Knockdown with siRNA WAC-03 resulted in a decrease VAMP3 message in both basal and starvation conditions (Figure 3.9a). As expected knockdown of WAC with 3 different siRNAs, -02, -03 and -04 reduced WAC protein levels (Figure 3.9b). However only WAC-03 siRNA reduced VAMP3 protein levels. Therefore VAMP3 is likely to be an off-target effect of the WAC-03 siRNA and regulation of VAMP3 by WAC does not explain WAC's effect on autophagy.

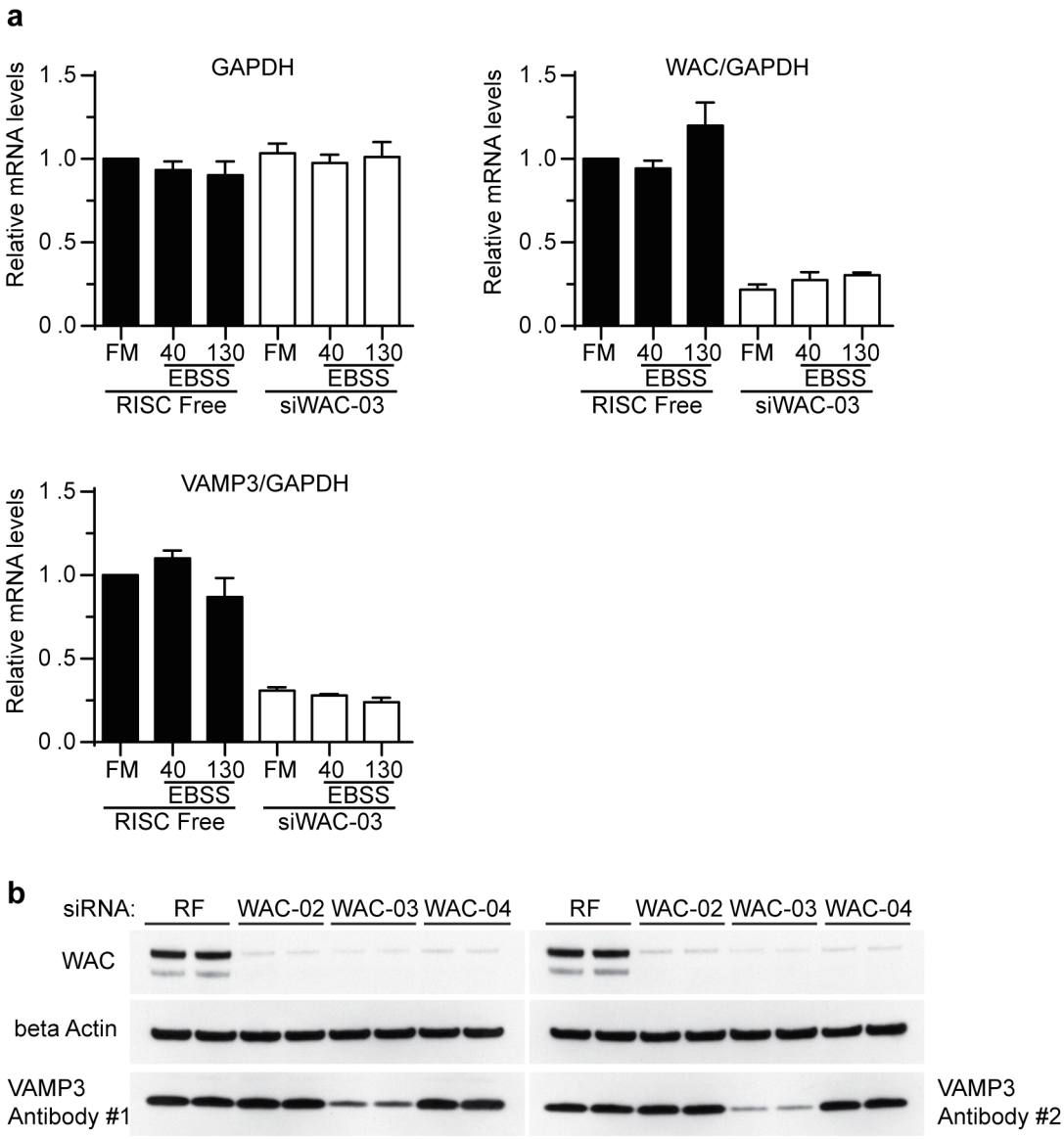

Figure 3.9 VAMP3 depletion is an off-target effect of WAC siRNA treatment

(a) HEK293A cells were treated with the specified siRNA for 72 hours, maintained in full medium or incubated in EBSS or 40 or 130 minutes followed by analysis by qRT-PCR for the indicated gene targets. Mean ± SEM from 3 independent experiments. **(b)** HEK293A cells were treated with the specified siRNA for 72 hours followed by immunoblot. Experiment performed once.

For further validation I decided to take a different approach. 551 genes downregulated after WAC knockdown were too numerous to validate by qRT-PCR and so I had to filter the dataset in some rational way. These 551 genes were cross-referenced against Nicole McKnight's siGenome screen as explained above (Table 7.1). This resulted in 145 genes which were both downregulated by WAC knockdown in my microarray and were putative positive regulators of autophagy based on the genome-wide screen. 44 of these 145 genes were highly significantly downregulated ($p \leq 0.005$) after WAC knockdown. LC3B did not remain after this filtering process. From this list of 44 genes, genes which were unlikely to be directly involved in autophagy were removed. This was done in a biased manner manually based first on UniProt annotations. For example if a gene was involved in translation or transcription, and thus may have affected expression of the GFP-LC3 readout in the genome-wide screen, this was removed. The list of 44 genes were then referenced against the autophagy interaction network (Behrends et al., 2010), to see if they were putative interactors of autophagy proteins. Genes which also caused cell death in the genome-wide screen were also removed, as these may indirectly stimulate the autophagy stress response. After this process 22 genes were taken for qRT-PCR analysis (Figure 3.10). mRNA expression was measured in HEK293A cells treated with WAC-02 or WAC-03 siRNA (Figure 3.10), whereas in the microarray a pool of WAC-03 and -04 siRNAs were used. As expected knockdown of WAC message had no effect on GAPDH expression levels (Figure 3.10a). 6 genes were not reduced by WAC depletion with either WAC-02 or -03 siRNAs (Figure 3.10b), suggesting that these may be off-target effects of WAC-04 siRNA from the microarray. 8 genes were likely off-target effects of the WAC-03 siRNA (Figure 3.10c). 8 genes were reduced after knockdown with both WAC siRNAs (Figure 3.10d) suggesting that these are on-target effects of WAC knockdown and genes that are specifically controlled by WAC independently of RNF20/40. A description of these on-target genes is given in Table 3.1.

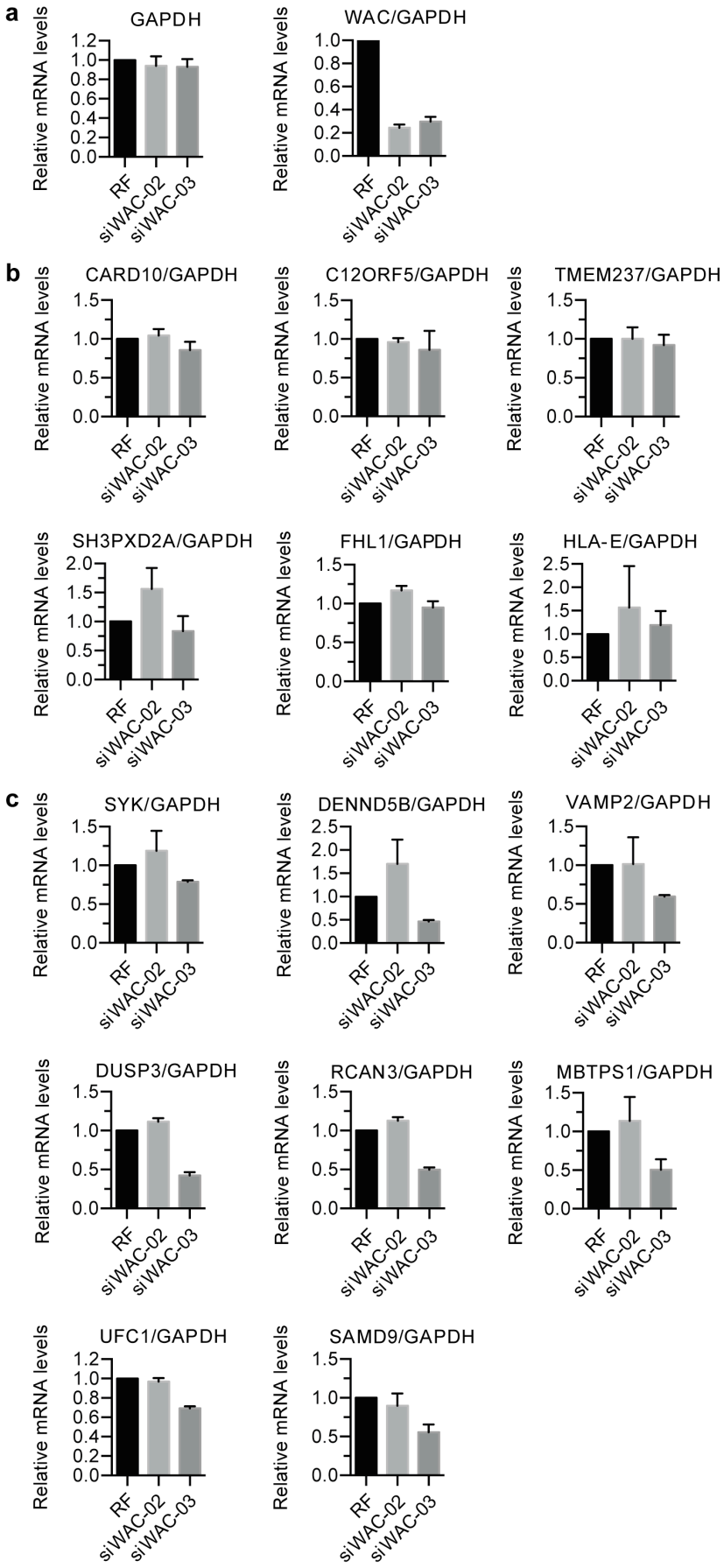
a
GAPDH
WAC/GAPDH
b
CARD10/GAPDH
C12ORF5/GAPDH
TMEM237/GAPDH
SH3PXD2A/GAPDH
FHL1/GAPDH
HLA-E/GAPDH
c
SYK/GAPDH
DENND5B/GAPDH
VAMP2/GAPDH
DUSP3/GAPDH
RCAN3/GAPDH
MBTPS1/GAPDH
UFC1/GAPDH
SAMD9/GAPDH
Relative mRNA levels
RF
siWAC-02
siWAC-03

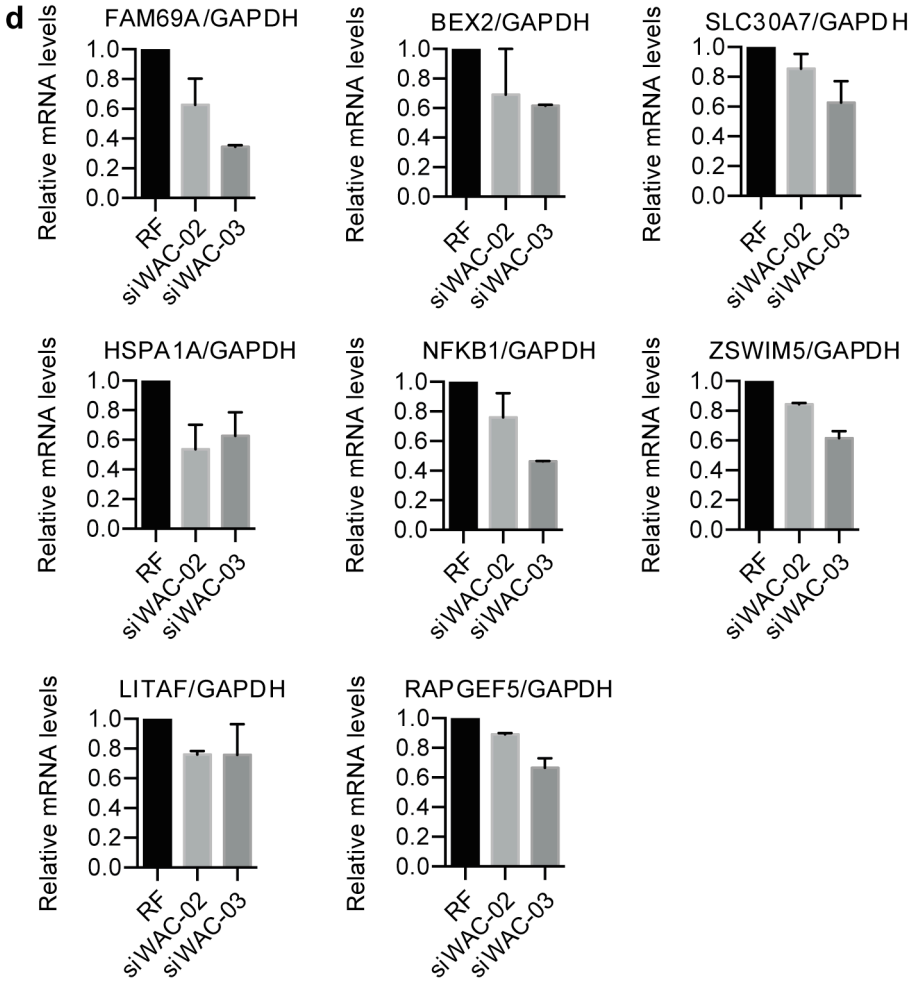

Figure 3.10 qRT-PCR validation of candidates from microarray

(a-d) HEK293A cells were treated with the specified siRNA for 72 hours followed by analysis by qRT-PCR for the indicated gene targets. Mean ± SD, biological triplicates from one experiment. **(a)** Efficacy of WAC siRNAs for WAC knockdown and effects on the 'housekeeping' gene GAPDH. **(b)** 6 transcripts did not recapitulate the results of the microarray analysis. **(c)** 8 transcripts were affected by WAC siRNA -03 only. **(d)** 8 transcripts were affected by both WAC-02 and -03 siRNAs and may be 'on-target' effects of WAC knockdown.

Gene	Description (UniProt annotation)	Published role in autophagy?
SLC30A7	Golgi membrane protein. Zinc transporter.	
RAPGEF5	GEF for RAP1A, RAP2A and MRAS.	
ZSWIM5	Uncharacterised.	
NFKB1	Pleiotropic transcription factor. Activating and repressing functions.	Yes. Inducer of BECN1 and p62 expresison. But also repressive function. (Fullgrabe et al., 2014)
LITAF	Lysosomal.	Colocalises with LC3. Positive regulator. (Bertolo et al., 2013)
FAM69A	ER transmembrane protein. Uncharacterised.	
BEX2	Positive regulator of BCL-2	BCL-2 inhibits Beclin1 in autophagy (Pattingre et al., 2005)
HSPA1A	Also known as HSP70. Protein chaperone. Interacts with TSC2.	Binds Beclin1-VPS34 complex and (indirectly) mediates SUMOylation of Vps34. Positive Role. (Yang et al., 2013)

Table 3.1 Putative autophagy regulating genes positively regulated by WAC independently of RNF20/40

Genes from Figure 3.10d are shown.

3.3.6 WAC function in histone ubiquitination does not require interaction with RNF40

The microarray analysis and qRT-PCR validation demonstrates that WAC regulates the expression of genes independently of RNF20/40. This could be through a direct function of WAC or a secondary effect of WAC depletion. This leads to the hypothesis that these WAC specific effects are also independent of the physical interaction between WAC and RNF20/40. To probe this, I made and used a double point mutant of WAC (I626S and L629S) that does not bind to RNF40, in rescue experiments. An explanation of the design of this mutant, along with evidence that it does not bind RNF40 is shown in Chapter 4.4.3.

Overexpression of EGFP-WAC was not sufficient to drive H2B monoubiquitination at lysine 120 in one experiment (Figure 3.11a), although expression of the ISLS mutant may increase it. The specificity of H2B ubiquitination

was shown by treatment with the drug 5,6-dichloro-1-β-D-ribofuranosyl-1H-benzimidazole (DRB) which inhibits CDK9 activity and therefore is thought to prevent phosphorylation of RNAP, recruitment of the WAC/RNF20/40 complex and H2B ubiquitination (Zhang and Yu, 2011). Depletion of WAC severely impaired H2B ubiquitination as expected (Figure 3.11b and c) and this was fully rescued by expression of siRNA resistant EGFP-WAC full length (aa1-647). However removal of the WAC C-terminal coiled-coil domain (EGFP-WAC aa1-610), ablated the rescue activity of WAC, suggesting that the coiled-coil domain is required for WAC's epigenetic function. However, surprisingly, the ISLS mutant, which does not bind RNF40, was able to fully rescue H2B ubiquitination. This is unlikely to be explained by RNF20, as RNF20/40 function as an obligate heterodimer (they stabilise one another) and knockdown of one member prevents H2B monoubiquitination (Shema et al., 2011, Karpiuk et al., 2012) (Zhang and Yu, 2011). This goes against the published model of WAC's function in the nucleus (Figure 1.10). These data suggest that WAC can promote epigenetic modification, and presumably activate transcription, without interacting with RNF20/40 but by promoting H2B monoubiquitination via another mechanism.

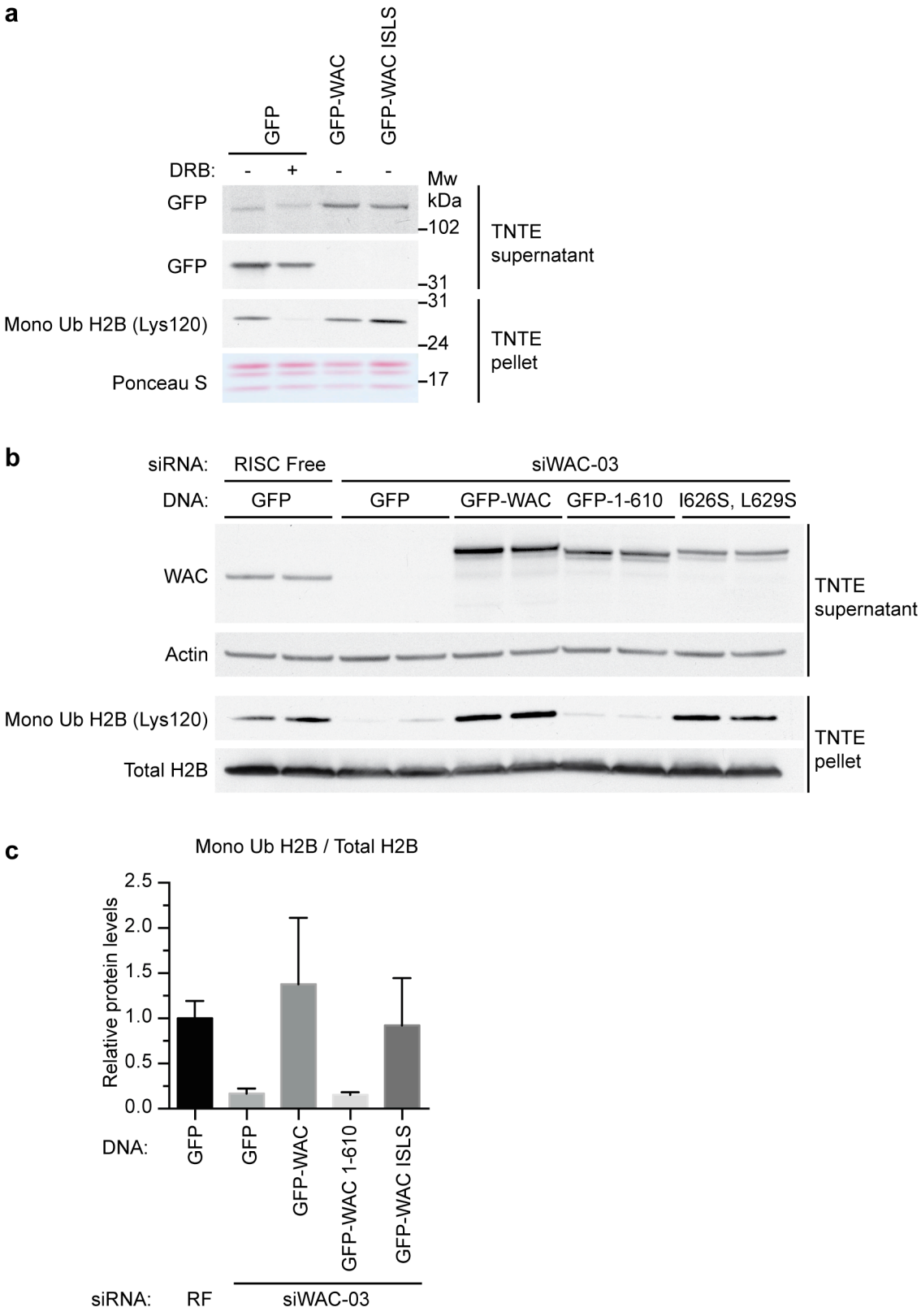
a
GFP
GFP-WAC
GFP-WAC ISLS
DRB: - + - -
Mw kDa
GFP
GFP
Mono Ub H2B (Lys120)
Ponceau S
102
31
31
24
17
TNTE supernatant
TNTE pellet
b
siRNA: RISC Free siWAC-03
DNA: GFP GFP GFP-WAC GFP-1-610 I626S, L629S
WAC
Actin
Mono Ub H2B (Lys120)
Total H2B
TNTE supernatant
TNTE pellet
c
Mono Ub H2B / Total H2B
Relative protein levels
2.5
2.0
1.5
1.0
0.5
0.0
DNA: GFP GFP GFP-WAC GFP-WAC 1-610 GFP-WAC ISLS
siRNA: RF siWAC-03

Figure 3.11 The interaction of WAC with RNF20/40 is not required for WAC-mediated H2B monoubiquitination at lysine 120

(a) HEK293A cells expressing the indicated construct were treated with 50 μM DRB for 4 hours or an equivalent volume of DMSO prior to immunoblot. Experiment was performed once. **(b)** HEK293A cells treated for 72 hours with the indicated siRNA were transfected with the specified constructs prior to immunoblot. **(c)** Quantification of **(b)** mean ± SD from 2 independent experiments.

3.4 Discussion

The majority of WAC present in the cell is localised to the nucleus, with only a small amount of WAC likely to be on the Golgi (Figure 3.2). Thus, an investigation of how WAC could affect autophagy cannot ignore the nuclear function of the WAC protein. The data presented in this chapter suggest that the first 162 amino acids of WAC control localisation to the nucleus, whereas the C-terminal half of WAC, which also contains a putative nuclear export signal (NES) (Figure 3.1), directs WAC's cytoplasmic localisation and association with membranes. Perhaps removal of the nuclear localising region of the WAC protein allows the NES to dominate, and shifts the equilibrium between nuclear import and export. How WAC associates with membranes is unknown, but as WAC has no transmembrane domain, some associated factor may recruit WAC to membranes. WAC has no nuclear localisation signal, however it may be that binding of WAC to RNA polymerase II facilitates its localisation to the nucleus. Binding of WAC to RNF20/40 is not required for WAC's nuclear retention, as removal of the C-terminal coiled-coil domain has no effect on nuclear localisation.

The qRT-PCR and microarray data presented here confirms that WAC controls the expression of genes, as previously demonstrated (Zhang and Yu, 2011). WAC, RNF20 and RNF40, which form a complex together with Rad6 that drives H2B monoubiquitination, also regulate a set of genes together, which could be direct targets of the complex. For example this complex promotes the expression of p53 and also of p53 target genes. It would be interesting to see if WAC, via modulation of p53, could act as a tumour suppressor gene. Of note, RNF20 may function as a tumour suppressor gene (Shema et al., 2008). This dataset provides for the first time a genome-wide list of transcripts regulated by the complex as a whole and by

WAC alone. However, most of the changes observed were quite modest, and effects on protein expression would also have to be validated separately in future studies. Perhaps surprisingly, there was a paucity of genes clustered into biological processes regulated by the WAC/RNF20/40 complex. However, bioinformatic analysis suggests that the complex may be involved in regulating transcription factor pathways such as SMAD or glucocorticoid receptor targets. Future studies could probe the functional relevance of this. Interestingly, almost as many genes were upregulated after knockdown of the complex members, as were downregulated (Shema et al., 2008). On first glance this may be surprising as H2B monoubiquitination is an epigenetic mark that is generally associated with active transcription, and is thought to promote transcriptional elongation by RNA polymerase II after the transcription start (Zhang and Yu, 2011). However, previous microarray analysis after RNF20 knockdown revealed a significant number of genes that were upregulated (Shema et al., 2008). These RNF20-suppressed genes were associated with increased H2B monoubiquitination. Thus it may not be surprising that some genes are repressed by the WAC/RNF20/40 complex and this could be due to its function in H2B monoubiquitination.

A large number of genes (961) may be regulated (551 positively, 410 negatively) by WAC independently of RNF20 and RNF40. This is in line what has been published for RNF20, where knockdown reduced the expression of ~3% of genes in HeLa cells and a similar percentage was upregulated (Shiloh et al., 2011, Shema et al., 2008). It should be mentioned though, that the WAC unique/specific gene set is less reliable then the gene set common to the whole complex. This may be because there are a significant number of hits that are off-target effects, which can only be discerned by further validation. Nevertheless, this suggests that WAC could regulate gene expression (e.g. LC3B) through some non-canonical, i.e. RNF20/40 independent, mechanism. The observation that WAC may promote the expression of antigen presentation genes is worthy of further investigation. Here I have focused more on the genes activated by WAC, in the search of autophagy promoting genes. However, it is also possible that WAC suppresses a negative regulator of autophagy, and therefore functions as a positive regulator. A non-canonical mechanism for WAC function in transcriptional regulation is supported by the discovery that the interaction of WAC with RNF40 is somehow not required for its role in H2B ubiquitination. It could be that the interaction of WAC with RNF20/40

per se is not required for H2B ubiquitination, but the function of the E3 ligase can be stimulated by WAC in an indirect manner by affecting another factor such as the E2 Rad6. Whether the ISLS WAC mutant interacts with Rad6 has not been determined. Alternatively, WAC may also activate some other E3 ligase that mediates H2B monoubiquitination at Lysine 120, which has yet to be identified. It would be interesting to see if the genes regulated by WAC independently of RNF20/40 also require WAC's RNF20/40 binding-independent function in H2B ubiquitination.

WAC's effect on autophagy is likely to be independent of RNF40, and is therefore unlikely to be explained by effects on p53 expression. WAC affected LC3B expression but none of the other Atg8 proteins were identified in the microarray. This specific effect on LC3B is unlikely to explain WAC's effect on autophagy due to the redundancy of the Atg8s (Weidberg et al., 2010). WAC does not simply effect LC3B expression but is required for autophagy flux in general (McKnight et al., 2012), this is investigated in greater detail in Chapter 5. The transcriptomic analysis reveals that WAC is not a broad or master regulator of autophagy gene expression, and is not a regulator of related processes such as lysosome function. Genes related to autophagy were affected in an unpredictable manner. Thus I would hypothesise that WAC's effect on autophagy may be due to its cytoplasmic function, rather than its control of gene expression. I cannot however completely rule out some effect of WAC on autophagy from its nuclear localisation. For example, WAC promotes the expression of at least 3 genes that promote autophagy (NFKB1, LITAF and HSPA1A) and 5 other genes which are possible autophagy regulators. The next steps in future studies addressing this would be to confirm similar effects on protein expression levels, effects on functional readouts of those proteins and that WAC is resident on those genetic loci.

Chapter 4. Identification of GM130 as a WAC binding partner and mapping the WAC-GM130 interaction

4.1 Introduction and aim

4.1.1 Introduction

The mechanisms by which WAC and GM130 exert their effects on autophagy are unknown. Although WAC promotes transcription through its nuclear function (Zhang and Yu, 2011), transcriptomic analysis (Chapter 3) suggests that WAC is neither a potent nor a broad regulator of autophagy gene expression. WAC's other known subcellular location is the Golgi where it interacts with VCP/p97, via the deubiquitinase VCIP135, to mediate Golgi complex reassembly post-mitosis (Totsukawa et al., 2011). VCP is a hexameric AAA ATPase that functions as a chaperone with unfoldase or segregase activity (the disassembly of protein complexes) and has been implicated in pathologies such as inclusion body myopathy with Paget's disease of bone and frontotemporal dementia (IBMPFD) and amyotrophic lateral sclerosis (ALS) (Yamanaka et al., 2012, Meyer et al., 2012). Through binding cofactors, VCP controls various cellular functions such as endoplasmic reticulum (ER), Golgi and nuclear envelope reassembly and ER-associated protein degradation (ERAD). VCP and its yeast homologue Cdc48 both positively regulate autophagy (Krick et al., 2010, Tresse et al., 2010), and VCP has been shown to mediate the selective degradation of depolarised mitochondria by autophagy, induced by the E3 ubiquitin ligase Parkin (Tanaka et al., 2010). Yeast Cdc48 is thought to promote phagophore elongation and autophagosome formation (Krick et al., 2010). In light of this, it is possible that WAC affects autophagy via modulation of VCP function. However, unlike its yeast homologue Cdc48, mammalian VCP promotes autophagosome maturation under basal conditions. In VCP depleted cells, or cells overexpressing a dominant-negative mutant of VCP, there was an accumulation of immature autophagosomes with ubiquitinated contents (Tresse et al., 2010). In contrast, WAC promotes autophagy initiation (McKnight et al., 2012) and ULK1 activation (Chapter 5); this phenotypic disconnect suggests a mode of action of WAC that is independent of VCP.

A number of autophagy machinery proteins are regulated at the Golgi complex (see Chapter 1.1.3). Thus, I postulated that WAC could affect autophagy through undiscovered interactions at the Golgi. In addition, the Golgi is also thought to directly contribute membranes to the forming phagophore (Biazik et al., 2015) and because WAC affects Golgi membrane fusion, it is possible that membrane flow from the Golgi to the phagophore could be altered in WAC depleted cells. This remains to be investigated and has not been addressed in my study.

Depletion of GM130 was found to induce autophagy (Chang et al., 2012). It was suggested that this was due to a loss of ER-to-Golgi transport and protein glycosylation. However, treatment with the drug Brefeldin A, which results in the disassembly of the Golgi complex and loss of protein secretion and glycosylation (Misumi et al., 1986), is thought not to affect autophagic flux (Weidberg et al., 2010, Nishida et al., 2009, Zoppino et al., 2010). Therefore, there may be an alternative outstanding explanation for GM130's effects on autophagy.

4.1.2 Aim

In order to further characterise the function of WAC in autophagy I began by carrying out an immunoprecipitation (IP) approach coupled with mass spectrometry to identify novel WAC interactors. To this end, I generated a HeLa stable cell line carrying a bacterial artificial chromosome (BAC) containing the human WAC gene (CTD-2309I17, Life Technologies) tagged at the C-terminus with a FLAP tag (WAC-FLAP) (Figure 4.3). The FLAP tag consists of FLAG-TEV site-S-peptide-3C site-EGFP (Figure 4.3a). It is named the FLAP tag because it is a localisation and affinity purification (LAP) tag with FLAG. The FLAP tag was added onto the C-terminus of WAC by homologous recombination (Figure 4.1), as the construct is too large to engineer by traditional cut-and-paste cloning. This was carried out using a previously described method (Poser et al., 2008) and the Quick & Easy BAC Modification Kit from Gene Bridges. I also attempted to generate N-terminally tagged FLAP-WAC, however this resulted in a truncated protein product. The WAC BAC contained the entire WAC gene (91 kb, UCSC Genome Browser) including introns and exons as well as large upstream and downstream regions, more than 10 kb either side. This means that the WAC-FLAP should be expressed under the

control of the WAC promoter and (short-range) regulatory elements and spliced into isoforms. As BACs normally integrate in the host genome as single or low copy number (Poser et al., 2008), this should mean that WAC-FLAP is spliced as different isoforms and expressed at near or below endogenous levels. Thus, this system circumvents problems associated with protein overexpression, such as mislocalisation and aberrant interactions, and provides a tractable way to modify genes with large tags. One disadvantage of BACs versus other technologies such as CRISPR is that protein expression levels are subject to the locus of integration of the BAC in the host genome, this can be somewhat ameliorated by screening multiple clones to identify the 'normal' expression level independent of integration locus (Figure 4.2).

The experimental design was to IP endogenous WAC from HEK293A cells and to also IP WAC-FLAP using GFP-Trap® (Chromotek) from HeLa cells, followed by analysis of protein complexes by mass spectrometry (Figure 4.4). The resulting datasets were then intersected to find proteins that bound to WAC and also to WAC-FLAP but not to the control (beads and lysate). One advantage of this approach is that it is high stringency, in the sense that proteins that non-specifically cross-react with either the WAC or the GFP antibody should be filtered out. This strategy proved to be fruitful, as I had attempted to validate endogenous WAC interactors only to conclude that they non-specifically bound to the WAC-antibody (data not shown). Another advantage of this strategy is that cell type specific interaction partners should be reduced, in order to focus on interactions with a broader biological meaning. It is also worth noting that a disadvantage to this technique is the possibility of false negatives, for example if fusion of the FLAP tag to the WAC C-terminus inhibits some subset of interactions, or if there are interactions specific to particular WAC isoforms.

4.2 Generation of a WAC-FLAP cell line

4.2.1 Modification of WAC BAC with a FLAP tag by homologous recombination

E. coli harbouring a BAC that contains your genomic locus of interest can be obtained commercially from Life Technologies. The UCSC genome browser can be used to map BACs to your genomic region of interest before ordering. In this case the BAC (clone identification: CTD-2309I17) contains the WAC gene (Figure 4.1). These bacteria are then transformed with a plasmid (pRed/ET) that encodes for recombinases. At 30^{o}C the pRed/ET plasmid can replicate. Concurrently, the FLAP tag should be prepared. A number of BAC tagging vectors are available, designed by the Tony Hyman Lab in Dresden, Germany. To tag the C-terminus of a gene with the FLAP tag, the R6Kamp-FLAP plasmid can be used as a template for PCR amplification. In order to target the FLAP tag to the C-terminus of your gene, regions of homology must be incorporated into your PCR product. Both the forward and reverse primers, designed to amplify the FLAP tag, contain 50 bp of homology to the WAC gene as shown by overhangs in Figure 4.1. This allows for precision in the site of integration. The primers are designed so that the FLAP tag is inserted before the stop codon of the WAC gene in exon 14 (the last exon of WAC isoform 1, UCSC genome browser and Ensembl). This is true in the case of WAC isoforms 1, 2 and 4 (UniProt nomenclature), which should therefore become tagged. However WAC isoform 3 uses a different stop codon and therefore should not be tagged. It is not clear if isoform 3 is even stable as it is predicted to be degraded by nonsense mediated decay (Ensembl).

E. coli transformed with pRed/ET and containing your BAC can now be induced to express recombinases by the addition of L-arabinose to the growth medium and by shifting the temperature from 30^{o}C to 37^{o}C. Although pRed/ET stops replicating at this temperature, because each cell should have multiple copies, it will be retained for at least a few division cycles. After this, the FLAP tag PCR product is electroporated into these bacteria to allow the recombination reaction to occur. The FLAP tag itself contains a neomycin/kanamycin resistance gene for selection in mammalian/bacterial cells respectively. Thus recombined

BACs can be selected for and subsequently screened. The design of the FLAP tag is quite elegant. The EGFP sequence within the FLAP tag has been split into 2 exons, with the intervening intron containing the antibiotic resistance gene (Neo/Kan) under the control of a PGK promoter and gb2 promoter for eukaryotic and bacterial expression respectively. In my experience it was very difficult to sequence directly from the BAC as a template, perhaps due to the DNA secondary structure of the large construct. Therefore it was necessary to sequence PCR products of the recombination region to identify the final modified WAC-FLAP BAC.

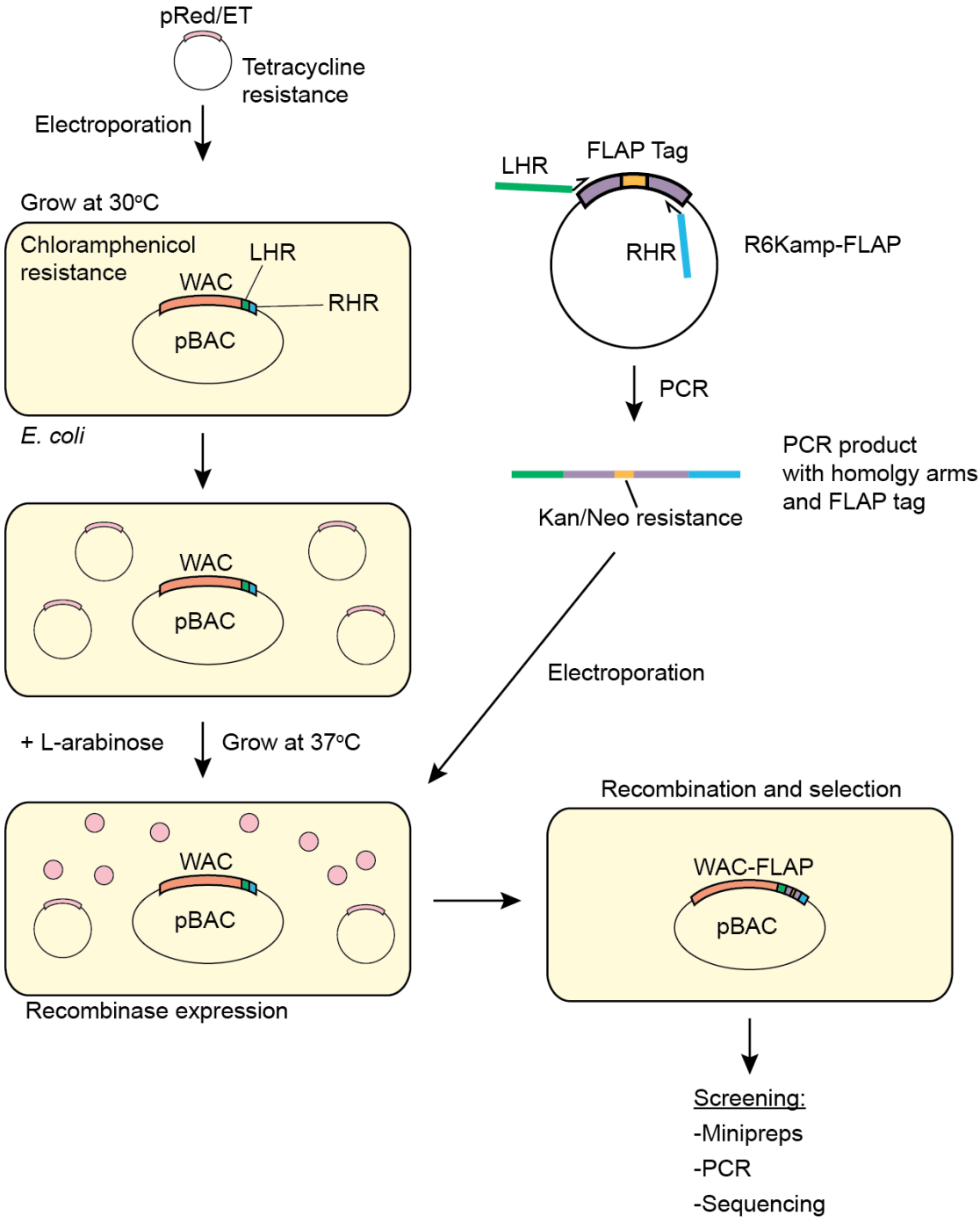

Figure 4.1 Recombineering of bacterial artificial chromosomes

Flow diagram showing steps to modify a BAC by homologous recombination. Left homology region, LHR; right homology region, RHR.

4.2.2 Generation of HeLa WAC-FLAP BAC cell line

After generation of the modified BAC, I then produced a stable cell line. HeLa, MEF and HEK293A cells were transfected with the WAC-FLAP BAC using Effectene transfection reagent (Qiagen) and the protocol developed by Ina Poser (Poser et al., 2008) (Figure 4.2). I was unable to isolate cells expressing full length WAC-FLAP in the case of MEFs and HEK293A cells. With HEK293A cells, spontaneous resistance to G418 developed during selection, even with control transfected cells. This is a problem that has been encountered in other labs (personal communication, Mark Petalcorin). However, I was successful in the case of HeLa cells. I also transfected HeLa cells with N-terminally tagged FLAP-WAC BAC.

After transfection, cells were selected in a high concentration of G418, the surviving colonies were pooled together and taken for FACs sorting. Forward and side scatter was first used to gate out doublet cells and cells with unusually high granularity. Analysis of fluorescence in two different channels, as shown in Figure 4.2, allows the exclusion of autofluorescent cells, which would lie on a gradient of 1 on the graphs shown. Cells with detectable EGFP were single-cell sorted into 96-well plates and kept under selection with a low concentration of G418. Clones were analysed by confocal microscopy. Some of these clones were unsuitable for generation of a cell line. These ‘bad’ clones had undesirable features such as high expression and/or heterogeneous expression. This could be due to genetic instability or the incorrect sorting of more than one cell into a well. ‘Good’ clones had low and homogenous expression and in addition these cells had similar morphological characteristics to wild-type HeLa cells.

Next, it was necessary to check that the expressed tagged protein was translated at the expected size and not truncated or degraded. HeLa cells expressing N-terminally tagged FLAP-WAC or C-terminally tagged WAC-FLAP were used for FLAG immunoprecipitation followed by western blotting with anti-GFP (Figure 4.2). Endogenous WAC (isoform 1) migrates with a molecular weight of around 80 kDa by SDS-PAGE (Figure 4.3d). However, FLAP-WAC was only expressed as a truncated product of around 55 kDa. This is unlikely to be due to instability induced by tagging because EGFP-WAC expresses at full length (Figure

4.6e). Instead this could be due to some recombination event within the BAC itself. Clearly FLAP-WAC was unsuitable for cell line generation. However, FLAP-WAC localised to the nucleus just like WAC-FLAP (data not shown). This suggests that the first 200aa (estimated) of the WAC protein (647aa) is sufficient to target WAC to the nucleus as expected (Figure 3.2).

WAC-FLAP was expressed as four bands all approximately the right size to be full-length protein (Figure 4.2). The largest 3 of these bands can be accounted for by tagged versions of the WAC isoforms 1, 2 and 4 as explained above. However, the presence of a smaller fourth band is interesting; this could be a post-translationally modified form of one of the isoforms. Alternatively, this could be evidence of expression of another WAC isoform (UniProt accession A0A0A0MRT2). There is currently no experimental evidence of expression of this isoform (mRNA or expressed sequence tag) but it is nonetheless predicted. A0A0A0MRT2 is predicted to be protein coding (Ensembl), is of the correct size to account for the lowest of the four bands and should also be tagged as it contains exon 14.

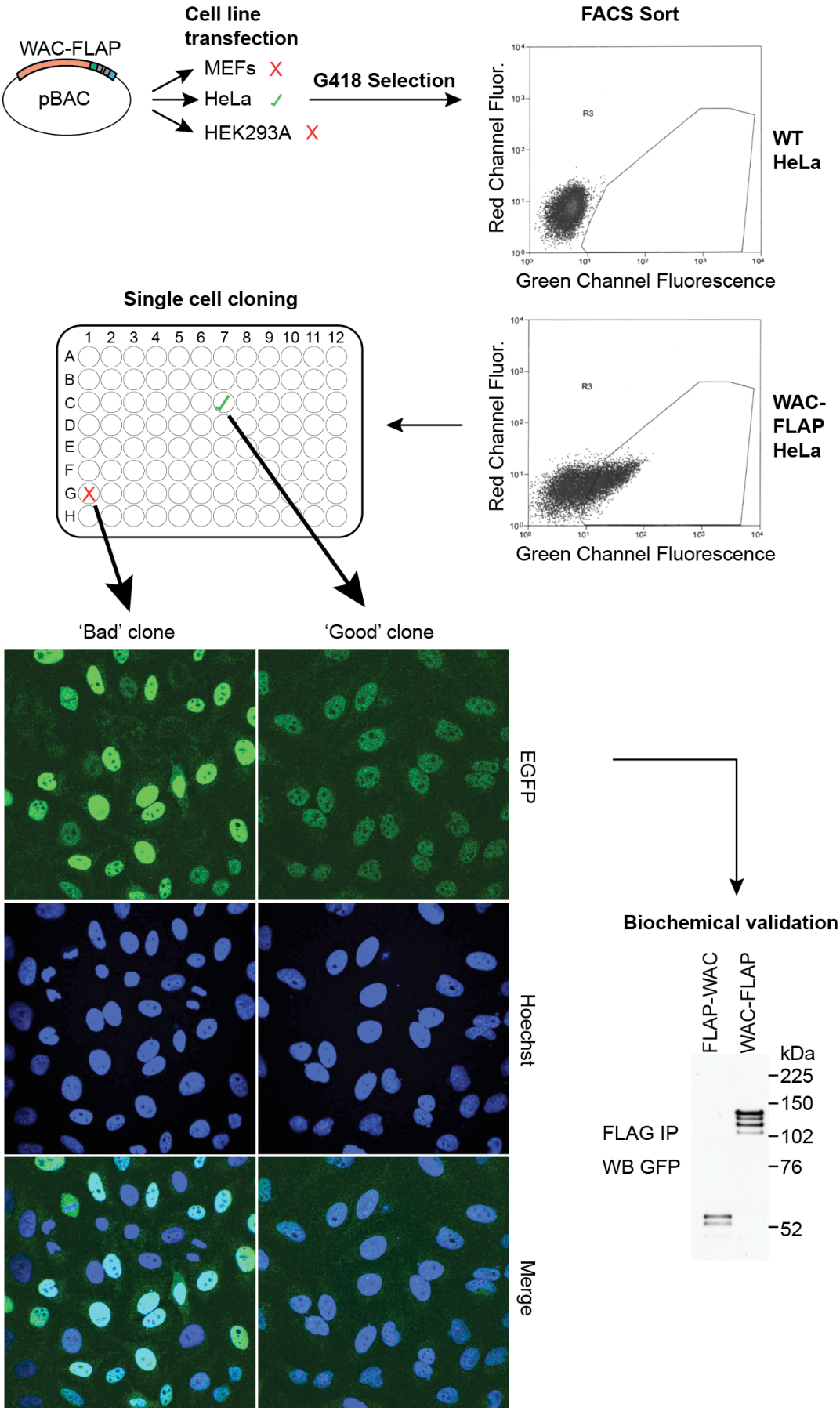
WAC-FLAP
pBAC
Cell line transfection
MEFs X
HeLa ✓
HEK293A X
G418 Selection
FACS Sort
Red Channel Fluor.
Green Channel Fluorescence
R3
WT HeLa
WAC-FLAP HeLa
Single cell cloning
1 2 3 4 5 6 7 8 9 10 11 12
A
B
C
D
E
F
G
H
'Bad' clone
'Good' clone
EGFP
Hoechst
Merge
Biochemical validation
FLAP-WAC
WAC-FLAP
kDa
225
150
102
76
52
FLAG IP
WB GFP

Figure 4.2 Transfection, selection and cloning of HeLa WAC-FLAP cell line

Schematic depicting stable cell line generation. FACS plots show 10,000 events per cell line. FACS sorting was carried out by Andy Filby. Fluorescence units are arbitrary. Confocal microscopy, immunoprecipitation and SDS-PAGE analysis was used to screen clones.

4.2.3 Validation of HeLa WAC-FLAP BAC stable cell line

Before using the WAC-FLAP cell line as a tool to identify novel WAC interactors, it was necessary to establish that WAC-FLAP behaved similarly to the endogenous WAC protein. Immunoblot analysis revealed that WAC-FLAP HeLa cells expressed tagged WAC isoforms 1 and 4 near to endogenous WAC protein levels (Figure 4.3b). Because BACs integrate in the host genome at usually single copy number (Poser et al., 2008) I expected to see expression of WAC-FLAP at a lower level than the endogenous WAC protein and indeed this was the case. The epitope used to generate the anti-WAC antibody is present only in isoforms 1 and 4, therefore only these can be detected.

Staining HeLa WAC-FLAP cells with anti-GFP and anti-GM130 antibodies, and comparing against wild-type control HeLa cells, revealed that WAC-FLAP localised both to the nucleus and to the Golgi apparatus as previously described for endogenous WAC (Totsukawa et al., 2011) (Figure 4.3c). Because WAC-FLAP is expressed at low levels under the control of the WAC promoter, I could not observe Golgi localised WAC by assessing EGFP fluorescence alone, thus it was necessary to stain WAC-FLAP cells with anti-GFP antibody. Even after staining, the signal was too low to detect by confocal microscopy and so the thicker z-sectioning of epifluorescence microscopy was required to enhance the signal.

Complementary to microscopy analysis, subcellular fractionation showed that WAC-FLAP isoforms 1 and 4 associated with a crude membrane extract and with a nuclear fraction, to a similar extent as the endogenous isoforms 1 and 4 (Figure 4.3d). Cytosolic WAC was not detected. These results were expected as membrane association of WAC has also been shown before by subcellular fractionation (Totsukawa et al., 2011). The transmembrane autophagy protein Atg9, which localises to the trans-Golgi network and endosomal system (Young et al., 2006), was used a marker for the membrane fraction. Superoxide dismutase (SOD1) was used as a marker for the cytosol, and a component of the nuclear

lamina, Lamin B, was used to identify the nuclear pellet. Only a small percentage (an estimated ≤ 10%) of WAC isoforms 1 and 4 localise to membranes both in WAC-FLAP HeLa and HEK293A cells (Figure 4.3d and e), with the majority of WAC being within the nucleus. This may explain why nuclear WAC-FLAP but not Golgi WAC-FLAP, could be detected without staining with anti-GFP antibody (Figure 4.2). One limitation of this fractionation technique is the presence of residual intact cells in the nuclear pellet as seen by Atg9 and SOD1 in this fraction. This is because a balance must be made during homogenisation of whole cells, too little results in insufficient plasma membrane breakage, too much risks damaging the nuclei and releasing nucleoplasmic proteins.

Immunoprecipitation of WAC-FLAP using GFP-Trap beads followed by western blotting with anti-GFP showed that WAC-FLAP interacted with the known WAC interaction partner RNF40 (Zhang and Yu, 2011) (Figure 4.3f). RNF40 binds the WAC C-terminal coiled-coil domain. Thus, at least in this instance, the C-terminal FLAP tag does not interfere with interactions at the C-terminal WAC coiled-coil domain. In conclusion, using a range of assays WAC-FLAP behaves similarly to the endogenous WAC protein and could be used to investigate WAC interactions and other biological functions of the WAC protein.

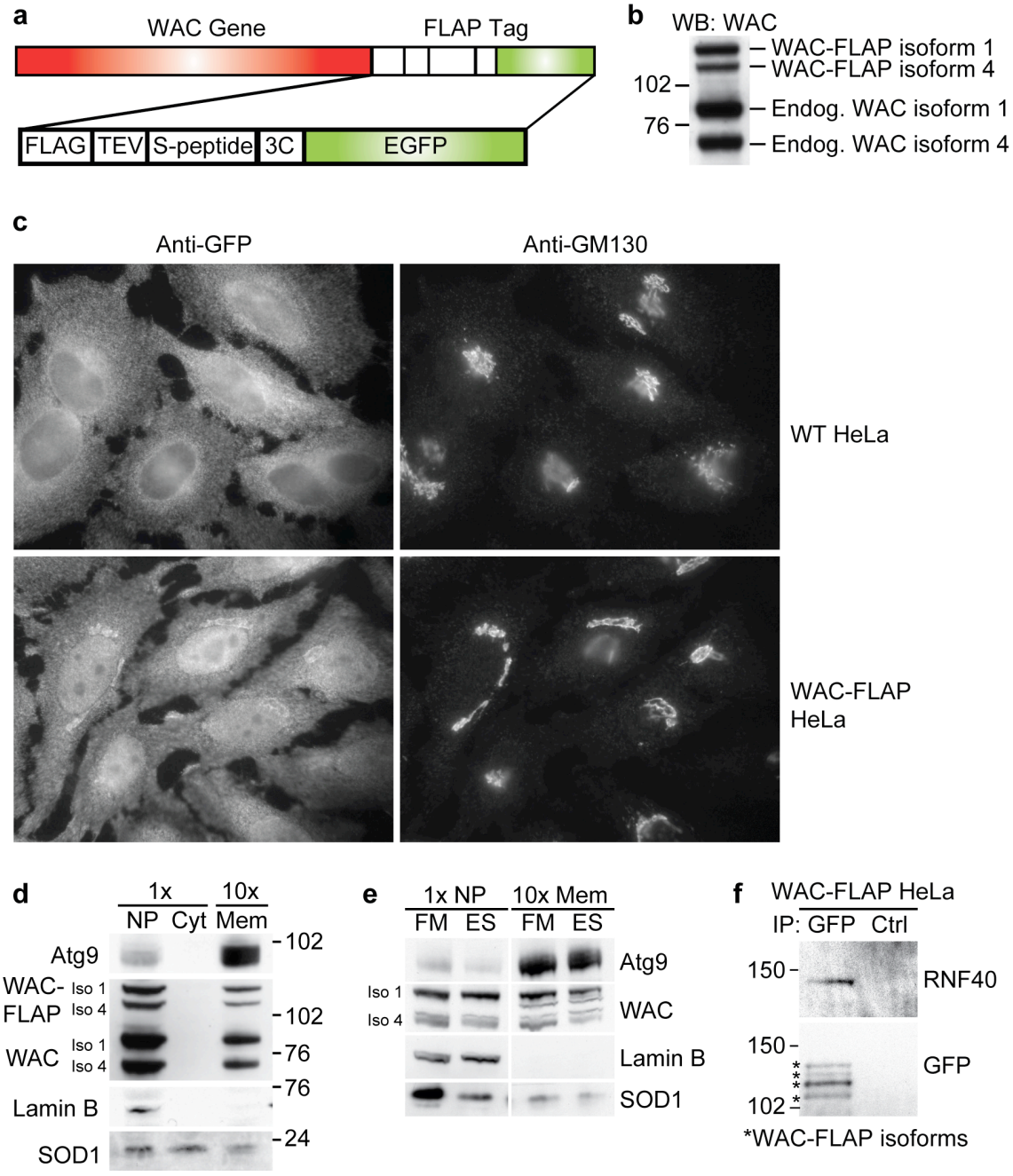
a
WAC Gene
FLAP Tag
FLAG
TEV
S-peptide
3C
EGFP
b
WB: WAC
WAC-FLAP isoform 1
WAC-FLAP isoform 4
102
76
Endog. WAC isoform 1
Endog. WAC isoform 4
c
Anti-GFP
Anti-GM130
WT HeLa
WAC-FLAP HeLa
d
1x
10x
NP
Cyt
Mem
Atg9
WAC-FLAP
Iso 1
Iso 4
WAC
Lamin B
SOD1
102
102
76
76
24
e
1x NP
10x Mem
FM
ES
FM
ES
Atg9
Iso 1
Iso 4
WAC
Lamin B
SOD1
f
WAC-FLAP HeLa
IP: GFP
Ctrl
150
RNF40
150
102
GFP
*WAC-FLAP isoforms

Figure 4.3 Validation of HeLa WAC-FLAP cell line

(a) Schematic of the WAC-FLAP BAC. TEV protease cleavage site, TEV; PreScission protease cleavage site, 3C. **(b)** WAC-FLAP HeLa lysate was analysed by SDS-PAGE and western blot. WAC antibody recognises isoforms 1 and 4 due to epitope position. **(c)** WT HeLa and WAC-FLAP HeLa cells were analysed by epifluorescence microscopy after staining with the indicated antibodies. **(d)** WAC-FLAP HeLa cells were homogenised before subcellular fractionation by differential centrifugation and analysis by SDS-PAGE and western blot. Membranes were loaded as a 10x concentrate compared to other fractions. Nuclear pellet, NP; cytosol, Cyt; membrane, Mem. **(e)** HEK293A cells were incubated in full medium (FM) or starvation medium EBSS (ES) for 2 hours prior to subcellular fractionation and western blotting. Nuclear pellet, NP; membrane, Mem. **(f)** Lysates from WAC-FLAP HeLa cells were subjected to GFP-Trap followed by SDS-PAGE and western blotting. Blocked agarose beads with lysate was used as a control (Ctrl). Markers indicate molecular weight in kilodaltons. Experiments shown were performed once.

4.3 Identification of GM130 as a novel WAC interactor by mass spectrometry

4.3.1 Experimental design of co-immunoprecipitation coupled with mass spectrometry

As outlined in the aims section of this chapter, my experimental plan was to immunoprecipitate WAC from HEK293A cells and compare these protein complexes with those from WAC-FLAP HeLa cells (Figure 4.4). The relative advantages/disadvantages of this approach have also been discussed.

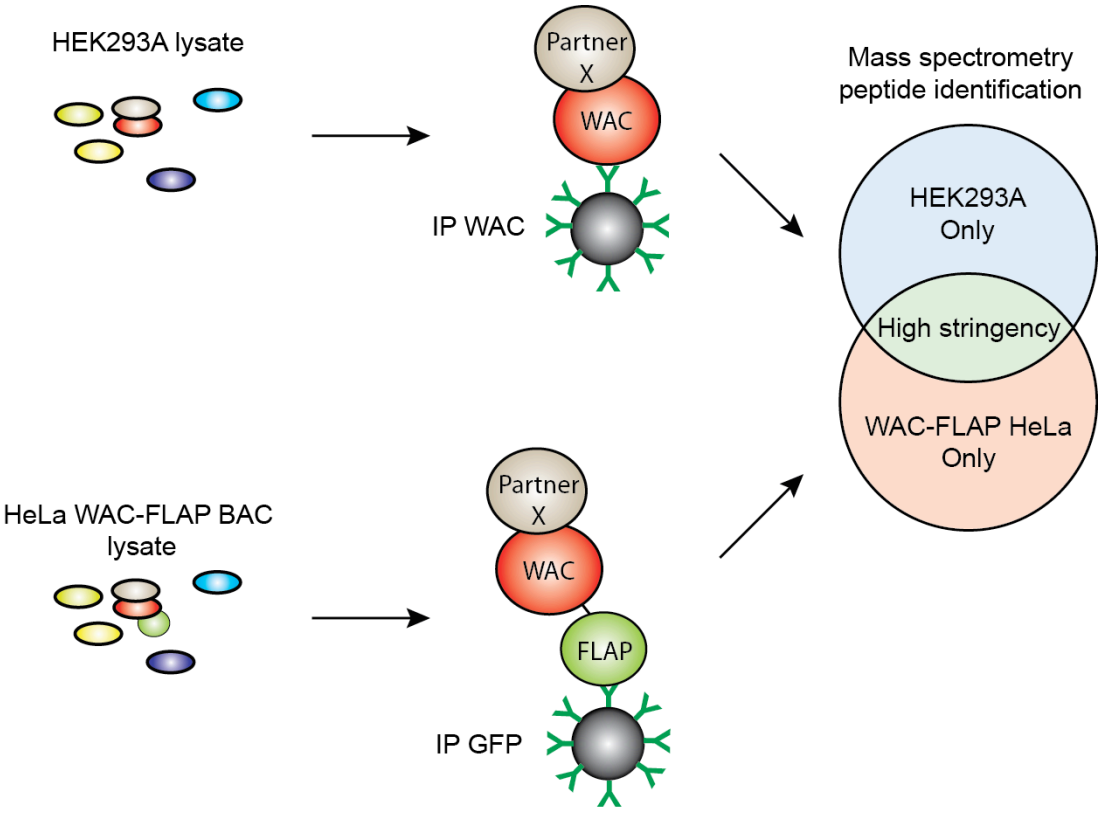

Figure 4.4 Experimental design of immunoprecipitation coupled to mass spectrometry

4.3.2 Analysis of mass spectrometry datasets to reveal high stringency WAC interactors

HEK293A cells or HeLa WAC-FLAP cells (not shown) were maintained in full medium or starved in EBSS for 2 hours prior to lysis and anti-WAC or anti-GFP immunoprecipitation (Figure 4.5a and b). Protein complexes were ran on SDS-PAGE gels before MeOH and glacial acetic acid fixation and staining with colloidal Coomassie. The gels were only ran for a short time and each lane was cut into bands and submitted for LC-MS mass spectrometry analysis (by David Frith and Bram Snijders, see Chapter 2.3.9 for method). The bands predicted to be WAC and the known interacting proteins RNF20 and RNF40, which are of similar size, are indicated (Figure 4.5a). The efficacy of immunoprecipitation was confirmed by Western blot analysis of supernatants after pull-down (Figure 4.5b).

After mass spectrometry the datasets were analysed as follows (Figure 4.5c, d and e). There were only small differences in the proteins identified between fed and starved samples (data not shown), and so the comparison was carried out between fed samples (HEK293A versus WAC-FLAP HeLa). Intensity based absolute quantification (iBAQ) was used as a label-free quantitative method to analyse WAC interactors (Schwanhausser et al., 2011, Fabre et al., 2014). The advantage of iBAQ is that I could distinguish between high abundance and low abundance WAC interactions, without the need for generating a labelled cell line such as with SILAC (Stable Isotope Labelling by Amino acids in Cell culture). The drawback with iBAQ quantification is that you cannot prove a true negative. If your protein of interest is missing in one sample, it may be that by chance the peptide was not detected in that particular case. With SILAC, heavy and light labelled samples are mixed, injected and compared together, which means true negatives can be established. More specifically, the atomic weight of the amino acid *per se* does not affect the hydrophobicity or therefore retention time during high-performance liquid chromatography (HPLC). So identical heavy and light peptides should fly together during mass spectrometry. The absence of either the heavy or light peptide will be apparent from mass. Nonetheless, iBAQ is still a useful technique. During iBAQ the sum of the all the observed peptide intensities is normalised to the number of observable peptides of a protein. This means that if 1

peptide is found from a very small protein this is scored much more highly than 1 peptide identified from a very large protein. This is a simplification though as the analysis is influenced by the tryptic digest pattern of a particular protein, not just the size.

The table in Figure 4.5 shows that 19 proteins, including WAC, were pulled down from both HEK293A and HeLa WAC-FLAP cells. These 19 proteins were filtered from the original list of 1,536 identified proteins. The 18 interactors identified were only in the experiment (both WAC and WAC-FLAP immunoprecipitation) but not the control. Extra information is given in the table to aid interpretation of the data. The posterior error probably (PEP) is a measurement of how reliable the peptide identification is: the smaller the number the smaller the possible error. The intensity column shows the sum of the observed signal intensities from the two datasets. As a further quality parameter, CRAPome frequencies are displayed http://www.crapome.org/ (Mellacheruvu et al., 2013). The CRAPome is a database of common contaminating proteins found in affinity purification mass spectrometry experiments. Where multiple gene names are given in the same row, these are either alternative names for the same gene, or the genes may be so similar that the identified peptides may belong to any of them.

As expected, nuclear and Golgi proteins, as described by UniProt annotations, were identified as WAC interactors: RNF20, RNF40, UBE2A, PRPF40A, WTAP, RBM15, MCM4, THOC2 (nuclear) and GOLGA2, ERC1, RAB1 and MYO18A (Golgi). As a validation of the technique known WAC interactors were identified, these were RNF20, RNF40 and UBE2A. UBE2A (Rad6) is the E2 ubiquitin-conjugating enzyme that acts in conjunction with the RNF20/40 E3 ubiquitin ligase complex (Zhang and Yu, 2011).

In particular, I chose to focus on GM130 (GOLGA2) as a novel WAC interactor, because GM130 affects autophagy via an unknown mechanism (Chang et al., 2012). Furthermore, multiple GM130 peptides were identified in both experiments. The iBAQ values (Figure 4.5d and e) suggest that WAC-RNF20-RNF40 exists as a stoichiometric complex. This supports the suggestion that WAC-RNF20-RNF40 exists as a 2:2:2 heterohexameric complex (Zhang and Yu, 2011). The WAC-GM130 interaction is likely to be substoichiometric.

It should be mentioned that Golgi-localised WAC interactors VCIP135 (direct) and VCP/p97 (indirect) were not identified as WAC interactors in my hands,

even in the individual datasets (IP WAC or IP WAC-FLAP) before intersection. This may be because I did not have exogenous ATP in my buffer, whereas these interactions were originally studied in the presence of ATP (Totsukawa et al., 2011). As VCP is an ATPase, this could possibly affect conformation and interactions. Alternatively, WAC-VCIP135-VCP may occur at a very low incidence.

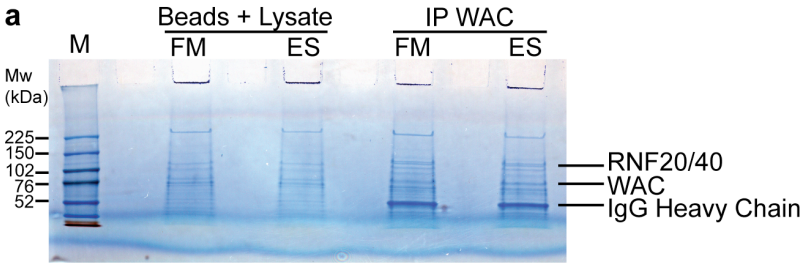

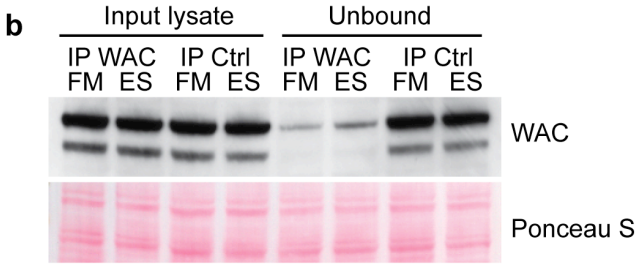

c

Gene names	PEP	Intensity	Unique peptides Ctrl	Unique peptides IP WAC	Unique peptides Ctrl	Unique peptides IP WAC-FLAP	Crapome Num of Expt. (found/total)
RNF20	0	1.05E+12	0	65	0	52	27 / 411
RNF40	0	9.78E+11	0	35	0	33	19 / 411
WAC	0	3.51E+11	0	23	0	19	14 / 411
ERC1	5.30E-116	1.11E+08	0	21	0	1	44 / 411
GOLGA2	4.68E-28	9.31E+08	0	6	0	3	26 / 411
ADD2	1.89E-28	2.04E+10	0	5	0	1	12 / 411
PRPF40A	8.18E-09	8.03E+07	0	2	0	1	76 / 411
CYTSA;SPECC1L	9.85E-210	4.73E+10	0	1	0	20	17 / 411
WTAP	2.52E-214	1.94E+10	0	1	0	7	41 / 411
RBM15	6.52E-57	1.80E+10	0	1	0	9	40 / 411
UBE2A	2.29E-09	1.65E+10	0	1	0	1	
PSRC1	0.0014697	6.91E+09	0	1	0	2	
RAB1A;RAB1B;RAB1C	1.99E-08	6.39E+09	0	1	0	2	69 / 411
MYO18A	3.99E-34	5.42E+09	0	1	0	7	11 / 411
MCM4	4.76E-05	8.24E+08	0	1	0	2	113 / 411
EGFR;ERBB4;ERBB2	4.41E-05	7.47E+08	0	1	0	1	16 / 411
THOC2	1.96E-10	1.38E+08	0	1	0	1	64 / 411
MAP7D1;RPRC1	1.30E-07	1.38E+07	0	1	0	1	24 / 411
NACA;hCG_2016482	5.59E-07	2.65E+05	0	1	0	1	125 / 411

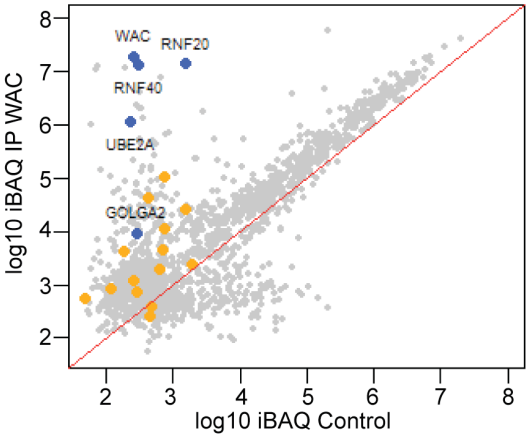

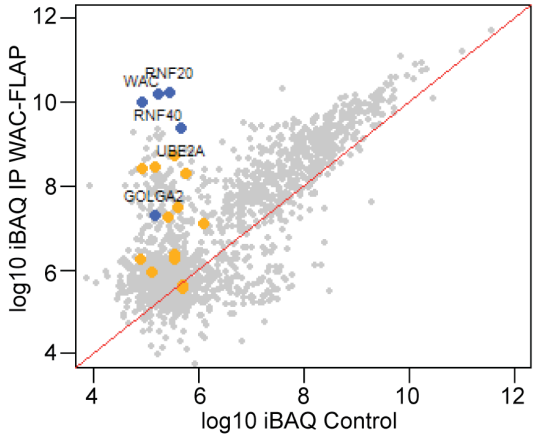

Figure 4.5 Immunoprecipitation of WAC complexes and mass spectrometry peptide identification

(a) HEK293A cells were incubated with full medium (FM) or starved in EBSS (ES) for 2 hours. Lysates were incubated with protein G beads or with protein G beads plus anti-WAC antibody. Immunoprecipitated complexes were eluted followed by SDS-PAGE and colloidal Coomassie staining. Fixed gel slices were processed for mass spectrometry analysis by David Frith. Markers (M) shown in kilodaltons. **(b)** Western blot of lysates from **(a)** before and after immunoprecipitation. **(c)** Table displaying high stringency WAC interactors after filtering mass spectrometry datasets from HEK293A cells and HeLa WAC-FLAP cells. WAC and previously published interactors are highlighted in blue, GM130 (GOLGA2) is highlighted in orange. Posterior error probability, PEP. Data analysis performed by Bram Snijders. **(d, e)** Intensity based absolute quantification (iBAQ) values of identified proteins after immunoprecipitation of WAC from HEK293A cells **(d)** or immunoprecipitation of WAC-FLAP from HeLa cells **(e)**. 19 proteins from table **(c)** are shown as blue or orange dots. WAC, published interactors and GM130 are shown as blue dots. Experiments shown were performed once.

4.4 Validation of mass spectrometry data and mapping the WAC-GM130 interaction

4.4.1 WAC interacts with COPI and with GM130

After analysis of the mass spectrometry datasets I wanted to validate interactions by co-immunoprecipitation and western blotting. When analysing the unfiltered mass spectrometry data I noticed that a COPI coatomer subunit, alpha-COP, was clearly enriched in pull-downs from HEK293A and HeLa WAC-FLAP cells (Table 4.1). The alpha-COP peptides did not meet the mass spectrometry filtering criteria in Figure 4.5c, as there was some background binding of alpha-COP in the control samples. Nevertheless, I questioned whether WAC could interact with the COPI complex. This relevant because COPI was shown to regulate autophagy by maintaining endosome function and hence is important in the maturation stages of autophagy (Razi et al., 2009). COPI is a vesicle coat protein complex involved in retrograde trafficking (Golgi-to-ER) (Letourneur et al., 1994, Cosson and Letourneur, 1994) and also in bidirectional intra-Golgi transport (Orci et al., 1997, Malhotra et al., 1989). COPI has also been implicated in anterograde transport (Bednarek et al., 1995) and is involved in maintaining the structure of the Golgi apparatus (Guo et al., 1994). I also sought to validate the WAC-GM130 interaction as highlighted before.

	HEK293A cells		HeLa WAC-FLAP cells	
Protein	Unique peptides - Beads and lysate	Unique peptides - IP WAC	Unique peptides - Beads and lysate	Unique peptides - IP GFP
αCOP	3	9	3	13

Table 4.1 alpha COP peptides are enriched in WAC or WAC-FLAP immunoprecipitates

Immunoprecipitation of endogenous WAC from HEK293A cells indicated that WAC interacts with GM130 and with COPI, as shown by detection of another COPI subunit, beta'-COP (Figure 4.6a). In my hands and with our reagents western blot detection of co-immunoprecipitated alpha-COP was unsuccessful. A small amount of beta'-COP was found sticking to the control, whereas GM130 had little background binding. Thus, this experiment essentially replicates the findings of mass spectrometry. It should be noted that WAC interacts only with a very small percentage (estimated at < 5%) of GM130 and beta'-COP, even when the immunoprecipitation of the target (WAC) is efficient.

At this stage I decided to study in greater detail WAC-GM130 interactions, rather than COPI. This was because of the reduced background binding of GM130 versus COPI. More importantly perhaps, was that COPI depletion elicits a maturation defect in autophagy (Tooze and Razi, 2009), and hence is phenotypically dissimilar to WAC (Chapter 5 and (McKnight et al., 2012)).

After starvation of HEK293A cells in EBSS to induce autophagy, I saw a small increase in the amount of co-immunoprecipitated GM130 in WAC pull-downs (Figure 4.6b and c). However, the interaction of WAC with RNF40 did not appear to be regulated by starvation. Densitometry and quantification of 3 experiments revealed that the increase in the WAC-GM130 interaction upon nutrient starvation was statistically significant (Figure 4.6c). In the HeLa WAC-FLAP cells I saw a similar effect from one experiment (Figure 4.6d): the amount of GM130 pulled-down with WAC-FLAP increased upon starvation whereas RNF40 was unaffected.

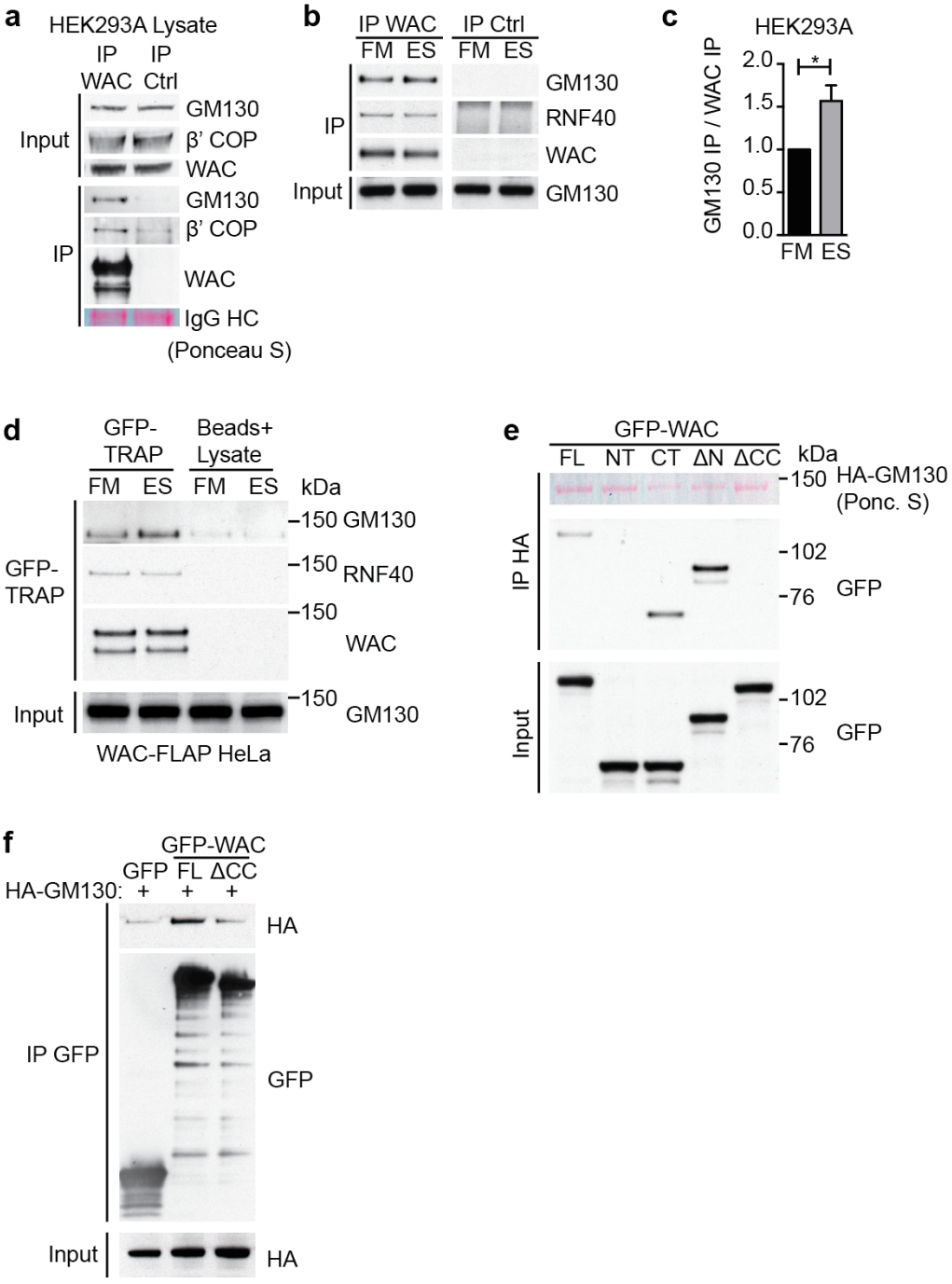
a
HEK293A Lysate
IP WAC
IP Ctrl
Input
IP
GM130
β' COP
WAC
GM130
β' COP
WAC
IgG HC
(Ponceau S)
b
IP WAC
IP Ctrl
FM ES
FM ES
IP
Input
GM130
RNF40
WAC
GM130
c
HEK293A
GM130 IP / WAC IP
2.0
1.5
1.0
0.5
0.0
*
FM ES
d
GFP-TRAP
Beads+ Lysate
FM ES FM ES
kDa
GFP-TRAP
Input
150 GM130
150 RNF40
150 WAC
150 GM130
WAC-FLAP HeLa
e
GFP-WAC
FL NT CT ΔN ΔCC
kDa
IP HA
Input
150 HA-GM130 (Ponc. S)
102
76 GFP
102
76 GFP
f
GFP-WAC
GFP FL ΔCC
HA-GM130: + + +
IP GFP
Input
HA
GFP
HA

Figure 4.6 WAC interacts with GM130 through its coiled-coil domain in a starvation regulated manner

(a) WAC was immunoprecipitated using an anti-WAC antibody from HEK293A cells incubated in full medium before immunoblotting. Anti-GFP was used as control (Ctrl). HC, heavy chain. **(b)** WAC was immunoprecipitated from HEK293A cells before immunoblotting. Anti-GFP was used as control (Ctrl). Cells were maintained in full medium (FM) or EBSS (ES) for 2 hr prior to lysis. **(c)** Quantification of **(b)**, co-immunoprecipitated GM130 was normalised to amount of WAC immunoprecipitated. Statistics were performed using an unpaired Student's t test, *, $p \leq 0.05$. Mean ± SEM from 3 independent experiments. **(d)** Lysates from HeLa cells stably expressing WAC-FLAP were used for GFP-Trap pull-down before immunoblot. Cells were maintained in full medium (FM) or EBSS (ES) for 2 hr prior to lysis. Blocked agarose beads (the same matrix as GFP-TRAP beads) incubated with lysate were used as control. The two WAC bands visible are WAC-FLAP isoforms 1 and 4. Experiment was performed once **(e)** Lysates from HEK293A cells co-transfected with 3xHA-GM130 (rat) and EGFP-WAC (human) full length (FL), aa1-319 (NT), aa320-647 (CT), aa163-647 (ΔN) or aa1-610 (ΔCC) were used for HA immunoprecipitation followed by immunoblot. Experiment was performed once. **(f)** Lysates from HEK293A cells co-transfected with 3xHA-GM130 (rat) and EGFP, EGFP-WAC human full length aa1-647 (FL) or aa1-610 (ΔCC) were used for GFP-Trap pull-down followed by immunoblot. Experiment was performed once.

4.4.2 The WAC coiled-coil domain is required for the interaction with GM130

I next wanted to see which domain(s) of WAC were required for its interaction with GM130. I cloned a series of truncated EGFP-WAC constructs in pEGFP C2 and these are shown in Figure 4.7. These were: EGFP-WAC full length aa1-647 (FL), N-terminal half aa1-319 (NT), C-terminal half aa320-647 (CT), aa163-647 (ΔN) and aa1-610 (ΔCC). The ΔCC truncation removes the highly conserved coiled-coil domain of WAC. The ΔN truncation removes a large section of the WAC N-terminus, up to and including the conserved WW domain of WAC. The rest of the WAC protein is not predicted to contain any known domains and there is no three dimensional structure of WAC (Protein Data Bank). So to make some sort of informed decision on my truncation strategy I used the FoldIndex© tool (Prilusky et al., 2005) (Figure 4.8). The first half of the WAC protein is predicted to be unfolded. Although, presumably incorrectly, the WW domain (aa130-168, InterPro) is predicted to be unfolded, this is probably because the FoldIndex tool does not take into account domains but rather uses hydrophobicity and charge of amino acids. The C-terminal half of WAC is predicted to possess more structure than the first

half and may constitute some sort of functional module. This is why I decided to clone the two halves of WAC.

After immunoprecipitation of 3xHA-GM130 (rat, gift from Joachim Seemann) (Figure 4.6e) I saw that WAC pieces FL, CT and ΔN were all co-immunoprecipitated. Proportionately, in this experiment at least, the CT and ΔN truncation of EGFP-WAC interacted more with 3xHA-GM130 than FL WAC. This may be related to the enhanced ability of these truncations to exit the nucleus (Figure 3.2). NT and ΔCC did not interact with 3xHA-GM130. This suggests that the coiled-coil domain of WAC is required to interact with GM130. In support of this, a reciprocal assay where EGFP-WAC or ΔCC WAC was immunoprecipitated also suggested that the coiled-coil domain of WAC was crucial for interaction with 3xHA-GM130 (Figure 4.6f).

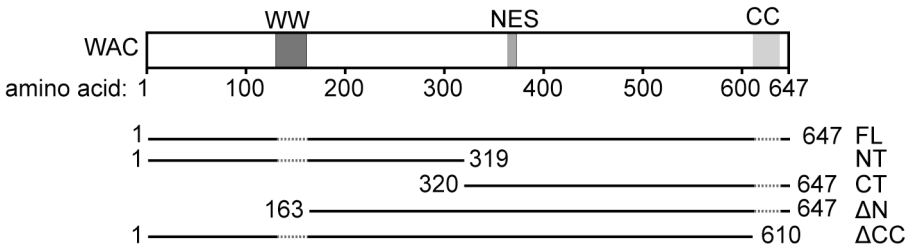

Figure 4.7 Human WAC isoform 1 primary structure and truncation constructs

Boxed regions indicate the highly conserved WW and coiled-coil (CC) domains of WAC. The putative nuclear export signal (NES) of WAC is also shown. The dashed lines in the truncation constructs indicate the positions of the WW and CC domains.

a

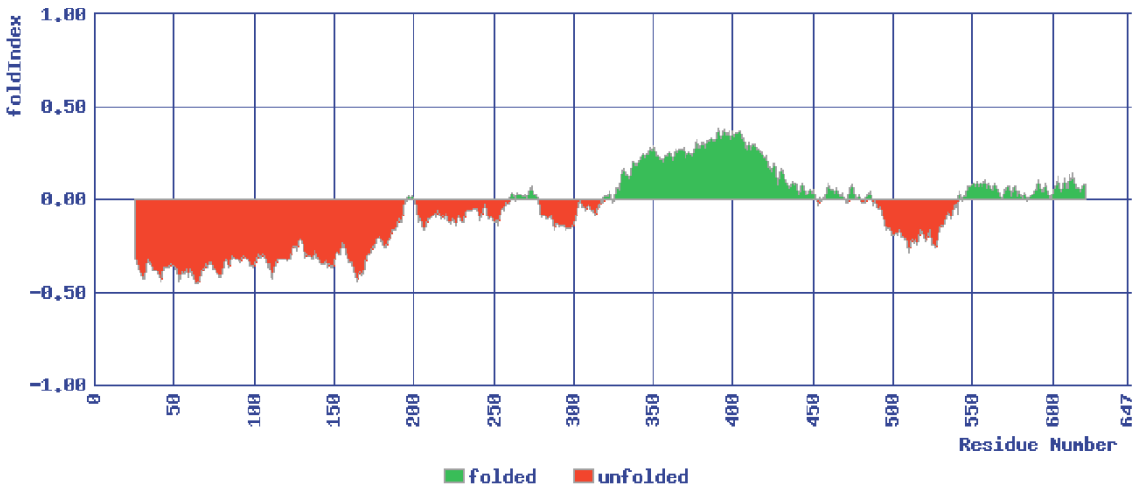

b

```
  1 MVMYARKQQR LSDGCHDRRG DSQPYQALKY SSKSHPSSGD HRHEKMRDAG
 51 DPSPPNKMLR RSDSPENKYS DSTGHSKAKN VHTHRVRERD GGTSYSPQEN
101 SHNHSALHSS NSHSSNPSNN PSKTSDAPYD SADDWSEHIS SSGKKYYYNC
151 RTEVSQWEKP KEWLEREQRQ KEANKMAVNS FPKDRDYRRE VMQATATSGF
201 ASGMEDKHSS DASSLLPQNI LSQTSRHNDR DYRLPRAETH SSSTPVQHPI
251 KPVVHPTATP STVPSSPFTL QSDHQPKKSF DANGASTLSK LPTPTSSVPA
301 QKTERKESTS GDKPVSHSCT TPSTSSASGL NPTSAPPTSA SAVPVSPVPQ
351 SPIPPLLQDP NLLRQLLPAL QATLQLNNSN VDISKINEVL TAAVTQASLQ
401 SIIHKFLTAG PSAFNITSLI SQAAQLSTQA QPSNQSPMSL TSDASSPRSY
451 VSPRISTPQT NTVPIKPLIS TPPVSSQPKV STPVVKQGPV SQSATQQPVT
501 ADKQQGHEPV SPRSLQRSSS QRSPSPGPNH TSNSSNASNA TVVPQNSSAR
551 STCSLTPALA AHFSENLIKH VQGWPADHAE KQASRLREEA HNMGTIHMSE
601 ICTELKNLRS LVRVCEIQAT LREQRILFLR QQIKELEKLK NQNSFMV

 ( Predicted disordered segment )
```

Figure 4.8 FoldIndex© analysis of human WAC isoform 1

(a) Probability plot of ability of the WAC protein to fold. 1=folded, -1=unfolded. **(b)** Primary structure of WAC isoform 1 with predicted ordered (green) and disordered regions (red) highlighted.

4.4.3 Amino acids 611-620 in the WAC coiled-coil domain are necessary but not sufficient for GM130 binding

GM130 and RNF20/40 interact with the WAC coiled-coil domain. RNF20 and RNF40 both contain coiled-coil domains, which bind WAC. Removal of the C-terminal region aa559-647 of WAC resulted in the loss of both RNF20 and RNF40 binding (Zhang and Yu, 2011). I wanted to investigate if GM130 and RNF20/40 bound WAC at the same or different regions and if binding of one required or inhibits the binding of the other. With this aim in mind I designed a series of finer truncations, deletions and mutations of the WAC coiled-coil domain (Figure 4.9c). In addition to the EGFP-WAC aa1-160 (ΔCC) truncation, I cloned aa1-620 and aa1-630. To probe the contribution of the structure of the coiled-coil domain I made the double point mutant I626S and L629S (ISLS mutant). These two residues are conserved from *Drosophila* and reside in the 'a' and 'd' positions of the WAC coiled-coiled domain, in the centre of the predicted coiled-coil region (Figure 4.9d). The 'a' and 'd' positions of a coiled-coil domain are especially important for the structure of coiled-coils. Amino acids at these positions are usually hydrophobic and are buried at the interface between the alpha-helices that form the coiled-coil structure (Burkhard et al., 2001). By mutating these residues to polar serines I hoped to disrupt the structure of the WAC coiled-coil domain, with my functional readout being interactions with RNF40 or GM130.

EGFP-WAC aa1-610 does not bind GM130 (or binds very weakly) but aa1-620 restores the interaction, suggesting that the highly conserved 10 amino acids 611-620 are required for GM130 binding (Figure 4.9a, b and d). However, aa611-647, which includes the entire predicted coiled-coil domain, did not bind GM130. Thus amino acids 611-620 are necessary but not alone sufficient to bind GM130. The ISLS mutation completely ablated WAC binding to RNF40, however binding of GM130 was unaffected. As RNF20/40 directly binds WAC in the nucleus (Zhang and Yu, 2011), this suggests that the WAC-GM130 interaction (presumably on the Golgi), can occur independently of RNF20/40. As a proportion of the input, WAC interacts with much more RNF40 than GM130, as predicted by mass spectrometry (Figure 4.5d and e). All of my coiled-coil domain truncations resulted in the complete loss of RNF40 binding to WAC. This indicates that in addition to I626 and

L629, the adjacent sequence is critical for RNF40 binding. Interestingly, WAC aa611-647 did not bind RNF40 at all.

When taking a closer look at the coiled-coil domain of WAC (Figure 4.9d), I noticed that the domain may actually extend past the predicted region in the N-terminal direction, because amino acids at the 'a' and 'd' positions of heptads still remain hydrophobic. Thus it was suspected that aa611-647 did not contain all of the information to encode for the WAC coiled-coil domain and might not adopt the native conformation. In support of this hypothesis, aa580-647, which includes all possible residues encoding for the WAC coiled-coil domain, binds RNF40 (Figure 4.9b). No binding to GM130 was detected suggesting that RNF40 binding to WAC occurs independently of WAC-GM130 interaction.

One concern I had was that maybe the WAC truncation aa1-610 does not interact with GM130 because too many amino acids have been removed, leading to misfolding of the protein. To help address this, I made more precise deletions of the WAC coiled-coil domain using inverse PCR and PCR SOEing (Splicing by Overlap Extension) (Ho et al., 1989). Inverse PCR uses primers pointing away from each other, in my case on a plasmid template. These primers are designed to exclude the region to be deleted. The resulting linear amplicon is then subjected to intramolecular ligation to restore a circular plasmid with the targeted region removed. In PCR SOEing two PCR products are made of the two halves you want to join together, these are designed to flank the region to be deleted. The primers used to amplify one fragment contain an overhang, which is homologous to the end region of the other fragment, and vice versa. Thus the two PCR products from the first two PCR reactions are now mixed and used as both the primers and template in a third PCR reaction. The resulting amplicon contains the two halves spliced together with the original intervening sequence removed. Using these techniques I removed a 10 amino acid region (Δ611-620) as well as one heptad (Δ612-618) (Figure 4.9b). Removal of one heptad in WAC reduced binding to GM130 and removed binding to RNF40. Deletion of aa611-620 reduced WAC-GM130 binding to greater extent, where only very little binding was observed. Again the RNF40 interaction was lost. These results further confirm the essential 10aa region for GM130 interaction. Although I saw degradation products of GFP-WAC (degraded from the C-terminus) in my GFP-Trap experiments (Figure 4.9a and b) even in the presence of the protease inhibitors (Roche), this does not seem to have altered the

results of the experiment.

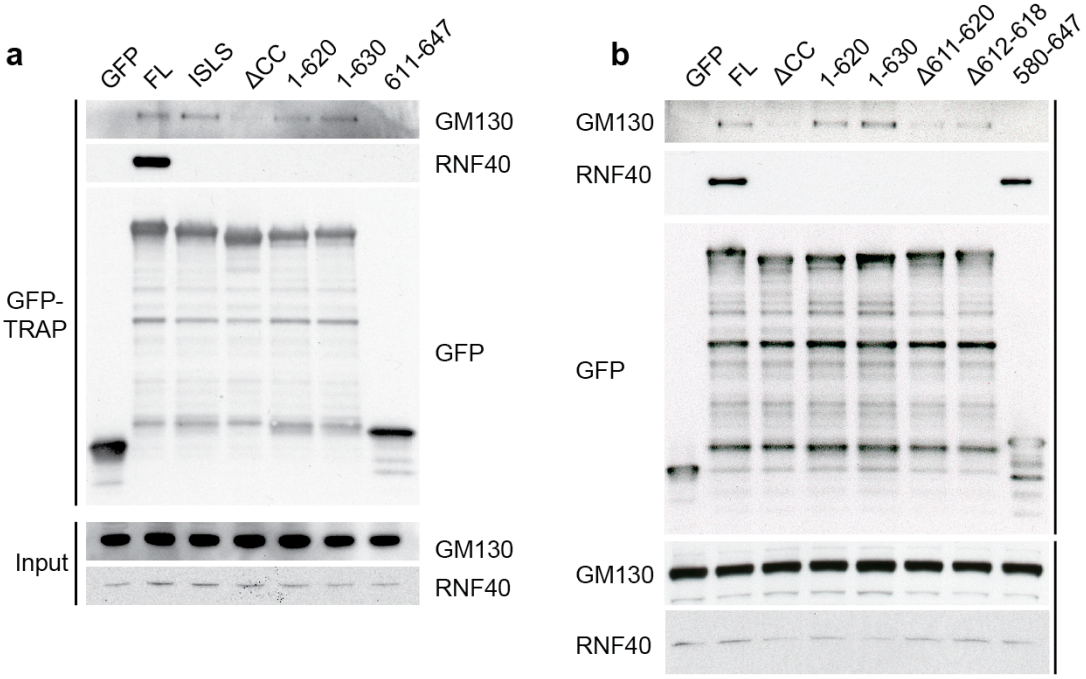

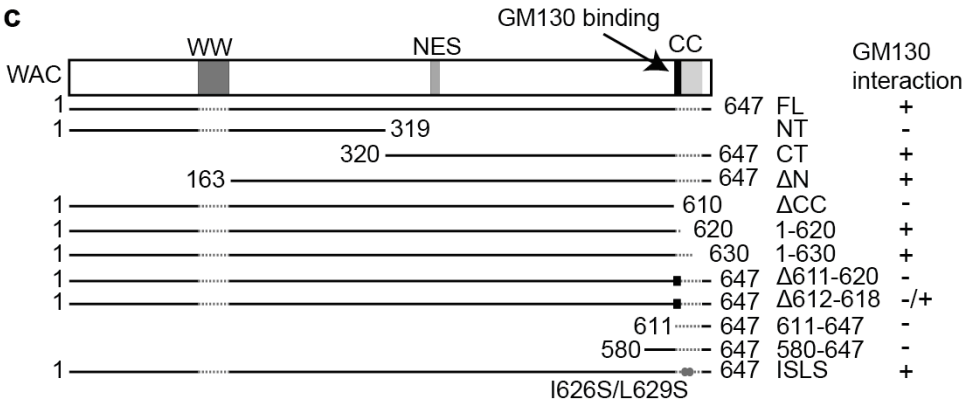

d

```
                                                                  abcdefg abcdefg a
Human     553  CSLTPALAAHFSENLIKHVQGWPADHAEKQASRLREEAHNMGTIHMSEICTELKNLRSLV  612
Rat       552  CSLTPTLAAHFNDNLIKHVQGWPADHAEKQASRLREEAHNMGSVHMSEICTELKNLRSLV  611
Mouse     552  CSLTPTLAAHFNDNLIKHVQGWPADHAEKQASRLREEAHNMGSVHMSEICTELKNLRSLV  611
Chicken   478  CSLTPTLAAHFNENLIKHVQGWPADHAEKQASRLREEAHNMGSVHMSEICTELKNLRSLV  537
Frog      534  CSLTPTLAAYFNENLVKHVQGWPADHAEKQASRLREEAHNMGSIHMSEVCTELKNLRSLV  593
Zebrafish 464  CSFTPTLAAHFNENLIKHVQGWPAEHVEKQASRLREEAHTMGSIYMSENCTELKNLRSLV  523
Fruit fly 737  PEISPKLAKYFRADLIAHVTNWHAEVLERQAQKCCEDTHLFGDITCTRICAELKCARSLV  796
                 .::* ** :*  :*: **  * *:  *:**.:  *::* :* :  :. *:***  ****
                 bcdefg abcdefg abcdefg abcdefg abcdefg a
Human     613  RVCEIQATLREQRILFLRQQIKELEKLKNQNSFMV---                      647
Rat       612  RVCEIQATLREQRILFLRQQIKELEKLKNQNSFMV---                      646
Mouse     612  RVCEIQATLREQRILFLRQQIKELEKLKNQNSFMV---                      646
Chicken   538  RVCEIQATLREQRILFLRQQIKELEKLKNQNSFMV---                      572
Frog      594  RVCEIQATLREQRILFLRQQIKELEKLKNQNSFMV---                      628
Zebrafish 524  RVCEIQATLREQRILFLRQQIKELEKLKNQNSFMV---                      558
Fruit fly 797  RSTEINATLQEQKIMYLRHQIRRIEESKTQNAFMSDDT                      834
               *  **:***:**:*::**:**:.:*: *.**:**
```

Figure 4.9 10 amino acids in the WAC coiled-coil domain are crucial for GM130 interaction

(a) Lysates from HEK293A cells transiently expressing EGFP or EGFP-WAC constructs FL, ISLS, ΔCC, aa1-620, aa1-630 or aa611-647 were used for GFP-Trap pull-down followed by Western blotting. Endogenous GM130 and RNF40 interaction was analysed by immunoblot. **(b)** Lysates from HEK293A cells transiently expressing EGFP, EGFP-WAC FL, ΔCC, aa1-620, aa1-630, Δ611-620, Δ612-618 or aa580-647 were used for GFP-Trap pull-down followed by immunoblot analysis. **(c)** Scheme of human WAC isoform 1 and deletion mutants used for mapping experiments, showing the WW domain, putative nuclear export signal (NES) and C-terminal coiled-coil (CC) domain, which includes the required sequence for GM130 binding. Domains are indicated by dashed lines. GM130 binding ability is summarised on right. Deletion of 10aa region or 7aa heptad is indicated by a black square. Grey circles show ISLS mutations. **(d)** Alignment of protein sequence of human WAC (coiled-coil region) and its orthologues using UniProt. Alignment is using described algorithm (Soding, 2005). Sequences aligned were: Q9BTA9-1 *Homo sapiens*, G3XEV5 *Rattus norvegicus*, Q924H7-1 *Mus musculus*, E1C6W1 *Gallus gallus*, Q5U4Q0 *Xenopus tropicalis*, Q7ZUK7 *Danio rerio*, Q9VX88 (CG8949 isoform A) *Drosophila melanogaster*. Conserved amino acid sequence (*), conservative change (:), semi-conservative change (.), non-conservative change ( ). Coiled-coil region is denoted by heptads assigned abcdefg positions. Green letters show predicted coiled-coil region using the COILS tool (Lupas et al., 1991) a 4-heptad window and a probably of > 0.5. Blue letters show extended heptads that are not predicted by bioinformatics to be coiled-coil but nevertheless possess some of the characteristics of a coiled-coil. Mutated residues for mapping experiments are shown in red.

4.4.4 The WAC coiled-coil domain is required for direct interaction with GM130 *in vitro*

Coiled-coils are protein interaction domains that form direct interactions with coiled-coil domains on other polypeptide chains (Burkhard et al., 2001). The majority of GM130 has predicted coiled-coil structure (Nakamura et al., 1995) and thus it is possible that the predicted WAC coiled-coil domain interacts directly with GM130. In order to test this I sought to purify both WAC and GM130 and investigate if they bound each other *in vitro* directly (Figure 4.10). Firstly I tested expression of GST-WAC and GST-1-610 (ΔCC) in *E. coli* (Figure 4.10a). WAC has no homologue in *E. coli* (BLASTP, data not shown). By assaying fusion protein expression in different colonies I could detect IPTG-induced proteins of the correct size to be GST-WAC or GST-1-610, as marked by asterisks. Although most of GST-WAC was insoluble (Figure 4.10b), enough of the protein was soluble to use

for purification purposes. Removal of the WAC coiled-coil domain greatly enhanced the solubility of GST-1-610.

To purify GM130 my strategy was to express the protein in HEK293A cells. Although it is possible to express full length GM130 in bacterial cells (Ishida et al., 2015), I was informed that this was difficult because GM130 often becomes insoluble (personal communication, Joachim Seemann). The advantage of expressing GM130 in HEK293A cells is that I know it is soluble (Figure 4.6), and it should be post-translationally modified. These modifications could be important for GM130 interaction; for example, it is known that phosphorylation of GM130 on Ser25 by Cdc2 disrupts interaction with p115 (Lowe et al., 1998). The disadvantage is that known GM130 interactors may contaminate my purification procedure. I tried to ameliorate this problem in two ways. Firstly, I cloned full-length rat GM130 with an N-terminal Strep-II tag (WSHPQFEK) with a 2xGly linker. The Strep-II tag binds with high affinity and selectivity to Strep-Tactin (a modified form of streptavidin) (Schmidt and Skerra, 2007). This is useful because I can wash the immobilised StrepII-GM130 with a high salt buffer to remove interaction partners. StrepII-GM130 can then be specifically eluted with biotin to separate proteins that non-specifically bind to the matrix. Biotin binds to Strep-Tactin thereby competing off StrepII-GM130. Most of StrepII-GM130 was eluted off Strep-Tactin after 5 minutes with biotin (Figure 4.10c). Secondly, I co-expressed StrepII-GM130 with HA-VP35. VP35 (virus protein 35) is an Ebola virus protein that antagonises the protein kinase R (PKR)-mediated repression of translation (Feng et al., 2007), which is triggered in HEK293 cells in response to transfection with plasmid DNA (Schumann et al., 2009). Thus co-expression of VP35 with your protein of interest can boost recombinant protein levels (Gantke et al., 2013). This is useful not just to improve yield, but also for stoichiometric reasons. In theory I should be able to saturate interactions with binding partners of GM130 to maximise the amount of uncomplexed protein. As seen in Figure 4.10c and d, expression of HA-VP35 improved the yield of StrepII-GM130 and in conjunction with the Strep-II tag-Strep-Tactin purification system, allowed for GM130 purification from human cells without detectable contaminants.

GST-WAC and GST-1-610 (ΔCC) were immobilised on glutathione sepharose resin (Figure 4.10e), washed multiple times in a high salt buffer and then incubated with equal volumes of StrepII-GM130 *in vitro*. After binding, the

beads were washed and boiled before SDS-PAGE and western blotting. The levels of GST-WAC and ΔCC were monitored by Ponceau S staining. StrepII-GM130 was detected by Western blotting. This experiment was repeated three times and suggests that GM130 binds directly to the C-terminal coiled-coil domain of WAC. It should be noted that I had degradation problems with full length GST-WAC (data not shown), and that future investigations into the direct binding could make use of smaller more stable domains of WAC.

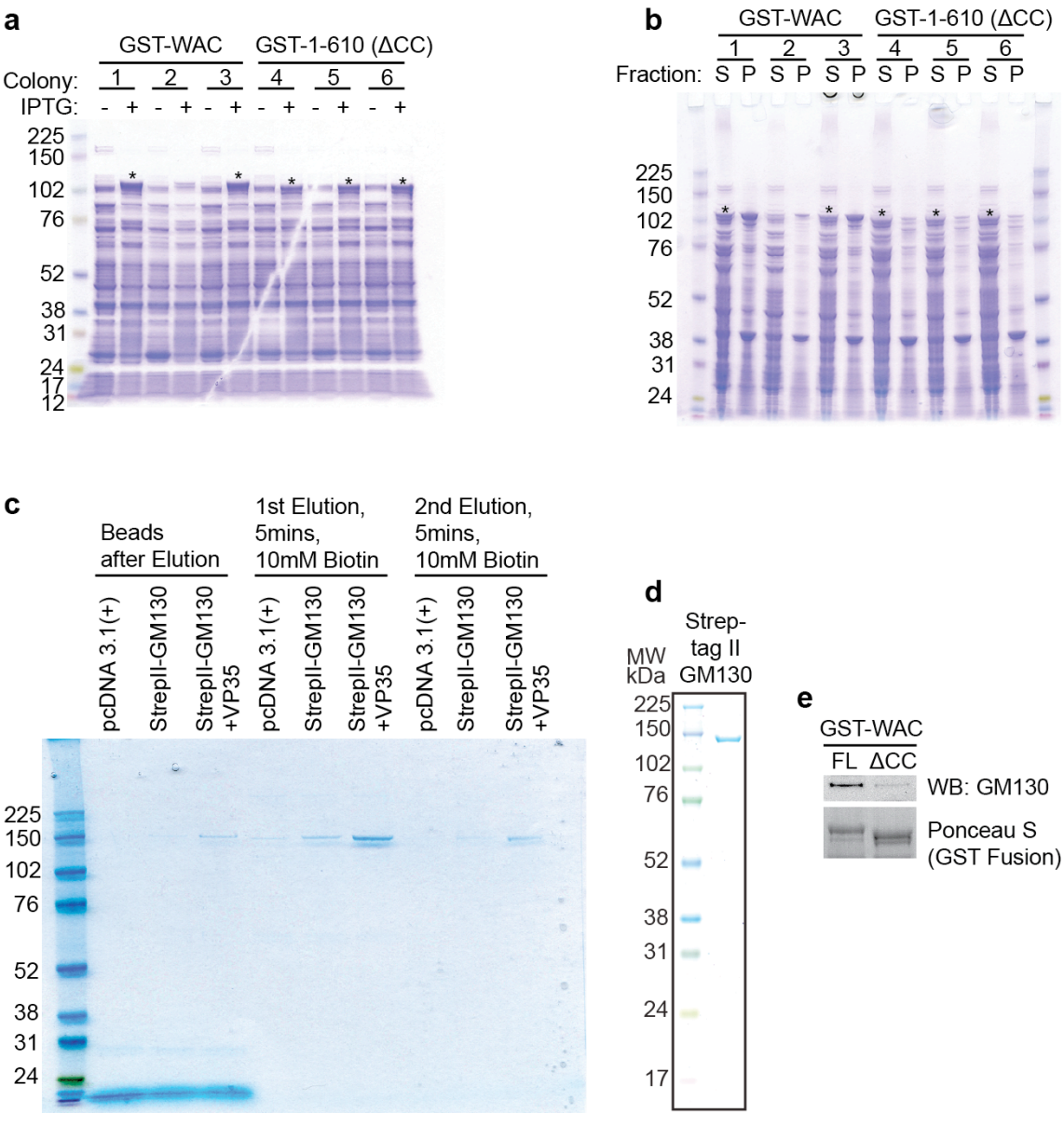

Figure 4.10 *In vitro* binding of GST-WAC and StrepII-GM130 requires the WAC coiled-coil domain

(a) *E. coli* BL21-CodonPlus(DE3)-RIL cells were transformed with pGEX-4T-2 GST-WAC or GST-1-610 (ΔCC), individual colonies were picked and cultured followed by protein expression induction with 1mM IPTG at OD_{600} = 0.6. Whole cell lysates of bacterial cultures were analysed by SDS-PAGE and Coomassie Blue staining. GST-WAC and GST-1-610 are indicated (*). **(b)** Solubility of GST-WAC and GST-1-610 from colonies picked in **(a)** was assessed by SDS-PAGE and Coomassie Blue staining. Bacterial cultures were lysed by sonication and subjected to centrifugation to separate soluble supernatant (S) and insoluble pellet (P) fractions. GST-WAC and GST-1-610 are indicated (*). **(c)** HEK293A cells were transiently transfected with empty vector (pcDNA 3.1 (+)), StrepII-GM130 (rat) or StrepII-GM130 and HA-VP35. Cells were lysed and incubated with Strep-Tactin beads (Qiagen) before stringent washing in buffer containing 1% Triton X-100 and 1M NaCl. StrepII-GM130 was eluted by the addition of 10mM biotin to the buffer and incubation at 4^{o}C. Purification procedure was monitored by SDS-PAGE and colloidal Coomassie staining. **(d)** Purity of StrepII-GM130 used in *in vitro* binding assays **(e)** was confirmed by SDS-PAGE and colloidal Coomassie staining. **(e)** GST-WAC and GST-1-610 (ΔCC) were immobilised on glutathione sepharose beads. Equal volumes of soluble StrepII-GM130 were incubated with GST-WAC or GST-1-610 beads before washing. Bound proteins were eluted by boiling and ran on SDS-PAGE gels followed by western blotting. Protein levels of GST fusions were assessed by Ponceau S staining. *In vitro* binding experiment was repeated three times in total. Molecular weights in kilodaltons are indicated.

4.4.5 WAC binds to a C-terminal region of GM130 that encompasses the 5th and 6th coiled-coil domains

After identifying a 10 amino acid region of WAC that is required for GM130 binding (Figure 4.9), I wanted see which region of GM130 was sufficient to bind to WAC. The majority of GM130 is predicted to adopt a coiled-coil structure, and interaction partners have been mapped to different regions of the protein, both within and outside of the coiled-coil domains (Figure 4.11c). I used truncations of human GM130 (gift from Angelika Barnekow) to map where WAC bound. Unfortunately, at this point I did not have full-length human GM130, so I had to use full-length rat GM130 as my positive control for EGFP-WAC binding (Figure 4.11a). Although, rat and human GM130 have high similarity as out of 1002 amino acids in human GM130, 748 are identical in the rat protein (UniProt alignment tool). This initial experiment suggested the first 445 amino acids of human GM130 isoform 1 are dispensable for interaction with EGFP-WAC. Moreover, removal of these amino

acids did not seem to positively or negative regulate the interaction, at least from this one experiment. One caveat to keep in mind, is the rat full-length GM130 has 3 HA tags, whereas the human truncations only have one HA tag each. This could affect IP efficiency and Western blot signal. To further extend these results, I used smaller truncations of human GM130 (Figure 4.11b). Full-length EGFP-WAC, but as expected not ΔCC, interacted with both aa692-1002 and aa774-1002. This suggests that WAC interacts with the C-terminal region of GM130, which includes the binding sites for ZFPL1, syntaxin 5 and GRASP65 (Chiu et al., 2008, Diao et al., 2008, Barr et al., 1998). This experiment was repeated twice with the same result. These smaller pieces of GM130 had more variable expression, especially when co-expressed with EGFP-WAC (data not shown). Thus I had to express these constructs separately, mix the lysates and then perform the IP, this gave me more control over the ectopic protein levels. It would be interesting to see in future studies if the interaction of WAC with GM130 is in competition with other GM130 protein interactions.

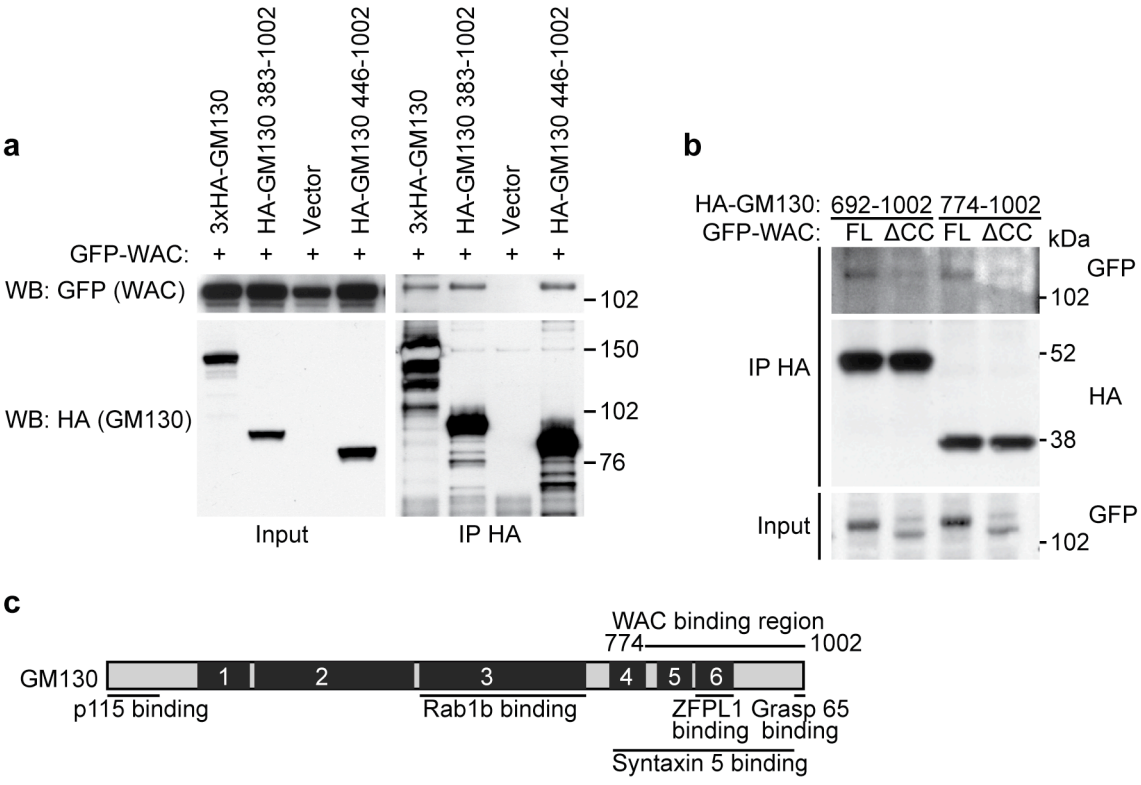

Figure 4.11 EGFP-WAC interacts with the last 227 amino acids of HA-GM130

(a) HEK293A cells were transiently transfected with EGFP-WAC and GM130 constructs: 3xHA-GM130 full length (rat), HA-383-1002 (human), HA-446-1002 (human) or pGADT7 (vector control). Cell lysates were subjected to anti-HA immunoprecipitation before SDS-PAGE and Western blotting. Experiment was performed once. **(b)** HEK293A cells were transfected separately with EGFP-WAC full length (FL), ΔCC or GM130 constructs HA-692-1002 or HA-774-1002. Lysates were mixed followed by anti-HA immunoprecipitation, SDS-PAGE and Western blotting. This experiment was repeated twice. **(c)** Schematic showing primary structure of human GM130 isoform 1. The six coiled-coil domains are indicated as well as interaction regions with known binding partners.

4.5 GM130 tethers WAC to the Golgi apparatus and this requires export of WAC from the nucleus

4.5.1 WAC localisation to the Golgi and ERGIC requires the expression of GM130

WAC colocalises with the cis-Golgi marker GM130 (Totsukawa et al., 2011). How this subcellular localisation occurs is unknown. After co-staining WAC with different markers of the secretory pathway, I saw that WAC colocalised with GM130 as expected, and also with another Golgi marker beta-COP (Duden et al., 1991) (Figure 4.12a). This was predicted, as WAC likely interacts with the COPI coatomer, of which beta-COP is a component (Figure 4.6a). In addition to this, WAC colocalised with the ER-Golgi intermediate compartment (ERGIC) as marked by ERGIC-53. The ERGIC is a membrane compartment of the secretory pathway that mediates trafficking between the endoplasmic reticulum and the Golgi (Appenzeller-Herzog and Hauri, 2006). More colocalisation of WAC was seen with the juxtanuclear ERGIC, which is likely to be juxta-Golgi also, than with the peripheral ERGIC puncta that closely are apposed to ER-exit sites (Figure 4.12a). In contrast, there was less colocalisation of WAC with the trans-Golgi network (TGN) markers p230 and TGN46. In conclusion, WAC localises to membrane compartments of the secretory pathway, namely the ERGIC and the cis-Golgi, but minimally with the TGN.

WAC interacts and colocalises with GM130. GM130 functions as a tethering molecule and has multiple interaction partners. This leads to the question: does GM130 tether WAC to the Golgi apparatus? To begin answering this I knocked down GM130 in HEK293A cells (Figure 4.12c). In cells with little or no detectable GM130 expression (see asterisked cell Figure 4.12c) I never observed juxtanuclear WAC localisation, even if the TGN remained intact, as judged by TGN46 staining. This experiment is supportive of GM130-mediated tethering of WAC to the Golgi. This experiment was performed once and would need to be repeated, but I provide additional evidence for GM130 tethering of WAC to the Golgi in (Figure 4.13).

I next investigated whether GM130 was required to recruit WAC to a crude membrane isolate by subcellular fractionation. Surprisingly, knockdown of GM130

did not alter the amount of WAC recovered from the membrane pellet (Figure 4.12d). Although this experiment was performed once, it suggests that a significant population of WAC may also localise to GM130-negative membrane compartments.

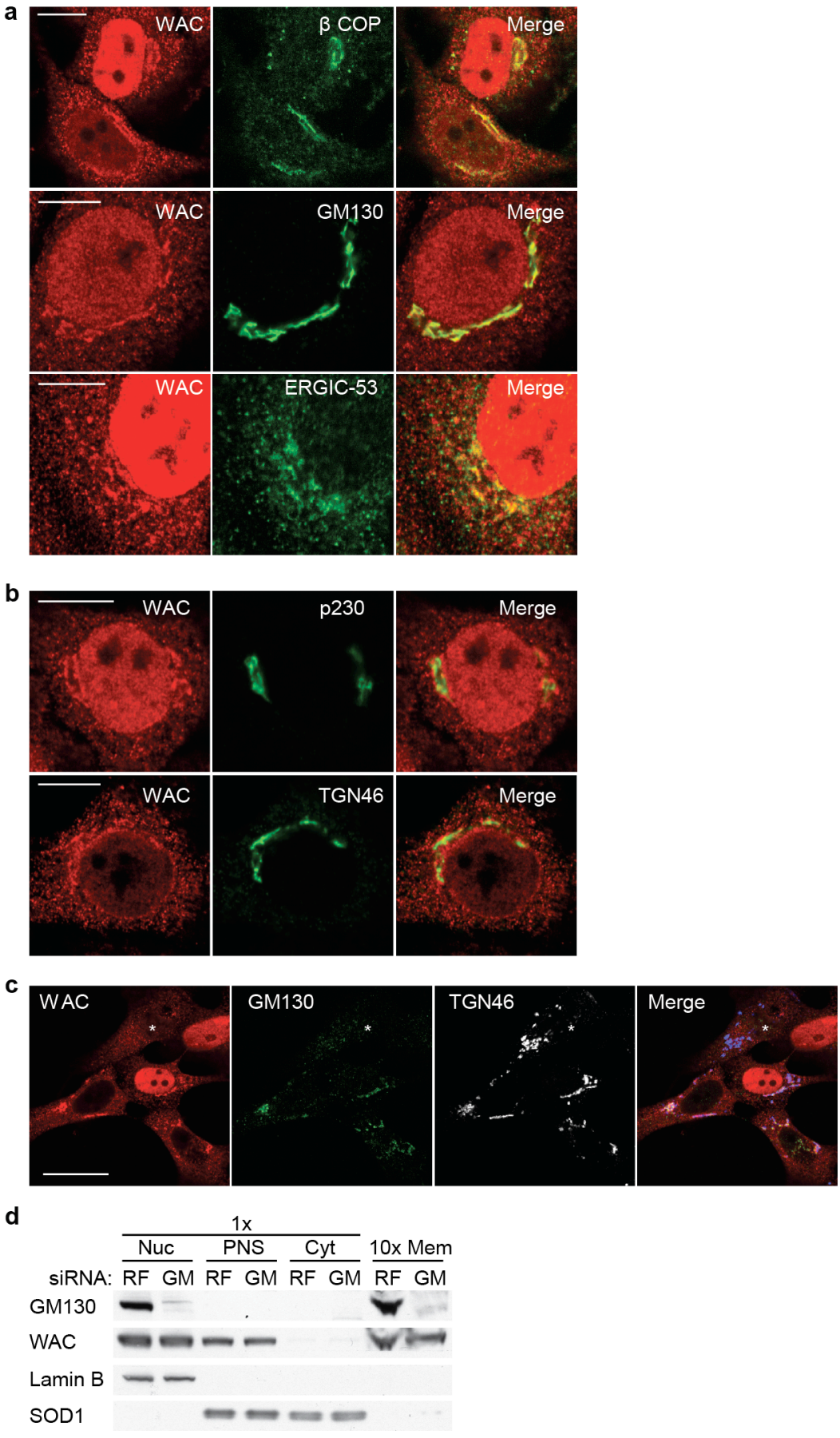
a
WAC
β COP
Merge
WAC
GM130
Merge
WAC
ERGIC-53
Merge
b
WAC
p230
Merge
WAC
TGN46
Merge
c
WAC
GM130
TGN46
Merge
d
1x
Nuc
PNS
Cyt
10x Mem
siRNA: RF GM RF GM RF GM RF GM
GM130
WAC
Lamin B
SOD1

Figure 4.12 WAC localises to the cis-Golgi and the ERGIC and this requires GM130 expression

(a) HeLa cells or HEK293A cells were fixed and labelled with antibodies to WAC, β-COP, GM130 (HeLa) or ERGIC-53 (HEK293A) and analysed by indirect immunofluorescence and confocal microscopy. Scale bars, 10 μm. **(b)** HeLa cells were fixed and labelled with antibodies against p230 and TGN46 before analysis by indirect immunofluorescence and confocal microscopy. Scale bars, 10 μm. **(c)** HEK293A cells were treated with GM130 siRNA (01) for 72 hr before analysis by confocal microscopy using the indicated antibodies. (*) Cell expressing very low levels of GM130. Scale bars, 25 μm. Experiment performed once. **(d)** HEK293A cells were treated with RISC free (RF) or GM130 (GM) siRNA (01) for 72 hr before subcellular fractionation by differential centrifugation and SDS-PAGE followed by Western blotting. Nuclear pellet, Nuc; post-nuclear supernatant , PNS; cytosol, Cyt; membrane pellet, Mem. Experiment performed once. **(a-c)** Cells display variable nuclear WAC signal because of variable nuclear envelope permeabilisation by saponin.

4.5.2 GM130 tethers WAC to the Golgi

There is evidence that GM130 controls the structural organisation of the Golgi complex (see Chapter 1.4 for details). If GM130 knockdown does disrupt the cis-Golgi, this may indirectly affect WAC Golgi localisation. To address this concern I carried out additional experiments (Figure 4.13).

Firstly, I depleted the endogenous WAC protein by siRNA knockdown in HEK293A cells. Knockdown efficacy was assessed by confocal microscopy (Figure 4.13a). After knockdown there was a reduction of nuclear and Golgi WAC signal, indicating that the antibody is specific. This antibody, from Hisao Kondo, has previously been validated in HeLa cells, where WAC knockdown also reduced anti-WAC signal in the nucleus and Golgi (Totsukawa et al., 2011). It is worth noting that Golgi-localised WAC is a heterogeneous phenotype, in that I do not see this in every cell. After knockdown of WAC, I attempted to rescue Golgi WAC localisation by expression of siRNA resistant EGFP-WAC or ΔCC, which binds GM130 very poorly or not at all (Figure 4.13b). In cells expressing EGFP-WAC full-length, I could detect Golgi-localised WAC by staining with the WAC antibody. However, in cells expressing EGFP-ΔCC I never detected Golgi-localised WAC. The EGFP signal was not detectable on the Golgi, but only in the nucleus, even for full-length EGFP-WAC. This is probably because the amount of total WAC on the Golgi is too low to be detected by EGFP fluorescence alone and therefore indirect immunofluorescence is required, as with the HeLa WAC-FLAP cells (Figure 4.2

and Figure 4.3c). This experiment supports my data that WAC is tethered to the Golgi via its interaction with GM130 mediated via its C-terminal coiled-coil domain.

Finally, I made use of a recently developed tool from the Sean Munro lab (Wong and Munro, 2014). To explain, GM130 is truncated at the C-terminus in order to remove its Golgi localisation ability, which is directed by Grasp65 binding (Barr et al., 1998), and fused to the trans-membrane domain of mono amine oxidase, allowing localisation of GM130 to the outer membrane of the mitochondria. Mitochondrial localisation of this construct was confirmed in my hands by treatment of cells with MitoTracker Red (Figure 4.13c). This construct was originally used to determine the trafficking itinerary of vesicular secretory cargo, encoded by golgin specific tethering events. However, this tool could also be used to study protein interaction-partners of GM130. With this goal in mind, I saw that co-expression of EGFP-WAC with GM130-ΔCterm-HA-MAO drove the relocalisation of EGFP-WAC to the mitochondria, mitochondrially tethered WAC was enriched to the extent that antibody staining of WAC was not required (Figure 4.13d). In contrast EGFP-WAC aa1-319 (NT), which does not bind GM130 (Figure 4.6e), always remained exclusively nuclear, and no mitochondrial relocalisation was induced with GM130-ΔCterm-HA-MAO co-expression. This experiment was repeated twice with the same result.

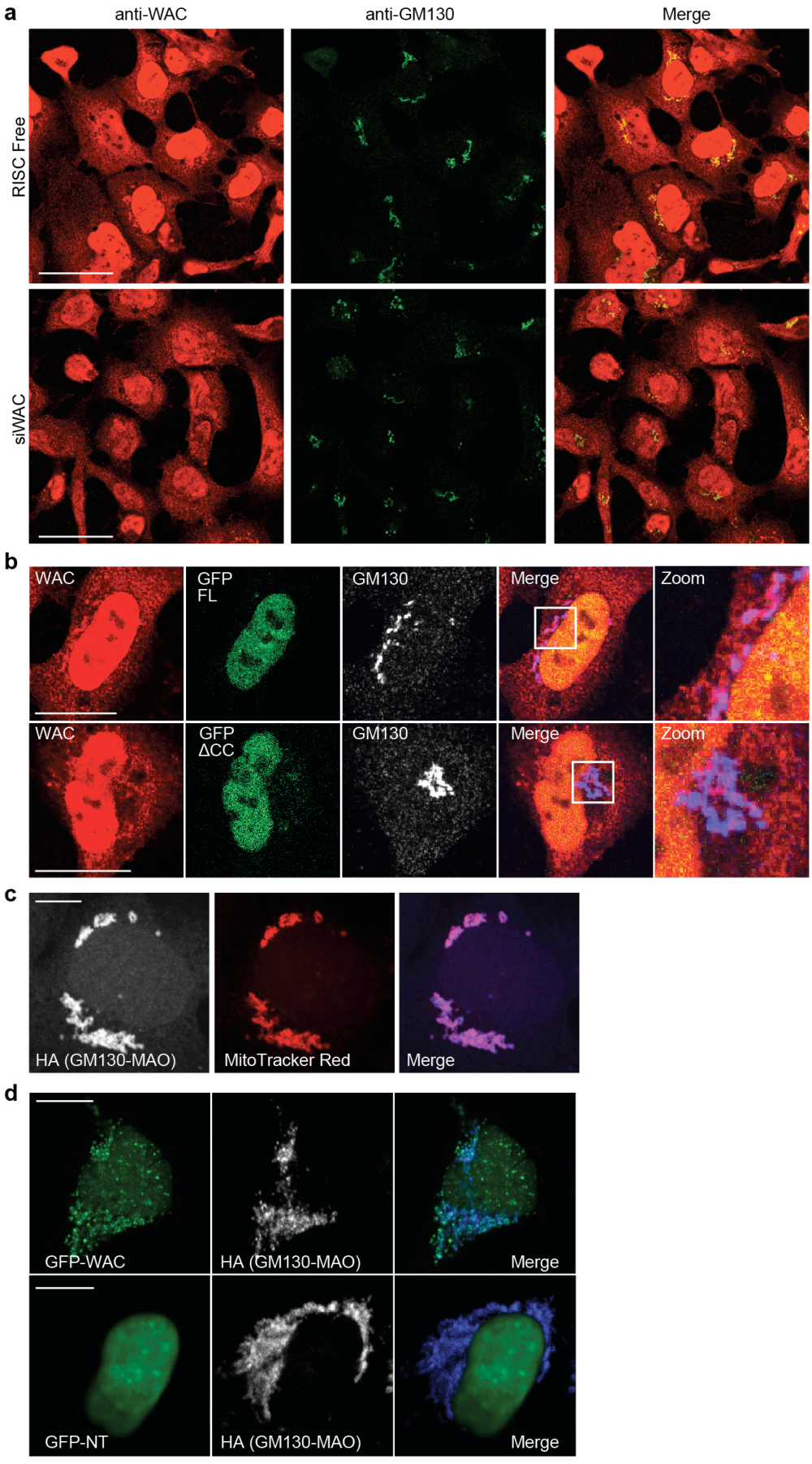
a
anti-WAC
anti-GM130
Merge
RISC Free
siWAC
b
WAC
GFP FL
GM130
Merge
Zoom
WAC
GFP ΔCC
GM130
Merge
Zoom
c
HA (GM130-MAO)
MitoTracker Red
Merge
d
GFP-WAC
HA (GM130-MAO)
Merge
GFP-NT
HA (GM130-MAO)
Merge

Figure 4.13 WAC localisation to the Golgi requires the WAC coiled-coil domain

(a) HEK293A cells were treated with WAC siRNA (03) and analysed after 72 hr by indirect immunofluorescence and confocal microscopy using the indicated antibodies. Scale bars, 50 μm. **(b)** siRNA resistant EGFP-WAC FL or ΔCC were expressed in HEK293A cells treated with WAC siRNA (03) for 72 hr before analysis by confocal microscopy using the indicated antibodies. Scale bars, 20 μm. Experiment performed once. **(c)** HEK293A cells expressing GM130-ΔCterm-HA-MAO were incubated in full medium with MitoTracker Red for 2 hr before staining with anti-HA antibody and analysis by confocal microscopy. Scale bars, 10 μm. **(d)** EGFP-WAC (FL) or aa1-319 (NT) were co-expressed with GM130-ΔCterm-HA-MAO (monoamine oxidase (MAO) aa481-528) in HEK293A cells before labelling with anti-HA, and confocal microscopy. Scale bars, 10 μm. This experiment was repeated twice.

4.5.3 Exportin1-dependent nuclear export is required to maintain the WAC-GM130 interacting pool

I wanted to gain some understanding of the relationship between the nuclear and cytoplasmic pools of the WAC protein. I noticed that WAC contains a putative nuclear export signal (NES) in the middle of the protein starting at aa367 LPALQATLQL (Figure 4.9c). This was predicted using the NetNES tool (la Cour et al., 2004). NESs are hydrophobic leucine-rich sequences that are recognised by CRM1 (exportin1) to facilitate nuclear export (Fornerod et al., 1997). CRM1-dependent nuclear export can be inhibited using the compound Leptomycin B (Wolff et al., 1997). I wanted to see if nuclear export affect recruitment of EGFP-WAC to mitochondrially targeted GM130 (Figure 4.14). I used the autophagy cargo receptor p62 as a control readout, because p62 has a NES and rapidly accumulates in the nucleus upon Leptomycin B (LMB) treatment (Pankiv et al., 2010). In fed control cells, EGFP-WAC could be targeted to the mitochondria when GM130-ΔCterm-HA-MAO was expressed and I could also detect some cytoplasmic p62 puncta. Two hours treatment with LMB was sufficient to robustly retain p62 in the nucleus, however I still found EGFP-WAC retained on the mitochondria. When I incubated cells with LMB for 24 hours, despite some toxicity, under these conditions there was even more accumulation of p62 in the nucleus, however WAC was not detected on mitochondrially localised GM130, suggesting that the NES in the WAC protein is functional. This experiment was repeated twice with the same result. It suggests that unlike cytosolic p62, WAC tethered to the Golgi (or in this case the mitochondria) is not free to diffuse. In fact the dissociation rate of WAC-

GM130 would be predicted to be quite slow from this experiment. However, during extended inhibition of CRM1-dependent nuclear export, EGFP-WAC eventually dissociates from GM130 and relocalises to the nucleus. Thus, the cytoplasmic pool of WAC is predicted to exchange with nuclear WAC and vice versa, and this exchange is predicted to maintain Golgi WAC.

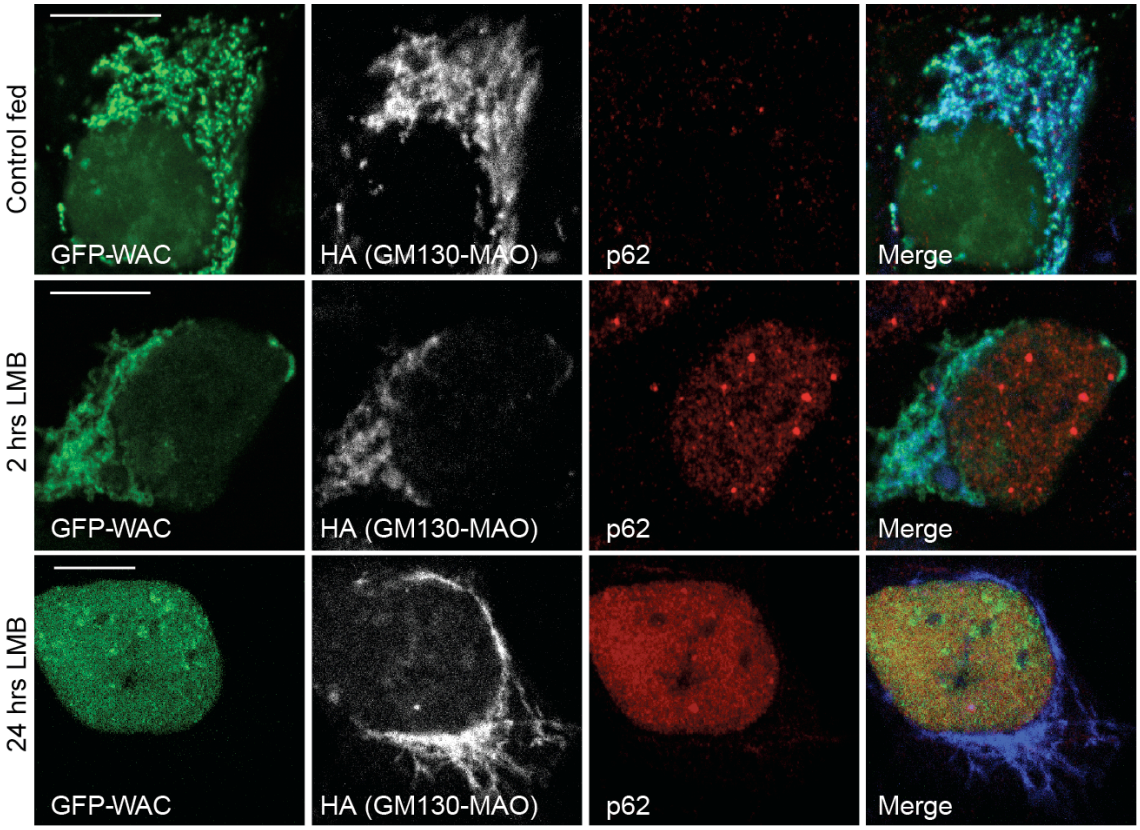

Figure 4.14 Nuclear export of EGFP-WAC is required to maintain interaction with cytoplasmic GM130

HEK293A cells expressing EGFP-WAC and GM130-ΔCterm-HA-MAO were incubated in full medium without or with Leptomycin B (LMB) for the indicated time before staining with anti-HA and anti-p62 antibodies and analysis by confocal microscopy. Scale bars, 10 μm. This experiment was repeated twice in total.

4.6 Discussion

In this chapter I have developed a strategy for identifying novel WAC interactors, by intersecting mass spectrometry datasets from immunoprecipitation experiments from different cell lines. Modification of a bacterial artificial chromosome by homologous recombination permitted the benefits of tagging and the use of the high affinity GFP-Trap® system (Chromotek), as well as protein expression at low levels. A COPI subunit (beta'-COP) and GM130 were both validated as novel WAC interactors. alpha-COP was also suggested as a WAC interactor by mass spectrometry. Interestingly, α-cop and β'-cop are both part of the same coatomer subcomplex and interact directly with each other (Eugster et al., 2000). I assumed that this suggested WAC interacts with the COPI complex because COPI is stable with a half-life of around 28 hours and free subunits are scarce in interphase cells (Lowe and Kreis, 1996), but I concede this may not necessarily be the case without confirmation of other COPI subunits interacting with WAC. GM130 is thought to tether COPI vesicles to the Golgi (Sonnichsen et al., 1998). More specifically, GM130 binds the vesicle tethering protein p115, which in turn binds to Giantin on COPI vesicles. Docking of COPI vesicles to the Golgi can be inhibited by pre-treatment of the Golgi with GM130 antibodies. This functional link between GM130 and COPI offers the exciting possibility that WAC may also affect tethering of COPI. Knockdown of WAC results in vesiculation of the Golgi at the ultrastructural level (Totsukawa et al., 2011). It may be that this phenotype is related to WAC interactions with GM130 and/or COPI. Interestingly, Rab1, which interacts with GM130 to regulate COPII tethering (Moyer et al., 2001, Weide et al., 2001), may also interact with WAC (Figure 4.5c).

The WAC-GM130 interaction is slightly enhanced upon starvation. How this occurs is unknown. However as both WAC and GM130 are modified by post-translational modifications (Xu and Arnaout, 2002, Lowe et al., 1998), this could provide a way for nutrient status to signal to WAC-GM130. Although this effect is statistically significant, the biological significance of this finding remains to be proven.

I have mapped the WAC-GM130 interaction on both sides, with more resolution on WAC, identifying a 10 amino acid region (aa611-620) in the coiled-

coil domain required to bind GM130. This 10 amino acid region is highly conserved back to *Drosophila* (Figure 4.9d). It is worth mentioning that WAC and GM130 both have homologues in *Drosophila*, however only GM130 has an identified homologue in yeast (Bug1) (Behnia et al., 2007, Xu and Arnaout, 2002). It would be interesting to see if the WAC binding region on GM130 was conserved in yeast and if a functional WAC homologue does indeed exist in yeast. Finer mapping experiments would be needed to begin this.

The interaction between WAC and GM130 appears to be direct. With this in mind, the 5th and/or 6th coiled-coil domains of GM130 are the best candidates for the WAC interaction site because coiled-coil domains often associate with one another (Burkhard et al., 2001). In contrast to the WAC-GM130 interaction, any perturbation of the WAC coiled-coil domain completely disrupted the WAC-RNF40 interaction, suggesting the whole domain is required for interaction with RNF40. In fact, the WAC coiled-coil domain may be larger than previously predicted by bioinformatics (Xu and Arnaout, 2002). It may be that WAC-RNF40 is especially sensitive to any changes in the coiled-coil structure as probed by the I626S, L629S mutations, whereas WAC-GM130 may be more tolerant of changes in structure. Alternatively, the WAC-GM130 interaction may not be dictated by the structure of the coiled-coil *per se*, but other factors may be important such as ionic interactions. These binding assays suggest that WAC-GM130 and WAC-RNF40 can bind in a mutually exclusive manner and one might infer that they possess separate functions too. GM130 did not bind to the WAC region aa580-647, which suggests that a secondary region of WAC is required to bind GM130 in addition to the 10 amino acid region (aa611-620). In support of this, I sometimes observed residual binding of GM130 to WAC even in the absence of the WAC coiled-coil domain (Figure 4.9a and b). As WAC aa320-647 does bind to GM130 (Figure 4.6e), this suggests that aa320-579 are also required for binding to GM130. This region of the protein is predicted to be folded (Figure 4.8). The presence of two regions on WAC that are required to interact with GM130 may suggest a multivalent interaction or perhaps some cooperativity between interaction sites. Ultimately, understanding these interactions at the three dimensional level would be crucial in unravelling this.

How WAC is localised to the Golgi was unknown (Totsukawa et al., 2011). WAC localises to and co-purifies with the Golgi complex, purified from rat liver, and like GM130, WAC is stably associated with the Golgi, remaining on the Golgi after

1M KCl wash (Totsukawa et al., 2011, Nakamura et al., 1995). A number of experiments suggest that GM130 tethers WAC to the Golgi, however WAC appears to also associate with (presumably non-Golgi) membranes in a manner not dependent on GM130 (Figure 4.12d). Peptides of the epidermal growth factor receptor (EGFR) were detected by mass spectrometry for WAC interactors (Figure 4.5c), it could be that WAC localises to EGFR-positive GM130-negative membrane compartments such as endosomes or the plasma membrane (Tomas et al., 2014). WAC localisation to the Juxtanuclear region, which included the ERGIC and Golgi, required GM130 expression (Figure 4.12). GM130 is known to cycle between the ERGIC and Golgi (Marra et al., 2001), and this could be why depletion of GM130 resulted in loss of WAC from both the Golgi and the ERGIC. Experiments with the drug Leptomycin B suggest that the GM130-binding and nuclear pools of the WAC protein exchange with one another. How WAC nucleocytoplasmic translocation is regulated still remains a mystery.

No autophagy machinery components were identified as WAC interactors, which would have been a more straightforward path. However, as GM130 regulates autophagy (Chang et al., 2012), it makes sense to further investigate this as a mechanism for how WAC could modulate autophagy.

Chapter 5. Elucidation of WAC function in the autophagy pathway

5.1 Introduction and aim

5.1.1 Introduction

As described previously (Chapter 1) WAC and GM130 both regulate autophagy. Depletion of WAC by siRNA reduced LC3 lipidation and impaired p62 degradation (McKnight et al., 2012). Conversely, depletion of GM130 by shRNA resulted in an increase in lipidated LC3 and an accumulation of autophagosomes (Chang et al., 2012). Thus WAC and GM130 appear to be positive and negative regulators of autophagy respectively. The data presented in Chapter 4 suggests that WAC interacts with GM130. This leads to the hypothesis that WAC may act to repress some negative function of GM130 on autophagy, in order to regulate and maintain high autophagic flux during starvation. I predict this function to be regulatory rather than absolutely required for autophagy. The question is therefore: how does this occur? One explanation could be that WAC and/or GM130 exert some direct effect on the autophagy machinery. Although no core autophagy proteins were identified as WAC interactors by mass spectrometry (Chapter 4), there is the possibility of false negatives as discussed, and it may be that WAC interactions with the autophagy machinery could be detected by other methods.

Interestingly, GM130 interacts with both Rab1b and Rab33b specifically in their GTP-bound states, and therefore could be an effector of these Rabs (Moyer et al., 2001, Weide et al., 2001, Valsdottir et al., 2001). Both Rab1b and Rab33b have been implicated in autophagy (Itoh et al., 2008, Itoh et al., 2011, Doring and Prange, 2015, Mochizuki et al., 2013, Zoppino et al., 2010, Huang et al., 2011). Rab proteins are small GTPases that control specificity in membrane trafficking pathways by regulating vesicle tethering and fusion events through interactions with effector molecules (Barr, 2013). Effectors bind to the Rabs in their active GTP-bound state. Active GTP-bound Rabs are targeted to membranes to exert their function, whereas GDP bound Rab proteins can be sequestered in the cytosol by binding to guanine nucleotide displacement inhibitor (GDI). Rab activation and deactivation is promoted by guanine nucleotide exchange factors (GEFs) and

GTPase activating proteins (GAPs), respectively. Although the GM130-Rab1 interaction is likely to be involved in the secretory pathway (Moyer et al., 2001), the involvement of Rab1 in autophagy is thought to be independent of its function in secretion (Huang et al., 2011). Rab1 exerts its effect on the autophagy at a very early stage during omegasome formation (Mochizuki et al., 2013). Rab33b on the other hand, interacts with Atg16L1 this is thought to modulate both autophagosome formation and maturation (Itoh et al., 2011, Itoh et al., 2008). Additionally, like Rab1b, Rab33b also appears to have a role in the secretory pathway (Valsdottir et al., 2001). One hypothesis I had was that GM130 may bind Rab1b and or Rab33b as an effector, to direct their function in secretion. WAC may be able to redirect these Rabs away from GM130 towards their autophagy specific function. Although this hypothesis was attractive to me, I could find no conclusive evidence that WAC regulated GM130-Rab interactions through the use of immunoprecipitation and immunofluorescence approaches (data not shown).

5.1.2 Aim

With this background in mind, I aimed to address WAC-GM130 function in the autophagy pathway in two stages. Firstly, I decided to characterise in more detail the effects of WAC and GM130 on autophagy. In the case of WAC I aimed to carry out a comprehensive analysis of WAC's effect on the autophagy pathway, which can be simplified as a hierarchy of signal transduction and protein recruitment events. With GM130, I aimed to reproduce and extend the published data that GM130 is a negative regulator of autophagy. This phenotypic approach, I hoped, could give insights into the mechanism by which WAC and GM130 affect autophagosome formation. Secondly, In order to elucidate how WAC-GM130 could impact on autophagy it is necessary to identify if any interactions with the autophagy machinery exist. After I stopped working on GM130-Rab interactions I decided to change strategy. A former student in the lab Nicole McKnight, reported in her thesis that WAC colocalised with GABARAP. This led me to investigate WAC-GM130 interactions with GABARAP, by overexpression and co-immunoprecipitation studies combined with indirect immunofluorescence of endogenous protein staining. This was combined with siRNA knockdown

experiments that allowed me to dissect further WAC and GM130 effects on the GABARAP protein in terms of subcellular localisation and protein interactions.

5.2 WAC is required for maximal ULK1 kinase activation downstream of mTORC1 deactivation

5.2.1 WAC is required for efficient LC3 lipidation and p62 degradation

As stated in the aims above, I began by further investigating the impact of WAC on the autophagy hierarchy. It has been shown that WAC is a positive regulator of autophagy (McKnight et al., 2012) (see Chapter 1.3). WAC depletion resulted in impaired p62 degradation and reduced LC3 lipidation and GFP-LC3 puncta formation. I began by trying to reproduce and extend these data, using lipidation of LC3 and autophagic clearance of p62 as my readout for WAC's impact on autophagy. Depletion of WAC reduced the formation of LC3-II upon starvation and treatment with BafA (Figure 5.1a and b). Less effect on LC3-II levels was observed in fed/basal conditions, as seen previously (McKnight et al., 2012). Furthermore, introduction of siRNA resistant EGFP-WAC into WAC depleted cells reversed the reduction in LC3 lipidation, at least from one experiment (Figure 5.1c). This suggests that WAC's effect on LC3 lipidation is not a result of an off-target effect of the siRNA used. In support of this suggestion, a reduction of GFP-LC3 puncta and LC3 lipidation was seen with multiple WAC siRNA duplexes, previously described (McKnight et al., 2012) and Nicole McKnight, ("A Genome-wide Screen for Starvation-induced Autophagy Identifies New Modulators of Autophagy", 2010). Knockdown of WAC increased basal p62 protein levels in both HEK293A cells and mouse embryonic fibroblasts (MEFs) (Figure 5.1d, e and f) supporting the published data. Human WAC isoform 1 is 95% identical to the mouse protein at the amino acid level ((Xu and Arnaout, 2002) and UniProt), so one would expect the proteins to be functionally similar in MEFs and HEK293A cells.

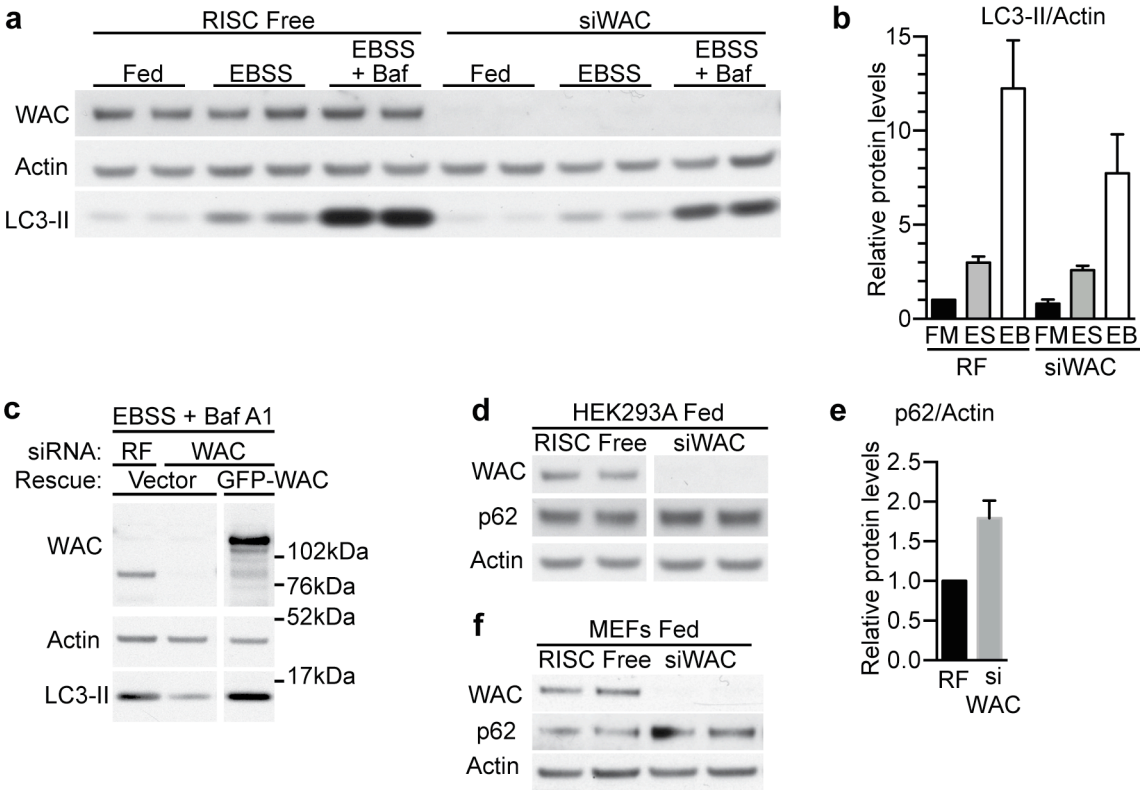

Figure 5.1 Depletion of WAC reduces LC3 lipidation and degradation of p62

(a) HEK293A cells were treated for 72 hr with RISC Free (RF) or WAC siRNA (03) and then incubated in full medium (Fed), EBSS or EBSS + Bafilomycin A1 (Baf) for 2 hr before immunoblot analysis. **(b)** Quantification of (A), mean ± SD from 2 independent experiments. Full medium, FM; EBSS, ES; EBSS + BafA1, EB. **(c)** siRNA-resistant EGFP-WAC or empty vector were expressed in HEK293A cells treated for 72 hr with either RISC free (RF) or WAC siRNA. After 2hr starvation with EBSS and BafA1, cells were analysed by immunoblot. Experiment performed once. **(d-f)** HEK293A or MEF cells were treated for 72 hr with RF or WAC siRNA before immunoblot analysis. Graph shows quantification from HEK293A cells, mean ± SD from 2 independent experiments.

5.2.2 WAC isoform 1 promotes LC3B puncta formation and this requires the GM130-interacting coiled-coil domain

Knockdown of WAC with different siRNA duplexes reduces the formation of GFP-LC3B spots in HEK293 cells (McKnight et al., 2012). In light of this, I wanted to investigate whether WAC regulated the formation of endogenous LC3B positive autophagosomes. In control HEK293A cells, LC3B positive puncta were formed after 2 hours starvation with EBSS, however fewer puncta were seen in cells treated with WAC siRNA (Figure 5.2a and b). This reduction in autophagosome formation was rescued by the expression of siRNA resistant Myc-WAC isoform 1 in WAC depleted cells. Cells expressing Myc-WAC were identified by nuclear Myc staining. However, introduction of truncated Myc-WAC aa1-610 (ΔC), which does not interact with GM130 (Figure 4.6e and f) did not rescue LC3B spot formation to control levels. This suggests that the coiled-coil domain of WAC is required for maximal autophagosome formation during starvation and that the interaction with GM130 may also be required.

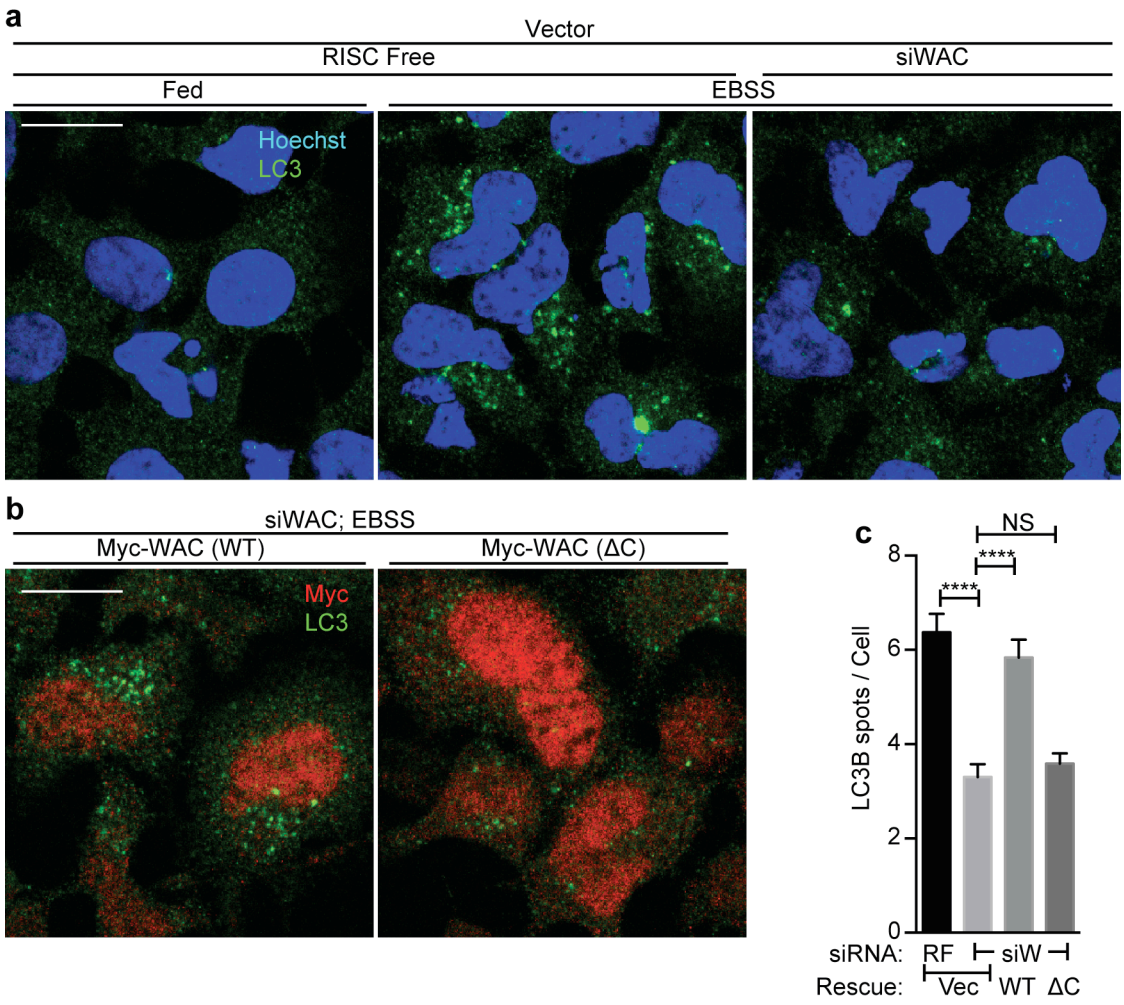

Figure 5.2 The WAC coiled-coil domain is required for maximal LC3B puncta formation during starvation

(a and b) RISC Free or WAC (siWAC) siRNA treated HEK293A cells for 72 hr transfected with empty vector **(a)**, siRNA resistant Myc-WAC (WT) or siRNA resistant Myc-WAC aa1-610 (ΔC) **(b)**, starved for 2 hr with EBSS. LC3B puncta were analysed by confocal microscopy. **(c)** LC3B puncta from **(a and b)** Mean ± SEM of 3 independent experiments, a total of >400 cells counted per condition, unpaired Student's t test, ****, $p \leq 0.0001$.

5.2.3 WAC promotes WIPI2 spot formation upon nutrient deprivation

WIPI2 binds to the pool of phosphatidylinositol 3-phosphate (PI3P) lipid formed by the Vps34-containing Beclin1 complex upon starvation (Polson et al., 2010). WIPI2 marks early autophagic structures such as phagophores rather than more mature structures like autolysosomes, and functions downstream of omegasomes. Thus, WIPI2 can be used as a specific marker for early autophagic structures. Furthermore, because WIPI2 functions to recruit the Atg12–5-16L1 complex to phagophores, thereby allowing LC3 lipidation (Dooley et al., 2014), WIPI2 is considered upstream of LC3 lipidation. I wanted to investigate whether WAC also affects autophagy upstream of LC3 lipidation.

Treatment of HEK293A cells with siRNA targeting WAC reduced WIPI2 puncta formation upon starvation, without affecting total WIPI2 protein levels (Figure 5.3a, b and c). Furthermore this reduction could be rescued by the transfection of siRNA resistant Myc-WAC (isoform 1) (Figure 5.3d). I saw a similar effect from one experiment in HeLa cells, using two different WAC siRNAs (Figure 5.4). In the HeLa cell experiment, I normalised the number of WIPI2 spots to the cell area (Figure 5.4b), rather than the cell number. This was in case WAC had some effect on cell size and thus an indirect effect on WIPI2 spot number. However normalisation to cell area did not change the phenotype observed. These data suggest that in the absence of WAC, there is less PI3P being produced by Vps34 and thus less recruitment of WIPI2 to cytoplasmic puncta. There are alternative interpretations of this data; for example in the absence of WAC, WIPI2 is tethered at some other compartment and unable to be recruited, or that PI3P phosphatase activity is enhanced upon WAC knockdown. Both of these conclusions are less likely given the additional data I will discuss.

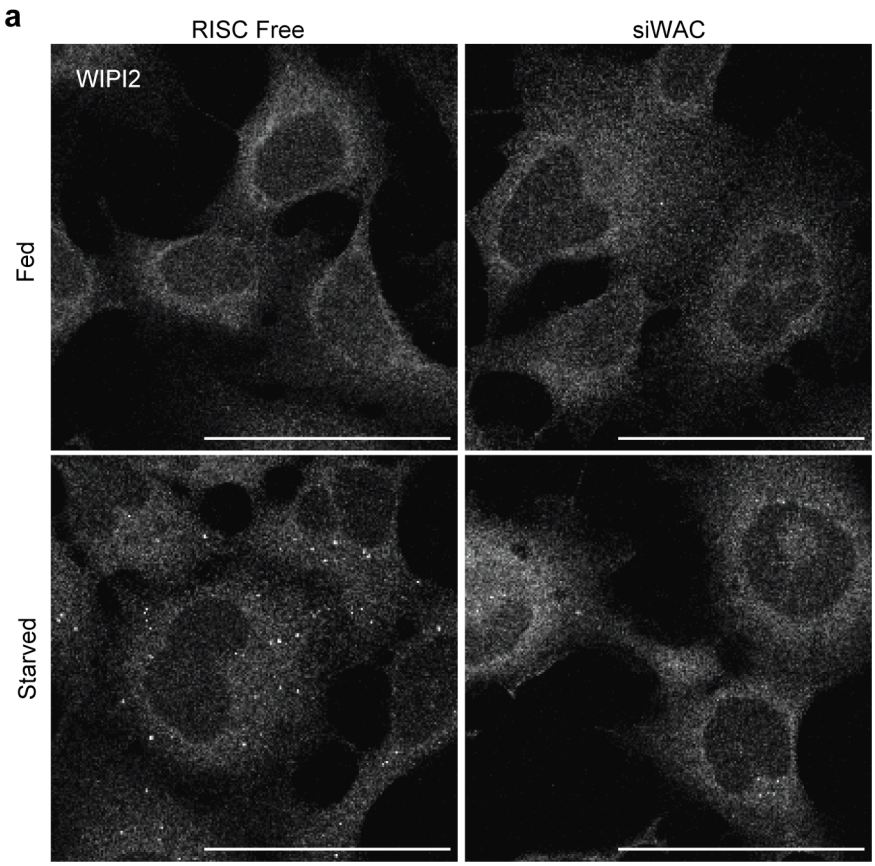
a
RISC Free
siWAC
WIPI2
Fed
Starved

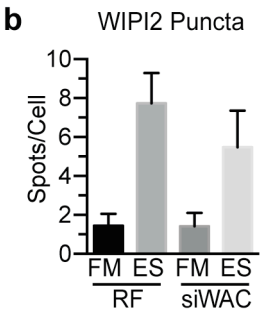
b
WIPI2 Puncta
Spots/Cell
10
8
6
4
2
0
FM ES FM ES
RF
siWAC

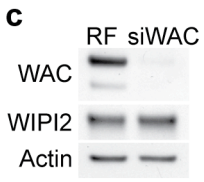
c
RF siWAC
WAC
WIPI2
Actin

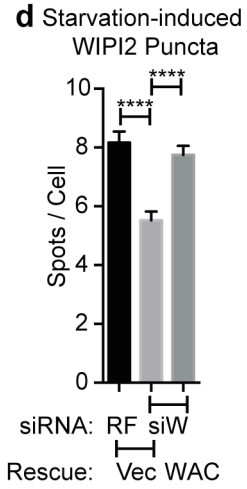
d Starvation-induced
WIPI2 Puncta
****
****
Spots / Cell
10
8
6
4
2
0
siRNA: RF siW
Rescue: Vec WAC

Figure 5.3 Knockdown of WAC attenuates starvation-induced WIPI2 puncta formation in HEK293A cells

(a) HEK293A cells were treated with RISC Free (RF) or WAC siRNA for 72 hr before starvation for 2 hr in EBSS, followed by fixation and labelling with WIPI2 antibody and confocal microscopy analysis. Scale bars, 50 μm. **(b)** WIPI2 puncta in **(a)** were counted, normalised to cell number. Mean ± SD from 2 independent experiments, >150 cells counted per condition in total. RISC Free, RF; Full medium, FM; EBSS, ES. **(c)** HEK293A cells were treated with RF or WAC (03) siRNA for 72 hr, at the same time as experiment shown in **(a)** before immunoblotting. **(d)** Empty vector (Vec) or Myc-WAC were expressed in HEK293A cells that were treated with RF or WAC (siW) siRNA for 72 hr followed by starvation in EBSS for 2 hr prior to WIPI2 staining and confocal microscopy. Statistics were performed using an unpaired Student's t test, ****, $p \leq 0.0001$. Mean ± SEM from 3 independent experiments, >300 cells were counted per condition in total.

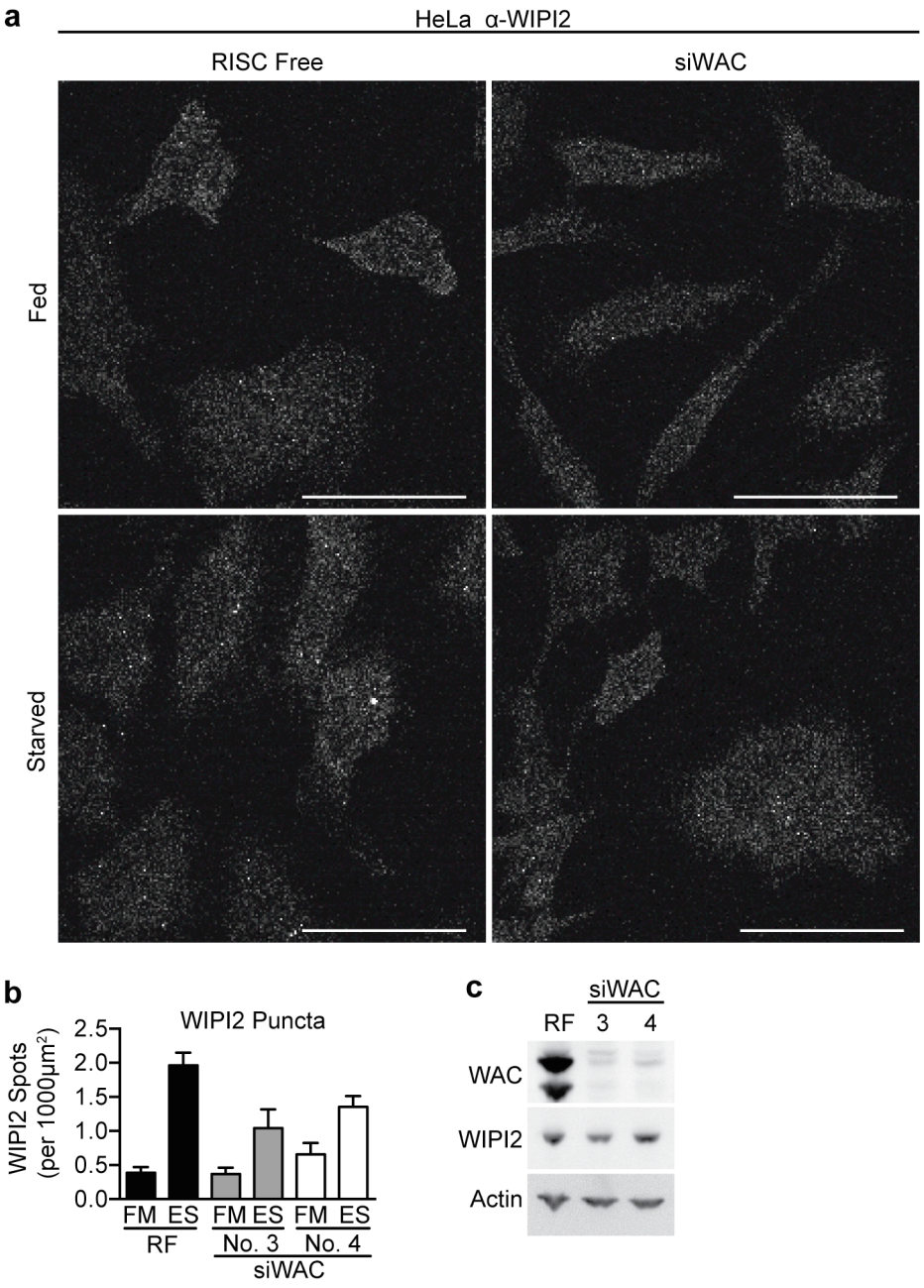

Figure 5.4 WAC depletion reduces WIPI2 spot formation in HeLa cells

(a) HeLa cells were treated for 72 hr with RISC Free or WAC siRNA (03 or 04, 03 is displayed only) and then incubated in full medium (Fed) or EBSS (Starved) for 2 hr prior to analysis by either confocal microscopy **(a)** or immunoblot **(c, fed)**. **(b)** Quantification of **(a)**, mean ± SD from at least 120 cells per condition. Full medium, FM; EBSS, ES. Number of WIPI2 spots were normalised to cell area.

5.2.4 WAC regulates ULK1 kinase activity downstream of mTORC1

In the presence of amino acids the autophagy-initiating protein kinase, ULK1, is phosphorylated and inhibited by mTORC1. mTORC1 is a master inhibitor of canonical ULK-dependent autophagy and this is reviewed in greater detail in Chapter 1. Phosphorylation of ULK1 at serine 757 by mTORC1 antagonises the pro-autophagic interaction between ULK1 and AMPK (Kim et al., 2011). This phosphorylation site should thus provide a functional readout of the autophagy specific arm of mTORC1 signalling, as opposed to translational control for example (Laplante and Sabatini, 2012). Upon amino acid starvation mTORC1 is deactivated, resulting in dephosphorylation of ULK1, ULK1 activation, autophosphorylation and phosphorylation of ULK1 substrates. The ULK complex member, Atg13, is phosphorylated at serine 318 by active ULK1 (Joo et al., 2011). However, Ser318 phosphorylation of Atg13 by ULK1 is thought to be involved in mitophagy, in a mechanism whereby Atg13 can dissociate from the ULK1 complex and localise to damaged mitochondria. The Atg13 S318A mutation has a dominant-negative effect on mitophagy, but does not inhibit basal or starvation-induced autophagy. This means that phosphorylation at Ser318 on Atg13 should in theory be a readout for active ULK1, but not necessarily a functional readout of starvation-induced autophagy.

In order to investigate if Atg13 phosphorylation at Ser318 responds as expected to nutrient starvation, I performed a starvation time course (Figure 5.5a and b). At the time I did the experiment it was unknown whether this phosphorylation event would be stimulated by EBSS starvation, but it was pleasing to see that Atg13 Ser318 phosphorylation was recently validated as a readout for ULK1 activity and nutrient status (Petherick et al., 2015). This was facilitated by the development of small molecule inhibitors of ULK1. This modification is now used as a readout in screens and biochemical assays (Rosenberg et al., 2015, Popovic and Dikic, 2014). After starving HEK293A cells for 15, 30 or 60 minutes there was a loss of phosphorylation of ULK1 at Ser757 that correlated with an increase of phosphorylation at Ser318 on Atg13, as expected (Figure 5.5a). In cells depleted of WAC the profile of mTORC1 deactivation upon starvation (ULK1 p-Ser757) was similar to control cells, however activation of the ULK1 complex (Atg13 p-Ser318)

was significantly reduced after 15 minutes and remained reduced after 1 hour (Figure 5.5b). This result suggests that knockdown of WAC does not affect starvation-induced deactivation of mTORC1, but does reduce activation of the ULK1 complex.

In order to strengthen this conclusion I performed immunofluorescence for WIPI2 after treating control HEK293A cells or WAC knockdown cells with Torin1 for 2 hours (Figure 5.5c). Torin1 is a potent ATP-competitive inhibitor of the both mTORC1 and mTORC2 that inhibits mTORC1 more completely than rapamycin (Thoreen et al., 2009). Thus Torin1 treatment induces autophagy and results in WIPI2 puncta formation (Polson et al., 2010). Knockdown of WAC reduced Torin1-induced WIPI2 puncta formation, to a similar extent as was seen during nutrient starvation (Figure 5.3b and Figure 5.4b). This further suggests that WAC exerts its effect on autophagy downstream of mTOR.

Another function of mTORC1 is to control protein synthesis (Laplante and Sabatini, 2012). One way this occurs is through the phosphorylation of S6 kinase 1 (S6K1) by active mTORC1 in the presence of nutrients. S6K1 in turn phosphorylates its substrate, ribosomal protein S6. Thus signalling to the translational arm of the mTORC1 pathway can also be monitored. Upon siRNA targeting of WAC I again saw a reduction of starvation-induced ULK1 activation as measured by Atg13 Ser318 phosphorylation, this time after 2 hours (Figure 5.5d). This reduction was modest suggesting WAC is a regulator of autophagy as I proposed before. mTORC1 deactivation during starvation, as measured by S6 phosphorylation at Ser240 and Ser244, was identical after 2 hours in both control and WAC knockdown cells. Taken together these data suggest that WAC is not involved in the signalling events of mTORC1 deactivation, but rather promotes activation of the ULK1 complex.

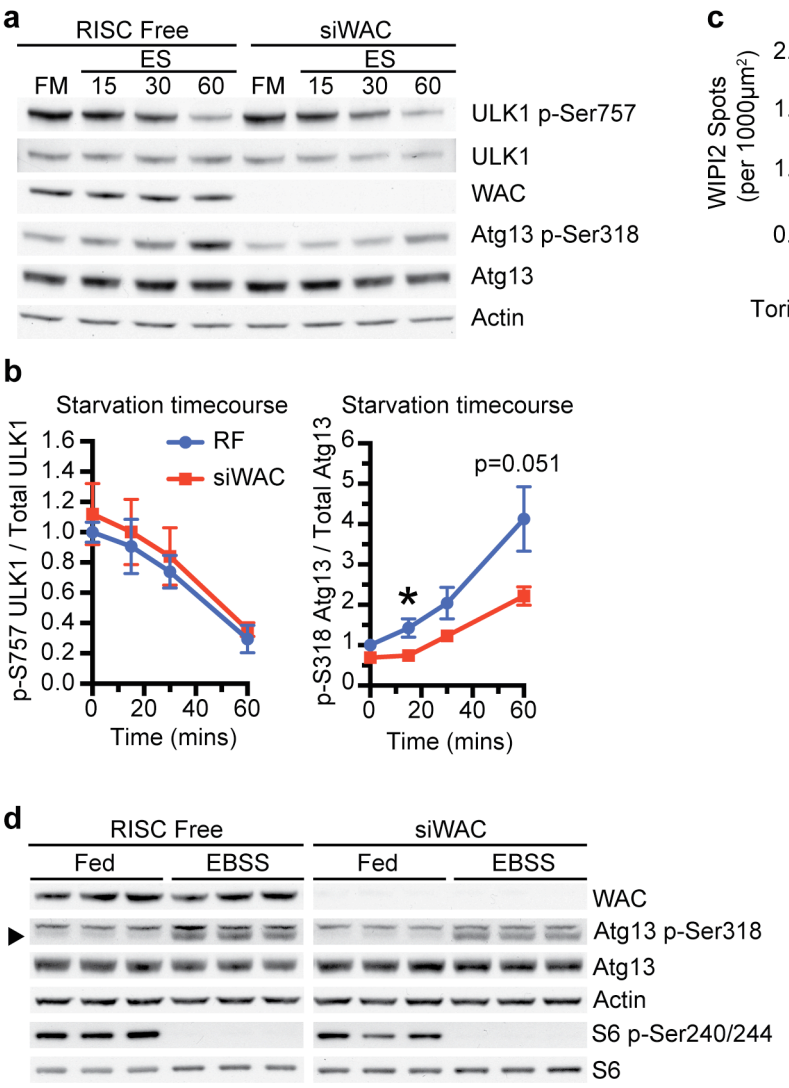

Figure 5.5 WAC is required for maximal ULK1 activation but not mTORC1 deactivation upon starvation

(a) HEK293A cells treated with RISC free (RF) or WAC siRNA (03) for 72 hr were incubated in full medium (FM) or EBSS (ES) for 15, 30 and 60 min prior to immunoblot analysis. **(b)** Quantification of **(a)**, statistical analysis unpaired Student's t test, Mean ± SEM from 3 independent experiments, *, $p \leq 0.05$. **(c)** HEK293A cells were treated for 72 hr with RF or WAC siRNA (03) and then incubated in full medium or full medium + Torin1 for 2 hr before analysis by confocal microscopy and quantification of WIPI2 puncta. Mean ± SD from at least 80 cells per condition. **(d)** HEK293A cells were treated for 72 hr with RF or WAC siRNA and then incubated in full medium (Fed) or EBSS for 2 hr before immunoblot analysis. Experiment performed once.

5.2.5 Depletion of WAC prevents redistribution of Atg9 away from the Golgi region during starvation

Atg9 is a transmembrane protein that is essential for autophagy and in mammals Atg9 is localised to a pool at the trans-Golgi network (TGN) in nutrient replete conditions (Young et al., 2006). A population of Atg9 has also been identified at the plasma membrane (Puri et al., 2013, Popovic and Dikic, 2014). During starvation, Atg9 relocalises from the TGN to endosomes, and this requires ULK1. Given that WAC knockdown reduces ULK1 activity, I reasoned that depletion of WAC should also affect relocalisation of Atg9 during starvation. This was important as a modest reduction in ULK1 signalling upon WAC knockdown may not necessarily be of biological significance. In HEK293A cells maintained in full medium Atg9 was concentrated in a juxtanuclear pool marked by GM130 (Figure 5.6). This was not necessarily colocalisation, as I had to open the pinhole of the confocal microscope to detect Atg9 signal. Upon starvation many cells lost this juxtanuclear concentration of Atg9, suggesting Atg9 had relocalised to another membrane compartment as previously published (Young et al., 2006). During starvation of ULK1 or WAC knockdown cells, Atg9 was retained at the Golgi region in many cases. This experiment was performed only once, and so it would be important to reproduce and quantify this effect for future studies.

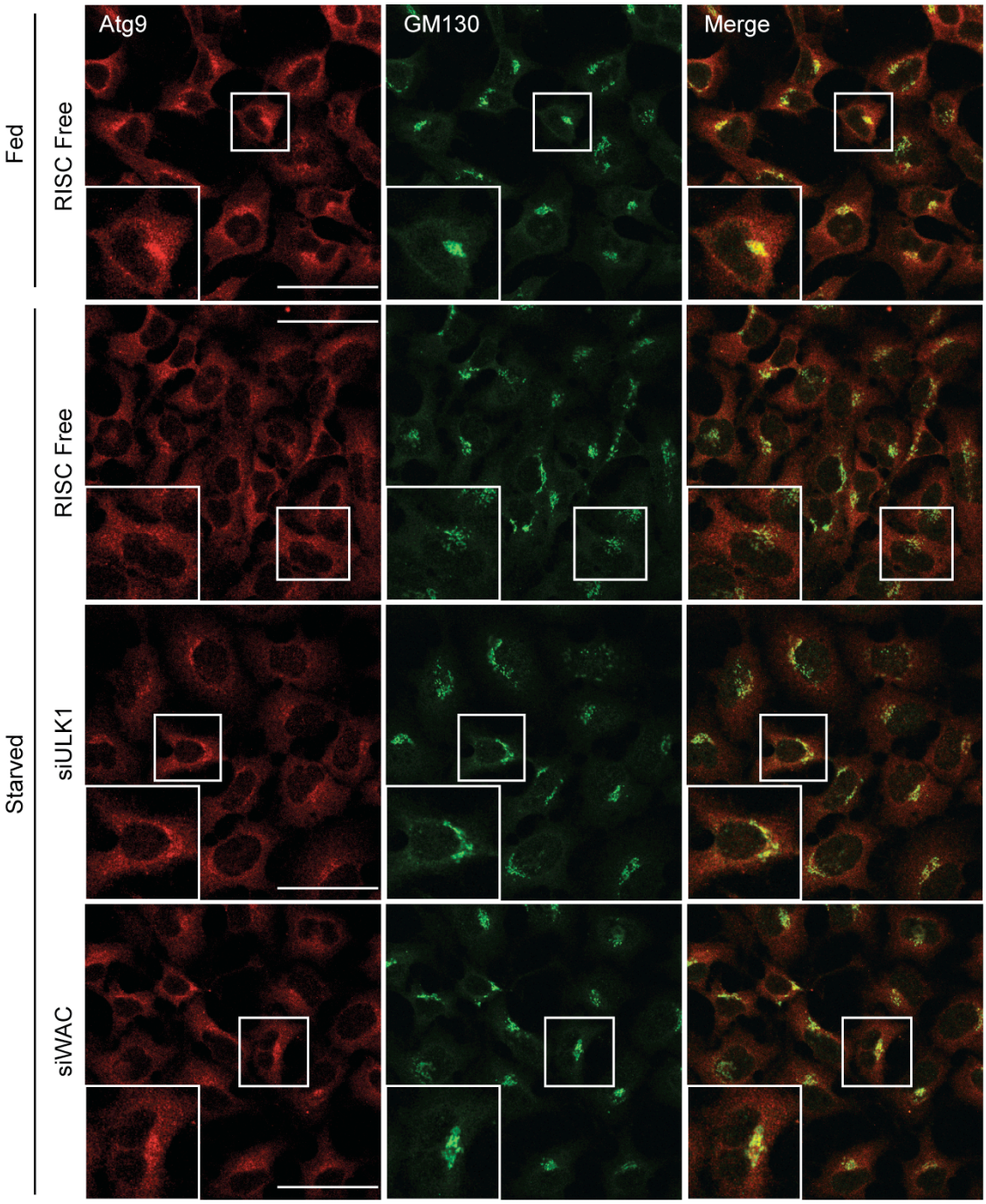

Figure 5.6 WAC knockdown prevented starvation-induced mAtg9 redistribution

HEK293A cells were treated with RISC free, ULK1 (04) or WAC (03) siRNA for 72 hr followed by treatment with full medium (Fed) or EBSS (Starved) for 2 hr, fixation and analysis by confocal microscopy. Scale bars, 50 μm. Experiment performed once.

5.3 GM130 is a negative regulator of autophagosome formation

5.3.1 Depletion of GM130 enhances LC3 Lipidation, p62 degradation and WIPI2 spot formation

It was previously published that GM130 is a negative regulator of autophagy based on the following observations (Chang et al., 2012): In A549 cells treatment with a shRNA targeted against GM130 increased the amount of lipidated LC3 under basal conditions as well endogenous LC3 puncta formation under basal conditions. In the K-ras^{LA1} lung cancer mouse model, aerosolised delivery of shRNA targeting GM130 to the lungs increased the levels of lipidated LC3, LC3 histopathological staining and autophagosome number by electron microscopy. However, despite these results, done without the use of tools to inhibit autophagic flux such as Bafilomycin A1 it is not clear whether depletion of GM130 blocks autophagic degradation or increases the levels of autophagy (as described in the guidelines (Klionsky et al., 2012)). In light of this, I sought to reproduce and extend the published findings that GM130 is a negative regulator of autophagy in our model HEK293A cell line, and to investigate the effects of GM130 on the early autophagy pathway, if any.

siRNA depletion of GM130 with two different duplexes showed a small increase of LC3II levels in both basal and starvation conditions, whereas no effect was seen on LC3I levels (Figure 5.7a and c). However, under conditions of starvation in the presence of BafA, LC3II levels were unaffected by GM130 knockdown. p62 protein levels relative to actin were also decreased to a small extent upon GM130 depletion with 2 different siRNAs, in both basal and starvation conditions (Figure 5.7b and d). However no effect was seen during BafA treatment. These results suggest that depletion of GM130 increases LC3 lipidation and p62 degradation and thus GM130 is negative regulator of basal and starvation induced autophagy. I proceeded to investigate markers of the early autophagy pathway after knockdown of GM130. WIPI2 puncta formation during starvation was significantly enhanced upon GM130 depletion, but no effect was seen on basal WIPI2 spot number (Figure 5.7e). ULK1 activity, as measured by phosphorylation of Atg13 on Ser318, was significantly increased in nutrient replete conditions with GM130-03 siRNA only but not with GM130-01 siRNA (Figure 5.7f and g). During

starvation, knockdown of GM130 had no effect on ULK1 activity. It may be that under starvation conditions Ser318 of Atg13 is maximally phosphorylated and further increases are not possible or detectable. The fact that only one siRNA to GM130 affected ULK1 activity suggest that this may be an off-target effect of the siRNA, or that the effect is very small and hard to reproduce. Nonetheless, these data suggest that like WAC, GM130 affects the early autophagy pathway. However, unlike WAC, GM130 appears to modestly inhibit the formation of autophagosomes.

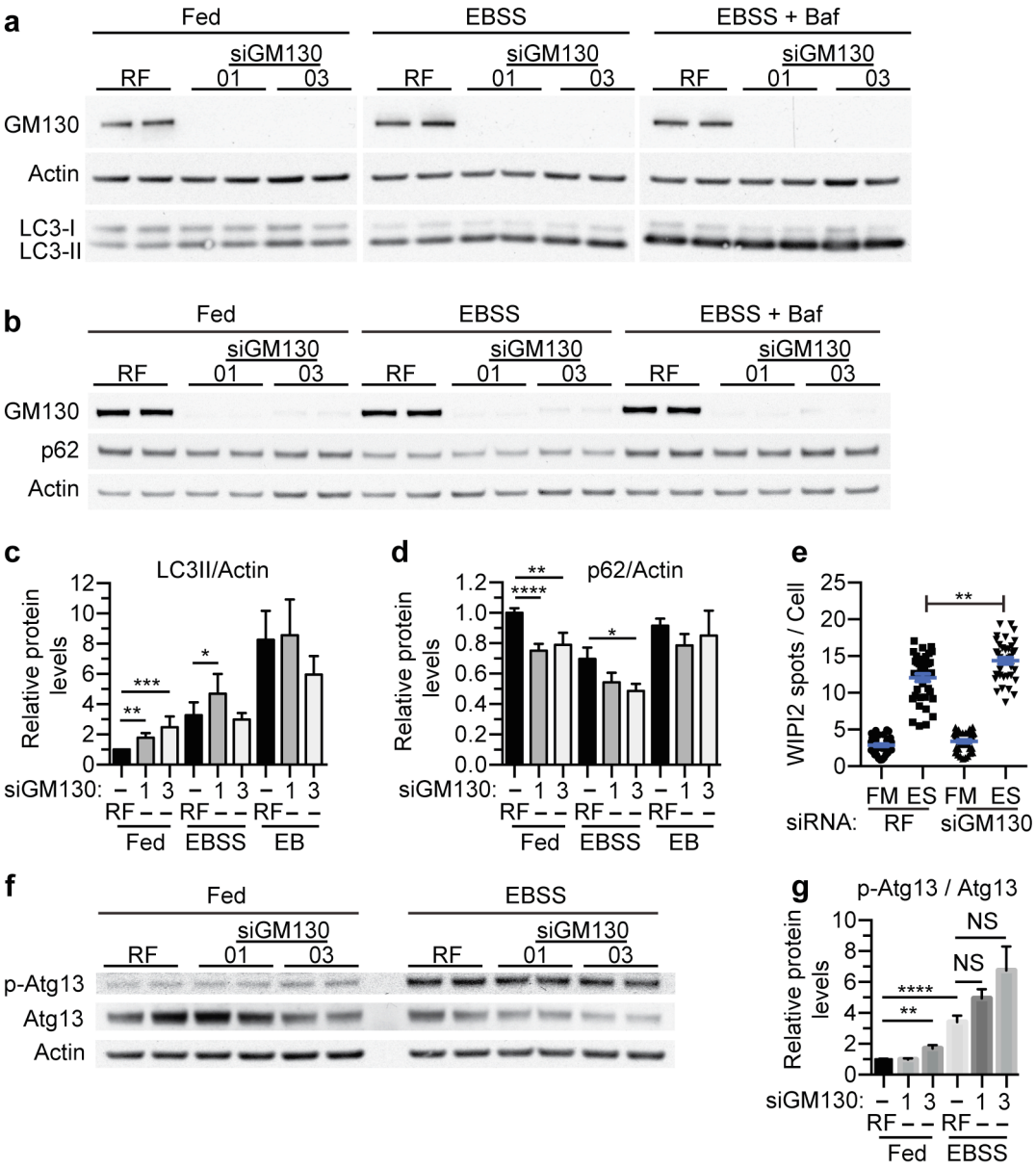

Figure 5.7 Knockdown of GM130 enhances autophagy at an early stage of the pathway

(a and b) HEK293A cells treated with RISC Free (RF) or GM130 siRNA-01 or -03 incubated in full medium (fed), or EBSS with or without Bafilomycin A1 for 2 hrs, followed by immunoblot. **(c)** LC3-II levels from **(a)** mean ± SEM of 4 independent experiments, Mann-Whitney test, *, $p \leq 0.05$. **(d)** p62 degradation from **(b)** mean ± SEM of 5 independent experiments, Mann-Whitney test, *, $p \leq 0.05$. **(e)** HEK293A cells treated with RF or GM130 siRNA (-01) incubated in full medium (FM), or EBSS (ES) for 2 hrs and fixed for labelling. Statistical analysis unpaired Student's t test, Mean ± SEM 4 independent experiments. **, $p \leq 0.01$. >30 fields of cells were analysed per condition in total. Spot counting and analysis was performed by Minoo Razi. **(f)** HEK293A cells treated with RF or GM130 siRNA-01 or -03 incubated in full medium (fed), or EBSS for 2 hrs and immunoblotted. **(g)** Quantification of **(f)**, statistical analysis unpaired Student's t test, Mean ± SEM 5 independent experiments, **, $p \leq 0.01$

5.3.2 Overexpression of GM130 inhibits LC3 lipidation

If knockdown of GM130 increases autophagy, overexpression of GM130 should in theory block autophagy at an early stage, assuming that the overexpressed protein in some way functionally replicates the endogenous protein. Overexpression of rat 3xHA-GM130 resulted in a robust decrease of LC3II accumulation during starvation and BafA treatment (Figure 5.8a and b), similar to knockdown of WAC (Figure 5.1a and b). This suggests that GM130 overexpression blocks the formation of lipidated LC3 during starvation. However, puzzlingly other markers of autophagy were unaffected by GM130 overexpression. The profile of p62 degradation was similar between vector transfected and GM130 overexpressing cells. WIPI2 spot formation was also unaffected after GM130 overexpression, in both basal and starvation conditions. In summary, although there is some evidence that GM130 overexpression blocks autophagy, this is not conclusive based on an investigation of multiple autophagic readouts. It has recently been published that overexpressed GM130 translocates to the nucleus (Wei et al., 2015), and it may be that GM130 overexpression may not be a good functional opposite of GM130 depletion.

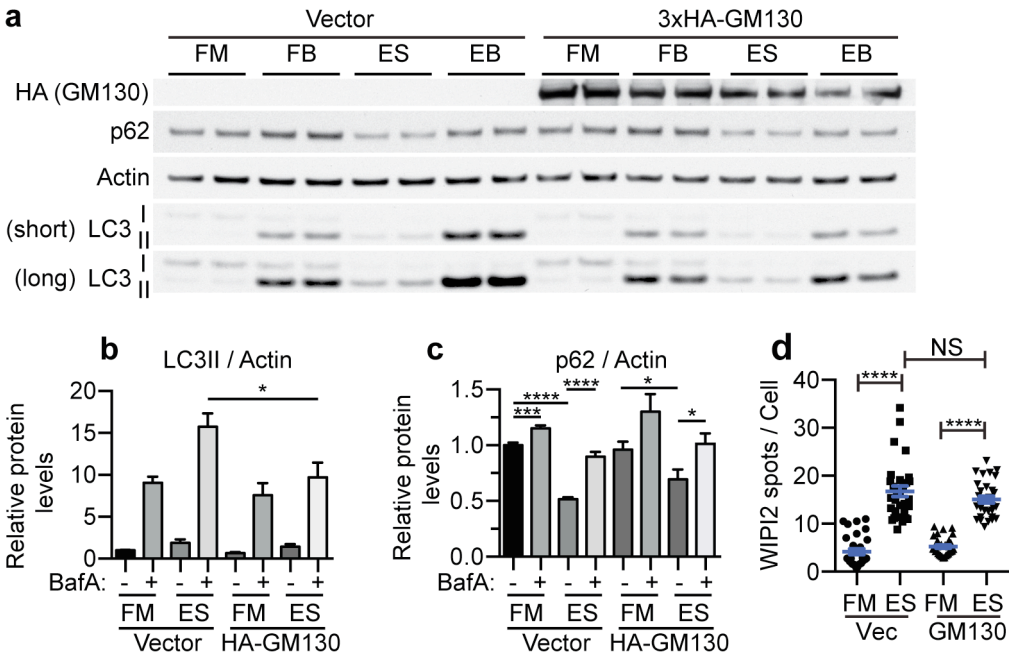

Figure 5.8 Overexpression of HA-GM130 suppresses LC3 lipidation but does not affect p62 degradation or WIPI2 spot formation

(a) HEK293A cells expressing empty vector or 3xHA-GM130 were incubated in full medium (FM), full medium with BafA (FB), EBSS (ES), or EBSS with BafA (EB) for 2 hr prior to immunoblot. Shorter and longer film exposures of LC3 immunoblot are denoted with (short) and (long) respectively. **(b)** Quantification of **(a)** statistics were performed using an unpaired Student's t test, *, $p \leq 0.05$. Mean ± SEM from 3 independent experiments. **(c)** Quantification of **(a)** statistics were performed using an unpaired Student's t test, *, $p \leq 0.05$. Mean ± SEM from 5 independent experiments. **(d)** HEK293A cells expressing empty vector or 3xHA-GM130 were incubated in full medium (FM) or EBSS (ES) for 2 hr prior to fixation, confocal microscopy and spot counting (performed by Minoo Razi).

5.4 GM130 directly interacts with GABARAP and WAC indirectly interacts with GABARAP

5.4.1 GM130 binds to GABARAP

After investigating the effects of WAC and GM130 on the hierarchy of the autophagy pathway, I wanted to understand how WAC and GM130 could regulate autophagy at a more molecular level. I decided to investigate GABARAP because Nicole Mcknight ("A Genome-wide Screen for Starvation-induced Autophagy Identifies New Modulators of Autophagy", 2010) had previously reported a colocalisation of GABARAP with WAC on punctate structures, although no colocalisation of WAC with GFP-LC3 was observed. I noticed that there was minor colocalisation between GM130 and GABARAP under both basal and starvation conditions (Figure 5.9a). Interestingly, GM130 was arranged around or juxtaposed to enlarged GABARAP structures that appeared larger than autophagosomes. As GM130 and GABARAP exhibited some colocalisation I tested if they could interact. After overexpressing the EGFP-tagged human Atg8 family of proteins in HEK293A cells followed by GFP-TRAP immunoprecipitations, I could show that out of the mAtg8 proteins tested endogenous GM130 interacted most abundantly with EGFP-GABARAP (Figure 5.9b). Myc-WAC was also detected as binding EGFP-GABARAP, but did not prefer GABARAP unlike GM130. Importantly, WAC and GM130 both interacted with GABARAP at the endogenous level, after immunoprecipitation of GABARAP (Figure 5.9c). The interaction between GM130 and GABARAP appears to be direct (Figure 5.9d). After incubation of two different concentrations (by volume) of soluble Strep II-GM130 (purified as per Figure 4.10d) with immobilised recombinant GST or GST-GABARAP on glutathione sepharose beads, more GM130 was seen binding to GST-GABARAP than to the GST alone control. This also suggests that the GM1130-GABARAP interaction is independent of lipidation.

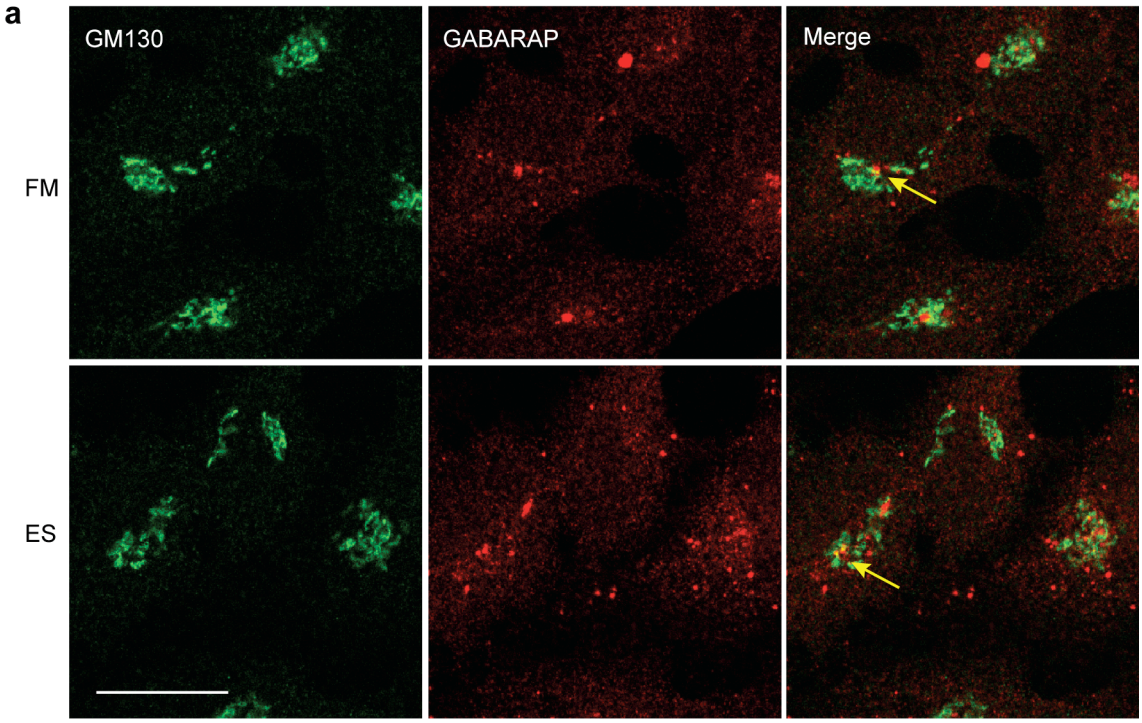
a
GM130
GABARAP
Merge
FM
ES

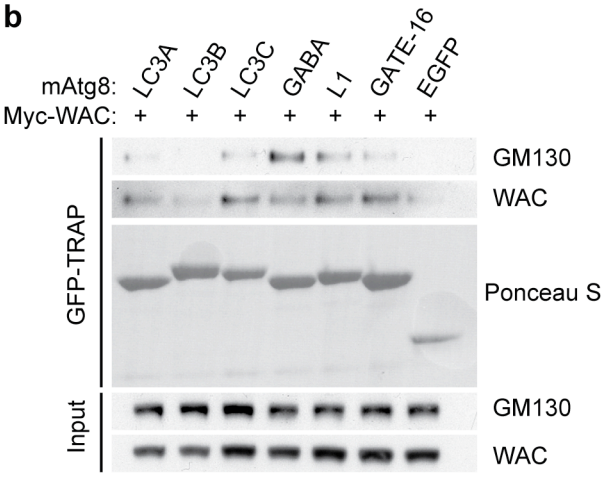
b
mAtg8:
LC3A
LC3B
LC3C
GABA
L1
GATE-16
EGFP
Myc-WAC: + + + + + + +
GFP-TRAP
GM130
WAC
Ponceau S
Input
GM130
WAC

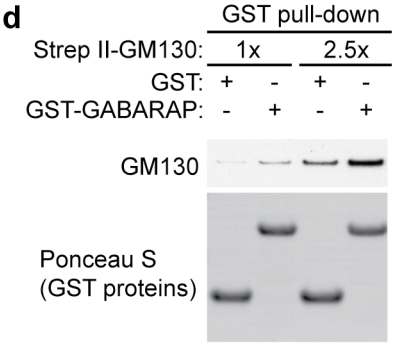
d
GST pull-down
Strep II-GM130:
1x
2.5x
GST: + - + -
GST-GABARAP: - + - +
GM130
Ponceau S
(GST proteins)

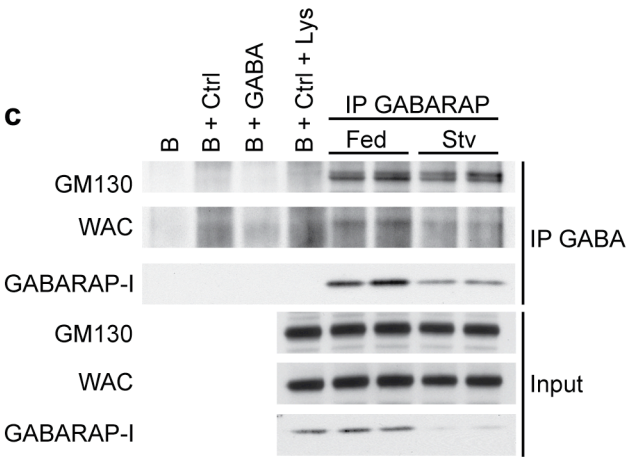
c
B
B + Ctrl
B + GABA
B + Ctrl + Lys
IP GABARAP
Fed
Stv
GM130
WAC
GABARAP-I
IP GABA
GM130
WAC
GABARAP-I
Input

Figure 5.9 WAC and GM130 interact with GABARAP

(a) HEK293A cells in full medium (FM) or EBSS (ES) for 2 hrs. Arrows indicate colocalisation. Scale bars, 20 μm. **(b)** Myc-WAC and EGFP, EGFP-LC3A, LC3B, LC3C, GABARAP, GABARAPL1 or GATE-16 co-expressed followed by GFP-Trap and immunoblot. Experiment performed twice. **(c)** Immunoprecipitation of GABARAP from fed or starved cells and immunoblot analysis. B, beads; Ctrl, Anti-GFP; GABA, Anti-GABARAP. Experiment performed twice. **(d)** Recombinant GST or GST-GABARAP beads were incubated with purified Strep II-GM130 before immunoblot. Purified GST proteins were provided by Harold Jefferies. Experiment performed once.

5.4.2 Mitochondrially targeted GM130 can recruit GABARAP, and WAC interacts with GABARAP indirectly

Expression of mitochondrially targeted GM130 was able to recruit EGFP-WAC to mitochondria (Figure 4.13d). I wanted to see if the same was true for GABARAP as it also interacts directly with GM130. After the expression of GM130-ΔCterm-HA-MAO, EGFP-GABARAP was also seen concentrated on the mitochondria (Figure 5.10a). In HEK293A cells transfected with empty control vector, GABARAP was found in puncta during starvation conditions that are likely to be autophagosomes (Figure 5.10b). I also observed an enlarged GABARAP structure as mentioned above. However after expression of GM130-ΔCterm-HA-MAO I noticed endogenous GABARAP concentrated around the mitochondria with some colocalisation with mitochondrially targeted GM130. This colocalisation was not complete and not to the extent of EGFP-tagged GABARAP. It may be that overexpressed GABARAP localises better with mitochondrial GM130 because of stoichiometric reasons or perhaps because of some dysregulation. The minor colocalisation of endogenous GABARAP with mitochondrially targeted GM130 is perhaps expected as only minor colocalisation between endogenous GABARAP and GM130 is observed.

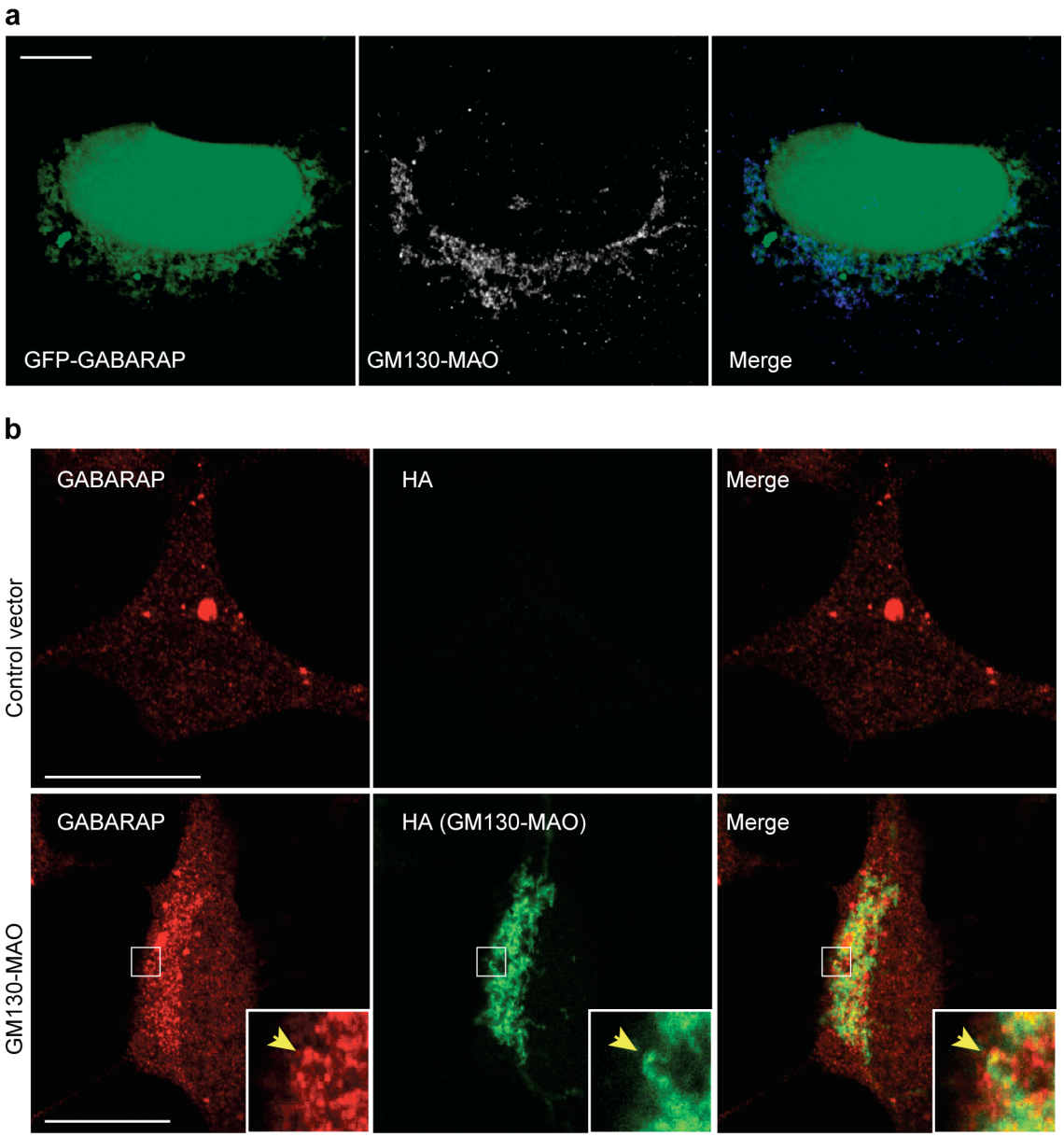

Figure 5.10 Mitochondrially localised GM130 can recruit GABARAP

(a) Co-expressed EGFP-GABARAP and GM130-ΔCterm-HA-MAO labelled with anti-HA. Scale bars, 10 μm. Experiment performed once. **(b)** Empty vector or GM130-ΔCterm-HA-MAO were expressed in HEK293A cells followed by 2 hr incubation with EBSS, anti-HA and anti-GABARAP labelling and analysis by confocal microscopy. Arrows indicate co-localization. Scale bars, 20 μm. Experiment performed twice.

I next wanted to further probe the WAC-GABARAP interaction. As shown (Figure 5.9b and c) both the overexpressed and endogenous forms of WAC and GABARAP interact. To investigate if this interaction occurred directly I used recombinant purified untagged human GABARAP, produced from *E. coli* (Figure 5.11a). In addition, I separately expressed EGFP-WAC in HEK293A cells and immunoprecipitated EGFP-WAC using GFP-TRAP (Figure 5.11b). Immobilised EGFP-WAC on beads was washed 5 times in 1M NaCl, followed by washing into a low salt buffer (Figure 5.11b). This was to help dissociate protein complexes immunoprecipitated from HEK293A cells, in support of this, endogenous GABARAP was not detected binding to its interactor mCherry-GFP-p62 (Pankiv et al., 2007), after 1M NaCl washes (Figure 5.11b). However, it is possible that interacting proteins may remain bound to EGFP-WAC after 1M NaCl washes, on the other hand the advantage of expressing EGFP-WAC in mammalian cells is that post-translational modifications on WAC that may influence protein-protein interactions should be maintained. mCherry-GFP-p62 was used as a control that directly interacts with GABARAP. It has previously been shown that p62 interacts directly with GABARAP and other Atg8 proteins (Pankiv et al., 2007). After the addition of purified recombinant untagged GABARAP (Figure 5.11a) to the salt washed GFP-Traps I could detect enhanced binding of GABARAP to mCherry-GFP-p62 over the EGFP alone control (Figure 5.11b and c), as would be expected (Pankiv et al., 2007). However no binding to EGFP-WAC was observed above the EGFP control levels (Figure 5.11b and c). Unfortunately, there was some background binding of GABARAP to the EGFP control (Figure 5.11b) and it may be possible that reduction of this background may reveal some low level binding of WAC and GABARAP. Nevertheless, under these conditions there was no evidence of direct binding of GABARAP to WAC. It is likely that WAC interacts with GABARAP in an indirect fashion, possibly by binding through GM130.

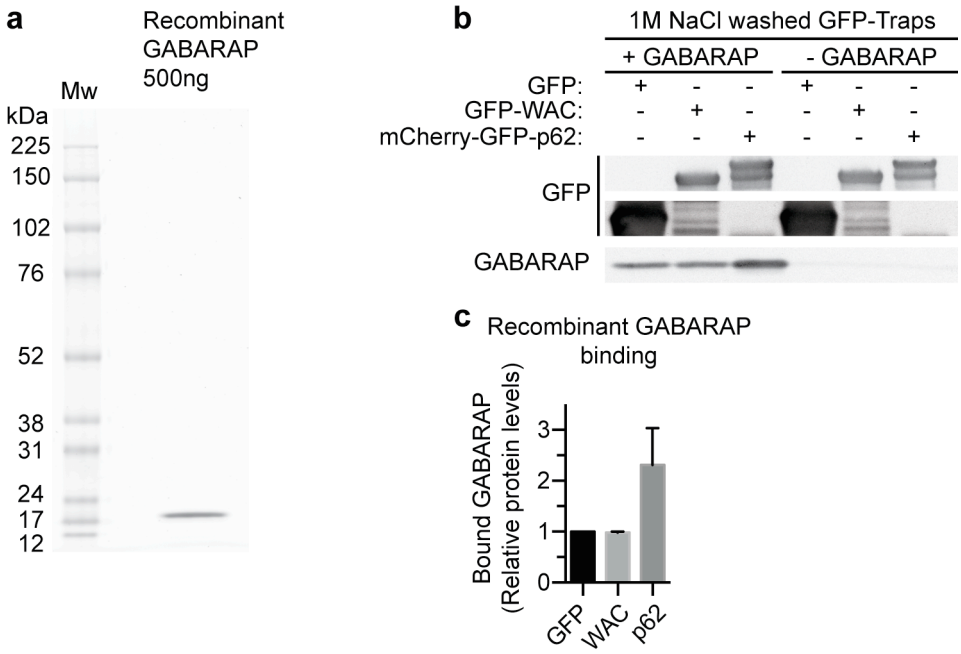

Figure 5.11 Recombinant GABARAP did not interact with GFP-WAC

(a) Colloidal Coomassie stained SDS-PAGE gel showing purified untagged human GABARAP from *E. coli*. Purified GABARAP was provided by Stephane Mouilleron. **(b)** Lysates from HEK293A cells expressing the indicated GFP constructs were used for GFP-TRAP followed by salt washes and incubation with purified recombinant GABARAP from **(a)** and immunoblot. mCherry-GFP-p62 was used as a positive control for GABARAP binding. GFP immunoblot shows the same gel and exposure for GFP, GFP-WAC and mCherry-GFP-p62. The intervening space between the faster migrating GFP band and the slower migrating GFP-WAC and mCherry-GFP-p62 bands has been removed, as indicated by an empty space. **(c)** Quantification of **(b)** from 2 independent experiments, mean ± SD.

5.5 Centrosomal GABARAP traffics to autophagosomes during starvation

5.5.1 GABARAP colocalises with γ-tubulin

The enlarged GABARAP structure that was juxtaposed to GM130 (Figure 5.9a and Figure 5.10b) did not appear to be an autophagosome because it was too large and was present under basal conditions. This structure was observed not in every cell but in many. The question remained as to what this structure represented. To my mind there were a few candidates of singular rounded structures that reside next to the cell nucleus such as the, endocytic recycling compartment, the aggresome, and the centrosome. GABARAP, via binding of p62, may be connected with aggresomes, which are enlarged aggregates of

ubiquitinated proteins (Pankiv et al., 2007). Furthermore, GABARAP has been seen at the basal body of the primary cilium (Pampliega et al., 2013), which is somewhat analogous to the centrosome. The primary cilium is a sensory organelle that grows from a mother centriole and is induced by serum starvation. After labelling for GABARAP with two different GABARAP antibodies under basal conditions I could observe GABARAP colocalising with γ-tubulin (Figure 5.12a and b), a marker for the pericentriolar material of the centrosome (Woodruff et al., 2014). The centrosome is comprised of two centrioles made of tubulin that are embedded in a matrix of coiled-coil proteins called the pericentriolar material (PCM). γ-tubulin ring complexes that nucleate microtubules are embedded in this matrix. The localisation of GABARAP to the centrosome was observed in cell lines derived from different tissues and species suggesting that it is not unique to the HEK293A model cell line (Figure 5.12a). However, the centrosome in HEK293A cells appeared enlarged and much more obvious than in the other cell lines tested. These enlarged γ-tubulin positive structures have been demonstrated before in HEK293A cells (Zhao et al., 2003). Low level expression of GFP-GABARAP using tetracycline-inducible HEK293 cells indicated that GFP-GABARAP could also localise to the centrosome (Figure 5.12c). This suggests that the GABARAP observed at the centrosome is unlikely to be due to an artefact of the antibody staining.

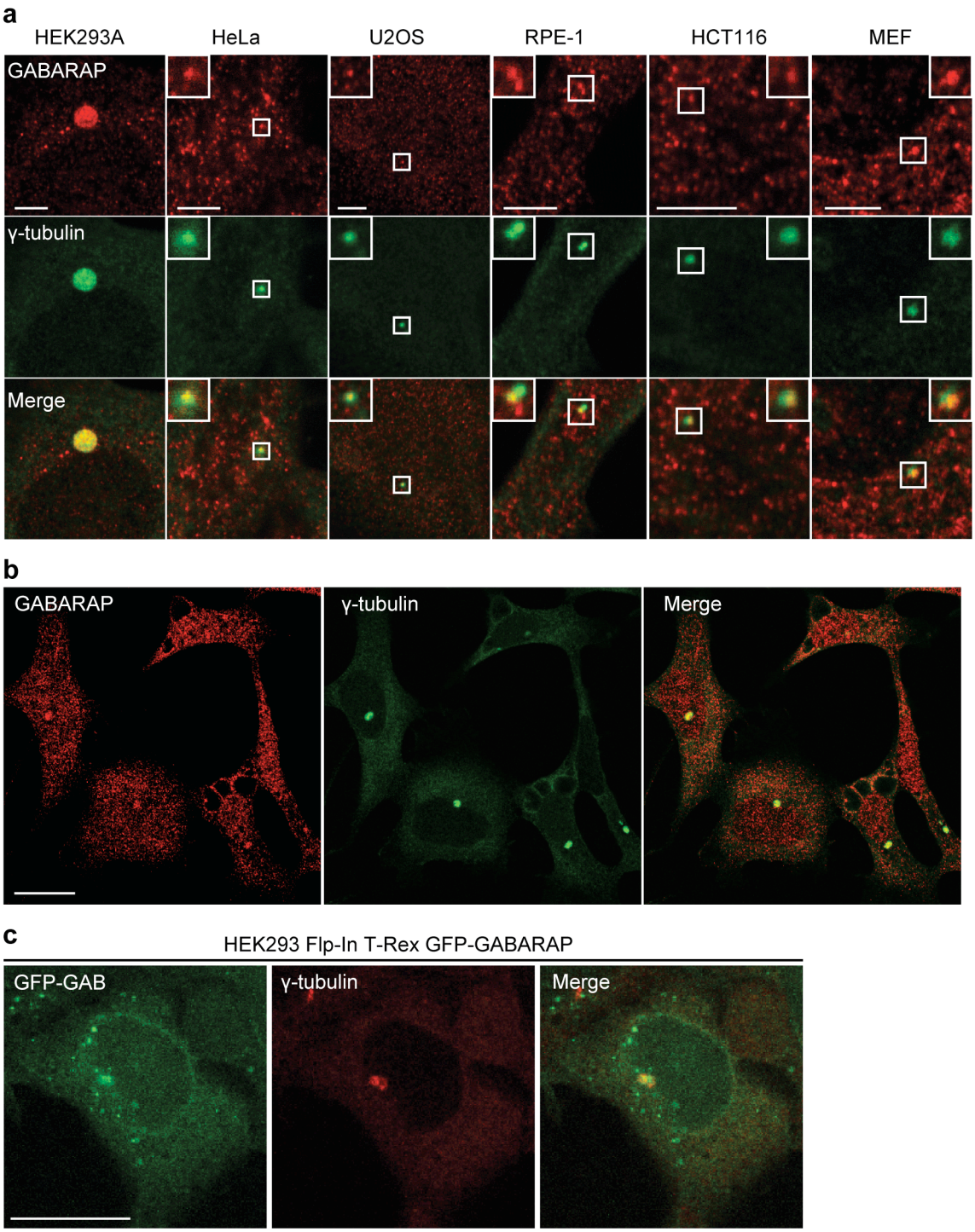

Figure 5.12 A population of GABARAP localises to the centrosome

(a) HEK293A, HeLa, U2OS, RPE-1, HCT116 and MEF cells were labelled as indicated. Scale bars, 5 μm. Rabbit anti-GABARAP was used. **(b)** HEK293A cells were stained with sheep anti-GABARAP antibody and mouse anti-γ-tubulin before analysis by confocal microscopy. Scale bars, 20 μm. **(c)** GFP-GABARAP expression in HEK293 Flp-In T-Rex cells after tetracycline treatment for 24 hr. Scale bars, 20 μm. Experiments performed once.

5.5.2 Non-lipidated GABARAP resides on the pericentriolar material of the centrosome

I wanted to further confirm the specificity of endogenous GABARAP staining at the centrosome. After treatment of HEK293A cells with siRNAs targeting GABARAP there was less GABARAP staining at the centrosome (Figure 5.13a), suggesting that the centrosomal GABARAP staining is indeed specific. By co-staining for GABARAP and Centrin-3 (Figure 5.13b), a marker for the centrioles (Middendorp et al., 2000), I noticed that the enlarged GABARAP structure was localised in a ring around Centrin-3, or sometimes juxtaposed to Centrin-3 (not shown). This further suggests that GABARAP localises to the pericentriolar material of the centrosome and not to the centrioles. I supposed enlarged GABARAP structures may be aggresomes and also because γ-tubulin marks aggresomes as well as centrosomes (Tanaka et al., 2004). I thus wanted to exclude the possibility that the enlarged GABARAP structure I observed was an aggresome. After nutrient starvation GABARAP puncta were observed that colocalised with p62 as expected (Figure 5.13c), these are likely to be autophagosomes, however the enlarged GABARAP structure was not positive for p62. Furthermore the enlarged GABARAP structure was negative for ubiquitin staining (Figure 5.13d), even after proteasomal inhibition with MG132 or epoxomycin (not shown). Thus, I conclude that GABARAP is present at the centrosome and that this population of GABARAP is distinct from the aggresome.

Finally, I wanted to see if GABARAP at the centrosome required lipidation for its localisation. In order to show this I transfected HEK293A cells with a G116A mutant of myc-GABARAP. This mutant of GABARAP cannot be processed into the lipidated form of GABARAP and thus remains non-lipidated (Chen et al., 2007). More specifically, the Atg8 proteins are produced as pro-proteins that are cleaved, exposing a C-terminal glycine that can be attached to phosphatidylethanolamine through an amide bond between the glycine and the amino group of phosphatidylethanolamine (Ichimura et al., 2000). Mutation of this Glycine to an Alanine prevents lipidation (Kirisako et al., 2000). Like the wild-type Myc-GABARAP, the G116A mutant could also localise at the centrosome (Figure 5.13e). This suggests that the pool of GABARAP at the centrosome is not lipidated. It is possible that G116A GABARAP may interact with the endogenous GABARAP

present on the centrosome, as GABARAP interacts with itself by crystal structure (Nymann-Andersen et al., 2002). To exclude this possibility, it would be interesting to repeat this experiment in the future with GABARAP knockout cells.

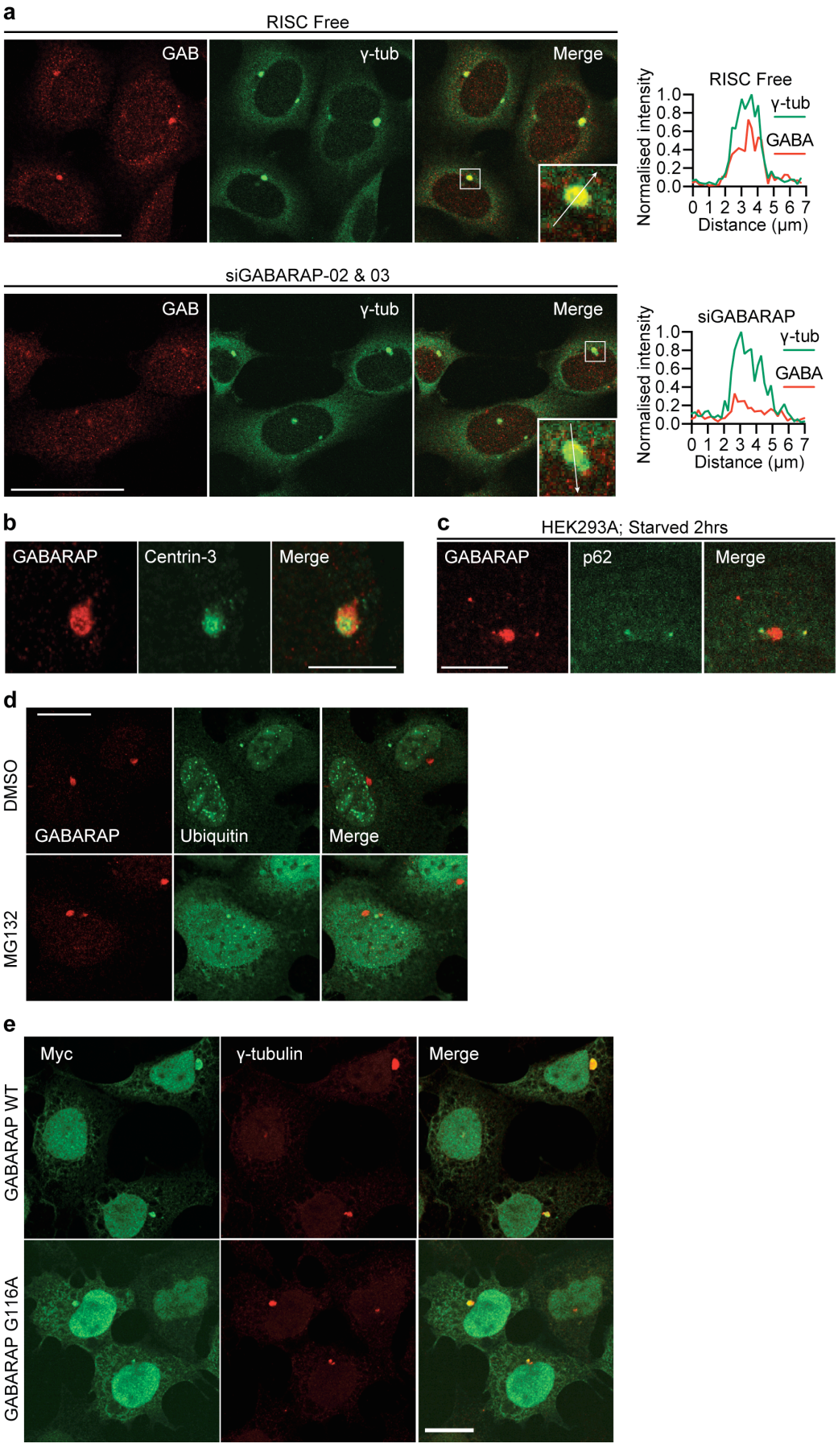
a
RISC Free
GAB
γ-tub
Merge
RISC Free
γ-tub
GABA
Normalised intensity
1.0
0.8
0.6
0.4
0.2
0.0
0 1 2 3 4 5 6 7
Distance (μm)
siGABARAP-02 & 03
GAB
γ-tub
Merge
siGABARAP
γ-tub
GABA
Normalised intensity
1.0
0.8
0.6
0.4
0.2
0.0
0 1 2 3 4 5 6 7
Distance (μm)
b
GABARAP
Centrin-3
Merge
c
HEK293A; Starved 2hrs
GABARAP
p62
Merge
d
DMSO
MG132
GABARAP
Ubiquitin
Merge
e
GABARAP WT
GABARAP G116A
Myc
γ-tubulin
Merge

Figure 5.13 Non-aggresomal and non-lipidated GABARAP localises to the pericentriolar material of the centrosome

(a) HEK293A cells were treated for 72 hr with RISC Free or GABARAP siRNAs, labelled with the indicated antibodies and analysed by confocal microscopy. Scale bars, 50 μm. Inset, line scan. Experiment performed twice. **(b)** HEK293A cells labelled as indicated. Scale bars, 10 μm. **(c)** HEK293A cells incubated in EBSS for 2 hr or **(d)** DMSO or MG132 for 2 hr and assessed using the indicated antibodies. Scale bars, 10 μm **(c)**, 20 μm **(d)**. **(e)** HEK293A cells expressing Myc-GABARAP or G116A mutant labelled as indicated. Scale bars 20 μm. Staining and microscopy was perfroemd by Minoo Razi. **(b-e)** Experiments performed once.

5.5.3 Centrosomal GABARAP localisation is regulated by the cell cycle but not by secretory membrane trafficking

In order to elucidate if centrosomal GABARAP had some function I began by investigating its dynamics, and if its localisation to the centrosome could be perturbed in some way. Surprisingly, in metaphase cells I noticed that the enlarged GABARAP structure was completely dissociated from the γ-tubulin positive spindle poles (Figure 5.14a). Although the mechanism or significance of this phenomenon is unknown, it suggests that centrosomal GABARAP is regulated by the cell cycle and is dynamically associated with the centrosome.

I next wanted to see if centrosomal GABARAP was regulated by membrane trafficking. To test this HEK293A cells were treated with Brefeldin A (BFA), a drug that causes the disassembly of the Golgi complex, and Golgi proteins relocalise to ER-exit sites (Ward et al., 2001). Glycosylation and protein secretion are inhibited after BFA treatment (Misumi et al., 1986). After BFA treatment the Golgi was indeed disassembled (Figure 5.14b). However, GABARAP positive puncta likely to be autophagosomes, were still formed upon starvation with BFA, and enlarged GABARAP structures (centrosomal GABARAP) were still observed. These data suggest that recruitment of GABRAP to the centrosome or to autophagosomes does not require secretion and agrees with previous findings that BFA treatment does not affect autophagic flux (Weidberg et al., 2010, Nishida et al., 2009, Zoppino et al., 2010).

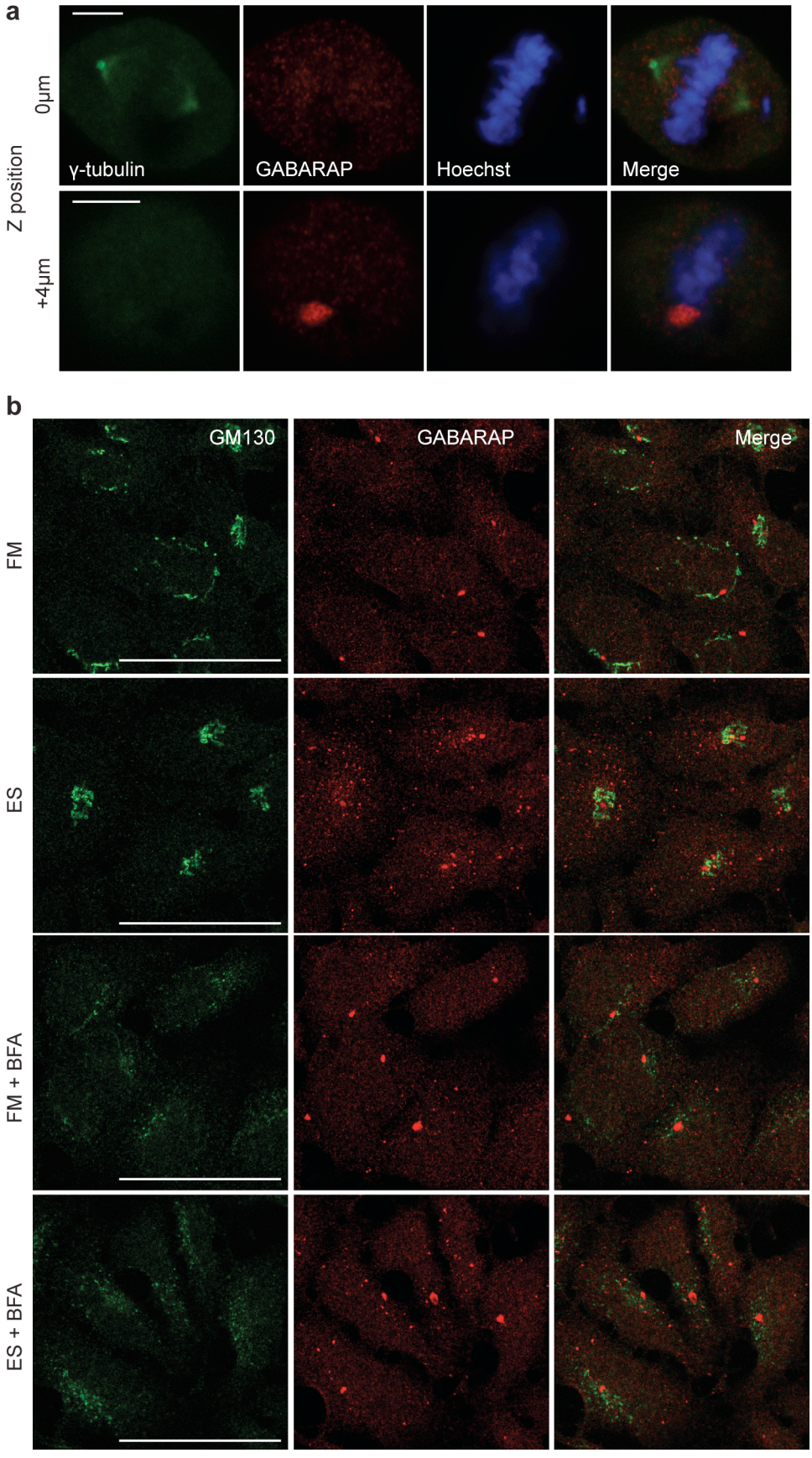
a
Z position
0µm
+4µm
γ-tubulin
GABARAP
Hoechst
Merge
b
FM
ES
FM + BFA
ES + BFA
GM130
GABARAP
Merge

Figure 5.14 GABARAP dissociates from γ-tubulin during metaphase but not after Brefeldin A treatment

(a) Asynchronous HEK293A cells were incubated in full medium and metaphase cells were analysed by confocal microscopy. A single mitotic cell is shown at two different positions in the Z-axis. Scale bars, 5 μm. This phenotype was observed in metaphase cells from 3 independent experiments, **(b)** HEK293A cells were incubated in full medium (FM) or EBSS (ES) with or without Brefeldin A (BFA) for 2 hr and assessed by confocal microscopy using the indicated antibodies. Scale bars, 50 μm. Experiment performed once.

5.5.4 Microtubules are required to concentrate non-lipidated GABARAP at the centrosome and away from the Golgi

GABARAP at the centrosome is not lipidated and does not require post-Golgi membrane secretion (Figure 5.13 and Figure 5.14). The centrosome functions as a microtubule organising centre. GABARAP is known to bind microtubules directly (Wang and Olsen, 2000) and thus the question arose as to whether centrosomal GABARAP was regulated by microtubules. Nocodazole is a compound that causes the disassembly of microtubules in cells and an accompanied fragmentation of the Golgi complex (Cole et al., 1996). The resultant Golgi mini stacks are relocalised adjacent to ER-exit sites. After treatment of HEK293A cells with a concentration of nocodazole that was sufficient to completely disassemble microtubules (Figure 5.15a), I saw the formation of GABARAP puncta under basal conditions (Figure 5.15b). Unlike autophagosomes, these puncta readily colocalised with GM130, on the Golgi ministacks. There was also a small but highly significant decrease of centrosomal GABARAP (Figure 5.15c), although GABARAP remained on the centrosome in many cells (data not shown). Golgi-localised GABARAP after microtubule depolymerisation was also observed in the presence of Wortmannin, a PI3 kinase inhibitor that also inhibits the Beclin 1 containing class III PI(3)K complex and thus prevents lipidation of Atg8 proteins (Kihara et al., 2001). These data suggest that in the absence of microtubules GABARAP relocalises from the centrosome to the Golgi, not as lipidated GABARAP but perhaps tethered by a protein such as GM130.

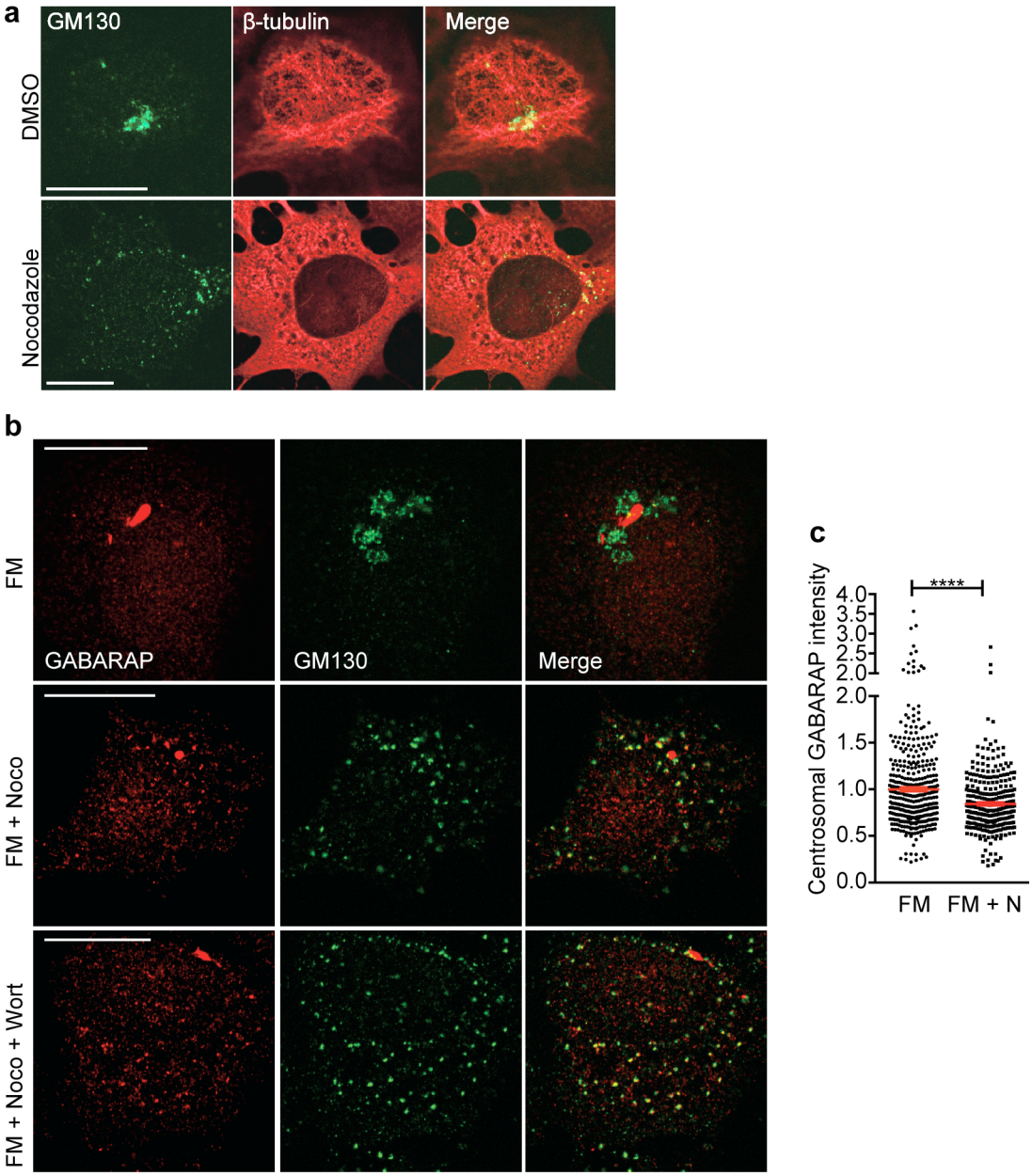

Figure 5.15 Nocodazole treatment reduces the amount of GABARAP at the centrosome and results in relocalisation of GABARAP to Golgi mini-stacks

(a) HEK293A cells were incubated in full medium with DMSO or nocodazole for 5 hr and assessed by confocal microscopy using the indicated antibodies. Scale bars, 20 μm. **(b)** HEK293A cells were incubated in full medium (FM), FM with nocodazole or FM with nocodazole and wortmannin for 5 hr and assessed by confocal microscopy using the indicated antibodies. Scale bars, 20 μm. **(c)** Quantification of centrosomal GABARAP intensity after nocodazole treatment. Mean ± SEM of 3 independent experiments, >300 cells in total were counted per condition, unpaired Student's t test, ****, $p \leq 0.0001$. Full medium plus nocodazole, FM + N. Enlarged GABARAP structures were taken as centrosomal GABARAP and their signal intensities were measured.

5.5.5 Nutrient starvation regulates the amount of GABARAP at the centrosome

GABARAP is recruited to autophagosomes upon nutrient starvation where it is lipidated and may function in driving closure of the forming autophagosome, as well as later functions in maturation (Weidberg et al., 2010, Wang et al., 2015). I hypothesised that the pool of non-lipidated GABARAP at the centrosome may provide a reservoir of GABARAP that could be used when autophagy is acutely induced. During starvation I saw the formation of GABARAP puncta (autophagosomes) as before (Figure 5.16a), which was completely inhibited by wortmannin treatment. I noticed a small reduction of GABARAP at the centrosome during starvation. After quantifying GABARAP signal intensity at the centrosome in hundreds of cells (Figure 5.16b), it was apparent that upon nutrient starvation there is a small but significant reduction in the amount of GABARAP at the centrosome that accompanies the formation of autophagosomes. This suggests that during starvation GABARAP could relocalise from a centrosomal reservoir to forming autophagosomes.

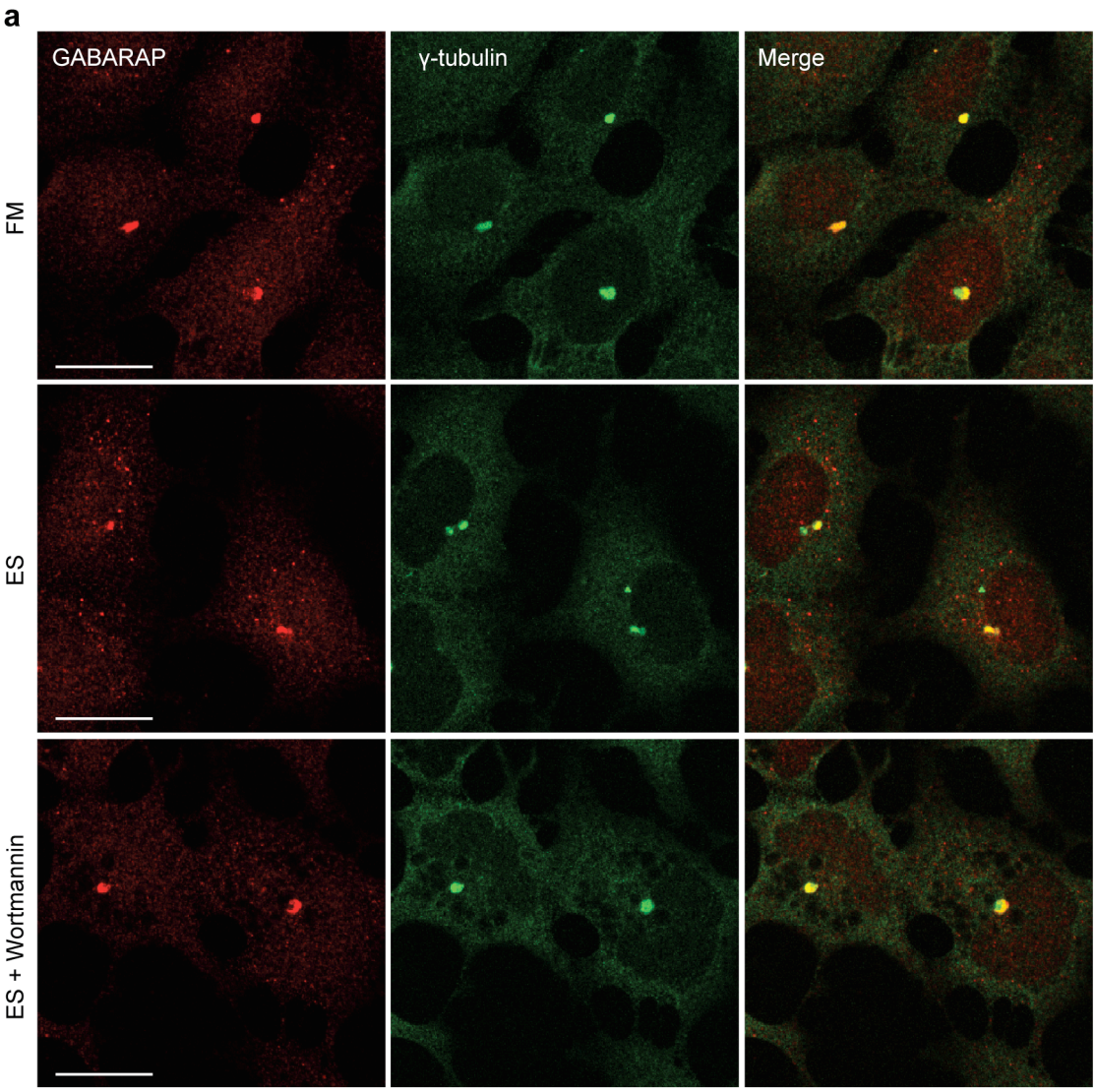
a
GABARAP
γ-tubulin
Merge
FM
ES
ES + Wortmannin
b
****
Centrosomal GABARAP intensity
4.0
3.0
2.0
2.0
1.5
1.0
0.5
0.0
FM
ES

Figure 5.16 Less GABARAP localises to the centrosome after 2 hr starvation, accompanied by GABARAP puncta formation

(a) HEK293A cells incubated in full medium (FM), EBSS (ES) or EBSS with wortmannin for 2 hr. Scale bars, 20 μm. **(b)** Quantification of centrosomal GABARAP after 2 hr with full medium (FM) or EBSS (ES). Mean ± SEM of 3 independent experiments, >420 cells were counted in total per condition, unpaired Student's t test, ****, $p \leq 0.0001$.

5.5.6 Photoactivatable GABARAP transports from the centrosome to forming autophagosomes during starvation

Although my experiments in fixed cells suggested that centrosomal GABARAP could contribute to autophagosomes (Figure 5.16), these were only suggestive. Hence I wanted to gather more evidence to support this hypothesis. In order to study the dynamics of specifically the centrosomal GABARAP pool, I attached a photoconvertible fusion protein, EosFP, to the N-terminus of GABARAP. EosFP is a fluorescent protein from coral that is constitutively green, but is converted from green fluorescence to red upon excitation with UV light (Wiedenmann et al., 2004). EosFP-GABARAP colocalised with γ-tubulin and WIPI2 in starved HEK293A cells (Figure 5.17a), thus suggesting that EosFP-GABARAP replicated endogenous GABARAP by localising to the centrosome and autophagosomes. EosFP-GABARAP formed rings around γ-tubulin, these were easily identifiable in live cells and were targeted in photoconversion experiments (Figure 5.17a, b and c). EosFP-GABARAP that was more homogenously distributed at the centrosome was hard to identify in live cells in the absence of a centrosomal marker. This is because these structures were confused with autophagosomes or aggregates of the overexpressed protein.

In starved live HEK293A cells, centrosomal EosFP-GABARAP was targeted for photoconversion, by irradiation with the 405nm laser. After photoconversion of the centrosomal green EosFP-GABARAP to red, GABARAP-positive red spots formed, which correlated with a decrease in the intensity of red centrosomal EosFP-GABARAP (Figure 5.17b, Figure 5.18a and Movie 1, see CD for movie and appendix for movie legend). Within minutes photoconverted centrosomal EosFP-GABARAP translocated to distal regions which were monitored by quantifying fluorescence intensities (Figure 5.18b). Like autophagosomes, EosFP-GABARAP

puncta were highly mobile (Kochl et al., 2006, Kimura et al., 2008) and additionally made transient interactions with centrosomal EosFP-GABARAP (Movie 2, see CD for movie and appendix for legend). Strikingly, peripheral green EosFP-GABARAP spots (that existed prior to photoconversion), acquired centrosomally-derived red photoactivated EosFP-GABARAP (Figure 5.17b, Figure 5.18a). After the live cell time-lapse microscopy the cells were fixed and stained with LC3 and γ-tubulin (Figure 5.17 and Figure 5.18). As the cells were seeded on gridded MatTek dishes during time-lapse imaging, I was able to find the same cells by correlative confocal microscopy. This technique confirmed that the photoconverted pool of GABARAP was at the centrosomal area, and that photoconverted centrosomal GABARAP had moved to peripheral puncta, many of which were LC3 positive, although some were LC3 negative (Figure 5.18c). Taken together these data suggest that forming and expanding autophagosomes acquire GABARAP derived from the PCM. It is also possible however that GABARAP is delivered to fully formed autophagosomes

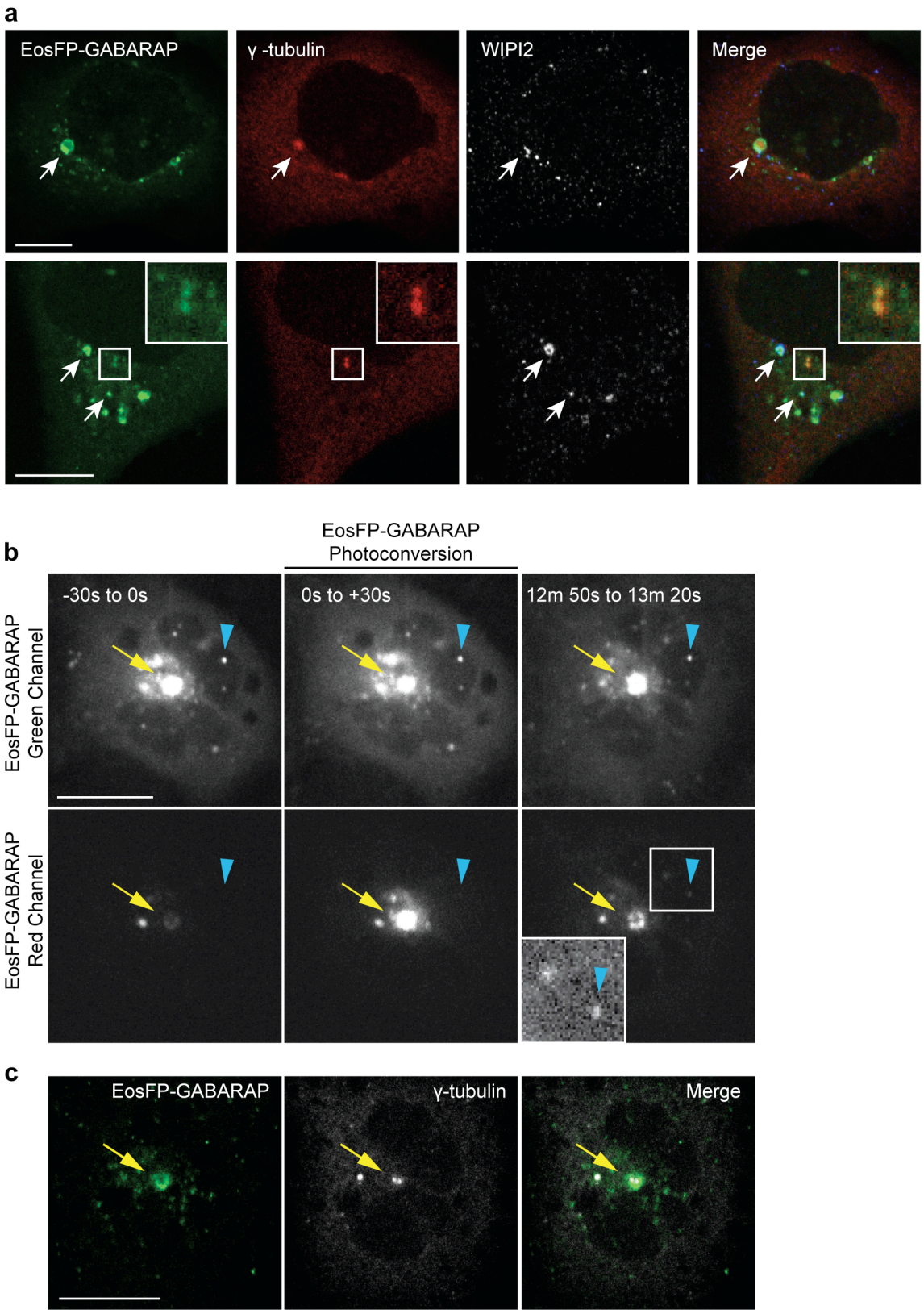
a
EosFP-GABARAP
γ -tubulin
WIPI2
Merge
b
EosFP-GABARAP
Photoconversion
-30s to 0s
0s to +30s
12m 50s to 13m 20s
EosFP-GABARAP
Green Channel
EosFP-GABARAP
Red Channel
c
EosFP-GABARAP
γ-tubulin
Merge

Figure 5.17 EosFP-GABARAP localises to the centrosome and WIPI2 puncta and forms puncta derived from the centrosomal region

(a) HEK293A cells expressing EosFP-GABARAP were incubated in EBSS for 2 hr before labelling with γ-tubulin and WIPI2 and analysis by confocal microscopy. Scale Bars, 10 μm. **(b)** Live HEK293A cells expressing EosFP-GABARAP were starved in EBSS and imaged every 5 s using a swept field confocal microscope. Photoconversion (PC) was performed with localised pulses of 405nm light. PC moment is set to 0 s. Yellow arrow indicates photoconverted region. Blue arrow shows defined punctum. To reduce noise, 6 sequential images, equal to 30 s timeframe, were averaged for each time period shown. Scale bar, 20 μm. Inset has been contrast adjusted for clarity. Experiment was performed 3 times on separate days, see also Figure 5.18. **(c)** Confocal microscopy performed on same cell from **(b)**. After time-lapse imaging, cells were fixed and stained for γ-tubulin. Yellow arrow indicates the same structure as in **(b)**. Scale bar, 20 μm.

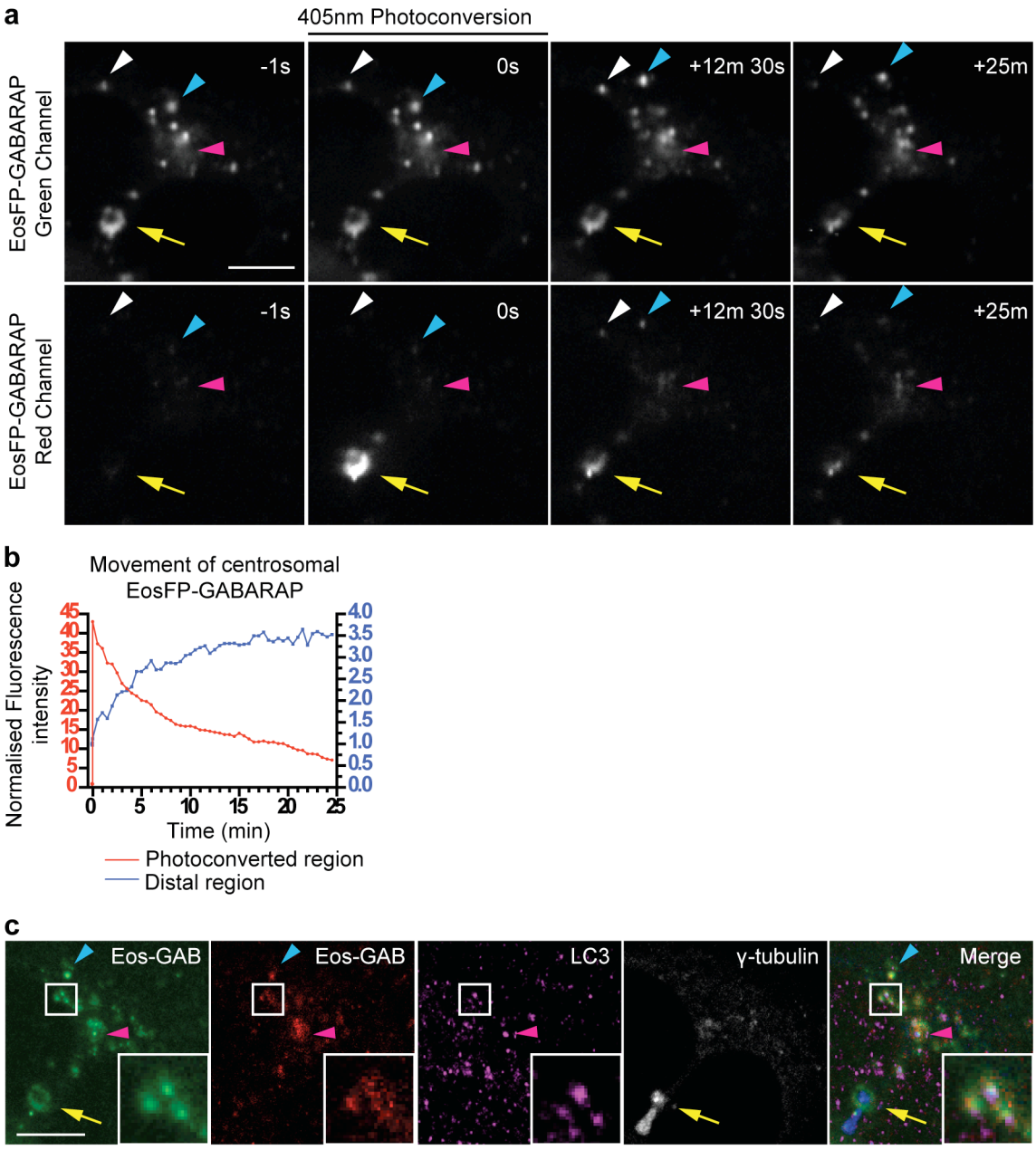

Figure 5.18 Photoconverted GABARAP translocates from the centrosomal area to LC3 positive puncta during starvation

(a) EosFP-GABARAP in starved HEK293A cells was imaged every 30 s using a swept field confocal microscope. 5 x 1 s images were captured prior to photoconversion (PC). PC moment is set to 0 s. Yellow arrow, photoconverted region. Magenta arrowhead, distal region. White and blue arrows track defined puncta. Scale bars, 10 μm. **(b)** Quantification of fluorescence intensity from video in **(a)**. PC region marked by yellow arrow and distal region marked by magenta arrowhead in **(a)**. Intensity 5 s prior to PC moment is set to 1 for normalisation. **(c)** Confocal microscopy performed on same cell from video in **(a)**. After imaging, cells were fixed and stained for LC3 and γ-tubulin. Arrows and arrowheads correspond to structures shown in **(a)**. Scale bars, 10 μm.

5.5.7 Cytosolic GABARAP translocates faster than centrosomal GABARAP

In contrast to the centrosomal pool, cytosolic EosFP-GABARAP diffused within seconds across the cell, rather than translocating in the timescale of minutes (compare Figure 5.18b and Figure 5.19b). This was measured by either assessing the movement of photoconverted EosFP-GABARAP across the cell (Figure 5.19a and b), or by looking at the diffusion of non-photoconverted (green) EosFP-GABARAP into a photoconverted (red) area (Figure 5.19c and d). Within seconds, this cytosolic photoconverted EosFP-GABARAP was recruited to punctate structures in the cell (Figure 5.19a). These puncta already had green non-photoconverted EosFP-GABARAP (data not shown). Perhaps this recruitment of cytosolic GABARAP to pre-existing GABARAP puncta occurred by lipidation or perhaps by homotypic interactions with other GABARAP molecules. Thus, given the kinetics of cytosolic diffusion versus translocation from the centrosomal area, it is likely that the red EosFP-GABARAP-puncta in Figure 5.17b and Figure 5.18a are derived from a centrosomal pool and not from unintentional photoconversion of the cytosolic pool.

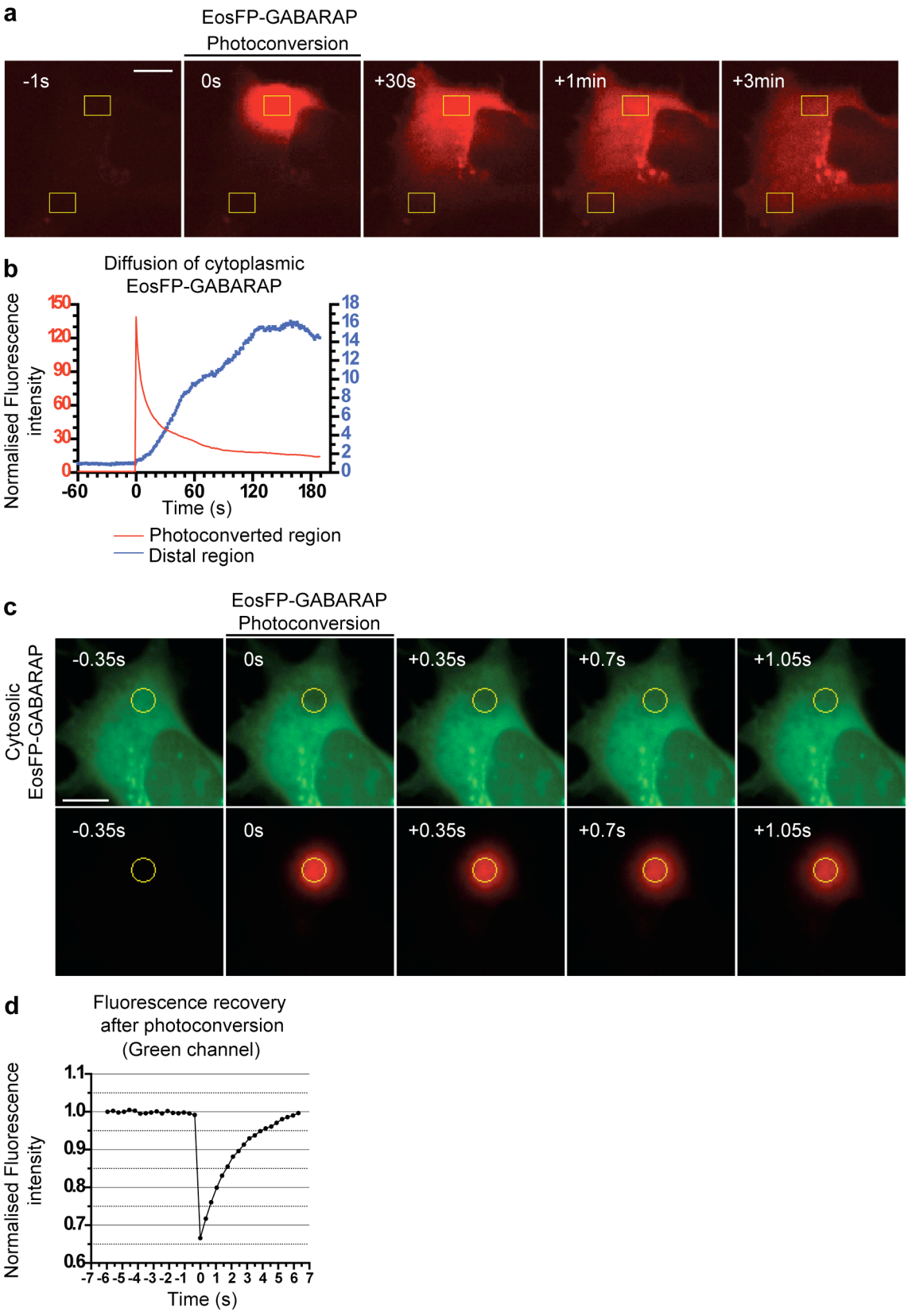
a
EosFP-GABARAP
Photoconversion
-1s
0s
+30s
+1min
+3min
b
Diffusion of cytoplasmic
EosFP-GABARAP
Normalised Fluorescence intensity
150
120
90
60
30
0
18
16
14
12
10
8
6
4
2
0
-60
0
60
120
180
Time (s)
Photoconverted region
Distal region
c
EosFP-GABARAP
Photoconversion
Cytosolic EosFP-GABARAP
-0.35s
0s
+0.35s
+0.7s
+1.05s
d
Fluorescence recovery
after photoconversion
(Green channel)
Normalised Fluorescence intensity
1.1
1.0
0.9
0.8
0.7
0.6
-7 -6 -5 -4 -3 -2 -1 0 1 2 3 4 5 6 7
Time (s)

Figure 5.19 Diffusion of cytosolic GABARAP occurs much more rapidly than movement of GABARAP from the centrosome

(a) HEK293A cell expressing EosFP-GABARAP, only red channel shown. Photoconversion (PC) moment is set to 0 s. Yellow box (top), photoconverted region. Yellow box (bottom), distal region. Scale bar, 10 μm. Experiment performed on multiple cells. **(b)** Quantification of intensities from boxed regions in **(a)**. Intensity 60 s prior to PC moment is set to 1 for normalisation. **(c)** HEK293A cell expressing high levels of cytosolic EosFP-GABARAP starved in EBSS and imaged every 0.35 s using a swept field confocal microscope. PC was performed with 405nm light. PC moment is set to 0 s. Scale bar, 10 μm. **(d)** Graph shows quantification of fluorescence intensity from yellow circle in images **(c)**, for green channel only. Intensity 6 s prior to PA moment is set to 1 for normalisation.

5.5.8 Golgi-localised GABARAP after nocodazole treatment is relatively immobile and does not contribute to *de novo* puncta formation

In order to further investigate the effect of depolymerising microtubules on GABARAP (Figure 5.15), I pre-treated live HEK293A cells expressing EosFP-GABARAP with nocodazole followed by incubation in EBSS with nocodazole (Figure 5.20). I wanted to ask if microtubules are required to translocate GABARAP from the centrosome to forming autophagosomes. However, in these cells I could never find the distinct ring-shaped structures of EosFP-GABARAP around the centrosome (not shown) I previously described (Figure 5.17a). Thus I could not target these for photoconversion experiments. This is perhaps reassuring though, as there is less endogenous GABARAP at the centrosome after nocodazole treatment (Figure 5.15c). After nocodazole treatment (Figure 5.20a) I noticed an accumulation of dispersed or peripherally distributed EosFP-GABARAP puncta. I targeted these puncta individually for photoconversion and performed time-lapse microscopy. These structures were relatively immobile over a 20 minute period after photoconversion. Furthermore, unlike with centrosomal EosFP-GABARAP, I did not observe translocation of photoconverted EosFP-GABARAP from these nocodazole-dispersed structures to other puncta. Correlative confocal microscopy revealed that similar to endogenous GABARAP (Figure 5.15b), EosFP-GABARAP was retained on Golgi mini-stacks (Figure 5.20b). This is another indicator that EosFP-GABARAP simulates the endogenous protein. This suggests that without microtubules centrosomal GABARAP relocalises to the Golgi where it becomes immobile. This population is unlikely to contribute to autophagosome formation. It

should be noted that I was only able to obtain one good video for the nocodazole experiment (Figure 5.20), and thus my observations may not be representative of variation in a heterogeneous cell population and should be repeated in future studies.

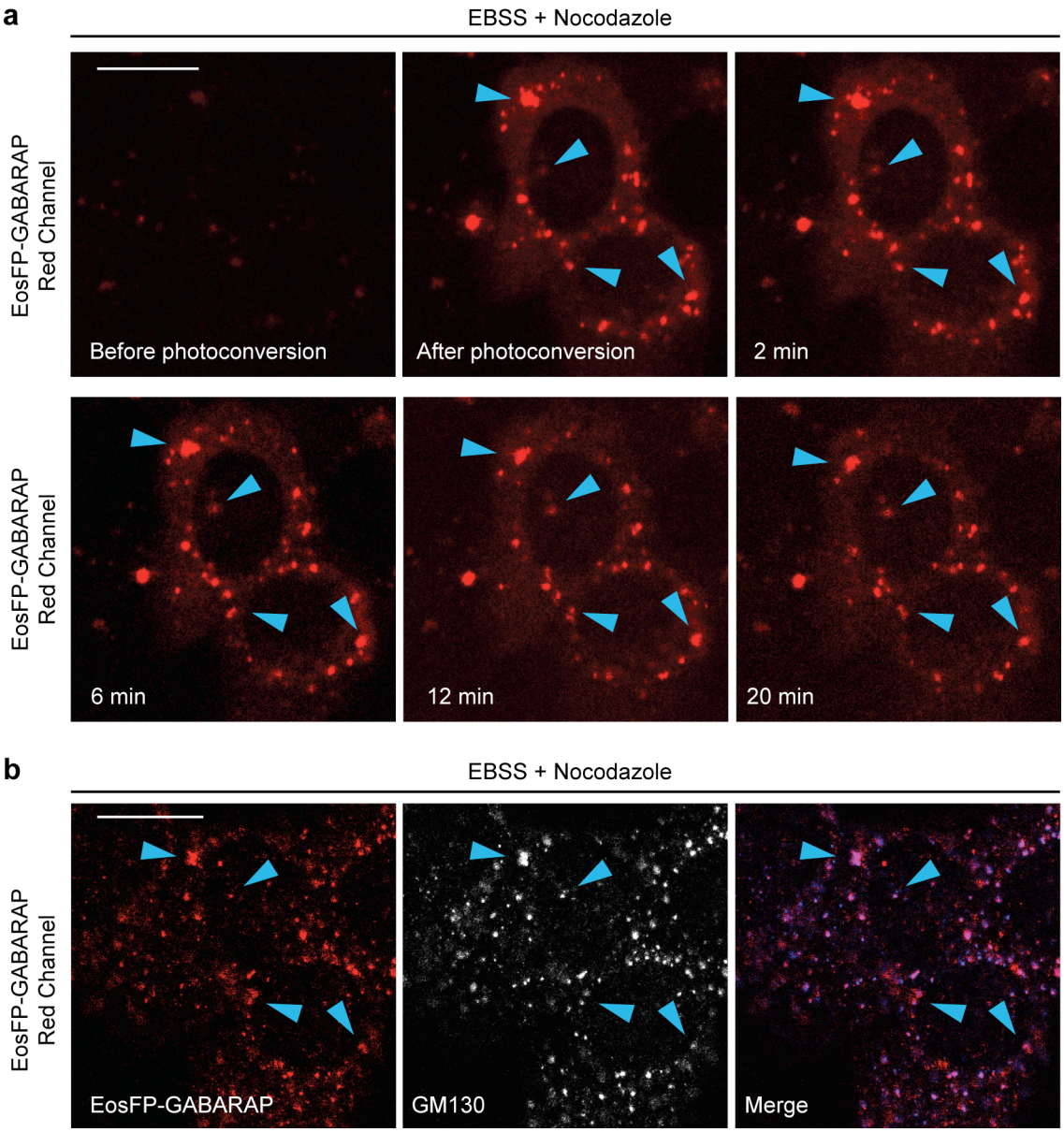

Figure 5.20 EosFP-GABARAP disperses after nocodazole treatment and relocalises to relatively immobile Golgi mini-stacks

(a) EosFP-GABARAP expressing HEK293A cells in full medium with nocodazole for 2 hr, then incubated in EBSS with nocodazole and imaged. Discrete structures were targeted for photoconversion and Images were captured every 3 s. All visible red structures after photoconversion were targeted individually for photoconversion. Blue arrows track a subset of these puncta. Scale bars, 20 μm. **(b)** Confocal microscopy performed on same cells from video in **(a)**. After imaging, cells were fixed and stained for GM130. Arrows correspond to structures shown in **(a)**. Scale bars, 20 μm. Experiment was performed once.

5.6 WAC inhibits binding of GABARAP to GM130 to promote centrosomal GABARAP localisation

5.6.1 WAC regulates GABARAP localisation

Since WAC and GM130 interact with GABARAP (Figure 5.9b and c), I next investigated if WAC and GM130 regulated the localisation of GABARAP to the centrosome or forming autophagosomes. Centrosomal GABARAP that colocalised with γ-tubulin, was seen in both fed and starved cells (Figure 5.22a), and in starved cells GABARAP-positive autophagosomes appeared (Figure 5.21). In starvation, WAC knockdown resulted in an accumulation of GABARAP on the Golgi (Figure 5.21) and ERGIC (Figure 5.22b) as marked by GM130 and ERGIC-53 respectively. This phenotype was characterised by an accumulation of GABARAP staining in the juxtanuclear region that exhibited a fragmented or dispersed pattern, and a reduction or loss of GABARAP contained within the enlarged GABARAP structure, the centrosome (Figure 5.21 and Figure 5.22a). It should be noted that not all WAC knockdown cells displayed this phenotype, and that this may be due to efficacy of the siRNA treatment or another heterogeneous property of the cell population such as cell cycle stage. The accumulation of GABARAP on the Golgi after WAC knockdown may be explained by an increase in the interaction of GABARAP with GM130 after WAC depletion (Figure 5.22c and d). This may also explain the accumulation of GABARAP on the ERGIC after WAC knockdown as GM130 is also known to traffic through the intermediate compartment (Marra et al., 2001).

GM130 can regulate centrosome morphology and function (Kodani and Sutterlin, 2008a) and after GM130 knockdown, I noticed that generally there was a small increase in the size and intensity of the centrosomal GABARAP pool Figure 5.21 and Figure 5.22a). These data suggest that WAC and GM130 control the localisation of centrosomal GABARAP in a reciprocal manner. WAC may promote GABARAP retention at a centrosomal reservoir, whereas GM130 may limit the pool of centrosomal GABARAP. Furthermore, WAC appears to negatively regulate GABARAP-GM130 binding. Future work should aim to further describe these phenotypes in a more quantitative manner.

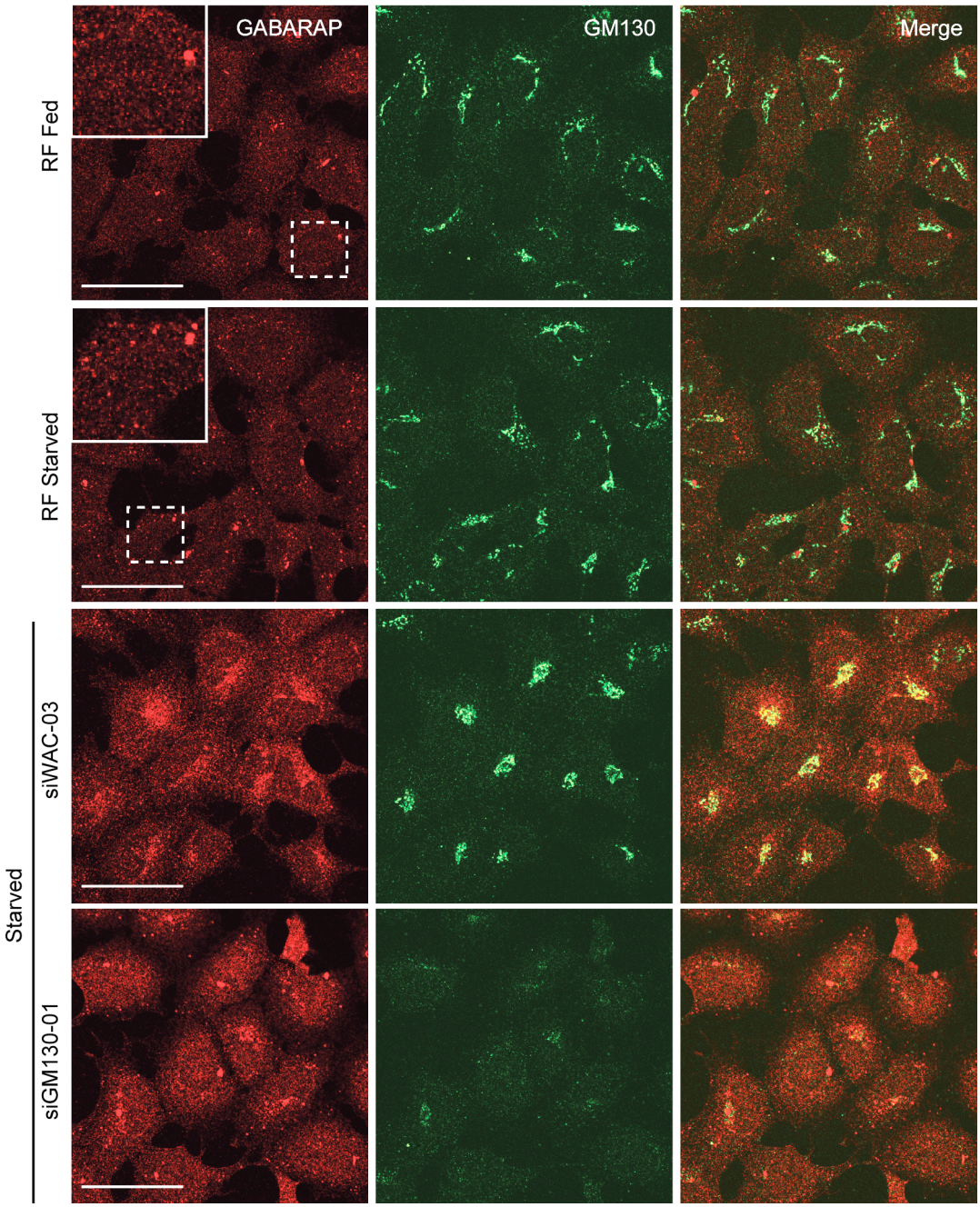

Figure 5.21 Depletion of WAC increases the amount of GABARAP at the Golgi

HEK293A cells were treated with RISC Free (RF), WAC or GM130 siRNAs for 72 hr and incubated with full medium (Fed) or EBSS (Starved) for 2 hr. Scale bars, 50 μm. Experiment was performed twice.

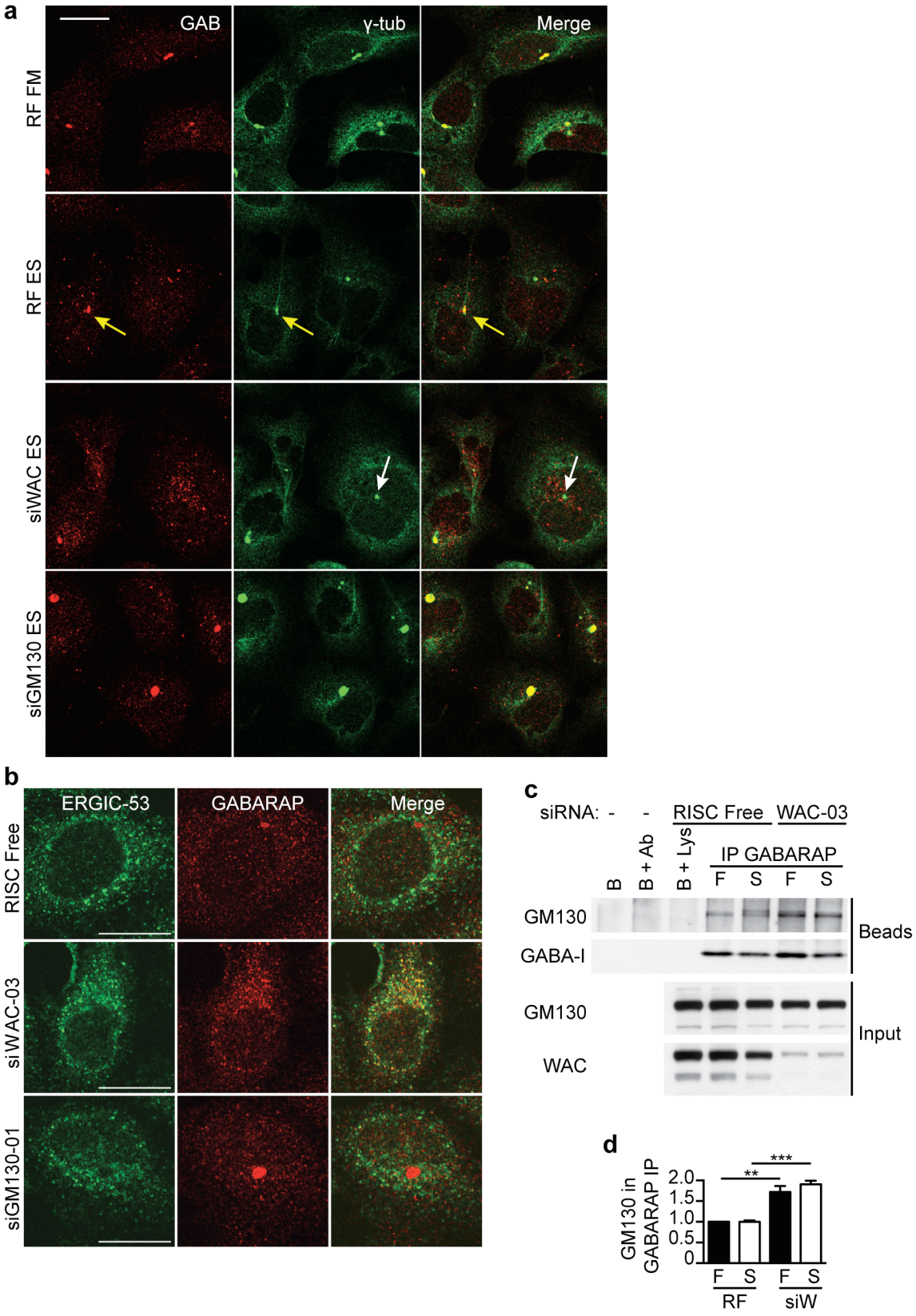
a
GAB
γ-tub
Merge
RF FM
RF ES
siWAC ES
siGM130 ES
b
ERGIC-53
GABARAP
Merge
RISC Free
siWAC-03
siGM130-01
c
siRNA: - - RISC Free WAC-03
B
B + Ab
B + Lys
IP GABARAP
F S F S
GM130
GABA-I
Beads
GM130
WAC
Input
d
GM130 in GABARAP IP
2.0
1.5
1.0
0.5
0
**
***
F S F S
RF
siW

Figure 5.22 WAC knockdown increases the amount of GABARAP on the ERGIC and increases GM130-GABARAP binding

(a) HEK293A cells were treated with RISC Free (RF), WAC or GM130 siRNAs for 72 hr, incubated with full medium (FM) or EBSS (ES) for 2 hr and analysed by confocal microscopy. Scale bars, 20 μm. Yellow arrows show GABARAP on the centrosome, white arrows show centrosomes without GABARAP. **(b)** HEK293A cells were treated with RISC Free, WAC or GM130 siRNAs for 72 hr, incubated with EBSS for 2 hr and analysed by confocal microscopy. Scale bars, 20 μm. **(a – b)** experiment performed once. **(c)** HEK293A cells were treated with RISC Free or WAC siRNAs for 72 hr and incubated with full medium (F) or EBSS (S) for 2 hr followed by GABARAP immunoprecipitation and immunoblotting. B, beads; Ab, GABARAP antibody; Lys, lysate. **(d)** Quantification of **(c)**, Student's t test, **, $p \leq 0.001$. Mean ± SEM of 3 independent experiments.

5.6.2 Golgi-localised GABARAP after WAC depletion is relatively immobile and does not contribute to *de novo* puncta formation

To investigate GABARAP dynamics in WAC depleted cells, I employed EosFP-GABARAP and photoconversion. After transfection of EosFP-GABARAP into HEK293A cells depleted of WAC (Figure 5.23a) I noticed an accumulation of EosFP-GABARAP in the juxtanuclear region. Photoconversion and time-lapse microscopy of the juxtanuclear-accumulated EosFP-GABARAP revealed that this pool of GABARAP is relatively immobile and did not form cytoplasmic GABARAP spots during starvation (Figure 5.23a and Movie 3, see CD for movie and appendix for legend). Fixation and correlative confocal microscopy of time-lapse imaged cells (Figure 5.23b) confirmed that juxtanuclear EosFP-GABARAP was localised on and around the Golgi, and that regions targeted for photoconversion were GM130 positive. This is similar to the accumulation of endogenous GABARAP at the Golgi upon WAC depletion (Figure 5.21). Thus, in the absence of WAC, GABARAP accumulates on the Golgi and this population is unlikely to contribute to autophagosome formation. In general WAC knockdown leads to reduced autophagosome formation.

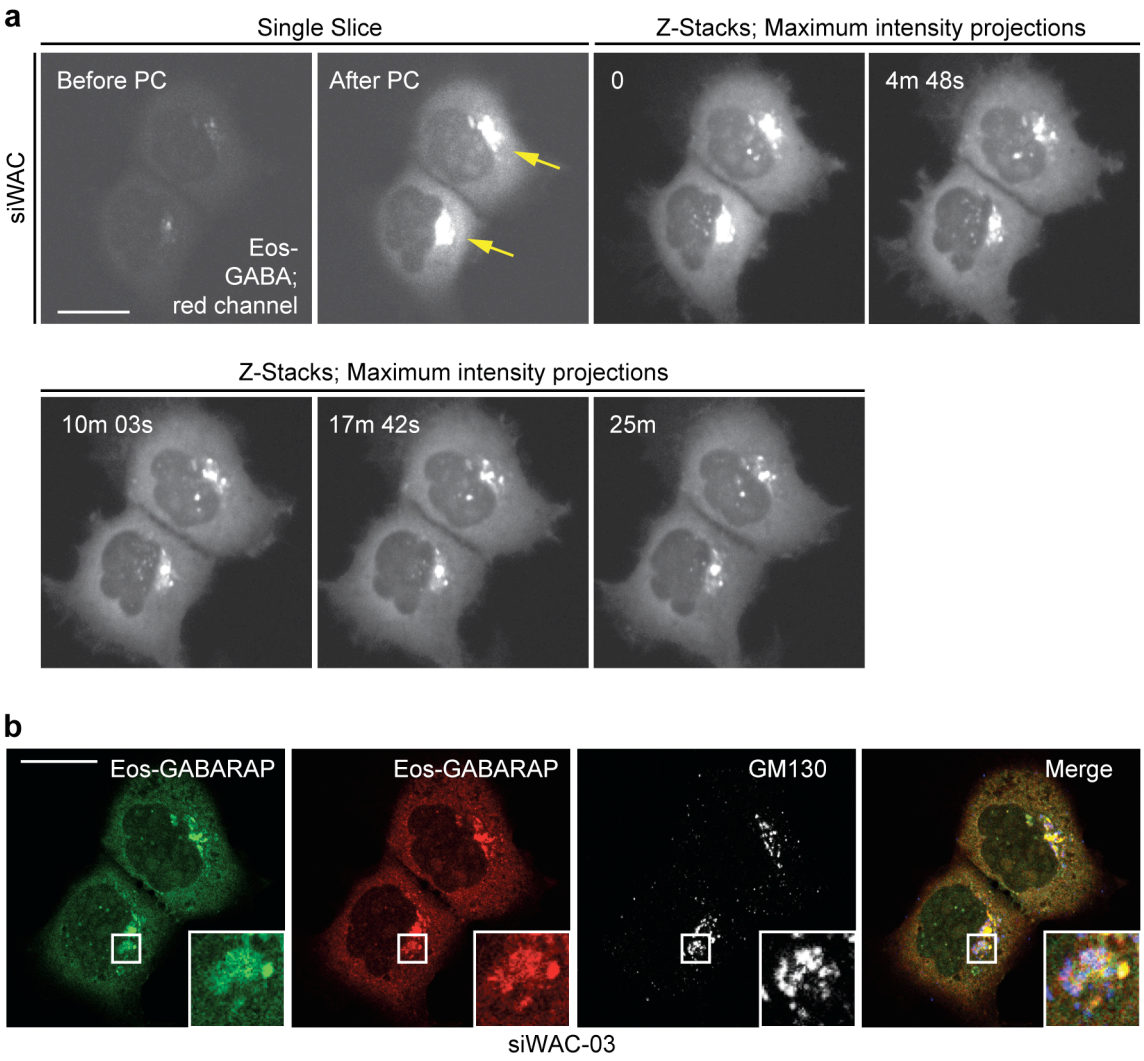

Figure 5.23 EosFP-GABARAP is retained on the Golgi after WAC knockdown and this population does not contribute to puncta formation during starvation

(a) EosFP-GABARAP expressed in HEK293A cells treated with WAC siRNA for 72 hr. Live cell imaging under starvation conditions. During photoconversion (PC), images from a single z-slice were acquired every 0.4 s. After PC z-stacks were acquired every 13 s. Shown are a selection of frames acquired at indicated times. Yellow arrows denote PC regions. Scale bars, 20 μm. Experiment was performed twice on separate days. **(b)** After time-lapse imaging, same cells shown in **(a)** were fixed and stained for GM130. Scale bars, 20 μm.

5.7 Non-lipidated GABARAP promotes ULK1 activity

5.7.1 GABARAP specifically promotes ULK1 activation likely by binding through the ULK1 LIR motif and independently of lipidation.

WAC depletion reduces activation of the ULK1 complex (Figure 5.5) but also likely inhibits GABARAP trafficking from the Golgi region to the centrosome (Figure 5.21). The question arises whether these two observations are independent or interconnected. GABARAP is thought to promote autophagosome closure and also fusion with lysosomes (Weidberg et al., 2010, Wang et al., 2015). I wanted to elucidate if knockdown of GABARAP could also attenuate ULK1 activation, thereby indicating a novel role of GABARAP in the early signalling events of autophagosome formation and demonstrating a phenotypic similarity between WAC and GABARAP. The clue that this could be the case is that GABARAP directly binds ULK1 complex members (Kraft et al., 2012, Alemu et al., 2012) (Okazaki et al., 2000). Atg13 p-Ser318 levels were significantly decreased after depletion of GABARAP, but not LC3B, GABARAPL1 or GATE-16 (Figure 5.24a, b, c and d). The efficacy of knockdown was confirmed at the mRNA level by qRT-PCR (Figure 5.24e), although I was only able to obtain a weak knockdown (< 50% reduction) of LC3A and LC3C (data not shown). By comparing the relative mRNA levels of the mAtg8 homologues to GAPDH (Figure 5.24f), my results suggested that in HEK293A cells, GABARAP is the most abundant mAtg8 protein followed by GATE-16, LC3B, GABARAPL1, LC3C and lastly by LC3A. This is similar to what has recently been published for the prostate cancer cell line LNCaP (Szalai et al., 2015), although in these cells LC3A was more abundant than LC3C. Thus GABARAP, the most abundant mAtg8 (at least in LNCaP cells and possibly in HEK293A cells) specifically promotes activation of ULK1. I should add that although I followed the published method (Szalai et al., 2015) to compare the expression of the mAtg8s, strictly speaking it could be problematic to compare the expression of different genes, unless it is demonstrated that the qRT-PCR amplification efficiencies for each gene target are similar, which I have not done. Future studies into mATG8 expression in HEK293A cells should address this. However, it is nonetheless interesting that I obtained very similar results to (Szalai et al., 2015), even when using independently-designed qRT-PCR primers.

I next wanted to see if overexpression of GABARAP could modulate ULK1 activity and if this depended on the ULK1 LIR motif. Overexpression of HA-ULK1 in fed HEK293 cells was sufficient to drive Atg13-FLAG phosphorylation even under basal conditions when ULK1 should not be active (as seen before (Chan et al., 2009)) and also when the ULK1 LIR was mutated (ΔLIR) (Figure 5.24g). As a negative control, expression of HA-ULK1 K46I ΔLIR, which has a kinase inactivating mutation (Chan et al., 2009), did not result in phosphorylation of Atg13-FLAG. The ULK1 LIR mutation used was generated in the Tooze lab (Kraft et al., 2012).These data suggest that the LIR motif of ULK1 *per se* is not required for the kinase activity of ULK1. In fact, there was a trend towards enhanced ULK1 activity upon mutation of the LIR motif, although this was not significant (Figure 5.24j). I next asked whether the LIR motif of ULK1 could regulate ULK1 activity in the presence of other overexpressed proteins. In the presence of EGFP-GABARAP and the non-lipidated G116A GABARAP mutant (Figure 5.24h), the ULK1 LIR was required for maximal phosphorylation of Atg13-FLAG (Figure 5.24g, i and j). However, when EGFP-LC3B was overexpressed in the presence of HA-ULK1 and Atg13-FLAG, mutation of the ULK1 LIR does not reduce ULK1 activity, similarly to transfection with an empty vector control.

These data suggest that overexpression of ULK1 leads to dysregulated phosphorylation of Atg13 under basal conditions when ULK1 should be turned off; this is used as a readout for ULK1 activity. ULK1 activity in this scenario is independent of the LIR motif of ULK1. However in the presence of GABARAP, which binds ULK1 and its complex members directly, the LIR motif of ULK1 is required for its full activity. This is independent of lipidation of GABARAP and may indicate that direct binding of GABARAP to ULK1 maintains ULK1 activity. This effect is specific because unlike GABARAP, LC3B does not affect the kinase activity of the ULK1 LIR mutant.

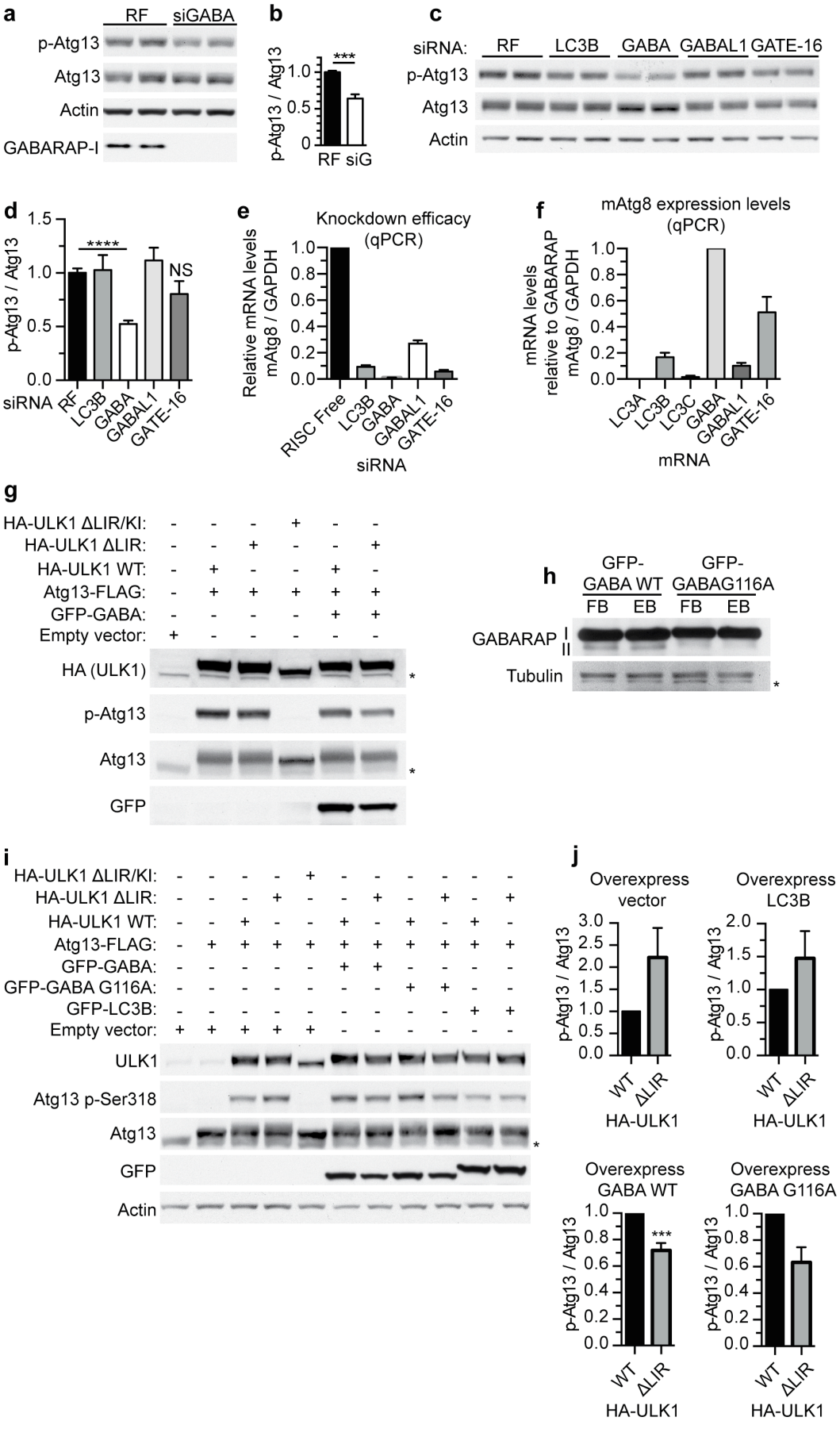
a
RF
siGABA
p-Atg13
Atg13
Actin
GABARAP-I
b
p-Atg13 / Atg13
***
RF siG
c
siRNA:
RF
LC3B
GABA
GABAL1
GATE-16
p-Atg13
Atg13
Actin
d
p-Atg13 / Atg13
****
NS
siRNA RF LC3B GABA GABAL1 GATE-16
e
Knockdown efficacy
(qPCR)
Relative mRNA levels
mAtg8 / GAPDH
RISC Free LC3B GABA GABAL1 GATE-16
siRNA
f
mAtg8 expression levels
(qPCR)
mRNA levels
relative to GABARAP
mAtg8 / GAPDH
LC3A LC3B LC3C GABA GABAL1 GATE-16
mRNA
g
HA-ULK1 ΔLIR/KI:
HA-ULK1 ΔLIR:
HA-ULK1 WT:
Atg13-FLAG:
GFP-GABA:
Empty vector:
HA (ULK1)
p-Atg13
Atg13
GFP
h
GFP-GABA WT
GFP-GABAG116A
FB EB FB EB
GABARAP I II
Tubulin
i
HA-ULK1 ΔLIR/KI:
HA-ULK1 ΔLIR:
HA-ULK1 WT:
Atg13-FLAG:
GFP-GABA:
GFP-GABA G116A:
GFP-LC3B:
Empty vector:
ULK1
Atg13 p-Ser318
Atg13
GFP
Actin
j
Overexpress vector
Overexpress LC3B
p-Atg13 / Atg13
WT ΔLIR
HA-ULK1
Overexpress GABA WT
Overexpress GABA G116A
***

Figure 5.24 Knockdown of GABARAP, but not other mAtg8s, attenuates ULK1 activity

(a) HEK293A cells treated with RISC Free (RF) or GABARAP siRNA for 72 hr, incubated in EBSS for 2 hr followed by immunoblot. p-Atg13, pSer318. **(b)** Quantification of **(a)**, Student's t test, ***, $p \leq 0.001$. Mean ± SEM of 3 independent experiments. **(c)** HEK293A cells treated with RF, LC3B, GABARAP, GABARAPL1 or GATE-16 siRNAs for 72 hr before 2 hr incubation in EBSS and immunoblot. p-Atg13, pSer318. **(d)** Quantification of **(c)** student's t test, ****, $p \leq 0.0001$. Mean ± SEM of 3 independent experiments. Not significant versus RF control, NS. **(e)** HEK293A cells were treated with RF, LC3B, GABARAP, GABARAPL1 or GATE-16 siRNA for 72 hr prior to analysis by qRT-PCR. Expression of each gene is normalised to the RISC Free sample. 3 independent experiments that are date matched with 3 experiments from **(d)**. **(f)** HEK293A cells were maintained in fed medium before analysis by qRT-PCR. 2 independent experiments; mean ± SD. **(g)** HEK293A cells expressing indicated proteins analysed by immunoblot. Full medium. *, non-specific band. KI, kinase inactive ULK1. **(h)** HEK293A cells expressing EGFP-GABARAP wild-type or the G116A mutant were incubated in full medium with BafA (FB) or EBSS with BafA (EB) for 2 hr prior to electrophoresis on an 8% SDS-PAGE gel and immunoblot. *, non-specific band. SDS-PAGE and western blotting were performed by Minoo Razi. **(i)** HEK293A cells expressing indicated proteins analysed by immunoblot. Full medium. *, non-specific band. KI, kinase inactive ULK1. **(j)** Quantifications of **(g and i)**, overexpressed vector, n=4 experiments; overexpressed LC3B, n=3 experiments; overexpressed GABARAP, n=5 experiments; overexpressed G116A, n=2 experiments. Statistics were performed using an unpaired Student's t test, ***, $p \leq 0.001$.

5.8 Discussion

WAC and GM130 are two regulators of autophagy, whose mechanism of action was unresolved and previously unconnected (McKnight et al., 2012, Chang et al., 2012). In this chapter I provide further evidence that WAC is a positive regulator of autophagosome formation and that GM130 functions as a negative regulator, using multiple readouts of the autophagic pathway. WAC drives autophagy initiation by maintaining ULK1 activation downstream of mTORC1. Another important autophagy regulator is AMP-activated protein kinase (AMPK), which is activated and activates ULK1 and autophagy in response to glucose starvation (Kim et al., 2011). Whether WAC regulates AMPK activity upstream of ULK1 is a possibility that has not been thoroughly investigated to date. In the model system I have used in my work to study autophagy, namely EBSS starvation of HEK293A cells, I did not see evidence of AMPK activation as measured by ULK1

phosphorylation at serine 555 (data not shown). However a study of glucose starvation has not been undertaken.

GM130 knockdown enhances WIPI2 puncta formation and thus GM130 may regulate autophagy at an early stage like WAC. There is some phenotypic disconnect between GM130 and WAC however, as it was not conclusive whether GM130 also regulates ULK1 activity. It may be that WAC has a more specific role in autophagy regulation, whereas GM130 may simply act to sequester GABARAP, perhaps for some unknown Golgi-localised function. Importantly though, the C-terminal GM130-interacting coiled-coil domain of WAC was required to rescue LC3B puncta formation after WAC depletion. This suggests that the WAC-GM130 interaction is indeed important for autophagy regulation. Although RNF20/40 also interacts with WAC through its coiled-coil domain it is less likely that this interaction is required for autophagosome formation, as RNF40 knockdown did not affect LC3 lipidation (Chapter 3.3.2).

In Chapter 4 I demonstrated that WAC and GM130 interacted with one another, although how this impacted on the autophagy machinery was unknown. Here I show that GM130 interacts with GABARAP directly and that WAC may interact with GABARAP via GM130. It may be that the GM130-GABARAP interaction is facilitated by a LIR motif in GM130, and this remains to be investigated. WAC appears to suppress GM130 binding to GABARAP and this could promote the maintenance of a centrosomal GABARAP ‘reservoir’ versus Golgi or ERGIC localised GABARAP. How this occurs is unknown. It may be that WAC could affect GABARAP binding to GM130 sterically, or by inducing some conformational change. The centrosomal GABARAP reservoir correlates with autophagic activity, as GM130 depletion resulted in a small increase in centrosomal GABARAP levels and also an increase in autophagy. How GABARAP translocates between the centrosome and the Golgi is not fully understood either. GABARAP binds microtubules directly (Wang and Olsen, 2000) and microtubules facilitate the concentration of GABARAP on the centrosome versus the Golgi. Under basal conditions GABARAP may continually traffic from the Golgi to the centrosome via microtubules, explaining why much greater colocalisation between GABARAP and GM130 is seen after nocodazole treatment to depolymerise the microtubule cytoskeleton. However, regulated GABARAP translocation likely involves motor proteins that impart directional control, analogous to the JIP1/Dynein mediated

translocation of LC3 positive autophagosomes in neurons (Fu et al., 2014). Whether GABARAP has a specific non-autophagosomal function at the centrosome is a question that remains unanswered. This would not be surprising as much of the centrosomal non-lipidated GABARAP remains localised there during starvation and indeed, many core autophagy proteins have non-autophagic functions (Subramani and Malhotra, 2013). Moreover, the factor that anchors non-lipidated GABARAP at the pericentriolar material also remains to be identified.

In more general terms, the Golgi acts as a hub for autophagy proteins under basal conditions as discussed in Chapter 1.1.3. Moreover, the Golgi complex is intimately linked with the centrosome and GM130 controls centrosome morphology and function (Kodani et al., 2009, Kodani and Sutterlin, 2008b). Golgi proteins such as AKAP450, which bind GM130 (and possibly WAC (Rolland et al., 2014)), GMAP-210 and HOOK3 connect the Golgi ribbon to the microtubule network and centrosome (Walenta et al., 2001, Hurtado et al., 2011, Rios et al., 2004, Rivero et al., 2009). Interestingly, Atg4D which processes GABARAPL1 is localised to the centrosome (Betin and Lane, 2009), and multiple autophagy proteins are localised around the centrioles at the basal body of the primary cilium (Pampliega et al., 2013). It will be interesting to see if other autophagy proteins localise to the PCM. Of special interest would be members of the ULK1 complex, which GABARAP directly binds.

The photoconversion data I present in this chapter suggests that non-lipidated centrosomal GABARAP is transported to autophagosomal structures. Presumably this pool of GABARAP becomes lipidated at some stage, this could be further elucidated by photoconversion of centrosomal GABARAP in the presence of wortmannin, which has not be done to date. It could be that this mobilised GABARAP performs some function in autophagosome closure, fusion or ULK1 activation or even a mixture of these. However, I hypothesise that in the absence of centrosomal GABARAP, cytosolic GABARAP can adequately contribute to autophagosome formation. Centrosomal GABARAP likely functions as an additional reservoir or provides some specialised role. This is because nocodazole treatment does not prevent autophagosome formation nor GABARAP puncta formation during starvation, (Kochl et al., 2006) and data not shown.

The ULK complex members ULK1/2, FIP200 and Atg13 bind GABARAP preferentially via LC3-interacting regions (LIRs) (Alemu et al., 2012, Kraft et al.,

2012, Okazaki et al., 2000). The identification of LIRs in the ULK complex suggested that the LC3 and GABARAP subfamilies act as a scaffold for recruitment of the ULK complex. However, in addition to this I show that knockdown of GABARAP specifically attenuates ULK1 activation whereas LC3B, GABARAPL1 and GATE-16 did not regulate ULK1 activity. In contrast, in yeast (Kraft et al., 2012), the Atg1 kinase is delivered to the vacuole via Atg8 to act as a brake on autophagy and the Atg8-Atg1 interaction does not modulate Atg1 kinase activity. The non-lipidated pool of GABARAP at the centrosome may somehow prime ULK1 activity. In support of this, ULK1 activation by GABARAP, but not LC3B, requires the ULK1 LIR motif but does not require GABARAP lipidation. Thus, LIR motifs could be functional regulatory elements rather than simply for recruitment of cargo or scaffolding. Data in the Tooze lab suggest that the interaction between GFP-GABARAP and endogenous ULK1 is not affected by starvation (data not shown). One important question arises though: how is the GABARAP-mediated activation of ULK1 regulated if not by lipidation or recruitment to the phagophore-localised pool of ULK? Presumably spatially uncontrolled activation of ULK1 would be unproductive. In the absence of WAC, aberrant GABARAP interaction with GM130 likely disrupts the centrosomal GABARAP reservoir, GABARAP retained on the Golgi is unlikely to contribute to autophagosome formation and this may impede GABARAP-mediated ULK1 activation. Hence GABARAP-mediated positive regulation of ULK1 provides an explanation for WAC's effect on ULK1 signalling.

Chapter 6. Discussion

In this thesis I have carried out an investigation of the mechanism by which WAC promotes the early stages of starvation-induced autophagy. This has involved studying WAC's role in the nucleus and in the cytoplasm. By assessing WAC's effect on the transcriptome it was apparent that WAC is not a master regulator of autophagy gene expression or of the expression of autophagy related processes. However, some individual autophagy genes were significantly affected by WAC depletion and I cannot rule out some nuclear effect of WAC on autophagy regulation. This analysis led to the surprising realisation that WAC may regulate gene expression independently of RNF20/40. This is surprising as WAC/RNF20/RNF40 are supposedly a stable complex involved in the same epigenetic mechanism (Zhang and Yu, 2011). WAC is thought to mediate H2B monoubiquitination by recruiting and activating the RNF20/40 E3 ligase complex by direct interaction. However, I found that a WAC mutant unable to bind RNF40 was able to rescue H2B monoubiquitination. These data point to a non-canonical mechanism of WAC-mediated gene regulation perhaps driven by H2B monoubiquitination independently of the RNF20/40 E3 ligase complex. The regulation of MHC class I-mediated antigen presentation genes is a candidate for further studying this possibility. In addition, the microarray data provides the first repository of genes regulated by all three members of the WAC/RNF20/40 complex and suggests novel pathways regulated by the complex as a whole, for example SMAD targets. Whether these genes are regulated directly or through secondary mechanisms would have to be further validated. There has been no direct proof of WAC's effect on splicing, however there are indications that WAC could be involved in splicing (Xu and Arnaout, 2002), although I was not able to investigate this with the tools used in my study

In the absence of clear indications that WAC regulated autophagy from the nucleus, I began by investigating its role in the cytoplasm and especially from the Golgi, an organelle implicated in autophagy. From mass spectrometry I could not detect members of the autophagy machinery as WAC interactors, however the negative autophagy regulator GM130 was identified as a novel WAC interactor. GM130 appeared to be a negative regulator of the early stages of autophagy from the literature (Chang et al., 2012). The WAC-GM130 interaction was validated and

delineated. In addition it appears that WAC interacts with COPI subunits. It would be fascinating to know if WAC affects GM130 mediated tethering of COPI vesicles or COPI-mediated retrograde or intra-Golgi transport. Moreover, WAC's maintenance of Golgi structure is thought to be through a mechanism involving p97 (Totsukawa et al., 2011) but it may be that WAC additionally modulates GM130-COPI to affect Golgi architecture. I did not find VCIP135 or p97 as WAC interactors from the mass spectrometry data, however RNF20/40 was confirmed. Other novel candidate WAC interactors from the mass spectrometry were less promising as they did not validate or appeared to be very low abundance interactions. It may be that to study and discover additional WAC interactions techniques to preserve transient or weak interactions, such as chemical crosslinking, should be used in the future.

The WAC-GM130 interaction is responsible for WAC's tethering to the Golgi and appears to be direct. WAC affects autophagy at the early ULK1 activation stage and GM130 affects autophagy at least at the WIPI2 spot formation stages, although effects on ULK1 activity were not clear. How WAC-GM130 could link to and affect the autophagy machinery was not clear until the discovery of the direct GM130-GABARAP and indirect WAC-GABARAP interactions. Surprisingly, I found a novel pool of non-lipidated GABARAP enriched at the pericentrosomal material of the centrosome. How this pool of GABARAP is anchored to the centrosome is unknown, but the biochemical purification of centrosomes and electron microscopy could determine the participating factors and whether membranes are involved. This structure was enlarged, and therefore tractable to study, in the HEK293A cell line that I used, but centrosomal GABARAP was present in a range of cell lines from different originating tissues. Moreover, this is a genuine localisation of the GABARAP protein as it is detected by different antibodies, the staining is sensitive to GABARAP siRNA, and three different tagged forms of GABARAP localise to the centrosome. The centrosomal-Golgi trafficking of GABARAP appears to be regulated by WAC and by microtubules (Figure 6.1). How this occurs is not known, but depletion of WAC results in increased binding of GM130 to GABARAP, GABARAP accumulation at the Golgi and ERGIC and less GABARAP at the centrosome, suggesting a competition by WAC for GABARAP-GM130 binding. Disassembly of the microtubule cytoskeleton also results in GABARAP accumulation at the Golgi and reduction at the centrosome. As GM130 binds

microtubules directly and controls microtubule nucleation (Wei et al., 2015) (Rivero et al., 2009), and GABARAP binds microtubules directly (Wang and Olsen, 2000), it could be that WAC alters microtubule mediated trafficking of GABARAP through an interaction with GM130. Interestingly, WAC interacts with AKAP450 by yeast two-hybrid (Rolland et al., 2014) and as AKAP450 binds GM130, centrosomal components and nucleates microtubules (Rivero et al., 2009), this could be another link to how WAC affects GABARAP localisation.

In addition, the role of motors in the centrosome-Golgi transport of GABARAP is not known, although my preliminary data suggest that cytoplasmic dynein could be involved in regulating this (data not shown). Importantly, centrosomally localised GABARAP can be transported to peripheral LC3-positive structures upon starvation, suggesting that the centrosomal pool of GABARAP may function in autophagosome formation. This likely requires microtubule mediated transport, however the centrosomal pool of GABARAP is probably not absolutely required for GABARAP targeting to the autophagosome, as microtubule disassembly did not prevent WIPI2-positive GABARAP puncta from forming (data not shown). This centrosome-to-autophagosome transport requires the action of WAC, perhaps by preventing the excessive tethering of GABARAP to GM130. The factors that mediate this transport are also unknown and remain to be investigated. A candidate for this could be kinesin motors, which mediate plus-end directed microtubule transport. In general the role of the centrosome in regulating autophagy proteins is a new idea, and how this relates to the concentration of autophagy proteins at the basal body of the primary cilium (Pampliega et al., 2013) is also an interesting consideration. The function of GABARAP at the centrosome, and on the Golgi, is also something that remains to be further explored and understood.

A trafficking route of GABARAP from Golgi to centrosome and from centrosome to autophagosome suggests a complicated relationship between GABARAP subcellular localisation and GABARAP function. I would tentatively predict that the centrosome-Golgi trafficking route of GABARAP may have some non-autophagic function and would be in competition with the centrosome-autophagosome transport of GABARAP. Perhaps analogous to this idea is the Golgi-mediated repression of Beclin1 autophagy function (Shoji-Kawata et al., 2013) and the autophagy-independent role of Beclin1 in maintaining centrosome

stability (Park et al., 2014). Disruption of the Golgi-centrosome axis of GABARAP trafficking may indirectly affect autophagy by depleting/increasing the centrosomal reservoir of GABARAP. I would speculate that under basal conditions of low autophagy, GABARAP may have some membrane trafficking function centred on the Golgi or could modulate some function of GM130. Thus it could be interesting to investigate the role of GABARAP in Golgi structural maintenance, vesicle tethering or protein secretion for example. Pertinent to this, GABARAP has been localised to the rims of Golgi cisternae by electron microscopy (Kittler et al., 2001). WAC could act as a switch to regulate the Golgi versus centrosome localisation of GABARAP, perhaps to toggle between GABARAP-mediated functions at those subcellular compartments and to maintain a centrosomal GABARAP reservoir that could be mobilised for autophagy. However, my data suggests that the WAC-mediated repression of GABARAP-GM130 interaction occurs constitutively (under basal and starvation conditions) and further work would be needed to elucidate if WAC's function is regulated by specific signals.

The role of GABARAP at the centrosome is poorly understood, but I would hypothesise that GABARAP has some non-autophagic constitutive function at the centrosome, as most of centrosomal GABARAP remains on the centrosome during starvation. Perhaps GABARAP could take part in centrosome-organised functions such as spindle assembly and cell polarity, or perhaps GABARAP mobilisation from the centrosome is more potently induced by other autophagy stimuli such as glucose starvation for example. Moreover, autophagy proteins including GABARAP localise to the basal body (mother centriole) and axoneme of the primary cilium, a sensory organelle that forms during G_1 and G_0 phases of the cell cycle (Pampliega et al., 2013). During long term (24 hour) serum starvation, a stimulus that drives the formation of autophagosomes and primary cilia, autophagy functions to degrade a centrosomally-localised inhibitor of ciliogenesis OFD1, to allow primary cilia formation (Tang et al., 2013). In addition, signalling to the primary cilium activates autophagy in the region of the plasma membrane/basal body (Pampliega et al., 2013). However, during nutrient replete conditions basal autophagy is involved in inhibiting the formation of the primary cilium through degrading IFT20 involved in ciliogenesis (Pampliega et al., 2013). Thus, it is plausible that GABARAP remains on the centrosome to coordinate the interlinked autophagosome and cilia formation pathways. The GABARAP reservoir at the centrosome may be co-opted for the

rapid and extensive formation of autophagosomes during acute 2 hour amino acid and serum starvation (EBSS starvation). However, a sufficient quantity of GABARAP may simultaneously need to remain at the centrosome to be able to function in cilia formation during the appropriate stage of the cell cycle, or during longer starvation periods. This could involve the GABARAP-mediated autophagic targeting of a ciliogenesis regulator such as OFD1, although this is unknown. One clue for a possible cell cycle regulation of GABARAP function is that I observed GABARAP dissociation from the spindle poles (centrosomes) during metaphase. Interestingly, this is a stage of the cell cycle where ciliogenesis is prevented, as centrosomes must be used for spindle formation (Ishikawa and Marshall, 2011). Whether GABARAP localisation at the centrosome is functionally linked to ciliogenesis is not understood. On the other hand, GABARAP at the basal body and axoneme of the primary cilium may be involved in converting extracellular cues to cytoplasmic autophagosome formation. Under these circumstances, GABARAP may also traffic from the basal body (mother centriole region) to forming autophagosomes. This remains to be investigated. In summary, I postulate that during starvation, the acute requirement for large-scale autophagosome formation would recruit a portion of the centrosomal pool of GABARAP. The remaining GABARAP pool could provide some centrosomally-localised function, such as in ciliogenesis.

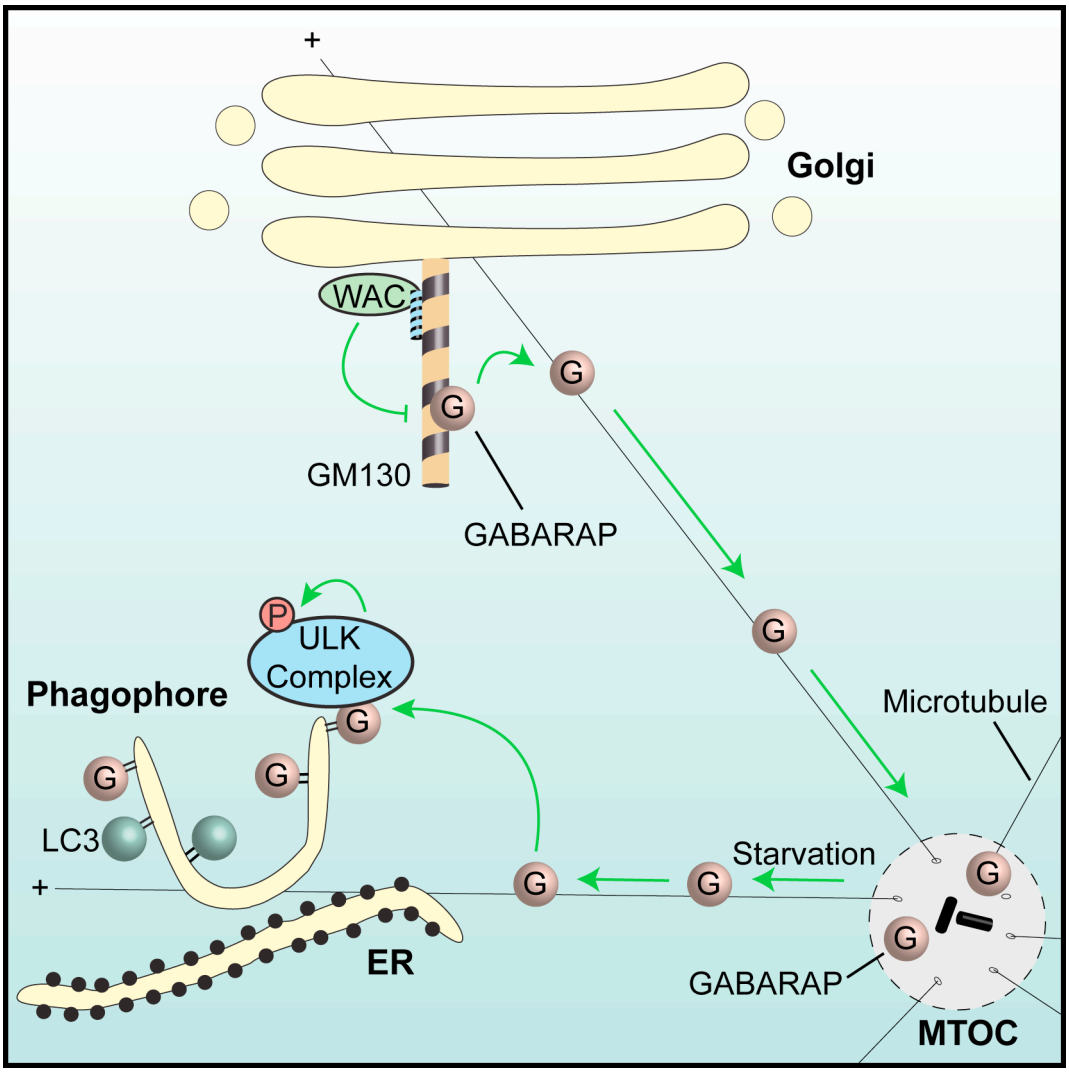

Figure 6.1 A model for WAC regulation of the centrosomal GABARAP reservoir

WAC inhibits the GM130-GABARAP interaction, which may maintain a pool of non-lipidated GABARAP at the centrosome. Microtubules control the Golgi-centrosome localisation of GABARAP. GABARAP at the centrosome can relocalise to LC3 positive structures and this likely requires microtubules. The role of motor proteins or membrane carriers in this process is not understood. At the phagophore, GABARAP may interact with ULK1 to keep it in an active state (see Figure 6.2).

The interactions between GABARAP and GM130 and WAC certainly pointed to the mechanism of autophagy regulation. However there was a problem in my hypothesis, in that WAC affects ULK1 regulation (initiation) whereas GABARAP is thought to act at a later stage (elongation). GABARAP is known to directly bind the ULK1 complex and it was hypothesised that ULK1 drives the function of GABARAP in elongation. However I hypothesised that GABARAP regulates ULK1 activity. In

the presence of GABARAP or G116A non-lipidated GABARAP, but not in the presence of LC3B or in the absence of GABARAP, maximal ULK1 activation requires the ULK1 LIR motif. Moreover depletion of GABARAP, but not other LC3 family members, results in reduced endogenous ULK1 activity. Thus it could be that binding of GABARAP to ULK1 maintains its activation, and this is independent of lipidation of GABARAP (Figure 6.2). Thus the WAC-GM130 interaction, which is likely involved in regulating the localisation of GABARAP, may in turn affect the activation of ULK1. However the fact remains that the LIR motif of ULK1 *per se* is not required for its kinase activity, but is only sensitised in the presence of GABARAP. Hence when the ULK1 LIR is mutated and GABARAP is present, it may be that GABARAP can bind to the LIRs on FIP200 and Atg13, and this intermediate complex may be semi-active.

Based on the presented data and existing literature, I would like to discuss a hypothetical model to explain the non-hierarchical GABARAP-ULK1 function (Figure 6.2). It is non-hierarchical in the sense that a protein that is downstream in the autophagy pathway (GABARAP) may regulate an upstream factor (ULK1). In summary, starvation activates the ULK complex leading to its recruitment to phagophore formation sites on the ER (Itakura and Mizushima, 2010). ULK1 is able to phosphorylate and activate the Beclin-1 complex (Russell et al., 2013), which creates a pool of PtdIns(3)P at the omegasome (Axe et al., 2008). PtdIns(3)P recruits WIPI2, which recruits the Atg12–5-16L1 complex (Dooley et al., 2014). Atg16L1 can simultaneously bind WIPI2b and FIP200, but FIP200 binding is downstream of WIPI2b and not required for LC3 lipidation (Dooley et al., 2014). Thus, recruitment of FIP200 (the ULK complex) to the phagophore by Atg16L1 is downstream of PtdIns(3)P, WIPI2, and Atg12–5-16L1 driven mAtg8 lipidation, see Figure 6.2. This hypothesis would provide an explanation for the PI3P mediated reinforcement of the ULK1 complex at the phagophore (Karanasios et al., 2013). The ULK complex bound to the Atg12–5-16L1 on the phagophore could then be activated by unlipidated GABARAP coming from the centrosome (or perhaps also the cytosol) or lipidated GABARAP on the phagophore membrane. GABARAP association then maintains ULK1 activation via a LIR interaction and ULK1 substrate phosphorylation during the final stages of phagophore formation, until the ULK1 complex dissociates prior to closure as shown previously (Karanasios et al., 2013).

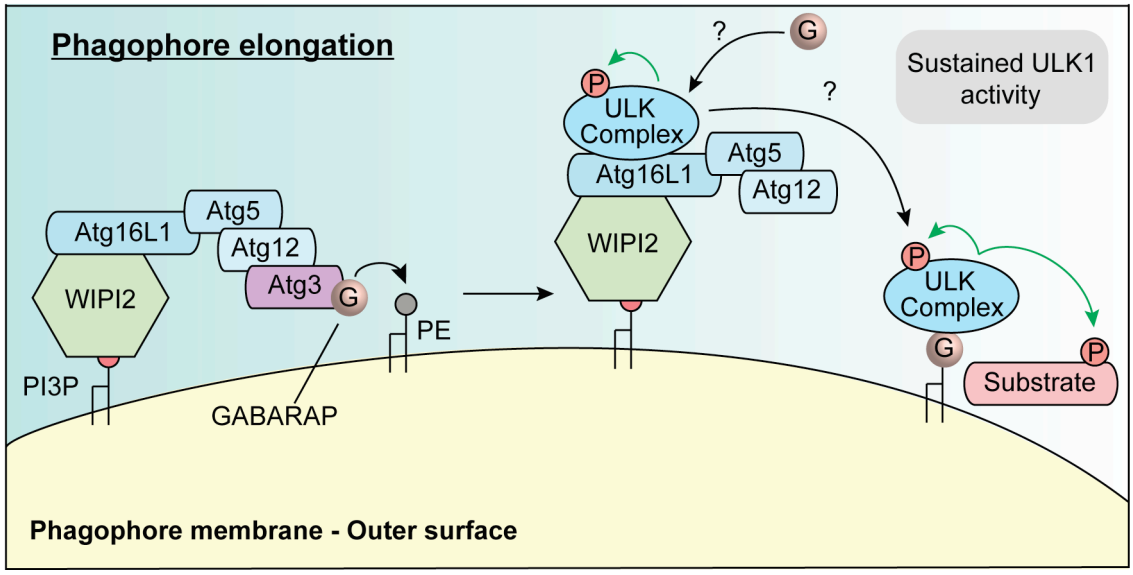

Figure 6.2 A hypothetical model for GABARAP-mediated maintenance of ULK1 activation at the phagophore

See main text for discussion.

Chapter 7. Appendix

7.1 Live cell imaging movies

Movies from photoconversion experiments of EosFP-GABARAP are on the CD found in the cover of this thesis. Legends are described below.

Movie 1) Related to Figure 5.18. Centrosomal GABARAP transports to forming autophagosomes.

Live cell imaging of a HEK293A cell expressing EosFP-GABARAP. Cells were washed into EBSS, imaged and photoconverted at 37^{o}C with 10% CO_2 using a Nikon Eclipse Ti Swept Field Confocal microscope. Arrows mark the structures shown in Figure 5.18a. Yellow arrow shows photoconverted centrosomal GABARAP. Blue arrow shows GABARAP punctum acquiring centrosomal GABARAP. Movie spans 25 mins played at 5 fps with 1 frame equal to 30 s. Note: first 5 frames are equal to 5 x 1 s images before photoconversion.

Movie 2). Related to Figure 5.18. GABARAP positive puncta are highly mobile and make transient interactions with the enlarged GABARAP structure.

Live cell imaging of a HEK293A cell expressing EosFP-GABARAP. Cells were washed into EBSS, imaged and photoconverted at 37^{o}C with 10% CO_2 using a Nikon Eclipse Ti Swept Field Confocal microscope. Enlarged EosFP-GABARAP structure in the centre of the cell is targeted for photoconversion and is assumed to be centrosomal GABARAP. Blue arrow shows GABARAP punctum making contact with centrosomal GABARAP before leaving in a different direction. Movie spans 26 mins played at 10 fps with 1 frame equal to 5 s. Note: first 12 frames span the 60 s before photoconversion.

Movie 3). Related to Figure 5.23. Depletion of WAC retains GABARAP on the Golgi where it becomes relatively immobile and does not make puncta

Live cell imaging of HEK293A cells depleted of WAC expressing EosFP-GABARAP. Cells were washed into EBSS, imaged and photoconverted at 37^{o}C with 10% CO_2 using a Nikon Eclipse Ti Swept Field Confocal microscope. Arrows mark the structures shown in Figure 5.23a. Golgi-localised GABARAP (yellow arrows) was targeted for photoconversion. Movie spans 25 mins played at 11.5 fps with 1 frame equal to 13.1 s. Maximum intensity projections of z-stacks are shown.

7.2 Microarray data

Table 7.1 961 genes significantly (p ≤ 0.05) up or downregulated after WAC knockdown only versus RISC Free control

Fold change versus RISC Free, FC. Adjusted p-value, adj. p-value. Top quarter-positive regulator: in the top quarter of genome-wide screen for novel positive regulators of starvation-induced autophagy (McKnight et al., 2012).

Gene symbol	Protein name	FC	adj. p-value	Top quarter -positive regulator
WAC	WW domain containing adaptor with coiled-coil	-3.719	2.4E-07	YES
SLC35B2	solute carrier family 35, member B2	-2.524	3.6E-07	NO
LYN	v-yes-1 Yamaguchi sarcoma viral related oncogene homolog	-2.354	9.3E-06	NO
DUSP3	dual specificity phosphatase 3	-2.264	1.4E-06	YES
ACOT7	acyl-CoA thioesterase 7	-2.184	1.2E-05	NO
MIS18A	MIS18 kinetochore protein homolog A (S. pombe)	-2.067	2.2E-05	NO
VAMP3	vesicle-associated membrane protein 3	-1.919	1.6E-05	NO
PLCB1	phospholipase C, beta 1 (phosphoinositide-specific)	-1.908	8.3E-06	NO
WDR12	WD repeat domain 12	-1.879	3.8E-05	YES
DENND5B	DENN/MADD domain containing 5B	-1.843	1.4E-04	YES
DHX40	DEAH (Asp-Glu-Ala-His) box polypeptide 40	-1.842	7.4E-04	NO
IMPDH1	IMP (inosine 5'-monophosphate) dehydrogenase 1	-1.815	1.4E-03	NO
CYP20A1	cytochrome P450, family 20, subfamily A, polypeptide 1	-1.799	2.7E-07	NO
CALD1	caldesmon 1	-1.798	6.3E-05	NO
CBR4	carbonyl reductase 4	-1.746	6.2E-04	NO
SHISA2	shisa homolog 2 (Xenopus laevis)	-1.745	2.9E-03	NO
AP3M1	adaptor-related protein complex 3, mu 1 subunit	-1.739	3.2E-04	NO
ZMAT3	zinc finger, matrin-type 3	-1.714	1.3E-03	NO
NFKB1	nuclear factor of kappa light polypeptide gene enhancer in B-cells 1	-1.695	3.2E-04	YES
LINC00152	long intergenic non-protein coding RNA 152	-1.690	2.1E-04	YES
HSPB8	heat shock 22kDa protein 8	-1.667	1.2E-04	NO
TTF2	transcription termination factor, RNA polymerase II	-1.654	1.1E-04	YES
TAF7L	TAF7-like RNA polymerase II, TATA box binding protein (TBP)-associated factor, 50kDa	-1.642	4.2E-04	NO
MCM3	minichromosome maintenance complex component 3	-1.629	6.7E-06	NO
ERAP2	endoplasmic reticulum aminopeptidase 2	-1.626	1.3E-03	NO
LTBR	lymphotoxin beta receptor (TNFR superfamily, member 3)	-1.625	4.1E-03	NO
FNDC3A	fibronectin type III domain containing 3A	-1.621	4.4E-05	NO
EIF3J	eukaryotic translation initiation factor 3, subunit J	-1.620	5.4E-04	NO
FAM69A	family with sequence similarity 69, member A	-1.615	3.9E-05	YES
KIAA0430	KIAA0430	-1.613	1.8E-03	NO
DDT	D-dopachrome tautomerase	-1.610	3.8E-05	NO
HLA-A	major histocompatibility complex, class I, A	-1.610	1.5E-05	NO
MAP2K4	mitogen-activated protein kinase kinase 4	-1.597	1.0E-04	NO
COMTD1	catechol-O-methyltransferase domain containing 1	-1.586	1.7E-03	NO
AKAP12	A kinase (PRKA) anchor protein 12	-1.586	3.7E-03	NO
SH3PXD2A	SH3 and PX domains 2A	-1.581	2.7E-04	YES
RPL29	ribosomal protein L29	-1.574	1.8E-03	NO
ACADVL	acyl-CoA dehydrogenase, very long chain	-1.545	7.3E-04	NO
OSTC	oligosaccharyltransferase complex subunit	-1.543	7.4E-04	NO
INTS2	integrator complex subunit 2	-1.538	4.4E-04	NO
AFF4	AF4/FMR2 family, member 4	-1.537	1.4E-02	YES

Gene symbol	Protein name	FC	adj. p-value	Top quarter -positive regulator
OAS3	2'-5'-oligoadenylate synthetase 3, 100kDa	-1.521	1.0E-03	YES
CMSS1	cms1 ribosomal small subunit homolog (yeast)	-1.515	1.7E-03	YES
ALDH2	aldehyde dehydrogenase 2 family (mitochondrial)	-1.514	2.0E-03	NO
BEX2	brain expressed X-linked 2	-1.510	3.1E-04	YES
MFSD3	major facilitator superfamily domain containing 3	-1.505	9.1E-03	NO
GPX3	glutathione peroxidase 3 (plasma)	-1.498	3.6E-03	YES
IMPAD1	inositol monophosphatase domain containing 1	-1.491	7.4E-04	NO
RAB21	RAB21, member RAS oncogene family	-1.489	3.7E-03	NO
MAPK13	mitogen-activated protein kinase 13	-1.486	5.6E-03	NO
MATN2	matrilin 2	-1.478	4.9E-03	NO
FHL1	four and a half LIM domains 1	-1.472	2.2E-04	YES
FBXO6	F-box protein 6	-1.471	1.9E-04	NO
TM7SF2	transmembrane 7 superfamily member 2	-1.467	9.6E-03	NO
SCARB2	scavenger receptor class B, member 2	-1.463	8.4E-03	NO
CWF19L2	CWF19-like 2, cell cycle control (S. pombe)	-1.463	5.8E-03	NO
CARD10	caspase recruitment domain family, member 10	-1.459	1.3E-03	YES
MBTPS1	membrane-bound transcription factor peptidase, site 1	-1.455	6.3E-05	YES
MTHFS	5,10-methenyltetrahydrofolate synthetase (5-formyltetrahydrofolate cyclo-ligase)	-1.454	3.3E-03	NO
NCR3LG1	natural killer cell cytotoxicity receptor 3 ligand 1	-1.451	1.9E-04	NO
TXNDC9	thioredoxin domain containing 9	-1.451	2.3E-03	NO
HLA-H	major histocompatibility complex, class I, H (pseudogene)	-1.447	3.8E-05	YES
AMZ2	archaelysin family metallopeptidase 2	-1.446	3.9E-04	NO
ADH5	alcohol dehydrogenase 5 (class III), chi polypeptide	-1.440	1.1E-03	NO
NPC2	Niemann-Pick disease, type C2	-1.437	6.9E-05	NO
SLC30A7	solute carrier family 30 (zinc transporter), member 7	-1.426	2.5E-03	YES
C17ORF80	chromosome 17 open reading frame 80	-1.423	1.2E-03	NO
SIL1	SIL1 homolog, endoplasmic reticulum chaperone (S. cerevisiae)	-1.422	2.5E-03	NO
NME4	NME/NM23 nucleoside diphosphate kinase 4	-1.422	5.9E-03	NO
LITAF	lipopolysaccharide-induced TNF factor	-1.419	1.5E-03	YES
PKMYT1	protein kinase, membrane associated tyrosine/threonine 1	-1.414	5.9E-03	NO
OCRL	oculocerebrorenal syndrome of Lowe	-1.411	3.5E-03	NO
LAMB2	laminin, beta 2 (laminin S)	-1.411	1.4E-03	YES
LINC00478	long intergenic non-protein coding RNA 478	-1.410	1.8E-04	NO
JAZF1	JAZF zinc finger 1	-1.409	2.1E-03	NO
HLA-E	major histocompatibility complex, class I, E	-1.406	2.9E-03	YES
XK	X-linked Kx blood group (McLeod syndrome)	-1.403	8.7E-03	YES
SULF2	sulfatase 2	-1.403	2.0E-03	NO
FHL2	four and a half LIM domains 2	-1.401	7.8E-03	NO
APOBEC3B	apolipoprotein B mRNA editing enzyme, catalytic polypeptide-like 3B	-1.400	4.7E-04	NO
PRKAG1	protein kinase, AMP-activated, gamma 1 non-catalytic subunit	-1.399	1.6E-03	NO
LAMA5	laminin, alpha 5	-1.398	1.2E-02	NO
GLG1	golgi glycoprotein 1	-1.395	1.3E-03	NO
SPATS2	spermatogenesis associated, serine-rich 2	-1.395	3.1E-04	NO
FAS	Fas (TNF receptor superfamily, member 6)	-1.393	3.0E-03	NO
CST3	cystatin C	-1.393	4.4E-03	NO
MEA1	male-enhanced antigen 1	-1.391	7.3E-04	NO
C11ORF54	chromosome 11 open reading frame 54	-1.389	3.1E-03	NO
SP110	SP110 nuclear body protein	-1.388	2.7E-03	YES
FAM83H	family with sequence similarity 83, member H	-1.388	2.7E-03	NO
RAB11FIP2	RAB11 family interacting protein 2 (class I)	-1.385	2.5E-03	NO
ITGB5	integrin, beta 5	-1.384	3.4E-04	NO
FIS1	fission 1 (mitochondrial outer membrane) homolog (S. cerevisiae)	-1.384	5.5E-03	NO
SMPDL3A	sphingomyelin phosphodiesterase, acid-like 3A	-1.384	4.6E-03	NO
FAM213A	family with sequence similarity 213, member A	-1.383	1.1E-02	NO

Gene symbol	Protein name	FC	adj. p-value	Top quarter -positive regulator
RRM2	ribonucleotide reductase M2	-1.383	2.2E-02	NO
NSF	N-ethylmaleimide-sensitive factor	-1.382	5.2E-03	NO
ZNF239	zinc finger protein 239	-1.381	2.8E-04	YES
HLA-B	major histocompatibility complex, class I, B	-1.380	4.1E-03	NO
C12ORF5	chromosome 12 open reading frame 5	-1.378	1.8E-03	YES
TMEM106B	transmembrane protein 106B	-1.378	8.5E-03	YES
NUCB1	nucleobindin 1	-1.375	1.5E-02	YES
RUNDC1	RUN domain containing 1	-1.371	1.5E-03	NO
CMTM6	CKLF-like MARVEL transmembrane domain containing 6	-1.368	5.2E-03	NO
MYCBP2	MYC binding protein 2, E3 ubiquitin protein ligase	-1.368	1.3E-02	YES
LRRCC1	leucine rich repeat and coiled-coil centrosomal protein 1	-1.363	1.9E-03	NO
CYCSP55	cytochrome c, somatic pseudogene 55	-1.360	2.9E-03	YES
VANGL2	vang-like 2 (van gogh, Drosophila)	-1.358	3.4E-03	NO
ITPRIPL2	inositol 1,4,5-trisphosphate receptor interacting protein-like 2	-1.356	8.8E-03	NO
SAMD9	sterile alpha motif domain containing 9	-1.356	1.2E-04	YES
MAP1LC3B	microtubule-associated protein 1 light chain 3 beta	-1.353	2.4E-02	YES
MOCS1	molybdenum cofactor synthesis 1	-1.353	5.8E-03	NO
CORO2A	coronin, actin binding protein, 2A	-1.352	1.5E-02	NO
GYPC	glycophorin C (Gerbich blood group)	-1.352	8.3E-04	NO
AVEN	apoptosis, caspase activation inhibitor	-1.350	3.5E-02	NO
XBP1	X-box binding protein 1	-1.347	1.6E-03	YES
ZNF219	zinc finger protein 219	-1.347	6.1E-03	NO
HMGA1	high mobility group AT-hook 1	-1.346	8.7E-03	NO
CEP55	centrosomal protein 55kDa	-1.345	7.8E-03	NO
GCDH	glutaryl-CoA dehydrogenase	-1.344	3.1E-03	NO
CAP2	CAP, adenylate cyclase-associated protein, 2 (yeast)	-1.344	5.0E-03	NO
ADAM23	ADAM metallopeptidase domain 23	-1.344	1.1E-03	NO
P4HA2	prolyl 4-hydroxylase, alpha polypeptide II	-1.343	3.8E-04	NO
P4HA1	prolyl 4-hydroxylase, alpha polypeptide I	-1.343	5.8E-04	YES
PRAME	preferentially expressed antigen in melanoma	-1.342	2.4E-03	NO
SUMF1	sulfatase modifying factor 1	-1.340	5.3E-04	NO
PITPNM1	phosphatidylinositol transfer protein, membrane-associated 1	-1.339	3.5E-02	NO
IRAK1	interleukin-1 receptor-associated kinase 1	-1.337	1.6E-03	NO
ITFG1	integrin alpha FG-GAP repeat containing 1	-1.336	2.0E-03	NO
RCOR3	REST corepressor 3	-1.336	1.2E-02	NO
CARD8	caspase recruitment domain family, member 8	-1.335	2.4E-02	YES
SSR4	signal sequence receptor, delta	-1.334	2.3E-03	NO
YOD1	YOD1 OTU deubiquinating enzyme 1 homolog (S. cerevisiae)	-1.332	4.0E-03	YES
LEPREL2	leprecan-like 2	-1.332	1.6E-02	NO
PFKP	phosphofructokinase, platelet	-1.331	1.5E-04	NO
VAMP2	vesicle-associated membrane protein 2 (synaptobrevin 2)	-1.330	6.1E-04	YES
RAB8B	RAB8B, member RAS oncogene family	-1.328	4.5E-03	NO
LGALS3BP	lectin, galactoside-binding, soluble, 3 binding protein	-1.326	3.1E-02	NO
ZSWIM5	zinc finger, SWIM-type containing 5	-1.326	1.0E-03	YES
SERPINH1	serpin peptidase inhibitor, clade H (heat shock protein 47), member 1, (collagen binding protein 1)	-1.326	1.1E-02	YES
ENPP4	ectonucleotide pyrophosphatase/phosphodiesterase 4 (putative)	-1.323	4.9E-03	NO
PGLS	6-phosphogluconolactonase	-1.323	7.0E-03	YES
ERO1L	ERO1-like (S. cerevisiae)	-1.323	7.3E-04	NO
RRM2B	ribonucleotide reductase M2 B (TP53 inducible)	-1.322	1.5E-03	NO
PNKP	polynucleotide kinase 3'-phosphatase	-1.321	3.7E-02	YES
CXCL16	chemokine (C-X-C motif) ligand 16	-1.320	1.5E-03	NO
PNMA2	paraneoplastic Ma antigen 2	-1.319	1.4E-03	NO
RAPGEF5	Rap guanine nucleotide exchange factor (GEF) 5	-1.319	5.0E-04	YES
KBTBD2	kelch repeat and BTB (POZ) domain containing 2	-1.318	9.8E-03	NO

Gene symbol	Protein name	FC	adj. p-value	Top quarter -positive regulator
LIG1	ligase I, DNA, ATP-dependent	-1.317	1.3E-02	NO
RBM4B	RNA binding motif protein 4B	-1.316	6.4E-04	NO
UFC1	ubiquitin-fold modifier conjugating enzyme 1	-1.316	4.3E-04	YES
WWOX	WW domain containing oxidoreductase	-1.315	7.3E-03	NO
RAP1B	RAP1B, member of RAS oncogene family	-1.315	4.2E-03	NO
CDK5RAP3	CDK5 regulatory subunit associated protein 3	-1.314	1.6E-02	NO
ZNF618	zinc finger protein 618	-1.313	6.8E-04	NO
SYK	spleen tyrosine kinase	-1.312	1.4E-03	YES
VPS35	vacuolar protein sorting 35 homolog (S. cerevisiae)	-1.311	7.3E-03	YES
KEAP1	kelch-like ECH-associated protein 1	-1.310	6.3E-03	NO
ITFG2	integrin alpha FG-GAP repeat containing 2	-1.307	1.3E-02	NO
MCM5	minichromosome maintenance complex component 5	-1.307	4.4E-02	NO
YEATS2	YEATS domain containing 2	-1.305	7.9E-03	YES
MIDN	midnolin	-1.304	7.3E-03	NO
NUP210	nucleoporin 210kDa	-1.302	4.9E-03	NO
SNX16	sorting nexin 16	-1.302	2.8E-03	NO
FAM45A	family with sequence similarity 45, member A	-1.302	1.9E-03	NO
PRNP	prion protein	-1.302	4.8E-03	NO
GALT	galactose-1-phosphate uridylyltransferase	-1.301	2.2E-02	NO
HSD17B7P2	hydroxysteroid (17-beta) dehydrogenase 7 pseudogene 2	-1.300	2.6E-03	YES
INSIG2	insulin induced gene 2	-1.298	4.0E-02	NO
KIAA1147	KIAA1147	-1.296	1.8E-02	YES
GOLIM4	golgi integral membrane protein 4	-1.296	4.2E-02	NO
DDR1	discoidin domain receptor tyrosine kinase 1	-1.295	1.3E-02	NO
ZDHHC8	zinc finger, DHHC-type containing 8	-1.294	4.0E-03	NO
PHF19	PHD finger protein 19	-1.294	6.7E-04	NO
NUFIP2	nuclear fragile X mental retardation protein interacting protein 2	-1.292	1.0E-02	NO
LOXL1	lysyl oxidase-like 1	-1.292	6.4E-03	YES
ZNF580	zinc finger protein 580	-1.291	4.9E-02	NO
MRPL34	mitochondrial ribosomal protein L34	-1.291	3.6E-02	NO
TRAK2	trafficking protein, kinesin binding 2	-1.289	3.7E-02	NO
CTSH	cathepsin H	-1.287	1.4E-02	NO
TP53I3	tumor protein p53 inducible protein 3	-1.286	2.5E-03	NO
RPS27L	ribosomal protein S27-like	-1.285	9.8E-04	YES
JMJD8	jumonji domain containing 8	-1.284	8.7E-03	NO
RBM47	RNA binding motif protein 47	-1.284	5.4E-04	YES
HSPA1A	heat shock 70kDa protein 1A	-1.283	1.5E-03	YES
TMTC1	transmembrane and tetratricopeptide repeat containing 1	-1.282	7.0E-04	NO
KLC3	kinesin light chain 3	-1.282	2.8E-02	NO
SEPN1	selenoprotein N, 1	-1.282	9.7E-03	NO
S100A13	S100 calcium binding protein A13	-1.281	2.4E-02	NO
HMGN5	high mobility group nucleosome binding domain 5	-1.280	3.4E-02	NO
IRF7	interferon regulatory factor 7	-1.280	1.1E-02	NO
PRRG4	proline rich Gla (G-carboxyglutamic acid) 4 (transmembrane)	-1.279	6.2E-03	NO
BBX	bobby sox homolog (Drosophila)	-1.279	2.6E-02	YES
ZNF672	zinc finger protein 672	-1.278	2.0E-02	NO
ARFGAP3	ADP-ribosylation factor GTPase activating protein 3	-1.278	2.7E-02	NO
EFCAB14	EF-hand calcium binding domain 14	-1.277	2.0E-02	NO
TMED1	transmembrane emp24 protein transport domain containing 1	-1.277	1.2E-02	NO
AKIP1	A kinase (PRKA) interacting protein 1	-1.276	3.8E-02	NO
TFPI	tissue factor pathway inhibitor (lipoprotein-associated coagulation inhibitor)	-1.276	3.3E-03	NO
TMEM59	transmembrane protein 59	-1.276	1.6E-03	NO
AKR1D1	aldo-keto reductase family 1, member D1	-1.275	2.4E-02	NO
BCAP29	B-cell receptor-associated protein 29	-1.275	6.3E-03	NO

Gene symbol	Protein name	FC	adj. p-value	Top quarter -positive regulator
TCEAL7	transcription elongation factor A (SII)-like 7	-1.274	3.8E-02	NO
CUTC	cutC copper transporter homolog (E. coli)	-1.274	1.2E-02	YES
NAGLU	N-acetylglucosaminidase, alpha	-1.274	2.4E-02	NO
PLAC9	placenta-specific 9	-1.272	4.2E-03	NO
CHST14	carbohydrate (N-acetylgalactosamine 4-0) sulfotransferase 14	-1.272	2.0E-02	NO
SMAD6	SMAD family member 6	-1.271	1.5E-02	YES
MGC72080	MGC72080 pseudogene	-1.271	2.7E-02	NO
CARD11	caspase recruitment domain family, member 11	-1.271	2.5E-02	YES
OSTM1	osteopetrosis associated transmembrane protein 1	-1.270	1.7E-02	NO
TBX18	T-box 18	-1.270	9.7E-03	NO
ANXA5	annexin A5	-1.270	1.4E-02	NO
CKB	creatine kinase, brain	-1.270	4.8E-03	NO
CUEDC1	CUE domain containing 1	-1.269	4.9E-02	NO
NPHP3	nephronophthisis 3 (adolescent)	-1.269	2.1E-03	NO
NXT2	nuclear transport factor 2-like export factor 2	-1.269	2.2E-03	YES
CAT	catalase	-1.268	7.0E-03	NO
DTNA	dystrobrevin, alpha	-1.268	2.8E-02	NO
RINL	Ras and Rab interactor-like	-1.267	2.1E-02	NO
SMAGP	small cell adhesion glycoprotein	-1.267	4.4E-03	NO
TSPAN31	tetraspanin 31	-1.267	4.7E-02	NO
FAAH	fatty acid amide hydrolase	-1.266	1.9E-02	NO
GLB1	galactosidase, beta 1	-1.265	4.8E-03	NO
C2CD5	C2 calcium-dependent domain containing 5	-1.263	4.6E-02	NO
SUPT3H	suppressor of Ty 3 homolog (S. cerevisiae)	-1.263	4.5E-03	NO
FAM111A	family with sequence similarity 111, member A	-1.261	7.3E-03	YES
UBA3	ubiquitin-like modifier activating enzyme 3	-1.260	1.1E-02	NO
ACVR1	activin A receptor, type I	-1.259	1.2E-03	NO
COMMD7	COMM domain containing 7	-1.259	5.0E-03	NO
GFM2	G elongation factor, mitochondrial 2	-1.258	1.4E-03	YES
HS3ST3A1	heparan sulfate (glucosamine) 3-O-sulfotransferase 3A1	-1.258	1.2E-02	NO
INPP1	inositol polyphosphate-1-phosphatase	-1.257	1.1E-02	NO
PMVK	phosphomevalonate kinase	-1.257	2.0E-02	NO
TMEM132A	transmembrane protein 132A	-1.257	3.9E-02	YES
PDCD4	programmed cell death 4 (neoplastic transformation inhibitor)	-1.257	2.6E-03	NO
PPARG	peroxisome proliferator-activated receptor gamma	-1.257	5.5E-03	NO
SCARA3	scavenger receptor class A, member 3	-1.257	4.8E-03	NO
BRD3	bromodomain containing 3	-1.257	1.1E-02	NO
GBE1	glucan (1,4-alpha-), branching enzyme 1	-1.257	2.0E-02	YES
DUS3L	dihydrouridine synthase 3-like (S. cerevisiae)	-1.256	1.3E-02	NO
NLRX1	NLR family member X1	-1.256	1.7E-02	YES
PRDX2	peroxiredoxin 2	-1.254	5.6E-03	NO
EFEMP1	EGF containing fibulin-like extracellular matrix protein 1	-1.254	2.7E-02	NO
DNAJC13	DnaJ (Hsp40) homolog, subfamily C, member 13	-1.253	8.7E-04	NO
MFI2	antigen p97 (melanoma associated) identified by monoclonal antibodies 133.2 and 96.5	-1.252	3.7E-02	YES
SRXN1	sulfiredoxin 1	-1.252	4.6E-02	NO
IFITM2	interferon induced transmembrane protein 2	-1.251	1.5E-02	NO
TAP1	transporter 1, ATP-binding cassette, sub-family B (MDR/TAP)	-1.251	1.2E-03	NO
PSEN2	presenilin 2 (Alzheimer disease 4)	-1.251	2.4E-03	NO
MSRB3	methionine sulfoxide reductase B3	-1.250	2.3E-02	YES
GBA	glucosidase, beta, acid	-1.249	2.5E-02	NO
TAF10	TAF10 RNA polymerase II, TATA box binding protein (TBP)-associated factor, 30kDa	-1.247	1.4E-02	YES
ZNF318	zinc finger protein 318	-1.247	2.6E-03	NO
AKR1B1	aldo-keto reductase family 1, member B1 (aldose reductase)	-1.246	1.8E-02	NO

Gene symbol	Protein name	FC	adj. p-value	Top quarter -positive regulator
LRP5	low density lipoprotein receptor-related protein 5	-1.246	4.6E-03	NO
BACE2	beta-site APP-cleaving enzyme 2	-1.246	1.6E-03	NO
PCSK5	proprotein convertase subtilisin/kexin type 5	-1.246	1.6E-02	NO
CYP2R1	cytochrome P450, family 2, subfamily R, polypeptide 1	-1.244	5.5E-03	NO
PTGFRN	prostaglandin F2 receptor inhibitor	-1.244	1.9E-02	NO
IVNS1ABP	influenza virus NS1A binding protein	-1.244	5.1E-03	YES
NEU1	sialidase 1 (lysosomal sialidase)	-1.243	3.8E-02	NO
IFI27L2	interferon, alpha-inducible protein 27-like 2	-1.243	3.2E-02	NO
CLDND1	claudin domain containing 1	-1.243	3.5E-02	NO
NR2C1	nuclear receptor subfamily 2, group C, member 1	-1.242	9.1E-03	NO
MEIS3P1	Meis homeobox 3 pseudogene 1	-1.241	2.3E-02	YES
NUPR1	nuclear protein, transcriptional regulator, 1	-1.241	2.4E-03	NO
KDM5A	lysine (K)-specific demethylase 5A	-1.240	1.5E-02	NO
HLA-F	major histocompatibility complex, class I, F	-1.240	2.1E-02	NO
CCNT1	cyclin T1	-1.240	2.3E-02	NO
FERMT2	fermitin family member 2	-1.239	1.7E-02	NO
VIM	vimentin	-1.239	2.0E-02	NO
SESN1	sestrin 1	-1.238	2.8E-02	YES
ELFN2	extracellular leucine-rich repeat and fibronectin type III domain containing 2	-1.238	1.2E-02	YES
P2RX4	purinergic receptor P2X, ligand-gated ion channel, 4	-1.238	1.7E-02	NO
CKLF	chemokine-like factor	-1.238	8.2E-03	NO
CCP110	centriolar coiled coil protein 110kDa	-1.238	5.7E-03	NO
C1ORF112	chromosome 1 open reading frame 112	-1.238	3.5E-02	YES
GSTO2	glutathione S-transferase omega 2	-1.238	2.2E-02	NO
PHYH	phytanoyl-CoA 2-hydroxylase	-1.235	8.1E-03	NO
PRCP	prolylcarboxypeptidase (angiotensinase C)	-1.233	4.8E-03	NO
C14ORF37	chromosome 14 open reading frame 37	-1.232	1.9E-02	NO
PON2	paraoxonase 2	-1.232	9.3E-03	NO
DNMT3B	DNA (cytosine-5-)-methyltransferase 3 beta	-1.232	1.0E-02	NO
DDAH1	dimethylarginine dimethylaminohydrolase 1	-1.231	1.0E-02	NO
N6AMT1	N-6 adenine-specific DNA methyltransferase 1 (putative)	-1.230	2.0E-03	NO
ALG13	ALG13, UDP-N-acetylglucosaminyltransferase subunit	-1.229	1.7E-02	NO
OTUD4	OTU domain containing 4	-1.229	1.5E-03	NO
CENPW	centromere protein W	-1.229	1.1E-02	YES
PDLIM7	PDZ and LIM domain 7 (enigma)	-1.228	3.0E-02	YES
MUTYH	mutY homolog (E. coli)	-1.228	4.9E-02	NO
ZFYVE16	zinc finger, FYVE domain containing 16	-1.228	2.3E-02	NO
DZIP1	DAZ interacting protein 1	-1.227	4.1E-02	NO
EHBP1L1	EH domain binding protein 1-like 1	-1.227	2.2E-02	NO
CTSC	cathepsin C	-1.227	4.3E-02	YES
RAD54L	RAD54-like (S. cerevisiae)	-1.227	1.1E-02	NO
UAP1L1	UDP-N-acteylglucosamine pyrophosphorylase 1-like 1	-1.227	4.8E-02	NO
C17ORF82	chromosome 17 open reading frame 82	-1.227	1.4E-03	NO
TMEM173	transmembrane protein 173	-1.227	1.3E-02	NO
SEMA4F	sema domain, immunoglobulin domain (Ig), transmembrane domain (TM) and short cytoplasmic domain, (semaphorin) 4F	-1.227	3.8E-02	YES
C17ORF58	chromosome 17 open reading frame 58	-1.226	1.5E-02	NO
TMEM237	transmembrane protein 237	-1.226	3.2E-03	YES
DMRT2	doublesex and mab-3 related transcription factor 2	-1.226	2.1E-02	YES
GGT1	gamma-glutamyltransferase 1	-1.226	1.3E-02	NO
B2M	beta-2-microglobulin	-1.225	4.5E-02	YES
SRSF5	serine/arginine-rich splicing factor 5	-1.224	1.9E-02	NO
SLMAP	sarcolemma associated protein	-1.223	4.1E-02	NO
PSMB5	proteasome (prosome, macropain) subunit, beta type, 5	-1.223	1.5E-03	YES

Gene symbol	Protein name	FC	adj. p-value	Top quarter -positive regulator
UBXN2A	UBX domain protein 2A	-1.222	2.5E-02	NO
PSME1	proteasome (prosome, macropain) activator subunit 1 (PA28 alpha)	-1.222	1.9E-02	NO
SNORA12	small nucleolar RNA, H/ACA box 12	-1.221	1.3E-02	YES
HAUS4	HAUS augmin-like complex, subunit 4	-1.221	4.7E-02	NO
SERF1B	small EDRK-rich factor 1B (centromeric)	-1.220	1.1E-02	NO
KIF13B	kinesin family member 13B	-1.220	3.2E-03	NO
PLXNB1	plexin B1	-1.220	3.0E-02	YES
C15ORF48	chromosome 15 open reading frame 48	-1.218	1.7E-02	NO
SEL1L3	sel-1 suppressor of lin-12-like 3 (C. elegans)	-1.218	2.0E-02	NO
SPG20	spastic paraplegia 20 (Troyer syndrome)	-1.218	5.9E-03	NO
RABAC1	Rab acceptor 1 (prenylated)	-1.217	3.1E-02	NO
CCDC90B	coiled-coil domain containing 90B	-1.217	1.5E-02	NO
ANGPTL2	angiopoietin-like 2	-1.217	1.0E-02	NO
IL1RAP	interleukin 1 receptor accessory protein	-1.217	8.5E-03	NO
DLG5-AS1	DLG5 antisense RNA 1	-1.216	2.7E-02	YES
TRAK1	trafficking protein, kinesin binding 1	-1.216	1.7E-02	YES
ZBTB8A	zinc finger and BTB domain containing 8A	-1.215	9.1E-03	YES
HELZ2	helicase with zinc finger 2, transcriptional coactivator	-1.215	6.2E-03	NO
CNOT10	CCR4-NOT transcription complex, subunit 10	-1.214	2.2E-02	YES
SLC2A12	solute carrier family 2 (facilitated glucose transporter), member 12	-1.214	8.5E-03	NO
KCTD18	potassium channel tetramerisation domain containing 18	-1.214	2.9E-02	NO
ZBTB4	zinc finger and BTB domain containing 4	-1.213	2.1E-03	YES
BANP	BTG3 associated nuclear protein	-1.213	3.6E-02	NO
TYMP	thymidine phosphorylase	-1.213	2.7E-02	NO
BTG3	BTG family, member 3	-1.211	1.2E-02	NO
WIPI1	WD repeat domain, phosphoinositide interacting 1	-1.211	3.1E-02	NO
ZCCHC9	zinc finger, CCHC domain containing 9	-1.211	1.7E-02	NO
SPCS3	signal peptidase complex subunit 3 homolog (S. cerevisiae)	-1.209	1.1E-02	NO
LRRK1	leucine-rich repeat kinase 1	-1.209	1.0E-02	NO
E2F5	E2F transcription factor 5, p130-binding	-1.207	7.9E-03	NO
WDR6	WD repeat domain 6	-1.207	8.7E-03	NO
RAMP1	receptor (G protein-coupled) activity modifying protein 1	-1.207	2.8E-03	NO
RCAN3	RCAN family member 3	-1.206	1.4E-03	YES
RRP7A	ribosomal RNA processing 7 homolog A (S. cerevisiae)	-1.206	4.9E-02	YES
YIPF4	Yip1 domain family, member 4	-1.205	1.1E-02	YES
CD58	CD58 molecule	-1.205	8.3E-03	NO
ILK	integrin-linked kinase	-1.204	4.7E-02	YES
DHRS4L2	dehydrogenase/reductase (SDR family) member 4 like 2	-1.204	3.2E-02	NO
NARS	asparaginyl-tRNA synthetase	-1.204	2.1E-02	NO
TRIM5	tripartite motif containing 5	-1.204	1.1E-02	NO
AQP11	aquaporin 11	-1.204	1.6E-02	YES
PDE8B	phosphodiesterase 8B	-1.203	1.4E-03	NO
TAX1BP3	Tax1 (human T-cell leukemia virus type I) binding protein 3	-1.202	3.8E-02	YES
STAG3L2	stromal antigen 3-like 2	-1.202	4.6E-02	NO
EPS8	epidermal growth factor receptor pathway substrate 8	-1.201	2.6E-02	NO
NUDT3	nudix (nucleoside diphosphate linked moiety X)-type motif 3	-1.201	1.8E-02	NO
TDRD7	tudor domain containing 7	-1.200	1.9E-02	YES
GTF3C2	general transcription factor IIIC, polypeptide 2, beta 110kDa	-1.200	1.7E-02	NO
C17ORF96	chromosome 17 open reading frame 96	-1.200	4.6E-02	YES
TERF2	telomeric repeat binding factor 2	-1.200	4.3E-02	NO
GABPB1	GA binding protein transcription factor, beta subunit 1	-1.198	7.0E-03	NO
TAGLN2	transgelin 2	-1.198	4.8E-02	NO
FAXC	failed axon connections homolog (Drosophila)	-1.197	3.4E-02	YES
SEPT10	septin 10	-1.197	2.0E-02	NO

Gene symbol	Protein name	FC	adj. p-value	Top quarter -positive regulator
ARSD	arylsulfatase D	-1.196	1.8E-02	NO
ARPC1B	actin related protein 2/3 complex, subunit 1B, 41kDa	-1.196	1.8E-02	NO
RIOK3	RIO kinase 3	-1.196	3.5E-02	YES
CALHM2	calcium homeostasis modulator 2	-1.195	4.3E-02	NO
ATL3	atlastin GTPase 3	-1.195	1.9E-02	NO
LPL	lipoprotein lipase	-1.195	4.7E-02	NO
GYG1	glycogenin 1	-1.194	1.9E-02	NO
CDC7	cell division cycle 7	-1.194	1.1E-02	NO
CCDC24	coiled-coil domain containing 24	-1.194	2.2E-02	NO
FAM50B	family with sequence similarity 50, member B	-1.193	3.2E-02	NO
MID2	midline 2	-1.192	6.2E-03	YES
RAB3IL1	RAB3A interacting protein (rabin3)-like 1	-1.192	3.6E-02	NO
AP1G2	adaptor-related protein complex 1, gamma 2 subunit	-1.192	1.9E-02	NO
ELOVL6	ELOVL fatty acid elongase 6	-1.192	5.8E-03	YES
IFI30	interferon, gamma-inducible protein 30	-1.192	3.1E-02	YES
BMP1	bone morphogenetic protein 1	-1.192	9.9E-03	NO
NDUFA8	NADH dehydrogenase (ubiquinone) 1 alpha subcomplex, 8, 19kDa	-1.192	2.7E-02	YES
VOPP1	vesicular, overexpressed in cancer, prosurvival protein 1	-1.191	4.2E-03	NO
RTCA	RNA 3'-terminal phosphate cyclase	-1.191	4.8E-02	NO
IKBIP	IKBKB interacting protein	-1.191	4.5E-03	NO
PARP12	poly (ADP-ribose) polymerase family, member 12	-1.191	1.0E-02	NO
DOCK8	dedicator of cytokinesis 8	-1.190	3.2E-02	YES
TRIM56	tripartite motif containing 56	-1.190	3.2E-02	NO
NUF2	NUF2, NDC80 kinetochore complex component, homolog (S. cerevisiae)	-1.189	2.2E-02	NO
DNASE2	deoxyribonuclease II, lysosomal	-1.189	1.5E-02	YES
MYL6	myosin, light chain 6, alkali, smooth muscle and non-muscle	-1.189	1.6E-02	YES
FER	fer (fps/fes related) tyrosine kinase	-1.189	4.4E-02	YES
TIA1	TIA1 cytotoxic granule-associated RNA binding protein	-1.189	4.1E-02	YES
FYCO1	FYVE and coiled-coil domain containing 1	-1.188	2.2E-02	YES
BCDIN3D	BCDIN3 domain containing	-1.188	4.7E-02	YES
ELMO2	engulfment and cell motility 2	-1.188	9.2E-03	NO
ZNF462	zinc finger protein 462	-1.185	1.7E-02	NO
HSD17B14	hydroxysteroid (17-beta) dehydrogenase 14	-1.185	4.0E-02	NO
MANEA	mannosidase, endo-alpha	-1.185	4.9E-02	YES
CHKB	choline kinase beta	-1.185	4.2E-02	YES
UXT	ubiquitously-expressed, prefoldin-like chaperone	-1.185	4.9E-03	NO
SCPEP1	serine carboxypeptidase 1	-1.184	2.0E-03	NO
MRPL3	mitochondrial ribosomal protein L3	-1.184	2.0E-02	NO
ZNF320	zinc finger protein 320	-1.183	3.2E-02	NO
MAN1A2	mannosidase, alpha, class 1A, member 2	-1.183	3.1E-02	NO
CELSR2	cadherin, EGF LAG seven-pass G-type receptor 2	-1.182	3.6E-02	NO
MATN3	matrilin 3	-1.181	3.7E-02	YES
CALML4	calmodulin-like 4	-1.181	8.2E-03	YES
NDST1	N-deacetylase/N-sulfotransferase (heparan glucosaminyl) 1	-1.181	4.8E-02	NO
NHLRC2	NHL repeat containing 2	-1.181	3.9E-02	NO
TMEM56	transmembrane protein 56	-1.180	3.0E-03	NO
BRSK1	BR serine/threonine kinase 1	-1.179	2.7E-02	NO
NDUFA3	NADH dehydrogenase (ubiquinone) 1 alpha subcomplex, 3, 9kDa	-1.179	4.6E-02	NO
ZNF641	zinc finger protein 641	-1.179	1.9E-02	NO
LONRF2	LON peptidase N-terminal domain and ring finger 2	-1.179	3.0E-02	NO
CYFIP2	cytoplasmic FMR1 interacting protein 2	-1.179	3.7E-02	NO
BRWD3	bromodomain and WD repeat domain containing 3	-1.178	3.0E-02	NO
LARGE	like-glycosyltransferase	-1.177	1.2E-02	NO
HHAT	hedgehog acyltransferase	-1.177	2.4E-02	NO

Gene symbol	Protein name	FC	adj. p-value	Top quarter -positive regulator
TSHZ1	teashirt zinc finger homeobox 1	-1.177	1.4E-02	YES
HOXD8	homeobox D8	-1.176	1.4E-02	YES
ZNF544	zinc finger protein 544	-1.176	2.6E-02	NO
SCMH1	sex comb on midleg homolog 1 (Drosophila)	-1.175	5.7E-03	NO
VLDLR	very low density lipoprotein receptor	-1.175	2.6E-02	YES
MIF	macrophage migration inhibitory factor (glycosylation-inhibiting factor)	-1.175	3.0E-02	NO
ARHGAP8	Rho GTPase activating protein 8	-1.174	1.1E-02	NO
KHNYN	KH and NYN domain containing	-1.173	2.0E-02	YES
TAPT1-AS1	TAPT1 antisense RNA 1 (head to head)	-1.172	9.1E-03	NO
PHLDB2	pleckstrin homology-like domain, family B, member 2	-1.171	3.9E-02	NO
HK1	hexokinase 1	-1.171	2.3E-03	NO
OSBPL10	oxysterol binding protein-like 10	-1.171	7.2E-03	NO
PCK2	phosphoenolpyruvate carboxykinase 2 (mitochondrial)	-1.171	4.3E-02	NO
SIGMAR1	sigma non-opioid intracellular receptor 1	-1.171	4.1E-02	NO
TMPO	thymopoietin	-1.170	3.1E-02	NO
PAQR7	progestin and adipoQ receptor family member VII	-1.170	2.1E-02	NO
CDH3	cadherin 3, type 1, P-cadherin (placental)	-1.170	7.1E-03	NO
CPQ	carboxypeptidase Q	-1.167	3.4E-02	NO
KLHL17	kelch-like family member 17	-1.167	4.6E-02	NO
C14ORF28	chromosome 14 open reading frame 28	-1.166	2.8E-02	NO
CREBRF	CREB3 regulatory factor	-1.166	8.9E-03	NO
PTPN4	protein tyrosine phosphatase, non-receptor type 4 (megakaryocyte)	-1.164	6.0E-03	NO
ENOSF1	enolase superfamily member 1	-1.164	4.5E-02	YES
RBM11	RNA binding motif protein 11	-1.163	2.8E-02	NO
GK5	glycerol kinase 5 (putative)	-1.163	3.0E-02	NO
CHST13	carbohydrate (chondroitin 4) sulfotransferase 13	-1.162	1.1E-02	NO
TMBIM1	transmembrane BAX inhibitor motif containing 1	-1.161	3.7E-02	NO
HLA-C	major histocompatibility complex, class I, C	-1.161	3.1E-02	NO
DNASE1L2	deoxyribonuclease I-like 2	-1.161	7.4E-03	YES
CD83	CD83 molecule	-1.161	3.5E-02	NO
SH3KBP1	SH3-domain kinase binding protein 1	-1.160	2.1E-02	NO
AADAT	aminoadipate aminotransferase	-1.160	3.1E-02	NO
CCDC8	coiled-coil domain containing 8	-1.160	4.9E-02	NO
FAM171A1	family with sequence similarity 171, member A1	-1.159	4.8E-02	NO
MFSD6	major facilitator superfamily domain containing 6	-1.159	3.0E-02	YES
ADCY10P1	adenylate cyclase 10 (soluble) pseudogene 1	-1.158	1.2E-02	NO
NAAA	N-acylethanolamine acid amidase	-1.158	4.6E-02	NO
TWF1	twinfilin, actin-binding protein, homolog 1 (Drosophila)	-1.158	1.7E-02	YES
PIGB	phosphatidylinositol glycan anchor biosynthesis, class B	-1.157	6.3E-03	NO
INTU	inturned planar cell polarity effector homolog (Drosophila)	-1.157	4.3E-02	YES
FAM129A	family with sequence similarity 129, member A	-1.156	4.4E-02	NO
RNF217	ring finger protein 217	-1.156	3.2E-02	NO
LOC550643	uncharacterized LOC550643	-1.156	2.5E-02	YES
ZBED1	zinc finger, BED-type containing 1	-1.155	2.8E-02	NO
CIB1	calcium and integrin binding 1 (calmyrin)	-1.155	2.7E-02	NO
CEP78	centrosomal protein 78kDa	-1.155	2.2E-02	NO
C21ORF67	chromosome 21 open reading frame 67	-1.154	4.3E-02	YES
RPL19	ribosomal protein L19	-1.154	4.9E-02	YES
BRE	brain and reproductive organ-expressed (TNFRSF1A modulator)	-1.153	9.0E-03	YES
LSM4	LSM4 homolog, U6 small nuclear RNA associated (S. cerevisiae)	-1.152	3.9E-02	NO
METRNL	meteorin, glial cell differentiation regulator-like	-1.152	3.5E-02	NO
SNORD52	small nucleolar RNA, C/D box 52	-1.152	1.3E-02	YES
ZNF514	zinc finger protein 514	-1.152	1.1E-02	NO
PDHB	pyruvate dehydrogenase (lipoamide) beta	-1.152	4.4E-02	NO

Gene symbol	Protein name	FC	adj. p-value	Top quarter -positive regulator
TP53I11	tumor protein p53 inducible protein 11	-1.151	2.1E-02	NO
GABBR1	gamma-aminobutyric acid (GABA) B receptor, 1	-1.151	3.6E-02	NO
ANKRD6	ankyrin repeat domain 6	-1.150	2.0E-02	YES
RAB38	RAB38, member RAS oncogene family	-1.150	4.4E-02	NO
GNAS-AS1	GNAS antisense RNA 1	-1.149	3.0E-02	YES
MCL1	myeloid cell leukemia sequence 1 (BCL2-related)	-1.149	1.4E-02	NO
AADACL4	arylacetamide deacetylase-like 4	-1.149	2.6E-02	NO
NEDD4	neural precursor cell expressed, developmentally down-regulated 4, E3 ubiquitin protein ligase	-1.149	1.3E-02	NO
SULT1A3	sulfotransferase family, cytosolic, 1A, phenol-preferring, member 3	-1.149	3.7E-02	NO
CD109	CD109 molecule	-1.148	2.2E-02	NO
U2SURP	U2 snRNP-associated SURP domain containing	-1.148	4.9E-02	NO
EPHX2	epoxide hydrolase 2, cytoplasmic	-1.148	4.3E-02	NO
ACADL	acyl-CoA dehydrogenase, long chain	-1.147	2.1E-02	NO
IL12A	interleukin 12A (natural killer cell stimulatory factor 1, cytotoxic lymphocyte maturation factor 1, p35)	-1.147	3.9E-02	YES
SPAG1	sperm associated antigen 1	-1.147	4.9E-02	NO
FAIM	Fas apoptotic inhibitory molecule	-1.146	4.2E-02	NO
TBC1D2B	TBC1 domain family, member 2B	-1.146	1.8E-02	YES
DDX60	DEAD (Asp-Glu-Ala-Asp) box polypeptide 60	-1.146	2.8E-02	YES
TFDP2	transcription factor Dp-2 (E2F dimerization partner 2)	-1.146	4.5E-02	YES
SCARNA16	small Cajal body-specific RNA 16	-1.145	3.2E-02	YES
NUP37	nucleoporin 37kDa	-1.145	3.7E-02	NO
DNAJC22	DnaJ (Hsp40) homolog, subfamily C, member 22	-1.145	3.5E-02	NO
MCOLN3	mucolipin 3	-1.144	4.3E-02	NO
TLX1	T-cell leukemia homeobox 1	-1.143	3.7E-02	YES
GPER	G protein-coupled estrogen receptor 1	-1.143	3.7E-02	YES
C9ORF3	chromosome 9 open reading frame 3	-1.142	3.9E-02	NO
MTX1	metaxin 1	-1.140	2.7E-02	NO
PTPRM	protein tyrosine phosphatase, receptor type, M	-1.140	3.9E-02	NO
BID	BH3 interacting domain death agonist	-1.140	4.8E-02	NO
SORT1	sortilin 1	-1.139	3.9E-02	NO
NT5DC1	5'-nucleotidase domain containing 1	-1.138	4.8E-02	NO
ZNF226	zinc finger protein 226	-1.138	4.1E-02	YES
UNC50	unc-50 homolog (C. elegans)	-1.138	2.9E-02	NO
MX1	myxovirus (influenza virus) resistance 1, interferon-inducible protein p78 (mouse)	-1.137	2.8E-02	NO
KCNG3	potassium voltage-gated channel, subfamily G, member 3	-1.137	2.0E-02	NO
AGXT2L2	alanine-glyoxylate aminotransferase 2-like 2	-1.137	2.3E-02	YES
SLFN12	schlafen family member 12	-1.137	3.3E-02	YES
TMCO4	transmembrane and coiled-coil domains 4	-1.136	3.5E-02	NO
HVCN1	hydrogen voltage-gated channel 1	-1.136	9.1E-03	NO
PANK3	pantothenate kinase 3	-1.136	4.4E-02	NO
PJA2	praja ring finger 2, E3 ubiquitin protein ligase	-1.134	3.0E-02	NO
FNDC4	fibronectin type III domain containing 4	-1.133	2.5E-02	NO
CD19	CD19 molecule	-1.132	4.4E-02	NO
CNPY4	canopy 4 homolog (zebrafish)	-1.132	4.5E-02	NO
NES	nestin	-1.131	2.8E-02	NO
SLC12A6	solute carrier family 12 (potassium/chloride transporters), member 6	-1.131	4.1E-02	NO
ANGEL1	angel homolog 1 (Drosophila)	-1.131	4.2E-02	YES
MPZL2	myelin protein zero-like 2	-1.131	2.0E-02	NO
ECE1	endothelin converting enzyme 1	-1.131	4.1E-02	NO
ABCA10	ATP-binding cassette, sub-family A (ABC1), member 10	-1.131	4.5E-02	NO
POU6F1	POU class 6 homeobox 1	-1.130	1.6E-02	NO
IRS1	insulin receptor substrate 1	-1.129	3.5E-02	YES

Gene symbol	Protein name	FC	adj. p-value	Top quarter -positive regulator
EMILIN3	elastin microfibril interfacer 3	-1.128	3.7E-02	NO
MYL9	myosin, light chain 9, regulatory	-1.128	3.2E-02	YES
IL17RC	interleukin 17 receptor C	-1.127	1.2E-02	NO
SMUG1	single-strand-selective monofunctional uracil-DNA glycosylase 1	-1.126	4.8E-02	NO
ADAM19	ADAM metallopeptidase domain 19	-1.125	1.7E-02	YES
LIMK2	LIM domain kinase 2	-1.125	4.6E-02	YES
C17ORF98	chromosome 17 open reading frame 98	-1.125	2.7E-02	NO
LRRC40	leucine rich repeat containing 40	-1.124	4.1E-02	NO
TTC39B	tetratricopeptide repeat domain 39B	-1.124	3.5E-02	NO
ICA1L	islet cell autoantigen 1,69kDa-like	-1.124	4.8E-02	NO
TOB2P1	transducer of ERBB2, 2 pseudogene 1	-1.123	3.1E-02	NO
UGT3A2	UDP glycosyltransferase 3 family, polypeptide A2	-1.122	2.3E-02	NO
RBPMS	RNA binding protein with multiple splicing	-1.122	3.0E-02	NO
STON1	stonin 1	-1.121	2.6E-02	NO
C7ORF13	chromosome 7 open reading frame 13	-1.120	2.7E-02	NO
EVA1A	eva-1 homolog A (C. elegans)	-1.120	3.6E-02	NO
MAST4	microtubule associated serine/threonine kinase family member 4	-1.120	3.7E-02	NO
CCDC91	coiled-coil domain containing 91	-1.119	3.9E-02	NO
FES	feline sarcoma oncogene	-1.119	2.8E-02	NO
CLPSL2	colipase-like 2	-1.118	3.2E-02	NO
USF2	upstream transcription factor 2, c-fos interacting	-1.118	3.1E-02	NO
TMCO6	transmembrane and coiled-coil domains 6	-1.117	2.8E-02	YES
DARS	aspartyl-tRNA synthetase	-1.115	4.3E-02	NO
CDH23	cadherin-related 23	-1.115	3.2E-02	NO
NLRP11	NLR family, pyrin domain containing 11	-1.110	4.9E-02	YES
GPR56	G protein-coupled receptor 56	-1.110	4.1E-02	NO
IRX6	iroquois homeobox 6	-1.105	4.8E-02	YES
PMEPA1	prostate transmembrane protein, androgen induced 1	-1.094	4.8E-02	YES
MTFR2	mitochondrial fission regulator 2	1.100	3.3E-02	
PSG6	pregnancy specific beta-1-glycoprotein 6	1.110	4.9E-02	
INHBB	inhibin, beta B	1.113	3.3E-02	
ZNF207	zinc finger protein 207	1.114	2.8E-02	
PSMG1	proteasome (prosome, macropain) assembly chaperone 1	1.115	4.0E-02	
HSD17B13	hydroxysteroid (17-beta) dehydrogenase 13	1.117	3.2E-02	
MMGT1	membrane magnesium transporter 1	1.120	4.6E-02	
SPANXA2	SPANX family, member A2	1.122	3.2E-02	
CIDECP	cell death-inducing DFFA-like effector c pseudogene	1.126	4.4E-02	
GNG10	guanine nucleotide binding protein (G protein), gamma 10	1.128	4.4E-02	
SNAP91	synaptosomal-associated protein, 91kDa	1.129	2.4E-02	
CRSP8P	mediator complex subunit 27 pseudogene	1.130	3.3E-02	
RAE1	RAE1 RNA export 1 homolog (S. pombe)	1.131	2.0E-02	
TIMM17A	translocase of inner mitochondrial membrane 17 homolog A (yeast)	1.131	4.9E-02	
SELRC1	Sel1 repeat containing 1	1.133	2.7E-02	
NDUFS3	NADH dehydrogenase (ubiquinone) Fe-S protein 3, 30kDa (NADH-coenzyme Q reductase)	1.133	1.7E-02	
STK16	serine/threonine kinase 16	1.133	2.8E-02	
RTFDC1	replication termination factor 2 domain containing 1	1.136	9.8E-03	
RLF	rearranged L-myc fusion	1.136	4.6E-02	
CMC2	COX assembly mitochondrial protein 2 homolog (S. cerevisiae)	1.139	2.1E-02	
SUCO	SUN domain containing ossification factor	1.140	4.6E-02	
WARS	tryptophanyl-tRNA synthetase	1.142	3.1E-02	
C17ORF76-AS1	C17orf76 antisense RNA 1	1.143	4.7E-02	
CDK8	cyclin-dependent kinase 8	1.143	3.0E-02	
MT1H	metallothionein 1H	1.144	2.5E-02	

Gene symbol	Protein name	FC	adj. p-value	Top quarter -positive regulator
CNOT8	CCR4-NOT transcription complex, subunit 8	1.144	3.9E-02	
UBE2J2	ubiquitin-conjugating enzyme E2, J2	1.144	4.5E-02	
RAP1A	RAP1A, member of RAS oncogene family	1.144	8.5E-03	
ARRDC2	arrestin domain containing 2	1.145	1.3E-02	
ADPRM	ADP-ribose/CDP-alcohol diphosphatase, manganese-dependent	1.145	2.4E-02	
TBC1D10A	TBC1 domain family, member 10A	1.145	1.3E-02	
BCL7B	B-cell CLL/lymphoma 7B	1.146	4.9E-02	
ABHD12	abhydrolase domain containing 12	1.146	3.4E-02	
OSGEP	O-sialoglycoprotein endopeptidase	1.146	2.6E-02	
PRUNE	prune homolog (Drosophila)	1.147	4.8E-02	
IFT46	intraflagellar transport 46 homolog (Chlamydomonas)	1.150	2.9E-02	
ZC3H18	zinc finger CCCH-type containing 18	1.150	2.7E-02	
SNORA18	small nucleolar RNA, H/ACA box 18	1.150	3.4E-02	
NDUFAF2	NADH dehydrogenase (ubiquinone) complex I, assembly factor 2	1.151	2.7E-02	
ETS2	v-ets erythroblastosis virus E26 oncogene homolog 2 (avian)	1.151	1.5E-02	
RAB2A	RAB2A, member RAS oncogene family	1.151	3.2E-02	
TTC9C	tetratricopeptide repeat domain 9C	1.152	1.3E-02	
TBC1D13	TBC1 domain family, member 13	1.152	7.6E-03	
REXO1	REX1, RNA exonuclease 1 homolog (S. cerevisiae)	1.152	3.9E-02	
SYS1	SYS1 Golgi-localized integral membrane protein homolog (S. cerevisiae)	1.153	3.9E-02	
GIGYF2	GRB10 interacting GYF protein 2	1.153	2.7E-02	
GOLGA4	golgin A4	1.154	3.9E-02	
RPS14	ribosomal protein S14	1.154	3.9E-02	
ALKBH3	alkB, alkylation repair homolog 3 (E. coli)	1.154	4.4E-02	
GLIPR2	GLI pathogenesis-related 2	1.155	4.8E-02	
TIMM23	translocase of inner mitochondrial membrane 23 homolog (yeast)	1.156	4.6E-02	
ZFP36L1	ZFP36 ring finger protein-like 1	1.156	2.7E-02	
MC2R	melanocortin 2 receptor (adrenocorticotropic hormone)	1.156	2.4E-02	
ZBTB3	zinc finger and BTB domain containing 3	1.157	3.4E-02	
PRDX1	peroxiredoxin 1	1.157	1.3E-02	
PIP4K2B	phosphatidylinositol-5-phosphate 4-kinase, type II, beta	1.158	2.2E-02	
CEP72	centrosomal protein 72kDa	1.159	1.6E-02	
AGAP10	ArfGAP with GTPase domain, ankyrin repeat and PH domain 10	1.159	3.9E-02	
PIP4K2C	phosphatidylinositol-5-phosphate 4-kinase, type II, gamma	1.159	4.7E-02	
TMEM158	transmembrane protein 158 (gene/pseudogene)	1.159	1.9E-02	
CSNK1A1	casein kinase 1, alpha 1	1.160	4.8E-02	
BCS1L	BC1 (ubiquinol-cytochrome c reductase) synthesis-like	1.160	4.1E-02	
NFS1	NFS1 nitrogen fixation 1 homolog (S. cerevisiae)	1.161	9.2E-03	
FGFR1OP2	FGFR1 oncogene partner 2	1.161	2.4E-02	
SLC35C2	solute carrier family 35, member C2	1.161	4.8E-02	
GNG7	guanine nucleotide binding protein (G protein), gamma 7	1.162	1.6E-02	
DHDDS	dehydrodolichyl diphosphate synthase	1.162	2.4E-02	
C12ORF49	chromosome 12 open reading frame 49	1.162	4.8E-02	
OPRM1	opioid receptor, mu 1	1.162	2.5E-02	
EMC3	ER membrane protein complex subunit 3	1.162	1.5E-02	
SAFB2	scaffold attachment factor B2	1.162	4.4E-02	
SON	SON DNA binding protein	1.162	1.7E-02	
PPP2R5A	protein phosphatase 2, regulatory subunit B', alpha	1.162	1.1E-02	
ABCA11P	ATP-binding cassette, sub-family A (ABC1), member 11, pseudogene	1.162	2.8E-02	
GGA3	golgi-associated, gamma adaptin ear containing, ARF binding protein 3	1.163	4.6E-02	
SMYD3	SET and MYND domain containing 3	1.164	9.4E-03	
GTSE1	G-2 and S-phase expressed 1	1.165	2.2E-02	
C12ORF65	chromosome 12 open reading frame 65	1.165	7.3E-03	

Gene symbol	Protein name	FC	adj. p-value	Top quarter -positive regulator
PGK1	phosphoglycerate kinase 1	1.165	2.7E-02	
CDKN2A	cyclin-dependent kinase inhibitor 2A	1.166	2.4E-02	
CNOT7	CCR4-NOT transcription complex, subunit 7	1.167	3.2E-02	
REEP6	receptor accessory protein 6	1.167	2.4E-02	
GTF3C5	general transcription factor IIIC, polypeptide 5, 63kDa	1.168	3.1E-02	
MAU2	MAU2 chromatid cohesion factor homolog (C. elegans)	1.168	3.5E-02	
EIF3E	eukaryotic translation initiation factor 3, subunit E	1.168	2.3E-02	
ATXN2	ataxin 2	1.168	1.2E-02	
EIF4EBP2	eukaryotic translation initiation factor 4E binding protein 2	1.168	2.2E-02	
DDX39A	DEAD (Asp-Glu-Ala-Asp) box polypeptide 39A	1.169	2.4E-02	
ZNF35	zinc finger protein 35	1.169	1.1E-02	
MARK1	MAP/microtubule affinity-regulating kinase 1	1.170	9.8E-03	
DPH3	DPH3, KTI11 homolog (S. cerevisiae)	1.170	2.4E-02	
MGP	matrix Gla protein	1.170	3.2E-02	
SPANXE	SPANX family, member E	1.171	1.6E-02	
ZNF668	zinc finger protein 668	1.171	1.7E-02	
FXR1	fragile X mental retardation, autosomal homolog 1	1.171	3.0E-02	
PRPS2	phosphoribosyl pyrophosphate synthetase 2	1.172	2.7E-02	
FNTA	farnesyltransferase, CAAX box, alpha	1.173	4.1E-02	
SLC25A28	solute carrier family 25 (mitochondrial iron transporter), member 28	1.173	3.0E-02	
NACC1	nucleus accumbens associated 1, BEN and BTB (POZ) domain containing	1.174	7.9E-03	
FOXD1	forkhead box D1	1.174	5.5E-03	
CA5B	carbonic anhydrase VB, mitochondrial	1.174	2.8E-02	
NFIA	nuclear factor I/A	1.175	2.3E-02	
MRPS17	mitochondrial ribosomal protein S17	1.175	3.8E-02	
ATP6V1B2	ATPase, H+ transporting, lysosomal 56/58kDa, V1 subunit B2	1.175	5.1E-03	
BBC3	BCL2 binding component 3	1.177	9.9E-03	
OTUB1	OTU domain, ubiquitin aldehyde binding 1	1.177	2.1E-02	
LOC730101	uncharacterized LOC730101	1.177	2.4E-02	
PIBF1	progesterone immunomodulatory binding factor 1	1.178	2.1E-02	
SETP3	septin 3	1.178	3.8E-02	
RPL13	ribosomal protein L13	1.179	4.8E-02	
RCL1	RNA terminal phosphate cyclase-like 1	1.179	3.1E-02	
OTUD3	OTU domain containing 3	1.180	2.6E-02	
INSIG1	insulin induced gene 1	1.181	2.0E-02	
HPS5	Hermansky-Pudlak syndrome 5	1.181	4.1E-02	
OLIG2	oligodendrocyte lineage transcription factor 2	1.181	2.2E-02	
RPS15A	ribosomal protein S15a	1.182	1.8E-02	
LOC642980	uncharacterized LOC642980	1.182	3.2E-02	
VAMP1	vesicle-associated membrane protein 1 (synaptobrevin 1)	1.182	2.9E-02	
SRFBP1	serum response factor binding protein 1	1.183	1.3E-02	
RNASEH1	ribonuclease H1	1.183	4.0E-02	
SMN2	survival of motor neuron 2, centromeric	1.183	4.9E-02	
WIPI2	WD repeat domain, phosphoinositide interacting 2	1.184	4.1E-02	
ZCCHC17	zinc finger, CCHC domain containing 17	1.184	2.8E-02	
PDCD6	programmed cell death 6	1.184	2.3E-03	
RFXAP	regulatory factor X-associated protein	1.185	2.7E-02	
SMIM8	small integral membrane protein 8	1.185	5.5E-03	
FBL	fibrillarin	1.185	2.8E-02	
SVEP1	sushi, von Willebrand factor type A, EGF and pentraxin domain containing 1	1.185	1.4E-02	
MRPL32	mitochondrial ribosomal protein L32	1.185	3.8E-02	
LARP4B	La ribonucleoprotein domain family, member 4B	1.185	3.2E-02	
UQCC	ubiquinol-cytochrome c reductase complex chaperone	1.186	4.4E-02	

Gene symbol	Protein name	FC	adj. p-value	Top quarter -positive regulator
TPD52	tumor protein D52	1.186	2.4E-02	
VDAC1	voltage-dependent anion channel 1	1.186	3.3E-02	
FBXW11	F-box and WD repeat domain containing 11	1.187	3.4E-02	
NCBP2	nuclear cap binding protein subunit 2, 20kDa	1.187	2.0E-02	
TMEM138	transmembrane protein 138	1.188	1.5E-02	
BRCC3	BRCA1/BRCA2-containing complex, subunit 3	1.188	3.9E-02	
HIF1A	hypoxia inducible factor 1, alpha subunit (basic helix-loop-helix transcription factor)	1.189	2.1E-02	
PTP4A3	protein tyrosine phosphatase type IVA, member 3	1.189	1.4E-02	
RUVBL1	RuvB-like 1 (E. coli)	1.189	4.9E-02	
ATXN1L	ataxin 1-like	1.189	1.3E-02	
EP400	E1A binding protein p400	1.189	2.5E-02	
SYNJ2BP	synaptojanin 2 binding protein	1.190	6.6E-03	
TMX2	thioredoxin-related transmembrane protein 2	1.190	2.4E-02	
SF3B4	splicing factor 3b, subunit 4, 49kDa	1.190	7.6E-03	
WDR20	WD repeat domain 20	1.190	2.8E-02	
ZBTB8OS	zinc finger and BTB domain containing 8 opposite strand	1.190	7.3E-03	
TMEM97	transmembrane protein 97	1.190	4.0E-02	
HSPD1	heat shock 60kDa protein 1 (chaperonin)	1.191	3.1E-02	
TTC25	tetratricopeptide repeat domain 25	1.191	9.0E-04	
KARS	lysyl-tRNA synthetase	1.191	3.5E-02	
CDX2	caudal type homeobox 2	1.192	4.1E-02	
PPM1H	protein phosphatase, Mg2+/Mn2+ dependent, 1H	1.192	4.8E-02	
RAB18	RAB18, member RAS oncogene family	1.192	4.8E-02	
MRPS31	mitochondrial ribosomal protein S31	1.194	8.1E-03	
USPL1	ubiquitin specific peptidase like 1	1.194	3.5E-02	
MTSS1	metastasis suppressor 1	1.194	5.8E-03	
DHX37	DEAH (Asp-Glu-Ala-His) box polypeptide 37	1.194	2.9E-02	
ANKRD10	ankyrin repeat domain 10	1.195	4.5E-02	
ACACA	acetyl-CoA carboxylase alpha	1.196	2.0E-02	
ACYP1	acylphosphatase 1, erythrocyte (common) type	1.196	5.0E-02	
MALSU1	mitochondrial assembly of ribosomal large subunit 1	1.198	3.1E-02	
C9ORF123	chromosome 9 open reading frame 123	1.198	4.4E-03	
L2HGDH	L-2-hydroxyglutarate dehydrogenase	1.198	3.4E-03	
HSPA14	heat shock 70kDa protein 14	1.199	3.2E-02	
FDX1	ferredoxin 1	1.199	1.9E-02	
ABL1	c-abl oncogene 1, non-receptor tyrosine kinase	1.200	4.8E-02	
LEPROTL1	leptin receptor overlapping transcript-like 1	1.200	4.5E-02	
TRMT6	tRNA methyltransferase 6 homolog (S. cerevisiae)	1.201	3.9E-02	
NT5C3	5'-nucleotidase, cytosolic III	1.202	2.9E-02	
PDPK1	3-phosphoinositide dependent protein kinase-1	1.202	2.7E-02	
MMS19	MMS19 nucleotide excision repair homolog (S. cerevisiae)	1.202	1.9E-02	
NXF1	nuclear RNA export factor 1	1.203	3.5E-03	
XAGE1D	X antigen family, member 1D	1.203	4.8E-02	
TIFA	TRAF-interacting protein with forkhead-associated domain	1.204	4.1E-02	
RAP1GDS1	RAP1, GTP-GDP dissociation stimulator 1	1.204	2.8E-02	
EIF1	eukaryotic translation initiation factor 1	1.204	4.7E-02	
AKAP17A	A kinase (PRKA) anchor protein 17A	1.205	4.2E-02	
NAP1L4	nucleosome assembly protein 1-like 4	1.206	1.7E-02	
SQLE	squalene epoxidase	1.206	2.7E-02	
BYSL	bystin-like	1.207	4.9E-02	
TDP1	tyrosyl-DNA phosphodiesterase 1	1.207	3.8E-02	
SLC25A17	solute carrier family 25 (mitochondrial carrier; peroxisomal membrane protein, 34kDa), member 17	1.207	3.0E-02	
ZNF322	zinc finger protein 322	1.207	2.1E-02	

Gene symbol	Protein name	FC	adj. p-value	Top quarter -positive regulator
MVD	mevalonate (diphospho) decarboxylase	1.208	2.2E-02	
TXNL4A	thioredoxin-like 4A	1.209	9.1E-03	
PUS1	pseudouridylate synthase 1	1.210	2.2E-02	
EDC3	enhancer of mRNA decapping 3 homolog (S. cerevisiae)	1.211	2.9E-02	
FDFT1	farnesyl-diphosphate farnesyltransferase 1	1.211	6.3E-03	
TRMT12	tRNA methyltransferase 12 homolog (S. cerevisiae)	1.211	1.2E-03	
COA4	cytochrome c oxidase assembly factor 4 homolog (S. cerevisiae)	1.212	2.7E-02	
GADD45G	growth arrest and DNA-damage-inducible, gamma	1.213	9.1E-03	
GGCX	gamma-glutamyl carboxylase	1.213	4.0E-02	
HTR3A	5-hydroxytryptamine (serotonin) receptor 3A, ionotropic	1.213	1.5E-03	
ELMO1	engulfment and cell motility 1	1.214	8.6E-03	
PSMD13	proteasome (prosome, macropain) 26S subunit, non-ATPase, 13	1.214	4.7E-02	
IFT27	intraflagellar transport 27 homolog (Chlamydomonas)	1.214	1.8E-02	
NUDT2	nudix (nucleoside diphosphate linked moiety X)-type motif 2	1.215	4.2E-02	
RDH11	retinol dehydrogenase 11 (all-trans/9-cis/11-cis)	1.215	8.6E-03	
ZDHHC7	zinc finger, DHHC-type containing 7	1.215	1.6E-02	
TBL1X	transducin (beta)-like 1X-linked	1.215	8.7E-03	
GFOD2	glucose-fructose oxidoreductase domain containing 2	1.216	2.7E-02	
NDUFB3	NADH dehydrogenase (ubiquinone) 1 beta subcomplex, 3, 12kDa	1.217	4.3E-03	
FAM220A	family with sequence similarity 220, member A	1.217	6.4E-03	
ZNF296	zinc finger protein 296	1.218	5.5E-03	
RAB1B	RAB1B, member RAS oncogene family	1.218	2.0E-02	
UBAP1	ubiquitin associated protein 1	1.219	1.0E-02	
TRAPPC2P1	trafficking protein particle complex 2 pseudogene 1	1.220	1.5E-02	
AXIN1	axin 1	1.222	3.5E-02	
GAK	cyclin G associated kinase	1.222	3.2E-02	
TP53BP2	tumor protein p53 binding protein, 2	1.222	4.5E-02	
FOXD4L1	forkhead box D4-like 1	1.223	1.5E-02	
LPCAT1	lysophosphatidylcholine acyltransferase 1	1.223	4.6E-02	
FARSA	phenylalanyl-tRNA synthetase, alpha subunit	1.223	4.8E-02	
PPME1	protein phosphatase methylesterase 1	1.224	4.6E-02	
PTRHD1	peptidyl-tRNA hydrolase domain containing 1	1.224	3.3E-02	
HSD17B10	hydroxysteroid (17-beta) dehydrogenase 10	1.224	2.9E-02	
GATS	GATS, stromal antigen 3 opposite strand	1.224	1.9E-03	
SMG5	smg-5 homolog, nonsense mediated mRNA decay factor (C. elegans)	1.224	5.0E-02	
DHX29	DEAH (Asp-Glu-Ala-His) box polypeptide 29	1.225	1.9E-02	
DPM2	dolichyl-phosphate mannosyltransferase polypeptide 2, regulatory subunit	1.225	1.0E-02	
ECHDC1	enoyl CoA hydratase domain containing 1	1.226	4.7E-02	
MAPT	microtubule-associated protein tau	1.226	8.5E-03	
USP37	ubiquitin specific peptidase 37	1.226	4.3E-02	
IQCK	IQ motif containing K	1.226	2.2E-02	
EDC4	enhancer of mRNA decapping 4	1.228	2.1E-02	
NRBF2	nuclear receptor binding factor 2	1.228	4.6E-02	
PRPF19	PRP19/PSO4 pre-mRNA processing factor 19 homolog (S. cerevisiae)	1.228	2.0E-02	
SRD5A1	steroid-5-alpha-reductase, alpha polypeptide 1 (3-oxo-5 alpha-steroid delta 4-dehydrogenase alpha 1)	1.228	3.2E-02	
ZNF446	zinc finger protein 446	1.228	2.5E-02	
RNMTL1	RNA methyltransferase like 1	1.228	5.3E-03	
ACSL3	acyl-CoA synthetase long-chain family member 3	1.228	1.3E-02	
SLC35E1	solute carrier family 35, member E1	1.228	4.0E-02	
CYP26A1	cytochrome P450, family 26, subfamily A, polypeptide 1	1.229	2.9E-03	
NME7	NME/NM23 family member 7	1.229	6.2E-03	
NOL11	nucleolar protein 11	1.229	2.1E-02	
POP5	processing of precursor 5, ribonuclease P/MRP subunit (S. cerevisiae)	1.230	3.8E-02	

Gene symbol	Protein name	FC	adj. p-value	Top quarter -positive regulator
GLRX5	glutaredoxin 5	1.230	4.6E-03	
HNRNPA1	heterogeneous nuclear ribonucleoprotein A1	1.230	1.7E-02	
PNO1	partner of NOB1 homolog (S. cerevisiae)	1.230	4.1E-03	
CFDP1	craniofacial development protein 1	1.231	7.1E-03	
NSMCE2	non-SMC element 2, MMS21 homolog (S. cerevisiae)	1.231	2.0E-02	
ZNF770	zinc finger protein 770	1.231	4.8E-02	
THADA	thyroid adenoma associated	1.232	5.3E-03	
ECSIT	ECSIT homolog (Drosophila)	1.232	2.0E-02	
MARCH7	membrane-associated ring finger (C3HC4) 7, E3 ubiquitin protein ligase	1.233	5.0E-02	
RNU4ATAC	RNA, U4atac small nuclear (U12-dependent splicing)	1.234	2.0E-02	
EPN1	epsin 1	1.234	9.7E-03	
BPGM	2,3-bisphosphoglycerate mutase	1.234	2.7E-02	
STC2	stanniocalcin 2	1.236	3.6E-02	
GNA11	guanine nucleotide binding protein (G protein), alpha 11 (Gq class)	1.236	9.3E-03	
FGF9	fibroblast growth factor 9 (glia-activating factor)	1.237	1.6E-02	
YDJC	YdjC homolog (bacterial)	1.237	3.6E-02	
ANKFY1	ankyrin repeat and FYVE domain containing 1	1.237	4.6E-02	
SLC30A9	solute carrier family 30 (zinc transporter), member 9	1.237	1.2E-02	
RNF167	ring finger protein 167	1.238	5.1E-03	
TNRC6A	trinucleotide repeat containing 6A	1.238	1.2E-02	
SMC1A	structural maintenance of chromosomes 1A	1.238	1.1E-02	
SAR1A	SAR1 homolog A (S. cerevisiae)	1.238	3.4E-02	
HES6	hairy and enhancer of split 6 (Drosophila)	1.239	2.2E-02	
PAG1	phosphoprotein associated with glycosphingolipid microdomains 1	1.239	3.3E-02	
MEF2D	myocyte enhancer factor 2D	1.239	1.3E-03	
CCT8	chaperonin containing TCP1, subunit 8 (theta)	1.239	3.0E-02	
RGS16	regulator of G-protein signaling 16	1.240	9.0E-03	
RNU1-3	RNA, U1 small nuclear 3	1.240	1.3E-02	
CHAF1A	chromatin assembly factor 1, subunit A (p150)	1.240	1.8E-02	
ACN9	ACN9 homolog (S. cerevisiae)	1.241	9.5E-03	
RHOA	ras homolog family member A	1.241	1.6E-02	
COX16	COX16 cytochrome c oxidase assembly homolog (S. cerevisiae)	1.241	4.2E-03	
SERP1	stress-associated endoplasmic reticulum protein 1	1.242	3.9E-02	
DRD4	dopamine receptor D4	1.243	3.0E-02	
BCYRN1	brain cytoplasmic RNA 1	1.243	2.8E-02	
C14ORF132	chromosome 14 open reading frame 132	1.244	1.7E-03	
MSMO1	methylsterol monooxygenase 1	1.245	2.3E-02	
NT5DC3	5'-nucleotidase domain containing 3	1.245	1.0E-02	
ILKAP	integrin-linked kinase-associated serine/threonine phosphatase	1.246	6.9E-03	
AP3D1	adaptor-related protein complex 3, delta 1 subunit	1.246	8.1E-03	
EMD	emerin	1.246	6.1E-03	
C4ORF46	chromosome 4 open reading frame 46	1.246	1.3E-03	
MED19	mediator complex subunit 19	1.246	2.4E-03	
ONECUT2	one cut homeobox 2	1.246	6.4E-03	
HDDC3	HD domain containing 3	1.247	2.0E-02	
FAM53B	family with sequence similarity 53, member B	1.251	1.3E-03	
GPHN	gephyrin	1.251	4.9E-02	
PRMT2	protein arginine methyltransferase 2	1.251	3.3E-03	
HILPDA	hypoxia inducible lipid droplet-associated	1.252	1.2E-02	
EBPL	emopamil binding protein-like	1.252	4.6E-02	
EIF2B2	eukaryotic translation initiation factor 2B, subunit 2 beta, 39kDa	1.252	2.2E-03	
LCMT1	leucine carboxyl methyltransferase 1	1.252	1.4E-02	
RRP8	ribosomal RNA processing 8, methyltransferase, homolog (yeast)	1.253	3.5E-02	
ZMYM4	zinc finger, MYM-type 4	1.253	6.4E-03	

Gene symbol	Protein name	FC	adj. p-value	Top quarter -positive regulator
RARS2	arginyl-tRNA synthetase 2, mitochondrial	1.253	4.6E-03	
PLD3	phospholipase D family, member 3	1.253	1.4E-02	
TCTN3	tectonic family member 3	1.254	1.1E-02	
C12ORF44	chromosome 12 open reading frame 44	1.255	2.7E-02	
DCAF6	DDB1 and CUL4 associated factor 6	1.255	8.1E-03	
KIAA0556	KIAA0556	1.255	1.4E-02	
ATP5J	ATP synthase, H+ transporting, mitochondrial Fo complex, subunit F6	1.255	6.4E-03	
MED31	mediator complex subunit 31	1.256	1.1E-02	
ZNF473	zinc finger protein 473	1.256	8.9E-03	
NIPA2	non imprinted in Prader-Willi/Angelman syndrome 2	1.257	2.7E-02	
USP7	ubiquitin specific peptidase 7 (herpes virus-associated)	1.257	2.9E-02	
GCSH	glycine cleavage system protein H (aminomethyl carrier)	1.257	1.9E-02	
DGCR14	DiGeorge syndrome critical region gene 14	1.258	6.7E-03	
MTPN	myotrophin	1.258	4.4E-02	
DHCR24	24-dehydrocholesterol reductase	1.259	1.2E-02	
NAP1L1	nucleosome assembly protein 1-like 1	1.260	4.6E-02	
AMOT	angiomotin	1.260	3.1E-02	
MRPL44	mitochondrial ribosomal protein L44	1.261	3.7E-03	
ZSCAN32	zinc finger and SCAN domain containing 32	1.263	3.1E-03	
KIF3B	kinesin family member 3B	1.263	7.3E-03	
TOMM20	translocase of outer mitochondrial membrane 20 homolog (yeast)	1.263	4.9E-02	
EPT1	ethanolaminephosphotransferase 1 (CDP-ethanolamine-specific)	1.264	3.7E-03	
EAF2	ELL associated factor 2	1.264	6.6E-03	
KCTD10	potassium channel tetramerisation domain containing 10	1.266	2.1E-02	
CA8	carbonic anhydrase VIII	1.266	2.4E-03	
EIF2S1	eukaryotic translation initiation factor 2, subunit 1 alpha, 35kDa	1.267	2.7E-02	
PPP1R7	protein phosphatase 1, regulatory subunit 7	1.268	1.0E-02	
PKP4	plakophilin 4	1.268	3.4E-03	
ZNF789	zinc finger protein 789	1.268	5.6E-04	
EFHD2	EF-hand domain family, member D2	1.270	1.9E-03	
C14ORF142	chromosome 14 open reading frame 142	1.270	2.1E-02	
MED26	mediator complex subunit 26	1.271	2.3E-02	
TOMM5	translocase of outer mitochondrial membrane 5 homolog (yeast)	1.273	1.2E-02	
LOC100293704	uncharacterized LOC100293704	1.273	6.5E-03	
MAPK1	mitogen-activated protein kinase 1	1.274	5.6E-03	
VMP1	vacuole membrane protein 1	1.274	6.8E-03	
ENOPH1	enolase-phosphatase 1	1.274	2.5E-02	
STRA13	stimulated by retinoic acid 13	1.274	2.3E-03	
PRADC1	protease-associated domain containing 1	1.277	1.2E-02	
EMC6	ER membrane protein complex subunit 6	1.277	1.0E-02	
MRPS12	mitochondrial ribosomal protein S12	1.279	3.1E-02	
SERF2	small EDRK-rich factor 2	1.279	2.1E-02	
RPL22	ribosomal protein L22	1.280	2.0E-02	
CISD2	CDGSH iron sulfur domain 2	1.281	1.4E-02	
PPP6R3	protein phosphatase 6, regulatory subunit 3	1.281	5.3E-03	
LMCD1	LIM and cysteine-rich domains 1	1.283	6.3E-04	
ARPC5L	actin related protein 2/3 complex, subunit 5-like	1.285	1.1E-03	
FAF1	Fas (TNFRSF6) associated factor 1	1.285	3.7E-03	
SNRPD3	small nuclear ribonucleoprotein D3 polypeptide 18kDa	1.286	1.1E-02	
PHF10	PHD finger protein 10	1.288	3.2E-02	
GATC	glutamyl-tRNA(Gln) amidotransferase, subunit C	1.288	3.4E-03	
MMAB	methylmalonic aciduria (cobalamin deficiency) cblB type	1.288	8.2E-04	
PRPF38A	PRP38 pre-mRNA processing factor 38 (yeast) domain containing A	1.288	3.8E-02	
CANX	calnexin	1.288	4.6E-02	

Gene symbol	Protein name	FC	adj. p-value	Top quarter -positive regulator
SETD8	SET domain containing (lysine methyltransferase) 8	1.289	5.3E-03	
AHCTF1	AT hook containing transcription factor 1	1.292	3.1E-02	
TUSC2	tumor suppressor candidate 2	1.295	2.0E-02	
TNFRSF19	tumor necrosis factor receptor superfamily, member 19	1.295	4.0E-02	
PGAM4	phosphoglycerate mutase family member 4	1.297	8.2E-03	
DIDO1	death inducer-obliterator 1	1.297	6.8E-03	
TRAPPC3	trafficking protein particle complex 3	1.297	2.5E-03	
RNF10	ring finger protein 10	1.298	4.4E-02	
RAB7A	RAB7A, member RAS oncogene family	1.298	2.1E-03	
VTA1	Vps20-associated 1 homolog (S. cerevisiae)	1.298	1.6E-02	
DACH1	dachshund homolog 1 (Drosophila)	1.298	8.9E-03	
ERLIN1	ER lipid raft associated 1	1.301	9.9E-03	
MPLKIP	M-phase specific PLK1 interacting protein	1.301	1.8E-02	
EBF2	early B-cell factor 2	1.302	2.2E-04	
RNFT2	ring finger protein, transmembrane 2	1.308	2.2E-04	
SS18L1	synovial sarcoma translocation gene on chromosome 18-like 1	1.308	3.6E-02	
GGA2	golgi-associated, gamma adaptin ear containing, ARF binding protein 2	1.308	2.1E-02	
ACLY	ATP citrate lyase	1.308	4.9E-02	
YTHDF1	YTH domain family, member 1	1.308	4.6E-03	
C9ORF37	chromosome 9 open reading frame 37	1.313	1.8E-02	
RABL2B	RAB, member of RAS oncogene family-like 2B	1.313	1.7E-02	
HMGCS1	3-hydroxy-3-methylglutaryl-CoA synthase 1 (soluble)	1.315	2.3E-02	
ILF3-AS1	ILF3 antisense RNA 1 (head to head)	1.320	3.8E-03	
DAZAP1	DAZ associated protein 1	1.322	1.0E-02	
HMGCR	3-hydroxy-3-methylglutaryl-CoA reductase	1.324	1.9E-02	
WRAP53	WD repeat containing, antisense to TP53	1.326	4.2E-02	
CCDC85C	coiled-coil domain containing 85C	1.326	1.6E-03	
PSMA2	proteasome (prosome, macropain) subunit, alpha type, 2	1.327	1.3E-03	
YWHAG	tyrosine 3-monooxygenase/tryptophan 5-monooxygenase activation protein, gamma polypeptide	1.327	9.1E-03	
RTN3	reticulon 3	1.331	6.4E-03	
H3F3B	H3 histone, family 3B (H3.3B)	1.332	2.0E-03	
TRAP1	TNF receptor-associated protein 1	1.333	1.4E-02	
STK3	serine/threonine kinase 3	1.335	2.5E-03	
MAGOHB	mago-nashi homolog B (Drosophila)	1.336	8.7E-03	
FAM84B	family with sequence similarity 84, member B	1.336	3.3E-02	
HNRNPH3	heterogeneous nuclear ribonucleoprotein H3 (2H9)	1.337	3.4E-02	
SGTA	small glutamine-rich tetratricopeptide repeat (TPR)-containing, alpha	1.340	8.7E-03	
ANKRD11	ankyrin repeat domain 11	1.341	6.4E-03	
LDHC	lactate dehydrogenase C	1.343	4.2E-04	
SELT	selenoprotein T	1.343	5.8E-03	
CITED1	Cbp/p300-interacting transactivator, with Glu/Asp-rich carboxy-terminal domain, 1	1.344	2.3E-03	
ZDHHC11	zinc finger, DHHC-type containing 11	1.345	3.1E-03	
RPRD1A	regulation of nuclear pre-mRNA domain containing 1A	1.349	7.4E-03	
RAB1A	RAB1A, member RAS oncogene family	1.356	1.3E-02	
NMT1	N-myristoyltransferase 1	1.358	5.9E-03	
FOXA2	forkhead box A2	1.359	7.4E-03	
CEBPG	CCAAT/enhancer binding protein (C/EBP), gamma	1.377	3.9E-02	
TMEM70	transmembrane protein 70	1.380	7.8E-04	
FGFBP1	fibroblast growth factor binding protein 1	1.385	8.3E-04	
LOC730020	uncharacterized LOC730020	1.389	3.6E-03	
KIF1A	kinesin family member 1A	1.402	1.3E-03	
G3BP2	GTPase activating protein (SH3 domain) binding protein 2	1.409	1.2E-02	
C12ORF76	chromosome 12 open reading frame 76	1.420	1.7E-04	

Gene symbol	Protein name	FC	adj. p-value	Top quarter -positive regulator
RNF126	ring finger protein 126	1.428	3.9E-04	
TRMT61B	tRNA methyltransferase 61 homolog B (S. cerevisiae)	1.439	1.1E-04	
TATDN1	TatD DNase domain containing 1	1.449	1.3E-03	
IPO5	importin 5	1.449	1.1E-02	
C2ORF68	chromosome 2 open reading frame 68	1.459	8.6E-05	
TEX19	testis expressed 19	1.474	2.5E-05	
SLC2A4RG	SLC2A4 regulator	1.475	1.5E-03	
RBBP4	retinoblastoma binding protein 4	1.480	4.1E-03	
UBE2N	ubiquitin-conjugating enzyme E2N	1.492	4.2E-03	
SOX3	SRY (sex determining region Y)-box 3	1.496	2.6E-03	
TKTL1	transketolase-like 1	1.730	1.8E-05	
IGFBP5	insulin-like growth factor binding protein 5	1.926	1.9E-04	

Table 7.2 Significantly (p ≤ 0.05) affected biological processes in 551 downregulated genes after WAC knockdown only

Analysis carried out using MetaCore™ pathway analysis tool (Thomson Reuters). Adjusted p-value, adj. p-value. Ratio: number of genes in my list/number of genes in entire process in whole genome.

#	Process name	adj. p-value	Ratio
1	Immune response_Antigen presentation	1.88E-06	26/188
2	Immune response_Phagosome in antigen presentation	9.48E-05	25/221
3	Inflammation_Amphoterin signaling	4.19E-04	16/115
4	Inflammation_NK cell cytotoxicity	3.23E-03	17/153
5	Inflammation_IL-10 anti-inflammatory response	8.32E-03	11/81
6	Inflammation_IgE signaling	1.43E-02	12/102
7	Response to hypoxia and oxidative stress	1.89E-02	12/107
8	Inflammation_Innate inflammatory response	3.87E-02	14/150
9	Immune response_Phagocytosis	4.90E-02	16/190
10	Inflammation_Protein C signaling	4.91E-02	10/94
11	Inflammation_TREM1 signaling	4.91E-02	12/126

Table 7.3 319 genes significantly (p ≤ 0.05) up or downregulated, common to WAC, RNF20 and RNF40 knockdown versus RISC Free control

Genes highlighted in red are not regulated in the same way (up or down) between the WAC, RNF20 and RNF40 knockdown samples. Fold change versus RISC free, FC.

Gene symbol	Protein name	FC in siWAC	FC in siRNF40	FC in siRNF20
TNFRSF12A	tumor necrosis factor receptor superfamily, member 12A	-2.0	-1.4	1.3
TAGLN	transgelin	-1.5	-1.9	1.5
DMKN	dermokine	-1.3	-1.3	1.3
RAC1	ras-related C3 botulinum toxin substrate 1 (rho family, small GTP binding protein Rac1)	-1.3	1.4	-1.2
TCTEX1D2	Tctex1 domain containing 2	1.2	-1.2	-1.6
MT1A	metallothionein 1A	1.3	-1.2	-1.3
HMGN2	high mobility group nucleosomal binding domain 2	1.3	-1.2	-1.3
EIF2AK1	eukaryotic translation initiation factor 2-alpha kinase 1	1.3	-1.3	-1.2
CTSL2	cathepsin L2	1.1	-1.1	-1.2
AK4	adenylate kinase 4	1.3	-1.2	-1.2
CD44	CD44 molecule (Indian blood group)	-1.3	-1.6	1.4
TUBB2B	tubulin, beta 2B class IIb	1.5	1.2	-1.2
POLR1D	polymerase (RNA) I polypeptide D, 16kDa	1.3	-1.3	1.2
HN1	hematological and neurological expressed 1	-1.5	1.3	1.3
PPFIA1	protein tyrosine phosphatase, receptor type, f polypeptide (PTPRF), interacting protein (liprin), alpha 1	1.3	-1.4	1.3
PRSS23	protease, serine, 23	-1.3	1.4	1.3
UBE2D2	ubiquitin-conjugating enzyme E2D 2	1.2	-1.2	1.3
SDHC	succinate dehydrogenase complex, subunit C, integral membrane protein, 15kDa	1.1	-1.2	1.2
TPM4	tropomyosin 4	-1.9	-1.5	-1.2
COL5A1	collagen, type V, alpha 1	-2.3	-2.3	-1.4
FBXO4	F-box protein 4	-1.6	-1.2	-1.3
SLC2A10	solute carrier family 2 (facilitated glucose transporter), member 10	-1.9	-1.5	-1.6
ACTA2	actin, alpha 2, smooth muscle, aorta	-2.0	-1.4	-1.6
DIRC2	disrupted in renal carcinoma 2	-1.6	-1.4	-1.2
TCEAL3	transcription elongation factor A (SII)-like 3	-1.5	-1.2	-1.3
LOXL4	lysyl oxidase-like 4	-2.1	-1.7	-2.1
TEAD2	TEA domain family member 2	-1.6	-1.4	-1.5
MDK	midkine (neurite growth-promoting factor 2)	-2.0	-1.1	-1.8
NYNRIN	NYN domain and retroviral integrase containing	-1.6	-1.2	-1.4
LINC00294	long intergenic non-protein coding RNA 294	-1.8	-1.5	-1.3
TMBIM4	transmembrane BAX inhibitor motif containing 4	-1.6	-1.2	-1.6
FEZ1	fasciculation and elongation protein zeta 1 (zygin I)	-1.6	-1.2	-2.0
LAMP2	lysosomal-associated membrane protein 2	-1.4	-1.6	-1.3
TMSB15A	thymosin beta 15a	-1.4	-1.1	-1.3
TRIP6	thyroid hormone receptor interactor 6	-1.7	-1.5	-1.4
TSPO	translocator protein (18kDa)	-1.4	-1.2	-1.3
EFEMP2	EGF containing fibulin-like extracellular matrix protein 2	-1.7	-1.7	-1.9
TST	thiosulfate sulfurtransferase (rhodanese)	-1.8	-1.2	-1.8
TRIOBP	TRIO and F-actin binding protein	-1.5	-1.3	-1.2
HIST1H2BJ	histone cluster 1, H2bj	-1.5	-1.4	-1.6
FTL	ferritin, light polypeptide	-1.4	-1.2	-1.2
MGST2	microsomal glutathione S-transferase 2	-1.5	-1.2	-1.3
FADS1	fatty acid desaturase 1	-1.5	-1.3	-1.5
MSRB2	methionine sulfoxide reductase B2	-1.6	-1.7	-2.0
PHPT1	phosphohistidine phosphatase 1	-1.4	-1.2	-1.2
HIST2H2AC	histone cluster 2, H2ac	-1.5	-1.2	-1.8
HSPB1	heat shock 27kDa protein 1	-1.4	-1.3	-1.5
MAGED1	melanoma antigen family D, 1	-1.5	-1.4	-1.6
FBLN1	fibulin 1	-1.4	-1.7	-1.8
PKD2	polycystic kidney disease 2 (autosomal dominant)	-1.4	-1.2	-1.2
MAP2	microtubule-associated protein 2	-1.4	-1.2	-1.3
BEX4	brain expressed, X-linked 4	-1.5	-1.4	-1.3
PAPLN	papilin, proteoglycan-like sulfated glycoprotein	-1.5	-1.3	-1.4
ABCB10	ATP-binding cassette, sub-family B (MDR/TAP), member 10	-2.1	-1.4	-1.7

Gene symbol	Protein name	FC in siWAC	FC in siRNF40	FC in siRNF20
FZD2	frizzled family receptor 2	-1.5	-1.3	-1.4
PHF11	PHD finger protein 11	-1.4	-1.2	-1.2
HIST2H4A	histone cluster 2, H4a	-1.5	-1.4	-1.6
MSRA	methionine sulfoxide reductase A	-1.3	-1.1	-1.2
ARHGEF39	Rho guanine nucleotide exchange factor (GEF) 39	-1.3	-1.3	-1.3
RNASE4	ribonuclease, RNase A family, 4	-1.4	-1.3	-1.2
CDC25B	cell division cycle 25B	-1.4	-1.5	-1.4
KLHL5	kelch-like family member 5	-1.3	-1.2	-1.1
ATP6V1B1	ATPase, H+ transporting, lysosomal 56/58kDa, V1 subunit B1	-1.3	-1.2	-1.5
FXYD5	FXYD domain containing ion transport regulator 5	-1.3	-1.2	-1.2
HIST2H2AA3	histone cluster 2, H2aa3	-1.7	-1.4	-2.1
MYADM	myeloid-associated differentiation marker	-1.5	-1.3	-1.4
HIST2H2AA4	histone cluster 2, H2aa4	-1.5	-1.3	-2.3
CDK19	cyclin-dependent kinase 19	-1.4	-1.3	-1.7
BRD2	bromodomain containing 2	-1.7	-1.4	-1.4
HIST2H4B	histone cluster 2, H4b	-1.3	-1.2	-1.3
SULT1A4	sulfotransferase family, cytosolic, 1A, phenol-preferring, member 4	-1.6	-1.3	-1.6
CD2BP2	CD2 (cytoplasmic tail) binding protein 2	-1.4	-1.3	-1.3
FAM120C	family with sequence similarity 120C	-1.3	-1.3	-1.4
VEGFB	vascular endothelial growth factor B	-1.3	-1.3	-1.4
PPA2	pyrophosphatase (inorganic) 2	-1.3	-1.5	-1.8
SMIM14	small integral membrane protein 14	-1.3	-1.6	-1.6
CPS1	carbamoyl-phosphate synthase 1, mitochondrial	-1.4	-1.5	-1.4
LPIN1	lipin 1	-1.3	-1.3	-1.4
HIST1H2BK	histone cluster 1, H2bk	-1.5	-1.7	-2.1
CCDC15	coiled-coil domain containing 15	-1.3	-1.2	-1.3
HEBP1	heme binding protein 1	-1.3	-1.2	-1.4
ARMCX1	armadillo repeat containing, X-linked 1	-1.3	-1.3	-1.2
ZNF362	zinc finger protein 362	-1.3	-1.2	-1.3
IL11RA	interleukin 11 receptor, alpha	-1.4	-1.2	-1.3
SLC16A9	solute carrier family 16, member 9 (monocarboxylic acid transporter 9)	-1.3	-1.3	-1.2
UCHL1	ubiquitin carboxyl-terminal esterase L1 (ubiquitin thiolesterase)	-1.3	-1.4	-1.1
EPSTI1	epithelial stromal interaction 1 (breast)	-1.2	-1.3	-1.1
FGGY	FGGY carbohydrate kinase domain containing	-1.2	-1.3	-1.3
THAP10	THAP domain containing 10	-1.3	-1.3	-1.6
NGFRAP1	nerve growth factor receptor (TNFRSF16) associated protein 1	-1.3	-1.5	-1.6
LSMD1	LSM domain containing 1	-1.4	-1.3	-1.6
ATRAID	all-trans retinoic acid-induced differentiation factor	-1.2	-1.3	-1.3
UBE2C	ubiquitin-conjugating enzyme E2C	-1.3	-1.3	-1.3
LINC00085	long intergenic non-protein coding RNA 85	-1.5	-1.4	-1.7
CPVL	carboxypeptidase, vitellogenic-like	-1.3	-1.2	-1.4
NUCKS1	nuclear casein kinase and cyclin-dependent kinase substrate 1	-1.5	-1.6	-1.9
ALDH7A1	aldehyde dehydrogenase 7 family, member A1	-1.3	-1.2	-1.2
CGNL1	cingulin-like 1	-1.4	-1.3	-1.5
ACSF2	acyl-CoA synthetase family member 2	-1.3	-1.2	-1.2
SLC44A1	solute carrier family 44, member 1	-1.5	-1.6	-1.9
HSPB1P1	heat shock 27kDa protein 1 pseudogene 1	-1.4	-1.4	-1.5
COQ2	coenzyme Q2 homolog, prenyltransferase (yeast)	-1.3	-1.2	-1.3
ARL6IP6	ADP-ribosylation-like factor 6 interacting protein 6	-1.4	-1.8	-1.2
AURKB	aurora kinase B	-1.3	-1.3	-1.2
C15ORF52	chromosome 15 open reading frame 52	-1.3	-1.2	-1.3
TNFAIP8L1	tumor necrosis factor, alpha-induced protein 8-like 1	-1.3	-1.3	-1.4
PTTG3P	pituitary tumor-transforming 3, pseudogene	-1.2	-1.3	-1.2
PTPLA	protein tyrosine phosphatase-like (proline instead of catalytic arginine), member A	-1.2	-1.3	-1.3
MTL5	metallothionein-like 5, testis-specific (tesmin)	-1.2	-1.1	-1.2
COMT	catechol-O-methyltransferase	-1.4	-1.4	-1.5
RLN2	relaxin 2	-1.2	-1.2	-1.4
HIST1H1C	histone cluster 1, H1c	-1.3	-1.6	-2.1
TMEM187	transmembrane protein 187	-1.3	-1.2	-1.3
GPX8	glutathione peroxidase 8 (putative)	-1.3	-1.2	-1.3
PPP1R3F	protein phosphatase 1, regulatory subunit 3F	-1.3	-1.3	-1.4
DECR2	2,4-dienoyl CoA reductase 2, peroxisomal	-1.2	-1.2	-1.3
CCT6B	chaperonin containing TCP1, subunit 6B (zeta 2)	-1.2	-1.2	-1.3
HMMR	hyaluronan-mediated motility receptor (RHAMM)	-1.5	-1.6	-1.6
SULT1A1	sulfotransferase family, cytosolic, 1A, phenol-preferring, member 1	-1.4	-1.3	-1.5
ATG10	autophagy related 10	-1.3	-1.4	-1.5
IRX3	iroquois homeobox 3	-1.2	-1.2	-1.2

Gene symbol	Protein name	FC in siWAC	FC in siRNF40	FC in siRNF20
SIRT5	sirtuin 5	-1.2	-1.3	-1.3
MGMT	O-6-methylguanine-DNA methyltransferase	-1.3	-1.3	-1.4
MRPS9	mitochondrial ribosomal protein S9	-1.2	-1.2	-1.3
CALY	calcyon neuron-specific vesicular protein	-1.3	-1.2	-1.4
STOX2	storkhead box 2	-1.2	-1.2	-1.3
SULT1A2	sulfotransferase family, cytosolic, 1A, phenol-preferring, member 2	-1.3	-1.3	-1.4
UCP2	uncoupling protein 2 (mitochondrial, proton carrier)	-1.3	-1.6	-1.4
BACE1	beta-site APP-cleaving enzyme 1	-1.2	-1.2	-1.3
TRO	trophinin	-1.3	-1.2	-1.3
N6AMT2	N-6 adenine-specific DNA methyltransferase 2 (putative)	-1.2	-1.2	-1.2
CD97	CD97 molecule	-1.3	-1.4	-1.4
NME3	NME/NM23 nucleoside diphosphate kinase 3	-1.3	-1.2	-1.3
RGS12	regulator of G-protein signaling 12	-1.3	-1.3	-1.3
B3GALT6	UDP-Gal:betaGal beta 1,3-galactosyltransferase polypeptide 6	-1.2	-1.2	-1.7
LPXN	leupaxin	-1.2	-1.3	-1.4
TGFB1I1	transforming growth factor beta 1 induced transcript 1	-1.2	-1.2	-1.3
TCEAL8	transcription elongation factor A (SII)-like 8	-1.2	-1.3	-1.3
RAD51C	RAD51 homolog C (S. cerevisiae)	-1.3	-1.2	-1.4
ESPNL	espin-like	-1.3	-1.3	-1.3
ALG9	ALG9, alpha-1,2-mannosyltransferase	-1.3	-1.3	-1.2
TP53	tumor protein p53	-1.4	-1.3	-1.3
ALG10B	ALG10B, alpha-1,2-glucosyltransferase	-1.2	-1.2	-1.1
HIST2H2BE	histone cluster 2, H2be	-1.2	-1.2	-1.3
VIPR1	vasoactive intestinal peptide receptor 1	-1.1	-1.2	-1.1
RBCK1	RanBP-type and C3HC4-type zinc finger containing 1	-1.2	-1.6	-1.5
PLTP	phospholipid transfer protein	-1.3	-1.3	-1.3
RPP25L	ribonuclease P/MRP 25kDa subunit-like	-1.3	-1.3	-1.4
APOA1BP	apolipoprotein A-I binding protein	-1.2	-1.2	-1.2
TCEAL1	transcription elongation factor A (SII)-like 1	-1.3	-1.6	-1.4
PKIA	protein kinase (cAMP-dependent, catalytic) inhibitor alpha	-1.2	-1.3	-1.4
MRPL35	mitochondrial ribosomal protein L35	-1.2	-1.2	-1.2
ATP11C	ATPase, class VI, type 11C	-1.2	-1.2	-1.2
SLC25A15	solute carrier family 25 (mitochondrial carrier; ornithine transporter) member 15	-1.3	-1.2	-1.2
CCDC92	coiled-coil domain containing 92	-1.2	-1.5	-1.5
HIST1H2AG	histone cluster 1, H2ag	-1.2	-1.1	-1.1
NUDT7	nudix (nucleoside diphosphate linked moiety X)-type motif 7	-1.2	-1.3	-1.3
POLA2	polymerase (DNA directed), alpha 2, accessory subunit	-1.2	-1.3	-1.2
AHSA2	AHA1, activator of heat shock 90kDa protein ATPase homolog 2 (yeast)	-1.4	-1.3	-1.5
OLFML2A	olfactomedin-like 2A	-1.2	-1.2	-1.1
ATP9A	ATPase, class II, type 9A	-1.3	-1.4	-1.4
TNS3	tensin 3	-1.2	-1.2	-1.2
SLX4IP	SLX4 interacting protein	-1.3	-1.3	-1.3
MFSD8	major facilitator superfamily domain containing 8	-1.2	-1.2	-1.3
ZWINT	ZW10 interactor, kinetochore protein	-1.3	-1.3	-1.3
FAM86A	family with sequence similarity 86, member A	-1.2	-1.2	-1.2
STEAP2	STEAP family member 2, metalloreductase	-1.2	-1.3	-1.2
CSTB	cystatin B (stefin B)	-1.2	-1.2	-1.1
DCAKD	dephospho-CoA kinase domain containing	-1.3	-1.4	-1.7
SLC2A6	solute carrier family 2 (facilitated glucose transporter), member 6	-1.2	-1.2	-1.2
MST1	macrophage stimulating 1 (hepatocyte growth factor-like)	-1.2	-1.2	-1.3
RAN	RAN, member RAS oncogene family	-1.1	-1.1	-1.4
GSTM2	glutathione S-transferase mu 2 (muscle)	-1.3	-1.4	-1.5
HMGB1P1	high mobility group box 1 pseudogene 1	-1.3	-1.3	-1.4
TCEAL4	transcription elongation factor A (SII)-like 4	-1.2	-1.2	-1.2
ARMCX6	armadillo repeat containing, X-linked 6	-1.2	-1.3	-1.1
RND2	Rho family GTPase 2	-1.2	-1.3	-1.2
TRMT5	tRNA methyltransferase 5 homolog (S. cerevisiae)	-1.2	-1.3	-1.2
EHHADH	enoyl-CoA, hydratase/3-hydroxyacyl CoA dehydrogenase	-1.2	-1.3	-1.3
POP4	processing of precursor 4, ribonuclease P/MRP subunit (S. cerevisiae)	-1.3	-1.3	-1.2
GCHFR	GTP cyclohydrolase I feedback regulator	-1.3	-1.3	-1.4
PHIP	pleckstrin homology domain interacting protein	-1.2	-1.2	-1.2
TACC1	transforming, acidic coiled-coil containing protein 1	-1.2	-1.3	-1.4
USP11	ubiquitin specific peptidase 11	-1.2	-1.2	-1.3
SPPL2A	signal peptide peptidase like 2A	-1.2	-1.2	-1.3
NIT2	nitrilase family, member 2	-1.2	-1.3	-1.3
MESP1	mesoderm posterior 1 homolog (mouse)	-1.2	-1.3	-1.4
MBLAC2	metallo-beta-lactamase domain containing 2	-1.2	-1.2	-1.3

Gene symbol	Protein name	FC in siWAC	FC in siRNF40	FC in siRNF20
HIST1H2AC	histone cluster 1, H2ac	-1.2	-1.3	-1.3
KHDC1	KH homology domain containing 1	-1.2	-1.4	-1.3
SLMO1	slowmo homolog 1 (Drosophila)	-1.2	-1.4	-1.5
CXXC4	CXXC finger protein 4	-1.2	-1.2	-1.2
TUBA1C	tubulin, alpha 1c	-1.1	-1.2	-1.1
GSTM1	glutathione S-transferase mu 1	-1.3	-1.4	-1.5
DARS2	aspartyl-tRNA synthetase 2, mitochondrial	-1.2	-1.2	-1.2
ALPK1	alpha-kinase 1	-1.1	-1.1	-1.2
RCCD1	RCC1 domain containing 1	-1.2	-1.2	-1.2
ANLN	anillin, actin binding protein	-1.3	-1.3	-1.3
GNB1L	guanine nucleotide binding protein (G protein), beta polypeptide 1-like	-1.1	-1.4	-1.4
XPC	xeroderma pigmentosum, complementation group C	-1.2	-1.5	-1.3
UBA52	ubiquitin A-52 residue ribosomal protein fusion product 1	2.1	1.3	1.9
BRK1	BRICK1, SCAR/WAVE actin-nucleating complex subunit	1.6	1.6	1.2
NASP	nuclear autoantigenic sperm protein (histone-binding)	1.8	1.4	1.9
ENAH	enabled homolog (Drosophila)	1.8	1.2	1.3
TUBB3	tubulin, beta 3 class III	1.6	1.4	1.9
BAMBI	BMP and activin membrane-bound inhibitor homolog (Xenopus laevis)	1.5	1.5	1.4
BCCIP	BRCA2 and CDKN1A interacting protein	1.6	1.3	1.4
HES5	hairy and enhancer of split 5 (Drosophila)	1.5	1.7	1.5
TPMT	thiopurine S-methyltransferase	1.3	1.1	1.2
ELAVL1	ELAV (embryonic lethal, abnormal vision, Drosophila)-like 1 (Hu antigen R)	1.5	1.2	1.2
EIF2S2	eukaryotic translation initiation factor 2, subunit 2 beta, 38kDa	1.5	1.2	1.4
PIN4	protein (peptidylprolyl cis/trans isomerase) NIMA-interacting, 4 (parvulin)	1.3	1.3	1.2
DYNLL2	dynein, light chain, LC8-type 2	1.3	1.3	1.4
BMP2	bone morphogenetic protein 2	1.4	1.5	1.6
CLTA	clathrin, light chain A	1.3	1.2	1.2
RBM12	RNA binding motif protein 12	1.4	1.2	1.3
FKBP1A	FK506 binding protein 1A, 12kDa	1.4	1.3	1.3
RPL37	ribosomal protein L37	1.7	1.2	1.3
C16ORF72	chromosome 16 open reading frame 72	1.3	1.2	1.3
GCNT1	glucosaminyl (N-acetyl) transferase 1, core 2	1.4	1.4	1.2
CSRP2BP	CSRP2 binding protein	1.3	1.1	1.2
RPRM	reprimo, TP53 dependent G2 arrest mediator candidate	1.4	1.2	1.6
EMC8	ER membrane protein complex subunit 8	1.3	1.1	1.3
YRDC	yrdC domain containing (E. coli)	1.3	1.2	1.2
PTRH2	peptidyl-tRNA hydrolase 2	1.4	1.3	1.2
BCL2L11	BCL2-like 11 (apoptosis facilitator)	1.2	1.2	1.2
DUSP5	dual specificity phosphatase 5	1.5	1.6	1.5
MARC2	mitochondrial amidoxime reducing component 2	-1.4	-1.2	-1.3
UBE2L3	ubiquitin-conjugating enzyme E2L 3	1.6	1.3	1.6
MYC	v-myc myelocytomatosis viral oncogene homolog (avian)	1.4	1.3	1.7
DKK1	dickkopf 1 homolog (Xenopus laevis)	1.4	1.8	2.1
VPS37B	vacuolar protein sorting 37 homolog B (S. cerevisiae)	1.3	1.2	1.3
PITPNB	phosphatidylinositol transfer protein, beta	1.2	1.1	1.1
C14ORF2	chromosome 14 open reading frame 2	1.5	1.3	1.3
CITED2	Cbp/p300-interacting transactivator, with Glu/Asp-rich carboxy-terminal domain, 2	1.3	1.2	1.6
RAPGEF1	Rap guanine nucleotide exchange factor (GEF) 1	1.5	1.6	1.5
LBH	limb bud and heart development	1.4	1.3	1.3
CPLX1	complexin 1	1.2	1.2	2.6
NKRF	NFKB repressing factor	1.2	1.2	1.2
SDHAP1	succinate dehydrogenase complex, subunit A, flavoprotein pseudogene 1	1.2	1.2	1.2
ZCCHC12	zinc finger, CCHC domain containing 12	1.4	1.3	1.5
C7ORF41	chromosome 7 open reading frame 41	1.4	1.3	1.3
HEY1	hairy/enhancer-of-split related with YRPW motif 1	1.4	1.5	1.2
PARM1	prostate androgen-regulated mucin-like protein 1	1.4	1.3	1.5
CCDC25	coiled-coil domain containing 25	1.4	1.3	1.2
NOP16	NOP16 nucleolar protein	1.5	1.4	1.3
PITHD1	PITH (C-terminal proteasome-interacting domain of thioredoxin-like) domain containing 1	1.3	1.3	1.5
CRK	v-crk sarcoma virus CT10 oncogene homolog (avian)	1.2	1.3	1.3
FAM189A1	family with sequence similarity 189, member A1	1.2	1.2	1.4
ZMYM5	zinc finger, MYM-type 5	1.2	1.1	1.2
SLBP	stem-loop binding protein	1.2	1.3	1.3
SNHG15	small nucleolar RNA host gene 15 (non-protein coding)	1.3	1.3	1.3
HBA2	hemoglobin, alpha 2	1.3	1.3	2.2
SUPV3L1	suppressor of var1, 3-like 1 (S. cerevisiae)	1.3	1.2	1.2

Gene symbol	Protein name	FC in siWAC	FC in siRNF40	FC in siRNF20
JAG1	jagged 1	1.3	1.4	1.4
FAM206A	family with sequence similarity 206, member A	1.2	1.2	1.4
COL12A1	collagen, type XII, alpha 1	1.3	1.4	2.0
MRTO4	mRNA turnover 4 homolog (S. cerevisiae)	1.3	1.3	1.2
SBK1	SH3-binding domain kinase 1	1.2	1.1	1.2
SRI	sorcin	1.2	1.2	1.4
TRAFD1	TRAF-type zinc finger domain containing 1	1.2	1.2	1.2
CKMT1A	creatine kinase, mitochondrial 1A	1.4	1.3	2.9
RBM4	RNA binding motif protein 4	1.3	1.3	1.3
PDCD2	programmed cell death 2	1.2	1.3	1.2
ZNF271	zinc finger protein 271	1.2	1.2	1.2
PLAGL2	pleiomorphic adenoma gene-like 2	1.3	1.3	1.3
C10ORF2	chromosome 10 open reading frame 2	1.2	1.2	1.2
EIF4H	eukaryotic translation initiation factor 4H	1.2	1.1	1.2
PPP2R2A	protein phosphatase 2, regulatory subunit B, alpha	1.3	1.3	1.4
FASTKD5	FAST kinase domains 5	1.3	1.2	1.2
TMEM150A	transmembrane protein 150A	1.1	1.3	1.2
EIF3B	eukaryotic translation initiation factor 3, subunit B	1.2	1.2	1.2
CD24	CD24 molecule	1.2	1.4	1.7
F12	coagulation factor XII (Hageman factor)	1.2	1.4	1.3
RNF114	ring finger protein 114	1.3	1.3	1.3
PDCD2L	programmed cell death 2-like	1.3	1.4	1.3
SPRY2	sprouty homolog 2 (Drosophila)	1.2	1.2	1.7
MMP12	matrix metallopeptidase 12 (macrophage elastase)	1.2	1.2	1.3
MTHFD2	methylenetetrahydrofolate dehydrogenase (NADP+ dependent) 2, methenyltetrahydrofolate cyclohydrolase	1.2	1.2	1.3
NEDD4L	neural precursor cell expressed, developmentally down-regulated 4-like, E3 ubiquitin protein ligase	1.2	1.3	1.3
TXNDC12	thioredoxin domain containing 12 (endoplasmic reticulum)	1.2	1.3	1.2
RNPS1	RNA binding protein S1, serine-rich domain	1.2	1.1	1.2
RSL1D1	ribosomal L1 domain containing 1	1.2	1.3	1.3
LLPH	LLP homolog, long-term synaptic facilitation (Aplysia)	1.2	1.2	1.2
NCLN	nicalin	1.3	1.3	1.3
PPRC1	peroxisome proliferator-activated receptor gamma, coactivator-related 1	1.2	1.2	1.2
MAGOH	mago-nashi homolog, proliferation-associated (Drosophila)	1.2	1.2	1.2
EPAS1	endothelial PAS domain protein 1	1.2	1.3	1.2
FARP1	FERM, RhoGEF (ARHGEF) and pleckstrin domain protein 1 (chondrocyte-derived)	1.2	1.3	1.2
CCDC12	coiled-coil domain containing 12	1.3	1.3	1.2
ZMYND19	zinc finger, MYND-type containing 19	1.3	1.3	1.2
POLR3F	polymerase (RNA) III (DNA directed) polypeptide F, 39 kDa	1.2	1.2	1.2
POLR1C	polymerase (RNA) I polypeptide C, 30kDa	1.2	1.2	1.2
C16ORF91	chromosome 16 open reading frame 91	1.2	1.2	1.2
SURF2	surfeit 2	1.3	1.3	1.2
CEBPZ	CCAAT/enhancer binding protein (C/EBP), zeta	1.2	1.2	1.2
DPF2	D4, zinc and double PHD fingers family 2	1.2	1.2	1.2
SEC24C	SEC24 family, member C (S. cerevisiae)	1.1	1.2	1.1
ID1	inhibitor of DNA binding 1, dominant negative helix-loop-helix protein	1.3	1.3	1.3
AFTPH	aftiphilin	1.2	1.2	1.1
PHLDA1	pleckstrin homology-like domain, family A, member 1	1.2	1.2	1.3
ATP6V0B	ATPase, H+ transporting, lysosomal 21kDa, V0 subunit b	1.2	1.2	1.2
PIGC	phosphatidylinositol glycan anchor biosynthesis, class C	1.1	1.2	1.1
ABCF2	ATP-binding cassette, sub-family F (GCN20), member 2	1.2	1.2	1.3
NTMT1	N-terminal Xaa-Pro-Lys N-methyltransferase 1	1.2	1.3	1.3
ID3	inhibitor of DNA binding 3, dominant negative helix-loop-helix protein	1.2	1.3	1.3
SEC23B	Sec23 homolog B (S. cerevisiae)	1.2	1.2	1.2
FLNB	filamin B, beta	1.2	1.2	1.2
EXOSC3	exosome component 3	1.1	1.2	1.2
TNFRSF10D	tumor necrosis factor receptor superfamily, member 10d, decoy with truncated death domain	1.2	1.2	1.6
RIMS4	regulating synaptic membrane exocytosis 4	1.3	1.4	1.3
NOP2	NOP2 nucleolar protein	1.2	1.2	1.2
EXOSC5	exosome component 5	1.3	1.4	1.4
GJA1	gap junction protein, alpha 1, 43kDa	1.3	1.4	1.6
KIF5C	kinesin family member 5C	1.3	1.4	2.0
SYT7	synaptotagmin VII	1.2	1.4	1.2
AEN	apoptosis enhancing nuclease	1.2	1.2	1.2
ZNF598	zinc finger protein 598	1.2	1.2	1.2

Gene symbol	Protein name	FC in siWAC	FC in siRNF40	FC in siRNF20
PCBP2	poly(rC) binding protein 2	1.2	1.3	1.5

Table 7.4 Significantly enriched (p ≤ 0.05) transcription factor targets in 118 genes commonly upregulated after WAC, RNF20 and RNF40 knockdown versus RISC free control

TF target group	No. found	p-value
CREB1	61	2.9E-10
SMAD5	7	7.3E-08
SMAD1	7	2.8E-06
SMAD3	8	1.7E-05
c-Myc	30	2.6E-05
c-Jun	14	7.7E-05
SMAD9 (SMAD8)	3	1.3E-04
TBX3	4	1.4E-04
b-Myb	5	1.6E-04
MSX1	3	2.9E-04
FOXO3A	6	4.5E-04
ZNF238	2	4.7E-04
NANOG	12	5.7E-04
YY1	16	6.1E-04
Lef-1	5	9.2E-04
SP1	18	2.0E-03
ATF-5	2	2.0E-03
TCF7L2 (TCF4)	7	2.5E-03
RUNX3	3	2.8E-03
hASH1	3	3.3E-03
E2F1	11	3.5E-03
C/EBPalpha	7	3.5E-03
c-Fos	6	3.8E-03

Table 7.5 Significantly enriched ($p \leq 0.05$) transcription factor targets in 183 genes commonly downregulated after WAC, RNF20 and RNF40 knockdown versus RISC free control

TF target group	No. found	p-value
c-Myc	37	5.3E-04
GCR-alpha	22	5.8E-04
CREB1	64	1.1E-03
Androgen receptor	17	1.7E-03
RREB1	2	2.6E-03
p53	18	2.8E-03
NOR1	2	6.5E-03
SP1	23	6.5E-03
Eomesodermin	2	7.4E-03
b-Myb	4	8.1E-03
FHL2	1	8.7E-03
BTF	1	8.7E-03
PHF20	1	8.7E-03
hASH1	3	1.1E-02
TEF-3	3	1.4E-02
KLF4	6	1.5E-02
E2F1	13	1.5E-02
RBMS1	1	1.7E-02
ZNF804A	1	1.7E-02
Parkin	1	1.7E-02
DP2	1	1.7E-02
PPAR-alpha	5	1.8E-02
NANOG	12	2.0E-02
SALL4	4	2.4E-02
NUP133	1	2.6E-02
KILLIN	1	2.6E-02
SP3	9	2.6E-02
TFIIB	3	3.1E-02
BARX2	2	3.2E-02
NeuroD2	1	3.5E-02
HOXB8	1	3.5E-02
IRX1	1	3.5E-02
PU.1	7	4.3E-02
NF-AT4(NFATC3)	2	4.8E-02

Reference List

ALBERTS, B. 2002. *Molecular biology of the cell,* New York, Garland Science.

ALEMU, E. A., LAMARK, T., TORGERSEN, K. M., BIRGISDOTTIR, A. B., LARSEN, K. B., JAIN, A., OLSVIK, H., OVERVATN, A., KIRKIN, V. & JOHANSEN, T. 2012. ATG8 family proteins act as scaffolds for assembly of the ULK complex: sequence requirements for LC3-interacting region (LIR) motifs. *J Biol Chem,* 287**,** 39275-90.

ALVAREZ, C., GARCIA-MATA, R., HAURI, H. P. & SZTUL, E. 2001. The p115-interactive proteins GM130 and giantin participate in endoplasmic reticulum-Golgi traffic. *J Biol Chem,* 276**,** 2693-700.

AMBIVERO, C. T., CILENTI, L., MAIN, S. & ZERVOS, A. S. 2014. Mulan E3 ubiquitin ligase interacts with multiple E2 conjugating enzymes and participates in mitophagy by recruiting GABARAP. *Cell Signal,* 26**,** 2921-9.

APPENZELLER-HERZOG, C. & HAURI, H. P. 2006. The ER-Golgi intermediate compartment (ERGIC): in search of its identity and function. *J Cell Sci,* 119**,** 2173-83.

ARIAS, E., KOGA, H., DIAZ, A., MOCHOLI, E., PATEL, B. & CUERVO, A. M. 2015. Lysosomal mTORC2/PHLPP1/Akt Regulate Chaperone-Mediated Autophagy. *Mol Cell,* 59**,** 270-84.

AXE, E. L., WALKER, S. A., MANIFAVA, M., CHANDRA, P., RODERICK, H. L., HABERMANN, A., GRIFFITHS, G. & KTISTAKIS, N. T. 2008. Autophagosome formation from membrane compartments enriched in phosphatidylinositol 3-phosphate and dynamically connected to the endoplasmic reticulum. *J Cell Biol,* 182**,** 685-701.

BARR, F. A. 2013. Review series: Rab GTPases and membrane identity: causal or inconsequential? *J Cell Biol,* 202**,** 191-9.

BARR, F. A., NAKAMURA, N. & WARREN, G. 1998. Mapping the interaction between GRASP65 and GM130, components of a protein complex involved in the stacking of Golgi cisternae. *EMBO J,* 17**,** 3258-68.

BARR, F. A., PUYPE, M., VANDEKERCKHOVE, J. & WARREN, G. 1997. GRASP65, a protein involved in the stacking of Golgi cisternae. *Cell,* 91**,** 253-62.

BASCHIERI, F., CONFALONIERI, S., BERTALOT, G., DI FIORE, P. P., DIETMAIER, W., LEIST, M., CRESPO, P., MACARA, I. G. & FARHAN, H. 2014. Spatial control of Cdc42 signalling by a GM130-RasGRF complex regulates polarity and tumorigenesis. *Nat Commun,* 5**,** 4839.

BASCHIERI, F., UETZ-VON ALLMEN, E., LEGLER, D. F. & FARHAN, H. 2015. Loss of GM130 in breast cancer cells and its effects on cell migration, invasion and polarity. *Cell Cycle,* 14**,** 1139-47.

BEDFORD, M. T., REED, R. & LEDER, P. 1998. WW domain-mediated interactions reveal a spliceosome-associated protein that binds a third class of proline-rich motif: the proline glycine and methionine-rich motif. *Proc Natl Acad Sci U S A,* 95**,** 10602-7.

BEDNAREK, S. Y., RAVAZZOLA, M., HOSOBUCHI, M., AMHERDT, M., PERRELET, A., SCHEKMAN, R. & ORCI, L. 1995. COPI- and COPII-coated vesicles bud directly from the endoplasmic reticulum in yeast. *Cell,* 83**,** 1183-96.

BEHNIA, R., BARR, F. A., FLANAGAN, J. J., BARLOWE, C. & MUNRO, S. 2007. The yeast orthologue of GRASP65 forms a complex with a coiled-coil protein that contributes to ER to Golgi traffic. *J Cell Biol,* 176**,** 255-61.

BEHRENDS, C. & FULDA, S. 2012. Receptor proteins in selective autophagy. *Int J Cell Biol,* 2012**,** 673290.

BEHRENDS, C., SOWA, M. E., GYGI, S. P. & HARPER, J. W. 2010. Network organization of the human autophagy system. *Nature,* 466**,** 68-76.

BERTOLO, C., ROA, S., SAGARDOY, A., MENA-VARAS, M., ROBLES, E. F., MARTINEZ-FERRANDIS, J. I., SAGAERT, X., TOUSSEYN, T., ORTA, A., LOSSOS, I. S., AMAR, S., NATKUNAM, Y., BRIONES, J., MELNICK, A., MALUMBRES, R. & MARTINEZ-CLIMENT, J. A. 2013. LITAF, a BCL6 target gene, regulates autophagy in mature B-cell lymphomas. *Br J Haematol,* 162**,** 621-30.

BETIN, V. M. & LANE, J. D. 2009. Caspase cleavage of Atg4D stimulates GABARAP-L1 processing and triggers mitochondrial targeting and apoptosis. *J Cell Sci,* 122**,** 2554-66.

BIAZIK, J., YLA-ANTTILA, P., VIHINEN, H., JOKITALO, E. & ESKELINEN, E. L. 2015. Ultrastructural relationship of the phagophore with surrounding organelles. *Autophagy,* 11**,** 439-51.

BJORKOY, G., LAMARK, T., BRECH, A., OUTZEN, H., PERANDER, M., OVERVATN, A., STENMARK, H. & JOHANSEN, T. 2005. p62/SQSTM1 forms protein aggregates degraded by autophagy and has a protective effect on huntingtin-induced cell death. *J Cell Biol,* 171**,** 603-14.

BONNET, J., DEVYS, D. & TORA, L. 2014. Histone H2B ubiquitination: signaling not scrapping. *Drug Discov Today Technol,* 12**,** e19-27.

BOYA, P., REGGIORI, F. & CODOGNO, P. 2013. Emerging regulation and functions of autophagy. *Nat Cell Biol,* 15**,** 713-20.

BUDANOV, A. V. & KARIN, M. 2008. p53 target genes sestrin1 and sestrin2 connect genotoxic stress and mTOR signaling. *Cell,* 134**,** 451-60.

BURKHARD, P., STETEFELD, J. & STRELKOV, S. V. 2001. Coiled coils: a highly versatile protein folding motif. *Trends Cell Biol,* 11**,** 82-8.

CHAN, D. C., BEDFORD, M. T. & LEDER, P. 1996. Formin binding proteins bear WWP/WW domains that bind proline-rich peptides and functionally resemble SH3 domains. *EMBO J,* 15**,** 1045-54.

CHAN, E. Y., KIR, S. & TOOZE, S. A. 2007. siRNA screening of the kinome identifies ULK1 as a multidomain modulator of autophagy. *J Biol Chem,* 282**,** 25464-74.

CHAN, E. Y., LONGATTI, A., MCKNIGHT, N. C. & TOOZE, S. A. 2009. Kinase-inactivated ULK proteins inhibit autophagy via their conserved C-terminal domains using an Atg13-independent mechanism. *Mol Cell Biol,* 29**,** 157-71.

CHAN, E. Y. & TOOZE, S. A. 2009. Evolution of Atg1 function and regulation. *Autophagy,* 5**,** 758-65.

CHANG, S. H., HONG, S. H., JIANG, H. L., MINAI-TEHRANI, A., YU, K. N., LEE, J. H., KIM, J. E., SHIN, J. Y., KANG, B., PARK, S., HAN, K., CHAE, C. & CHO, M. H. 2012. GOLGA2/GM130, cis-Golgi matrix protein, is a novel target of anticancer gene therapy. *Mol Ther,* 20**,** 2052-63.

CHAUHAN, S., GOODWIN, J. G., CHAUHAN, S., MANYAM, G., WANG, J., KAMAT, A. M. & BOYD, D. D. 2013. ZKSCAN3 is a master transcriptional repressor of autophagy. *Mol Cell,* 50**,** 16-28.

CHEN, D., FAN, W., LU, Y., DING, X., CHEN, S. & ZHONG, Q. 2012. A mammalian autophagosome maturation mechanism mediated by TECPR1 and the Atg12-Atg5 conjugate. *Mol Cell,* 45**,** 629-41.

CHEN, H. I. & SUDOL, M. 1995. The WW domain of Yes-associated protein binds a proline-rich ligand that differs from the consensus established for Src homology 3-binding modules. *Proc Natl Acad Sci U S A,* 92**,** 7819-23.

CHEN, Z. W., CHANG, C. S., LEIL, T. A. & OLSEN, R. W. 2007. C-terminal modification is required for GABARAP-mediated GABA(A) receptor trafficking. *J Neurosci,* 27**,** 6655-63.

CHEONG, H., LINDSTEN, T., WU, J., LU, C. & THOMPSON, C. B. 2011. Ammonia-induced autophagy is independent of ULK1/ULK2 kinases. *Proc Natl Acad Sci U S A,* 108**,** 11121-6.

CHIU, C. F., GHANEKAR, Y., FROST, L., DIAO, A., MORRISON, D., MCKENZIE, E. & LOWE, M. 2008. ZFPL1, a novel ring finger protein required for cis-Golgi integrity and efficient ER-to-Golgi transport. *EMBO J,* 27**,** 934-47.

CIOTTA, G., HOFEMEISTER, H., MARESCA, M., FU, J., SAROV, M., ANASTASSIADIS, K. & STEWART, A. F. 2011. Recombineering BAC transgenes for protein tagging. *Methods,* 53**,** 113-9.

CLEMENTS, A., SMOLLETT, K., LEE, S. F., HARTLAND, E. L., LOWE, M. & FRANKEL, G. 2011. EspG of enteropathogenic and enterohemorrhagic E. coli binds the Golgi matrix protein GM130 and disrupts the Golgi structure and function. *Cell Microbiol,* 13**,** 1429-39.

CODOGNO, P., MEHRPOUR, M. & PROIKAS-CEZANNE, T. 2012. Canonical and non-canonical autophagy: variations on a common theme of self-eating? *Nat Rev Mol Cell Biol,* 13**,** 7-12.

COLE, N. B., SCIAKY, N., MAROTTA, A., SONG, J. & LIPPINCOTT-SCHWARTZ, J. 1996. Golgi dispersal during microtubule disruption: regeneration of Golgi stacks at peripheral endoplasmic reticulum exit sites. *Mol Biol Cell,* 7**,** 631-50.

COLECCHIA, D., STRAMBI, A., SANZONE, S., IAVARONE, C., ROSSI, M., DALL'ARMI, C., PICCIONI, F., VERROTTI DI PIANELLA, A. & CHIARIELLO, M. 2012. MAPK15/ERK8 stimulates autophagy by interacting with LC3 and GABARAP proteins. *Autophagy,* 8**,** 1724-40.

CORDA, D., BARRETTA, M. L., CERVIGNI, R. I. & COLANZI, A. 2012. Golgi complex fragmentation in G2/M transition: An organelle-based cell-cycle checkpoint. *IUBMB Life,* 64**,** 661-70.

COSSON, P. & LETOURNEUR, F. 1994. Coatomer interaction with di-lysine endoplasmic reticulum retention motifs. *Science,* 263**,** 1629-31.

COX, J. & MANN, M. 2008. MaxQuant enables high peptide identification rates, individualized p.p.b.-range mass accuracies and proteome-wide protein quantification. *Nat Biotechnol,* 26**,** 1367-72.

COYLE, J. E., QAMAR, S., RAJASHANKAR, K. R. & NIKOLOV, D. B. 2002. Structure of GABARAP in two conformations: implications for GABA(A) receptor localization and tubulin binding. *Neuron,* 33**,** 63-74.

CUERVO, A. M. & WONG, E. 2014. Chaperone-mediated autophagy: roles in disease and aging. *Cell Res,* 24**,** 92-104.

DANTUMA, N. P., LINDSTEN, K., GLAS, R., JELLNE, M. & MASUCCI, M. G. 2000. Short-lived green fluorescent proteins for quantifying ubiquitin/proteasome-dependent proteolysis in living cells. *Nat Biotechnol,* 18**,** 538-43.

DESANTO, C., D'ACO, K., ARAUJO, G. C., SHANNON, N., STUDY, D., VERNON, H., RAHRIG, A., MONAGHAN, K. G., NIU, Z., VITAZKA, P., DODD, J., TANG, S., MANWARING, L., MARTIR-NEGRON, A., SCHNUR, R. E., JUUSOLA, J., SCHROEDER, A., PAN, V., HELBIG, K. L., FRIEDMAN, B. & SHINAWI, M. 2015. WAC loss-of-function mutations cause a recognisable syndrome characterised by dysmorphic features, developmental delay and hypotonia and recapitulate 10p11.23 microdeletion syndrome. *J Med Genet*.

DI BARTOLOMEO, S., CORAZZARI, M., NAZIO, F., OLIVERIO, S., LISI, G., ANTONIOLI, M., PAGLIARINI, V., MATTEONI, S., FUOCO, C., GIUNTA, L., D'AMELIO, M., NARDACCI, R., ROMAGNOLI, A., PIACENTINI, M., CECCONI,

F. & FIMIA, G. M. 2010. The dynamic interaction of AMBRA1 with the dynein motor complex regulates mammalian autophagy. *J Cell Biol,* 191**,** 155-68.

DIAO, A., FROST, L., MOROHASHI, Y. & LOWE, M. 2008. Coordination of golgin tethering and SNARE assembly: GM130 binds syntaxin 5 in a p115-regulated manner. *J Biol Chem,* 283**,** 6957-67.

DIAO, J., LIU, R., RONG, Y., ZHAO, M., ZHANG, J., LAI, Y., ZHOU, Q., WILZ, L. M., LI, J., VIVONA, S., PFUETZNER, R. A., BRUNGER, A. T. & ZHONG, Q. 2015. ATG14 promotes membrane tethering and fusion of autophagosomes to endolysosomes. *Nature,* 520**,** 563-6.

DING, L., LEY, T. J., LARSON, D. E., MILLER, C. A., KOBOLDT, D. C., WELCH, J. S., RITCHEY, J. K., YOUNG, M. A., LAMPRECHT, T., MCLELLAN, M. D., MCMICHAEL, J. F., WALLIS, J. W., LU, C., SHEN, D., HARRIS, C. C., DOOLING, D. J., FULTON, R. S., FULTON, L. L., CHEN, K., SCHMIDT, H., KALICKI-VEIZER, J., MAGRINI, V. J., COOK, L., MCGRATH, S. D., VICKERY, T. L., WENDL, M. C., HEATH, S., WATSON, M. A., LINK, D. C., TOMASSON, M. H., SHANNON, W. D., PAYTON, J. E., KULKARNI, S., WESTERVELT, P., WALTER, M. J., GRAUBERT, T. A., MARDIS, E. R., WILSON, R. K. & DIPERSIO, J. F. 2012. Clonal evolution in relapsed acute myeloid leukaemia revealed by whole-genome sequencing. *Nature,* 481**,** 506-10.

DOOLEY, H. C., RAZI, M., POLSON, H. E., GIRARDIN, S. E., WILSON, M. I. & TOOZE, S. A. 2014. WIPI2 links LC3 conjugation with PI3P, autophagosome formation, and pathogen clearance by recruiting Atg12-5-16L1. *Mol Cell,* 55**,** 238-52.

DORING, T. & PRANGE, R. 2015. Rab33B and its autophagic Atg5/12/16L1 effector assist in hepatitis B virus naked capsid formation and release. *Cell Microbiol,* 17**,** 747-64.

DU, P., KIBBE, W. A. & LIN, S. M. 2008. lumi: a pipeline for processing Illumina microarray. *Bioinformatics,* 24**,** 1547-8.

DUDEN, R., GRIFFITHS, G., FRANK, R., ARGOS, P. & KREIS, T. E. 1991. Beta-COP, a 110 kd protein associated with non-clathrin-coated vesicles and the Golgi complex, shows homology to beta-adaptin. *Cell,* 64**,** 649-65.

DUNLOP, E. A., HUNT, D. K., ACOSTA-JAQUEZ, H. A., FINGAR, D. C. & TEE, A. R. 2011. ULK1 inhibits mTORC1 signaling, promotes multisite Raptor phosphorylation and hinders substrate binding. *Autophagy,* 7**,** 737-47.

DUNLOP, E. A., SEIFAN, S., CLAESSENS, T., BEHRENDS, C., KAMPS, M. A., ROZYCKA, E., KEMP, A. J., NOOKALA, R. K., BLENIS, J., COULL, B. J., MURRAY, J. T., VAN STEENSEL, M. A., WILKINSON, S. & TEE, A. R. 2014. FLCN, a novel autophagy component, interacts with GABARAP and is regulated by ULK1 phosphorylation. *Autophagy,* 10**,** 1749-60.

ENGLISH, L., CHEMALI, M. & DESJARDINS, M. 2009. Nuclear membrane-derived autophagy, a novel process that participates in the presentation of endogenous viral antigens during HSV-1 infection. *Autophagy,* 5**,** 1026-9.

ESKELINEN, E. L., REGGIORI, F., BABA, M., KOVACS, A. L. & SEGLEN, P. O. 2011. Seeing is believing: the impact of electron microscopy on autophagy research. *Autophagy,* 7**,** 935-56.

EUGSTER, A., FRIGERIO, G., DALE, M. & DUDEN, R. 2000. COP I domains required for coatomer integrity, and novel interactions with ARF and ARF-GAP. *EMBO J,* 19**,** 3905-17.

FABRE, B., LAMBOUR, T., BOUYSSIÉ, D., MENNETEAU, T., MONSARRAT, B., BURLET-SCHILTZ, O. & BOUSQUET-DUBOUCH, M.-P. 2014. Comparison of label-free quantification methods for the determination of protein complexes subunits stoichiometry. *EuPA Open Proteomics,* 4**,** 82-86.

FAN, W., NASSIRI, A. & ZHONG, Q. 2011. Autophagosome targeting and membrane curvature sensing by Barkor/Atg14(L). *Proc Natl Acad Sci U S A,* 108**,** 7769-74.
FENG, Z., CERVENY, M., YAN, Z. & HE, B. 2007. The VP35 protein of Ebola virus inhibits the antiviral effect mediated by double-stranded RNA-dependent protein kinase PKR. *J Virol,* 81**,** 182-92.
FINLEY, D. 2009. Recognition and processing of ubiquitin-protein conjugates by the proteasome. *Annu Rev Biochem,* 78**,** 477-513.
FORNEROD, M., OHNO, M., YOSHIDA, M. & MATTAJ, I. W. 1997. CRM1 is an export receptor for leucine-rich nuclear export signals. *Cell,* 90**,** 1051-60.
FU, M. M., NIRSCHL, J. J. & HOLZBAUR, E. L. 2014. LC3 binding to the scaffolding protein JIP1 regulates processive dynein-driven transport of autophagosomes. *Dev Cell,* 29**,** 577-90.
FULLGRABE, J., KLIONSKY, D. J. & JOSEPH, B. 2014. The return of the nucleus: transcriptional and epigenetic control of autophagy. *Nat Rev Mol Cell Biol,* 15**,** 65-74.
FUNDERBURK, S. F., WANG, Q. J. & YUE, Z. 2010. The Beclin 1-VPS34 complex--at the crossroads of autophagy and beyond. *Trends Cell Biol,* 20**,** 355-62.
GANLEY, I. G., LAM DU, H., WANG, J., DING, X., CHEN, S. & JIANG, X. 2009. ULK1.ATG13.FIP200 complex mediates mTOR signaling and is essential for autophagy. *J Biol Chem,* 284**,** 12297-305.
GANTKE, T., BOUSSOUF, S., JANZEN, J., MORRICE, N. A., HOWELL, S., MUHLBERGER, E. & LEY, S. C. 2013. Ebola virus VP35 induces high-level production of recombinant TPL-2-ABIN-2-NF-kappaB1 p105 complex in co-transfected HEK-293 cells. *Biochem J,* 452**,** 359-65.
GE, L., MELVILLE, D., ZHANG, M. & SCHEKMAN, R. 2013. The ER-Golgi intermediate compartment is a key membrane source for the LC3 lipidation step of autophagosome biogenesis. *Elife,* 2**,** e00947.
GE, L., ZHANG, M. & SCHEKMAN, R. 2014. Phosphatidylinositol 3-kinase and COPII generate LC3 lipidation vesicles from the ER-Golgi intermediate compartment. *Elife,* 3**,** e04135.
GENAU, H. M., HUBER, J., BASCHIERI, F., AKUTSU, M., DOTSCH, V., FARHAN, H., ROGOV, V. & BEHRENDS, C. 2015. CUL3-KBTBD6/KBTBD7 ubiquitin ligase cooperates with GABARAP proteins to spatially restrict TIAM1-RAC1 signaling. *Mol Cell,* 57**,** 995-1010.
GENG, J., NAIR, U., YASUMURA-YORIMITSU, K. & KLIONSKY, D. J. 2010. Post-Golgi Sec proteins are required for autophagy in Saccharomyces cerevisiae. *Mol Biol Cell,* 21**,** 2257-69.
GUO, Q., VASILE, E. & KRIEGER, M. 1994. Disruptions in Golgi structure and membrane traffic in a conditional lethal mammalian cell mutant are corrected by epsilon-COP. *J Cell Biol,* 125**,** 1213-24.
GUO, Y., CHANG, C., HUANG, R., LIU, B., BAO, L. & LIU, W. 2012. AP1 is essential for generation of autophagosomes from the trans-Golgi network. *J Cell Sci,* 125**,** 1706-15.
GUTIERREZ, M. G., MUNAFO, D. B., BERON, W. & COLOMBO, M. I. 2004. Rab7 is required for the normal progression of the autophagic pathway in mammalian cells. *J Cell Sci,* 117**,** 2687-97.
HAILEY, D. W., RAMBOLD, A. S., SATPUTE-KRISHNAN, P., MITRA, K., SOUGRAT, R., KIM, P. K. & LIPPINCOTT-SCHWARTZ, J. 2010. Mitochondria supply membranes for autophagosome biogenesis during starvation. *Cell,* 141**,** 656-67.
HAMASAKI, M., FURUTA, N., MATSUDA, A., NEZU, A., YAMAMOTO, A., FUJITA, N., OOMORI, H., NODA, T., HARAGUCHI, T., HIRAOKA, Y., AMANO, A. & YOSHIMORI, T. 2013. Autophagosomes form at ER-mitochondria contact sites. *Nature,* 495**,** 389-93.

HAMDAN, F. F., SROUR, M., CAPO-CHICHI, J. M., DAOUD, H., NASSIF, C., PATRY, L., MASSICOTTE, C., AMBALAVANAN, A., SPIEGELMAN, D., DIALLO, O., HENRION, E., DIONNE-LAPORTE, A., FOUGERAT, A., PSHEZHETSKY, A. V., VENKATESWARAN, S., ROULEAU, G. A. & MICHAUD, J. L. 2014. De novo mutations in moderate or severe intellectual disability. *PLoS Genet,* 10**,** e1004772.

HANADA, T., NODA, N. N., SATOMI, Y., ICHIMURA, Y., FUJIOKA, Y., TAKAO, T., INAGAKI, F. & OHSUMI, Y. 2007. The Atg12-Atg5 conjugate has a novel E3-like activity for protein lipidation in autophagy. *J Biol Chem,* 282**,** 37298-302.

HARA, K., YONEZAWA, K., WENG, Q. P., KOZLOWSKI, M. T., BELHAM, C. & AVRUCH, J. 1998. Amino acid sufficiency and mTOR regulate p70 S6 kinase and eIF-4E BP1 through a common effector mechanism. *J Biol Chem,* 273**,** 14484-94.

HARA, T., TAKAMURA, A., KISHI, C., IEMURA, S., NATSUME, T., GUAN, J. L. & MIZUSHIMA, N. 2008. FIP200, a ULK-interacting protein, is required for autophagosome formation in mammalian cells. *J Cell Biol,* 181**,** 497-510.

HARDING, T. M., MORANO, K. A., SCOTT, S. V. & KLIONSKY, D. J. 1995. Isolation and characterization of yeast mutants in the cytoplasm to vacuole protein targeting pathway. *J Cell Biol,* 131**,** 591-602.

HAYASHI-NISHINO, M., FUJITA, N., NODA, T., YAMAGUCHI, A., YOSHIMORI, T. & YAMAMOTO, A. 2009. A subdomain of the endoplasmic reticulum forms a cradle for autophagosome formation. *Nat Cell Biol,* 11**,** 1433-7.

HE, S., NI, D., MA, B., LEE, J. H., ZHANG, T., GHOZALLI, I., PIROOZ, S. D., ZHAO, Z., BHARATHAM, N., LI, B., OH, S., LEE, W. H., TAKAHASHI, Y., WANG, H. G., MINASSIAN, A., FENG, P., DERETIC, V., PEPPERKOK, R., TAGAYA, M., YOON, H. S. & LIANG, C. 2013. PtdIns(3)P-bound UVRAG coordinates Golgi-ER retrograde and Atg9 transport by differential interactions with the ER tether and the beclin 1 complex. *Nat Cell Biol,* 15**,** 1206-19.

HO, S. N., HUNT, H. D., HORTON, R. M., PULLEN, J. K. & PEASE, L. R. 1989. Site-directed mutagenesis by overlap extension using the polymerase chain reaction. *Gene,* 77**,** 51-9.

HOSOKAWA, N., HARA, T., KAIZUKA, T., KISHI, C., TAKAMURA, A., MIURA, Y., IEMURA, S., NATSUME, T., TAKEHANA, K., YAMADA, N., GUAN, J. L., OSHIRO, N. & MIZUSHIMA, N. 2009a. Nutrient-dependent mTORC1 association with the ULK1-Atg13-FIP200 complex required for autophagy. *Mol Biol Cell,* 20**,** 1981-91.

HOSOKAWA, N., SASAKI, T., IEMURA, S., NATSUME, T., HARA, T. & MIZUSHIMA, N. 2009b. Atg101, a novel mammalian autophagy protein interacting with Atg13. *Autophagy,* 5**,** 973-9.

HU, F., SHI, X., LI, B., HUANG, X., MORELLI, X. & SHI, N. 2015. Structural Basis for the Interaction between the Golgi Reassembly-stacking Protein GRASP65 and the Golgi Matrix Protein GM130. *J Biol Chem,* 290**,** 26373-82.

HUANG, J., BIRMINGHAM, C. L., SHAHNAZARI, S., SHIU, J., ZHENG, Y. T., SMITH, A. C., CAMPELLONE, K. G., HEO, W. D., GRUENHEID, S., MEYER, T., WELCH, M. D., KTISTAKIS, N. T., KIM, P. K., KLIONSKY, D. J. & BRUMELL, J. H. 2011. Antibacterial autophagy occurs at PI(3)P-enriched domains of the endoplasmic reticulum and requires Rab1 GTPase. *Autophagy,* 7**,** 17-26.

HUANG, W., CHOI, W., HU, W., MI, N., GUO, Q., MA, M., LIU, M., TIAN, Y., LU, P., WANG, F. L., DENG, H., LIU, L., GAO, N., YU, L. & SHI, Y. 2012. Crystal structure and biochemical analyses reveal Beclin 1 as a novel membrane binding protein. *Cell Res,* 22**,** 473-89.

HURTADO, L., CABALLERO, C., GAVILAN, M. P., CARDENAS, J., BORNENS, M. & RIOS, R. M. 2011. Disconnecting the Golgi ribbon from the centrosome prevents directional cell migration and ciliogenesis. *J Cell Biol,* 193**,** 917-33.

ICHIMURA, Y., KIRISAKO, T., TAKAO, T., SATOMI, Y., SHIMONISHI, Y., ISHIHARA, N., MIZUSHIMA, N., TANIDA, I., KOMINAMI, E., OHSUMI, M., NODA, T. & OHSUMI, Y. 2000. A ubiquitin-like system mediates protein lipidation. *Nature,* 408**,** 488-92.

ISHIDA, R., YAMAMOTO, A., NAKAYAMA, K., SOHDA, M., MISUMI, Y., YASUNAGA, T. & NAKAMURA, N. 2015. GM130 is a parallel tetramer with a flexible rod-like structure and N-terminally open (Y-shaped) and closed (I-shaped) conformations. *FEBS J,* 282**,** 2232-44.

ISHIKAWA, H. & MARSHALL, W. F. 2011. Ciliogenesis: building the cell's antenna. *Nat Rev Mol Cell Biol,* 12**,** 222-34.

ITAKURA, E., KISHI, C., INOUE, K. & MIZUSHIMA, N. 2008. Beclin 1 forms two distinct phosphatidylinositol 3-kinase complexes with mammalian Atg14 and UVRAG. *Mol Biol Cell,* 19**,** 5360-72.

ITAKURA, E., KISHI-ITAKURA, C. & MIZUSHIMA, N. 2012. The hairpin-type tail-anchored SNARE syntaxin 17 targets to autophagosomes for fusion with endosomes/lysosomes. *Cell,* 151**,** 1256-69.

ITAKURA, E. & MIZUSHIMA, N. 2010. Characterization of autophagosome formation site by a hierarchical analysis of mammalian Atg proteins. *Autophagy,* 6**,** 764-76.

ITOH, T., FUJITA, N., KANNO, E., YAMAMOTO, A., YOSHIMORI, T. & FUKUDA, M. 2008. Golgi-resident small GTPase Rab33B interacts with Atg16L and modulates autophagosome formation. *Mol Biol Cell,* 19**,** 2916-25.

ITOH, T., KANNO, E., UEMURA, T., WAGURI, S. & FUKUDA, M. 2011. OATL1, a novel autophagosome-resident Rab33B-GAP, regulates autophagosomal maturation. *J Cell Biol,* 192**,** 839-53.

JEWELL, J. L., RUSSELL, R. C. & GUAN, K. L. 2013. Amino acid signalling upstream of mTOR. *Nat Rev Mol Cell Biol,* 14**,** 133-9.

JOHANSEN, T. & LAMARK, T. 2011. Selective autophagy mediated by autophagic adapter proteins. *Autophagy,* 7**,** 279-96.

JOO, J. H., DORSEY, F. C., JOSHI, A., HENNESSY-WALTERS, K. M., ROSE, K. L., MCCASTLAIN, K., ZHANG, J., IYENGAR, R., JUNG, C. H., SUEN, D. F., STEEVES, M. A., YANG, C. Y., PRATER, S. M., KIM, D. H., THOMPSON, C. B., YOULE, R. J., NEY, P. A., CLEVELAND, J. L. & KUNDU, M. 2011. Hsp90-Cdc37 chaperone complex regulates Ulk1- and Atg13-mediated mitophagy. *Mol Cell,* 43**,** 572-85.

JUNG, C. H., JUN, C. B., RO, S. H., KIM, Y. M., OTTO, N. M., CAO, J., KUNDU, M. & KIM, D. H. 2009. ULK-Atg13-FIP200 complexes mediate mTOR signaling to the autophagy machinery. *Mol Biol Cell,* 20**,** 1992-2003.

JUNG, C. H., SEO, M., OTTO, N. M. & KIM, D. H. 2011. ULK1 inhibits the kinase activity of mTORC1 and cell proliferation. *Autophagy,* 7**,** 1212-21.

KABEYA, Y., MIZUSHIMA, N., UENO, T., YAMAMOTO, A., KIRISAKO, T., NODA, T., KOMINAMI, E., OHSUMI, Y. & YOSHIMORI, T. 2000. LC3, a mammalian homologue of yeast Apg8p, is localized in autophagosome membranes after processing. *EMBO J,* 19**,** 5720-8.

KABEYA, Y., MIZUSHIMA, N., YAMAMOTO, A., OSHITANI-OKAMOTO, S., OHSUMI, Y. & YOSHIMORI, T. 2004. LC3, GABARAP and GATE16 localize to autophagosomal membrane depending on form-II formation. *J Cell Sci,* 117**,** 2805-12.

KANG, R., ZEH, H. J., LOTZE, M. T. & TANG, D. 2011. The Beclin 1 network regulates autophagy and apoptosis. *Cell Death Differ,* 18**,** 571-80.

KARANASIOS, E., STAPLETON, E., MANIFAVA, M., KAIZUKA, T., MIZUSHIMA, N., WALKER, S. A. & KTISTAKIS, N. T. 2013. Dynamic association of the ULK1 complex with omegasomes during autophagy induction. *J Cell Sci,* 126**,** 5224-38.

KARPIUK, O., NAJAFOVA, Z., KRAMER, F., HENNION, M., GALONSKA, C., KONIG, A., SNAIDERO, N., VOGEL, T., SHCHEBET, A., BEGUS-NAHRMANN, Y., KASSEM, M., SIMONS, M., SHCHERBATA, H., BEISSBARTH, T. & JOHNSEN, S. A. 2012. The histone H2B monoubiquitination regulatory pathway is required for differentiation of multipotent stem cells. *Mol Cell,* 46**,** 705-13.

KATO, Y., NAGATA, K., TAKAHASHI, M., LIAN, L., HERRERO, J. J., SUDOL, M. & TANOKURA, M. 2004. Common mechanism of ligand recognition by group II/III WW domains: redefining their functional classification. *J Biol Chem,* 279**,** 31833-41.

KAUFMANN, A., BEIER, V., FRANQUELIM, H. G. & WOLLERT, T. 2014. Molecular mechanism of autophagic membrane-scaffold assembly and disassembly. *Cell,* 156**,** 469-81.

KHAMINETS, A., HEINRICH, T., MARI, M., GRUMATI, P., HUEBNER, A. K., AKUTSU, M., LIEBMANN, L., STOLZ, A., NIETZSCHE, S., KOCH, N., MAUTHE, M., KATONA, I., QUALMANN, B., WEIS, J., REGGIORI, F., KURTH, I., HUBNER, C. A. & DIKIC, I. 2015. Regulation of endoplasmic reticulum turnover by selective autophagy. *Nature,* 522**,** 354-8.

KIHARA, A., KABEYA, Y., OHSUMI, Y. & YOSHIMORI, T. 2001. Beclin-phosphatidylinositol 3-kinase complex functions at the trans-Golgi network. *EMBO Rep,* 2**,** 330-5.

KIM, J., KUNDU, M., VIOLLET, B. & GUAN, K. L. 2011. AMPK and mTOR regulate autophagy through direct phosphorylation of Ulk1. *Nat Cell Biol,* 13**,** 132-41.

KIMURA, S., NODA, T. & YOSHIMORI, T. 2008. Dynein-dependent movement of autophagosomes mediates efficient encounters with lysosomes. *Cell Struct Funct,* 33**,** 109-22.

KIRISAKO, T., BABA, M., ISHIHARA, N., MIYAZAWA, K., OHSUMI, M., YOSHIMORI, T., NODA, T. & OHSUMI, Y. 1999. Formation process of autophagosome is traced with Apg8/Aut7p in yeast. *J Cell Biol,* 147**,** 435-46.

KIRISAKO, T., ICHIMURA, Y., OKADA, H., KABEYA, Y., MIZUSHIMA, N., YOSHIMORI, T., OHSUMI, M., TAKAO, T., NODA, T. & OHSUMI, Y. 2000. The reversible modification regulates the membrane-binding state of Apg8/Aut7 essential for autophagy and the cytoplasm to vacuole targeting pathway. *J Cell Biol,* 151**,** 263-76.

KITTLER, J. T., ROSTAING, P., SCHIAVO, G., FRITSCHY, J. M., OLSEN, R., TRILLER, A. & MOSS, S. J. 2001. The subcellular distribution of GABARAP and its ability to interact with NSF suggest a role for this protein in the intracellular transport of GABA(A) receptors. *Mol Cell Neurosci,* 18**,** 13-25.

KLIONSKY, D. J., ABDALLA, F. C., ABELIOVICH, H., ABRAHAM, R. T., ACEVEDO-AROZENA, A., ADELI, K., AGHOLME, L., AGNELLO, M., AGOSTINIS, P., AGUIRRE-GHISO, J. A., AHN, H. J., AIT-MOHAMED, O., AIT-SI-ALI, S., AKEMATSU, T., AKIRA, S., AL-YOUNES, H. M., AL-ZEER, M. A., ALBERT, M. L., ALBIN, R. L., ALEGRE-ABARRATEGUI, J., ALEO, M. F., ALIREZAEI, M., ALMASAN, A., ALMONTE-BECERRIL, M., AMANO, A., AMARAVADI, R., AMARNATH, S., AMER, A. O., ANDRIEU-ABADIE, N., ANANTHARAM, V., ANN, D. K., ANOOPKUMAR-DUKIE, S., AOKI, H., APOSTOLOVA, N., ARANCIA, G., ARIS, J. P., ASANUMA, K., ASARE, N. Y., ASHIDA, H., ASKANAS, V., ASKEW, D. S., AUBERGER, P., BABA, M., BACKUES, S. K., BAEHRECKE, E. H., BAHR, B. A., BAI, X. Y., BAILLY, Y., BAIOCCHI, R., BALDINI, G., BALDUINI, W., BALLABIO, A., BAMBER, B. A., BAMPTON, E. T.,

BANHEGYI, G., BARTHOLOMEW, C. R., BASSHAM, D. C., BAST, R. C., JR., BATOKO, H., BAY, B. H., BEAU, I., BECHET, D. M., BEGLEY, T. J., BEHL, C., BEHRENDS, C., BEKRI, S., BELLAIRE, B., BENDALL, L. J., BENETTI, L., BERLIOCCHI, L., BERNARDI, H., BERNASSOLA, F., BESTEIRO, S., BHATIA-KISSOVA, I., BI, X., BIARD-PIECHACZYK, M., BLUM, J. S., BOISE, L. H., BONALDO, P., BOONE, D. L., BORNHAUSER, B. C., BORTOLUCI, K. R., BOSSIS, I., BOST, F., BOURQUIN, J. P., BOYA, P., BOYER-GUITTAUT, M., BOZHKOV, P. V., BRADY, N. R., BRANCOLINI, C., BRECH, A., BRENMAN, J. E., BRENNAND, A., BRESNICK, E. H., BREST, P., BRIDGES, D., BRISTOL, M. L., BROOKES, P. S., BROWN, E. J., BRUMELL, J. H., et al. 2012. Guidelines for the use and interpretation of assays for monitoring autophagy. *Autophagy,* 8**,** 445-544.

KNAEVELSRUD, H., SORENG, K., RAIBORG, C., HABERG, K., RASMUSON, F., BRECH, A., LIESTOL, K., RUSTEN, T. E., STENMARK, H., NEUFELD, T. P., CARLSSON, S. R. & SIMONSEN, A. 2013. Membrane remodeling by the PX-BAR protein SNX18 promotes autophagosome formation. *J Cell Biol,* 202**,** 331-49.

KOCHL, R., HU, X. W., CHAN, E. Y. & TOOZE, S. A. 2006. Microtubules facilitate autophagosome formation and fusion of autophagosomes with endosomes. *Traffic,* 7**,** 129-45.

KODANI, A., KRISTENSEN, I., HUANG, L. & SUTTERLIN, C. 2009. GM130-dependent control of Cdc42 activity at the Golgi regulates centrosome organization. *Mol Biol Cell,* 20**,** 1192-200.

KODANI, A. & SUTTERLIN, C. 2008a. The Golgi protein GM130 regulates centrosome morphology and function. *Molecular Biology of the Cell,* 19**,** 745-753.

KODANI, A. & SUTTERLIN, C. 2008b. The Golgi protein GM130 regulates centrosome morphology and function. *Mol Biol Cell,* 19**,** 745-53.

KOMANDER, D. & RAPE, M. 2012. The ubiquitin code. *Annu Rev Biochem,* 81**,** 203-29.

KOMARNITSKY, P., CHO, E. J. & BURATOWSKI, S. 2000. Different phosphorylated forms of RNA polymerase II and associated mRNA processing factors during transcription. *Genes Dev,* 14**,** 2452-60.

KRAFT, C., KIJANSKA, M., KALIE, E., SIERGIEJUK, E., LEE, S. S., SEMPLICIO, G., STOFFEL, I., BREZOVICH, A., VERMA, M., HANSMANN, I., AMMERER, G., HOFMANN, K., TOOZE, S. & PETER, M. 2012. Binding of the Atg1/ULK1 kinase to the ubiquitin-like protein Atg8 regulates autophagy. *EMBO J,* 31**,** 3691-703.

KRICK, R., BREMER, S., WELTER, E., SCHLOTTERHOSE, P., MUEHE, Y., ESKELINEN, E. L. & THUMM, M. 2010. Cdc48/p97 and Shp1/p47 regulate autophagosome biogenesis in concert with ubiquitin-like Atg8. *J Cell Biol,* 190**,** 965-73.

KRICK, R., MUHE, Y., PRICK, T., BREDSCHNEIDER, M., BREMER, S., WENZEL, D., ESKELINEN, E. L. & THUMM, M. 2009. Piecemeal microautophagy of the nucleus: genetic and morphological traits. *Autophagy,* 5**,** 270-2.

KROEMER, G., MARINO, G. & LEVINE, B. 2010. Autophagy and the integrated stress response. *Mol Cell,* 40**,** 280-93.

LA COUR, T., KIEMER, L., MOLGAARD, A., GUPTA, R., SKRIVER, K. & BRUNAK, S. 2004. Analysis and prediction of leucine-rich nuclear export signals. *Protein Eng Des Sel,* 17**,** 527-36.

LAMB, C. A., YOSHIMORI, T. & TOOZE, S. A. 2013. The autophagosome: origins unknown, biogenesis complex. *Nat Rev Mol Cell Biol,* 14**,** 759-74.

LAPLANTE, M. & SABATINI, D. M. 2012. mTOR signaling in growth control and disease. *Cell,* 149**,** 274-93.

LEE, E. J. & TOURNIER, C. 2011. The requirement of uncoordinated 51-like kinase 1 (ULK1) and ULK2 in the regulation of autophagy. *Autophagy,* 7**,** 689-95.
LEE, I. H., KAWAI, Y., FERGUSSON, M. M., ROVIRA, II, BISHOP, A. J., MOTOYAMA, N., CAO, L. & FINKEL, T. 2012. Atg7 modulates p53 activity to regulate cell cycle and survival during metabolic stress. *Science,* 336**,** 225-8.
LEIL, T. A., CHEN, Z. W., CHANG, C. S. & OLSEN, R. W. 2004. GABAA receptor-associated protein traffics GABAA receptors to the plasma membrane in neurons. *J Neurosci,* 24**,** 11429-38.
LESA, G. M., SEEMANN, J., SHORTER, J., VANDEKERCKHOVE, J. & WARREN, G. 2000. The amino-terminal domain of the golgi protein giantin interacts directly with the vesicle-tethering protein p115. *J Biol Chem,* 275**,** 2831-6.
LETOURNEUR, F., GAYNOR, E. C., HENNECKE, S., DEMOLLIERE, C., DUDEN, R., EMR, S. D., RIEZMAN, H. & COSSON, P. 1994. Coatomer is essential for retrieval of dilysine-tagged proteins to the endoplasmic reticulum. *Cell,* 79**,** 1199-207.
LIANG, C., FENG, P., KU, B., DOTAN, I., CANAANI, D., OH, B. H. & JUNG, J. U. 2006. Autophagic and tumour suppressor activity of a novel Beclin1-binding protein UVRAG. *Nat Cell Biol,* 8**,** 688-99.
LIANG, X. H., JACKSON, S., SEAMAN, M., BROWN, K., KEMPKES, B., HIBSHOOSH, H. & LEVINE, B. 1999. Induction of autophagy and inhibition of tumorigenesis by beclin 1. *Nature,* 402**,** 672-6.
LIN, S. Y., LI, T. Y., LIU, Q., ZHANG, C., LI, X., CHEN, Y., ZHANG, S. M., LIAN, G., LIU, Q., RUAN, K., WANG, Z., ZHANG, C. S., CHIEN, K. Y., WU, J., LI, Q., HAN, J. & LIN, S. C. 2012. GSK3-TIP60-ULK1 signaling pathway links growth factor deprivation to autophagy. *Science,* 336**,** 477-81.
LINSTEDT, A. D., JESCH, S. A., MEHTA, A., LEE, T. H., GARCIA-MATA, R., NELSON, D. S. & SZTUL, E. 2000. Binding relationships of membrane tethering components. The giantin N terminus and the GM130 N terminus compete for binding to the p115 C terminus. *J Biol Chem,* 275**,** 10196-201.
LOFFLER, A. S., ALERS, S., DIETERLE, A. M., KEPPELER, H., FRANZ-WACHTEL, M., KUNDU, M., CAMPBELL, D. G., WESSELBORG, S., ALESSI, D. R. & STORK, B. 2011. Ulk1-mediated phosphorylation of AMPK constitutes a negative regulatory feedback loop. *Autophagy,* 7**,** 696-706.
LONGATTI, A., LAMB, C. A., RAZI, M., YOSHIMURA, S., BARR, F. A. & TOOZE, S. A. 2012. TBC1D14 regulates autophagosome formation via Rab11- and ULK1-positive recycling endosomes. *J Cell Biol,* 197**,** 659-75.
LOWE, M. & KREIS, T. E. 1996. In vivo assembly of coatomer, the COP-I coat precursor. *J Biol Chem,* 271**,** 30725-30.
LOWE, M., RABOUILLE, C., NAKAMURA, N., WATSON, R., JACKMAN, M., JAMSA, E., RAHMAN, D., PAPPIN, D. J. & WARREN, G. 1998. Cdc2 kinase directly phosphorylates the cis-Golgi matrix protein GM130 and is required for Golgi fragmentation in mitosis. *Cell,* 94**,** 783-93.
LU, P. J., ZHOU, X. Z., SHEN, M. & LU, K. P. 1999. Function of WW domains as phosphoserine- or phosphothreonine-binding modules. *Science,* 283**,** 1325-8.
LUPAS, A., VAN DYKE, M. & STOCK, J. 1991. Predicting coiled coils from protein sequences. *Science,* 252**,** 1162-4.
LYSTAD, A. H., ICHIMURA, Y., TAKAGI, K., YANG, Y., PANKIV, S., KANEGAE, Y., KAGEYAMA, S., SUZUKI, M., SAITO, I., MIZUSHIMA, T., KOMATSU, M. & SIMONSEN, A. 2014. Structural determinants in GABARAP required for the selective binding and recruitment of ALFY to LC3B-positive structures. *EMBO Rep,* 15**,** 557-65.
MA, P., SCHWARTEN, M., SCHNEIDER, L., BOESKE, A., HENKE, N., LISAK, D., WEBER, S., MOHRLUDER, J., STOLDT, M., STRODEL, B., METHNER, A.,

HOFFMANN, S., WEIERGRABER, O. H. & WILLBOLD, D. 2013. Interaction of Bcl-2 with the autophagy-related GABAA receptor-associated protein (GABARAP): biophysical characterization and functional implications. *J Biol Chem,* 288**,** 37204-15.

MAIURI, M. C., GALLUZZI, L., MORSELLI, E., KEPP, O., MALIK, S. A. & KROEMER, G. 2010. Autophagy regulation by p53. *Curr Opin Cell Biol,* 22**,** 181-5.

MALHOTRA, V., SERAFINI, T., ORCI, L., SHEPHERD, J. C. & ROTHMAN, J. E. 1989. Purification of a novel class of coated vesicles mediating biosynthetic protein transport through the Golgi stack. *Cell,* 58**,** 329-36.

MARI, M., GRIFFITH, J., RIETER, E., KRISHNAPPA, L., KLIONSKY, D. J. & REGGIORI, F. 2010. An Atg9-containing compartment that functions in the early steps of autophagosome biogenesis. *J Cell Biol,* 190**,** 1005-22.

MARRA, P., MAFFUCCI, T., DANIELE, T., TULLIO, G. D., IKEHARA, Y., CHAN, E. K., LUINI, A., BEZNOUSSENKO, G., MIRONOV, A. & DE MATTEIS, M. A. 2001. The GM130 and GRASP65 Golgi proteins cycle through and define a subdomain of the intermediate compartment. *Nat Cell Biol,* 3**,** 1101-13.

MARRA, P., SALVATORE, L., MIRONOV, A., JR., DI CAMPLI, A., DI TULLIO, G., TRUCCO, A., BEZNOUSSENKO, G., MIRONOV, A. & DE MATTEIS, M. A. 2007. The biogenesis of the Golgi ribbon: the roles of membrane input from the ER and of GM130. *Mol Biol Cell,* 18**,** 1595-608.

MARTIN, D. D., LADHA, S., EHRNHOEFER, D. E. & HAYDEN, M. R. 2015. Autophagy in Huntington disease and huntingtin in autophagy. *Trends Neurosci,* 38**,** 26-35.

MARTINA, J. A., CHEN, Y., GUCEK, M. & PUERTOLLANO, R. 2012. MTORC1 functions as a transcriptional regulator of autophagy by preventing nuclear transport of TFEB. *Autophagy,* 8**,** 903-14.

MARUYAMA, Y., SOU, Y. S., KAGEYAMA, S., TAKAHASHI, T., UENO, T., TANAKA, K., KOMATSU, M. & ICHIMURA, Y. 2014. LC3B is indispensable for selective autophagy of p62 but not basal autophagy. *Biochem Biophys Res Commun,* 446**,** 309-15.

MATSUNAGA, K., MORITA, E., SAITOH, T., AKIRA, S., KTISTAKIS, N. T., IZUMI, T., NODA, T. & YOSHIMORI, T. 2010. Autophagy requires endoplasmic reticulum targeting of the PI3-kinase complex via Atg14L. *J Cell Biol,* 190**,** 511-21.

MATSUNAGA, K., SAITOH, T., TABATA, K., OMORI, H., SATOH, T., KUROTORI, N., MAEJIMA, I., SHIRAHAMA-NODA, K., ICHIMURA, T., ISOBE, T., AKIRA, S., NODA, T. & YOSHIMORI, T. 2009. Two Beclin 1-binding proteins, Atg14L and Rubicon, reciprocally regulate autophagy at different stages. *Nat Cell Biol,* 11**,** 385-96.

MCALPINE, F., WILLIAMSON, L. E., TOOZE, S. A. & CHAN, E. Y. 2013. Regulation of nutrient-sensitive autophagy by uncoordinated 51-like kinases 1 and 2. *Autophagy,* 9.

MCEWAN, D. G., POPOVIC, D., GUBAS, A., TERAWAKI, S., SUZUKI, H., STADEL, D., COXON, F. P., MIRANDA DE STEGMANN, D., BHOGARAJU, S., MADDI, K., KIRCHOF, A., GATTI, E., HELFRICH, M. H., WAKATSUKI, S., BEHRENDS, C., PIERRE, P. & DIKIC, I. 2015. PLEKHM1 regulates autophagosome-lysosome fusion through HOPS complex and LC3/GABARAP proteins. *Mol Cell,* 57**,** 39-54.

MCKNIGHT, N. C., JEFFERIES, H. B., ALEMU, E. A., SAUNDERS, R. E., HOWELL, M., JOHANSEN, T. & TOOZE, S. A. 2012. Genome-wide siRNA screen reveals amino acid starvation-induced autophagy requires SCOC and WAC. *EMBO J,* 31**,** 1931-46.

MELLACHERUVU, D., WRIGHT, Z., COUZENS, A. L., LAMBERT, J. P., ST-DENIS, N. A., LI, T., MITEVA, Y. V., HAURI, S., SARDIU, M. E., LOW, T. Y., HALIM, V. A., BAGSHAW, R. D., HUBNER, N. C., AL-HAKIM, A., BOUCHARD, A., FAUBERT,

D., FERMIN, D., DUNHAM, W. H., GOUDREAULT, M., LIN, Z. Y., BADILLO, B. G., PAWSON, T., DUROCHER, D., COULOMBE, B., AEBERSOLD, R., SUPERTI-FURGA, G., COLINGE, J., HECK, A. J. R., CHOI, H., GSTAIGER, M., MOHAMMED, S., CRISTEA, I. M., BENNETT, K. L., WASHBURN, M. P., RAUGHT, B., EWING, R. M., GINGRAS, A. C. & NESVIZHSKII, A. I. 2013. The CRAPome: a contaminant repository for affinity purification-mass spectrometry data. *Nature Methods,* 10**,** 730-+.

MERCER, C. A., KALIAPPAN, A. & DENNIS, P. B. 2009. A novel, human Atg13 binding protein, Atg101, interacts with ULK1 and is essential for macroautophagy. *Autophagy,* 5**,** 649-62.

MEYER, H., BUG, M. & BREMER, S. 2012. Emerging functions of the VCP/p97 AAA-ATPase in the ubiquitin system. *Nat Cell Biol,* 14**,** 117-23.

MIDDENDORP, S., KUNTZIGER, T., ABRAHAM, Y., HOLMES, S., BORDES, N., PAINTRAND, M., PAOLETTI, A. & BORNENS, M. 2000. A role for centrin 3 in centrosome reproduction. *J Cell Biol,* 148**,** 405-16.

MISUMI, Y., MISUMI, Y., MIKI, K., TAKATSUKI, A., TAMURA, G. & IKEHARA, Y. 1986. Novel blockade by brefeldin A of intracellular transport of secretory proteins in cultured rat hepatocytes. *J Biol Chem,* 261**,** 11398-403.

MIZUSHIMA, N. 2007. Autophagy: process and function. *Genes Dev,* 21**,** 2861-73.

MIZUSHIMA, N. & KOMATSU, M. 2011. Autophagy: renovation of cells and tissues. *Cell,* 147**,** 728-41.

MIZUSHIMA, N., KUMA, A., KOBAYASHI, Y., YAMAMOTO, A., MATSUBAE, M., TAKAO, T., NATSUME, T., OHSUMI, Y. & YOSHIMORI, T. 2003. Mouse Apg16L, a novel WD-repeat protein, targets to the autophagic isolation membrane with the Apg12-Apg5 conjugate. *J Cell Sci,* 116**,** 1679-88.

MIZUSHIMA, N., NODA, T., YOSHIMORI, T., TANAKA, Y., ISHII, T., GEORGE, M. D., KLIONSKY, D. J., OHSUMI, M. & OHSUMI, Y. 1998. A protein conjugation system essential for autophagy. *Nature,* 395**,** 395-8.

MIZUSHIMA, N., OHSUMI, Y. & YOSHIMORI, T. 2002. Autophagosome formation in mammalian cells. *Cell Struct Funct,* 27**,** 421-9.

MIZUSHIMA, N., YAMAMOTO, A., HATANO, M., KOBAYASHI, Y., KABEYA, Y., SUZUKI, K., TOKUHISA, T., OHSUMI, Y. & YOSHIMORI, T. 2001. Dissection of autophagosome formation using Apg5-deficient mouse embryonic stem cells. *J Cell Biol,* 152**,** 657-68.

MIZUSHIMA, N., YOSHIMORI, T. & LEVINE, B. 2010. Methods in mammalian autophagy research. *Cell,* 140**,** 313-26.

MIZUSHIMA, N., YOSHIMORI, T. & OHSUMI, Y. 2011. The role of Atg proteins in autophagosome formation. *Annu Rev Cell Dev Biol,* 27**,** 107-32.

MOCHIZUKI, Y., OHASHI, R., KAWAMURA, T., IWANARI, H., KODAMA, T., NAITO, M. & HAMAKUBO, T. 2013. Phosphatidylinositol 3-phosphatase myotubularin-related protein 6 (MTMR6) is regulated by small GTPase Rab1B in the early secretory and autophagic pathways. *J Biol Chem,* 288**,** 1009-21.

MOLEJON, M. I., ROPOLO, A., RE, A. L., BOGGIO, V. & VACCARO, M. I. 2013. The VMP1-Beclin 1 interaction regulates autophagy induction. *Sci Rep,* 3**,** 1055.

MOYER, B. D., ALLAN, B. B. & BALCH, W. E. 2001. Rab1 interaction with a GM130 effector complex regulates COPII vesicle cis--Golgi tethering. *Traffic,* 2**,** 268-76.

NAKAMURA, N., LOWE, M., LEVINE, T. P., RABOUILLE, C. & WARREN, G. 1997. The vesicle docking protein p115 binds GM130, a cis-Golgi matrix protein, in a mitotically regulated manner. *Cell,* 89**,** 445-55.

NAKAMURA, N., RABOUILLE, C., WATSON, R., NILSSON, T., HUI, N., SLUSAREWICZ, P., KREIS, T. E. & WARREN, G. 1995. Characterization of a cis-Golgi matrix protein, GM130. *J Cell Biol,* 131**,** 1715-26.

NAKAMURA, T., HAYASHI, T., NASU-NISHIMURA, Y., SAKAUE, F., MORISHITA, Y., OKABE, T., OHWADA, S., MATSUURA, K. & AKIYAMA, T. 2008. PX-RICS mediates ER-to-Golgi transport of the N-cadherin/beta-catenin complex. *Genes Dev,* 22**,** 1244-56.

NATH, S., DANCOURT, J., SHTEYN, V., PUENTE, G., FONG, W. M., NAG, S., BEWERSDORF, J., YAMAMOTO, A., ANTONNY, B. & MELIA, T. J. 2014. Lipidation of the LC3/GABARAP family of autophagy proteins relies on a membrane-curvature-sensing domain in Atg3. *Nat Cell Biol,* 16**,** 415-24.

NAZIO, F., STRAPPAZZON, F., ANTONIOLI, M., BIELLI, P., CIANFANELLI, V., BORDI, M., GRETZMEIER, C., DENGJEL, J., PIACENTINI, M., FIMIA, G. M. & CECCONI, F. 2013. mTOR inhibits autophagy by controlling ULK1 ubiquitylation, self-association and function through AMBRA1 and TRAF6. *Nat Cell Biol*.

NEEFJES, J., JONGSMA, M. L., PAUL, P. & BAKKE, O. 2011. Towards a systems understanding of MHC class I and MHC class II antigen presentation. *Nat Rev Immunol,* 11**,** 823-36.

NISHIDA, Y., ARAKAWA, S., FUJITANI, K., YAMAGUCHI, H., MIZUTA, T., KANASEKI, T., KOMATSU, M., OTSU, K., TSUJIMOTO, Y. & SHIMIZU, S. 2009. Discovery of Atg5/Atg7-independent alternative macroautophagy. *Nature,* 461**,** 654-8.

NYMANN-ANDERSEN, J., WANG, H. & OLSEN, R. W. 2002. Biochemical identification of the binding domain in the GABA(A) receptor-associated protein (GABARAP) mediating dimer formation. *Neuropharmacology,* 43**,** 476-81.

OHASHI, Y. & MUNRO, S. 2010. Membrane delivery to the yeast autophagosome from the Golgi-endosomal system. *Mol Biol Cell,* 21**,** 3998-4008.

OKAMOTO, K. 2014. Organellophagy: eliminating cellular building blocks via selective autophagy. *J Cell Biol,* 205**,** 435-45.

OKAZAKI, N., YAN, J., YUASA, S., UENO, T., KOMINAMI, E., MASUHO, Y., KOGA, H. & MURAMATSU, M. 2000. Interaction of the Unc-51-like kinase and microtubule-associated protein light chain 3 related proteins in the brain: possible role of vesicular transport in axonal elongation. *Brain Res Mol Brain Res,* 85**,** 1-12.

ORCI, L., STAMNES, M., RAVAZZOLA, M., AMHERDT, M., PERRELET, A., SOLLNER, T. H. & ROTHMAN, J. E. 1997. Bidirectional transport by distinct populations of COPI-coated vesicles. *Cell,* 90**,** 335-49.

ORSI, A., RAZI, M., DOOLEY, H. C., ROBINSON, D., WESTON, A. E., COLLINSON, L. M. & TOOZE, S. A. 2012. Dynamic and transient interactions of Atg9 with autophagosomes, but not membrane integration, are required for autophagy. *Mol Biol Cell,* 23**,** 1860-73.

PAMPLIEGA, O., ORHON, I., PATEL, B., SRIDHAR, S., DIAZ-CARRETERO, A., BEAU, I., CODOGNO, P., SATIR, B. H., SATIR, P. & CUERVO, A. M. 2013. Functional interaction between autophagy and ciliogenesis. *Nature,* 502**,** 194-200.

PANKIV, S., CLAUSEN, T. H., LAMARK, T., BRECH, A., BRUUN, J. A., OUTZEN, H., OVERVATN, A., BJORKOY, G. & JOHANSEN, T. 2007. p62/SQSTM1 binds directly to Atg8/LC3 to facilitate degradation of ubiquitinated protein aggregates by autophagy. *J Biol Chem,* 282**,** 24131-45.

PANKIV, S., LAMARK, T., BRUUN, J. A., OVERVATN, A., BJORKOY, G. & JOHANSEN, T. 2010. Nucleocytoplasmic shuttling of p62/SQSTM1 and its role in recruitment of nuclear polyubiquitinated proteins to promyelocytic leukemia bodies. *J Biol Chem,* 285**,** 5941-53.

PARK, J. M., TOUGERON, D., HUANG, S., OKAMOTO, K. & SINICROPE, F. A. 2014. Beclin 1 and UVRAG confer protection from radiation-induced DNA damage

and maintain centrosome stability in colorectal cancer cells. *PLoS One,* 9**,** e100819.
PARMIGIANI, A., NOURBAKHSH, A., DING, B., WANG, W., KIM, Y. C., AKOPIANTS, K., GUAN, K. L., KARIN, M. & BUDANOV, A. V. 2014. Sestrins inhibit mTORC1 kinase activation through the GATOR complex. *Cell Rep,* 9**,** 1281-91.
PATTINGRE, S., TASSA, A., QU, X., GARUTI, R., LIANG, X. H., MIZUSHIMA, N., PACKER, M., SCHNEIDER, M. D. & LEVINE, B. 2005. Bcl-2 antiapoptotic proteins inhibit Beclin 1-dependent autophagy. *Cell,* 122**,** 927-39.
PETHERICK, K. J., CONWAY, O. J., MPAMHANGA, C., OSBORNE, S. A., KAMAL, A., SAXTY, B. & GANLEY, I. G. 2015. Pharmacological Inhibition of ULK1 Kinase Blocks Mammalian Target of Rapamycin (mTOR)-dependent Autophagy. *J Biol Chem,* 290**,** 11376-83.
PIRNGRUBER, J., SHCHEBET, A., SCHREIBER, L., SHEMA, E., MINSKY, N., CHAPMAN, R. D., EICK, D., AYLON, Y., OREN, M. & JOHNSEN, S. A. 2009. CDK9 directs H2B monoubiquitination and controls replication-dependent histone mRNA 3'-end processing. *EMBO Rep,* 10**,** 894-900.
POLSON, H. E., DE LARTIGUE, J., RIGDEN, D. J., REEDIJK, M., URBE, S., CLAGUE, M. J. & TOOZE, S. A. 2010. Mammalian Atg18 (WIPI2) localizes to omegasome-anchored phagophores and positively regulates LC3 lipidation. *Autophagy,* 6.
PONPUAK, M., MANDELL, M. A., KIMURA, T., CHAUHAN, S., CLEYRAT, C. & DERETIC, V. 2015. Secretory autophagy. *Curr Opin Cell Biol,* 35**,** 106-16.
POPOVIC, D. & DIKIC, I. 2014. TBC1D5 and the AP2 complex regulate ATG9 trafficking and initiation of autophagy. *EMBO Rep,* 15**,** 392-401.
POSER, I., SAROV, M., HUTCHINS, J. R., HERICHE, J. K., TOYODA, Y., POZNIAKOVSKY, A., WEIGL, D., NITZSCHE, A., HEGEMANN, B., BIRD, A. W., PELLETIER, L., KITTLER, R., HUA, S., NAUMANN, R., AUGSBURG, M., SYKORA, M. M., HOFEMEISTER, H., ZHANG, Y., NASMYTH, K., WHITE, K. P., DIETZEL, S., MECHTLER, K., DURBIN, R., STEWART, A. F., PETERS, J. M., BUCHHOLZ, F. & HYMAN, A. A. 2008. BAC TransgeneOmics: a high-throughput method for exploration of protein function in mammals. *Nat Methods,* 5**,** 409-15.
PREISINGER, C., SHORT, B., DE CORTE, V., BRUYNEEL, E., HAAS, A., KOPAJTICH, R., GETTEMANS, J. & BARR, F. A. 2004. YSK1 is activated by the Golgi matrix protein GM130 and plays a role in cell migration through its substrate 14-3-3zeta. *J Cell Biol,* 164**,** 1009-20.
PRILUSKY, J., FELDER, C. E., ZEEV-BEN-MORDEHAI, T., RYDBERG, E. H., MAN, O., BECKMANN, J. S., SILMAN, I. & SUSSMAN, J. L. 2005. FoldIndex: a simple tool to predict whether a given protein sequence is intrinsically unfolded. *Bioinformatics,* 21**,** 3435-8.
PROIKAS-CEZANNE, T., WADDELL, S., GAUGEL, A., FRICKEY, T., LUPAS, A. & NORDHEIM, A. 2004. WIPI-1alpha (WIPI49), a member of the novel 7-bladed WIPI protein family, is aberrantly expressed in human cancer and is linked to starvation-induced autophagy. *Oncogene,* 23**,** 9314-25.
PURI, C., RENNA, M., BENTO, C. F., MOREAU, K. & RUBINSZTEIN, D. C. 2013. Diverse autophagosome membrane sources coalesce in recycling endosomes. *Cell,* 154**,** 1285-99.
PUTHENVEEDU, M. A., BACHERT, C., PURI, S., LANNI, F. & LINSTEDT, A. D. 2006. GM130 and GRASP65-dependent lateral cisternal fusion allows uniform Golgi-enzyme distribution. *Nat Cell Biol,* 8**,** 238-48.
PUTHENVEEDU, M. A. & LINSTEDT, A. D. 2001. Evidence that Golgi structure depends on a p115 activity that is independent of the vesicle tether components giantin and GM130. *J Cell Biol,* 155**,** 227-38.

RAVIKUMAR, B., MOREAU, K., JAHREISS, L., PURI, C. & RUBINSZTEIN, D. C. 2010. Plasma membrane contributes to the formation of pre-autophagosomal structures. *Nat Cell Biol,* 12**,** 747-57.

RAZI, M., CHAN, E. Y. & TOOZE, S. A. 2009. Early endosomes and endosomal coatomer are required for autophagy. *J Cell Biol,* 185**,** 305-21.

RIOS, R. M., SANCHIS, A., TASSIN, A. M., FEDRIANI, C. & BORNENS, M. 2004. GMAP-210 recruits gamma-tubulin complexes to cis-Golgi membranes and is required for Golgi ribbon formation. *Cell,* 118**,** 323-35.

RITCHIE, M. E., PHIPSON, B., WU, D., HU, Y., LAW, C. W., SHI, W. & SMYTH, G. K. 2015. limma powers differential expression analyses for RNA-sequencing and microarray studies. *Nucleic Acids Res,* 43**,** e47.

RIVERO, S., CARDENAS, J., BORNENS, M. & RIOS, R. M. 2009. Microtubule nucleation at the cis-side of the Golgi apparatus requires AKAP450 and GM130. *EMBO J,* 28**,** 1016-28.

ROBOTI, P., SATO, K. & LOWE, M. 2015. The golgin GMAP-210 is required for efficient membrane trafficking in the early secretory pathway. *J Cell Sci,* 128**,** 1595-606.

ROCZNIAK-FERGUSON, A., PETIT, C. S., FROEHLICH, F., QIAN, S., KY, J., ANGAROLA, B., WALTHER, T. C. & FERGUSON, S. M. 2012. The transcription factor TFEB links mTORC1 signaling to transcriptional control of lysosome homeostasis. *Sci Signal,* 5**,** ra42.

ROGOV, V., DOTSCH, V., JOHANSEN, T. & KIRKIN, V. 2014. Interactions between autophagy receptors and ubiquitin-like proteins form the molecular basis for selective autophagy. *Mol Cell,* 53**,** 167-78.

ROLLAND, T., TASAN, M., CHARLOTEAUX, B., PEVZNER, S. J., ZHONG, Q., SAHNI, N., YI, S., LEMMENS, I., FONTANILLO, C., MOSCA, R., KAMBUROV, A., GHIASSIAN, S. D., YANG, X., GHAMSARI, L., BALCHA, D., BEGG, B. E., BRAUN, P., BREHME, M., BROLY, M. P., CARVUNIS, A. R., CONVERY-ZUPAN, D., COROMINAS, R., COULOMBE-HUNTINGTON, J., DANN, E., DREZE, M., DRICOT, A., FAN, C., FRANZOSA, E., GEBREAB, F., GUTIERREZ, B. J., HARDY, M. F., JIN, M., KANG, S., KIROS, R., LIN, G. N., LUCK, K., MACWILLIAMS, A., MENCHE, J., MURRAY, R. R., PALAGI, A., POULIN, M. M., RAMBOUT, X., RASLA, J., REICHERT, P., ROMERO, V., RUYSSINCK, E., SAHALIE, J. M., SCHOLZ, A., SHAH, A. A., SHARMA, A., SHEN, Y., SPIROHN, K., TAM, S., TEJEDA, A. O., TRIGG, S. A., TWIZERE, J. C., VEGA, K., WALSH, J., CUSICK, M. E., XIA, Y., BARABASI, A. L., IAKOUCHEVA, L. M., ALOY, P., DE LAS RIVAS, J., TAVERNIER, J., CALDERWOOD, M. A., HILL, D. E., HAO, T., ROTH, F. P. & VIDAL, M. 2014. A proteome-scale map of the human interactome network. *Cell,* 159**,** 1212-26.

ROSENBERG, L. H., LAFITTE, M., GRANT, W., CHEN, W., CLEVELAND, J. L. & DUCKETT, D. R. 2015. Development of an HTS-Compatible Assay for the Discovery of Ulk1 Inhibitors. *J Biomol Screen*.

ROWLAND, A. A. & VOELTZ, G. K. 2012. Endoplasmic reticulum-mitochondria contacts: function of the junction. *Nat Rev Mol Cell Biol,* 13**,** 607-25.

RUSSELL, R. C., TIAN, Y., YUAN, H., PARK, H. W., CHANG, Y. Y., KIM, J., KIM, H., NEUFELD, T. P., DILLIN, A. & GUAN, K. L. 2013. ULK1 induces autophagy by phosphorylating Beclin-1 and activating VPS34 lipid kinase. *Nat Cell Biol,* 15**,** 741-50.

SAGIV, Y., LEGESSE-MILLER, A., PORAT, A. & ELAZAR, Z. 2000. GATE-16, a membrane transport modulator, interacts with NSF and the Golgi v-SNARE GOS-28. *EMBO J,* 19**,** 1494-504.

SCHMIDT, T. G. & SKERRA, A. 2007. The Strep-tag system for one-step purification and high-affinity detection or capturing of proteins. *Nat Protoc,* 2**,** 1528-35.

SCHUMANN, M., GANTKE, T. & MUHLBERGER, E. 2009. Ebola virus VP35 antagonizes PKR activity through its C-terminal interferon inhibitory domain. *J Virol,* 83**,** 8993-7.

SCHWANHAUSSER, B., BUSSE, D., LI, N., DITTMAR, G., SCHUCHHARDT, J., WOLF, J., CHEN, W. & SELBACH, M. 2011. Global quantification of mammalian gene expression control. *Nature,* 473**,** 337-42.

SEEMANN, J., JOKITALO, E. J. & WARREN, G. 2000. The role of the tethering proteins p115 and GM130 in transport through the Golgi apparatus in vivo. *Mol Biol Cell,* 11**,** 635-45.

SETTEMBRE, C., DI MALTA, C., POLITO, V. A., GARCIA ARENCIBIA, M., VETRINI, F., ERDIN, S., ERDIN, S. U., HUYNH, T., MEDINA, D., COLELLA, P., SARDIELLO, M., RUBINSZTEIN, D. C. & BALLABIO, A. 2011. TFEB links autophagy to lysosomal biogenesis. *Science,* 332**,** 1429-33.

SETTEMBRE, C., ZONCU, R., MEDINA, D. L., VETRINI, F., ERDIN, S., ERDIN, S., HUYNH, T., FERRON, M., KARSENTY, G., VELLARD, M. C., FACCHINETTI, V., SABATINI, D. M. & BALLABIO, A. 2012. A lysosome-to-nucleus signalling mechanism senses and regulates the lysosome via mTOR and TFEB. *EMBO J,* 31**,** 1095-108.

SHEMA, E., KIM, J., ROEDER, R. G. & OREN, M. 2011. RNF20 inhibits TFIIS-facilitated transcriptional elongation to suppress pro-oncogenic gene expression. *Mol Cell,* 42**,** 477-88.

SHEMA, E., TIROSH, I., AYLON, Y., HUANG, J., YE, C., MOSKOVITS, N., RAVER-SHAPIRA, N., MINSKY, N., PIRNGRUBER, J., TARCIC, G., HUBLAROVA, P., MOYAL, L., GANA-WEISZ, M., SHILOH, Y., YARDEN, Y., JOHNSEN, S. A., VOJTESEK, B., BERGER, S. L. & OREN, M. 2008. The histone H2B-specific ubiquitin ligase RNF20/hBRE1 acts as a putative tumor suppressor through selective regulation of gene expression. *Genes Dev,* 22**,** 2664-76.

SHILOH, Y., SHEMA, E., MOYAL, L. & OREN, M. 2011. RNF20-RNF40: A ubiquitin-driven link between gene expression and the DNA damage response. *FEBS Lett,* 585**,** 2795-802.

SHOJI-KAWATA, S., SUMPTER, R., LEVENO, M., CAMPBELL, G. R., ZOU, Z., KINCH, L., WILKINS, A. D., SUN, Q., PALLAUF, K., MACDUFF, D., HUERTA, C., VIRGIN, H. W., HELMS, J. B., EERLAND, R., TOOZE, S. A., XAVIER, R., LENSCHOW, D. J., YAMAMOTO, A., KING, D., LICHTARGE, O., GRISHIN, N. V., SPECTOR, S. A., KALOYANOVA, D. V. & LEVINE, B. 2013. Identification of a candidate therapeutic autophagy-inducing peptide. *Nature,* 494**,** 201-6.

SHPILKA, T., WEIDBERG, H., PIETROKOVSKI, S. & ELAZAR, Z. 2011. Atg8: an autophagy-related ubiquitin-like protein family. *Genome Biol,* 12**,** 226.

SHVETS, E., ABADA, A., WEIDBERG, H. & ELAZAR, Z. 2011. Dissecting the involvement of LC3B and GATE-16 in p62 recruitment into autophagosomes. *Autophagy,* 7**,** 683-8.

SIMONSEN, A. & TOOZE, S. A. 2009. Coordination of membrane events during autophagy by multiple class III PI3-kinase complexes. *J Cell Biol,* 186**,** 773-82.

SODING, J. 2005. Protein homology detection by HMM-HMM comparison. *Bioinformatics,* 21**,** 951-60.

SOHDA, M., MISUMI, Y., OGATA, S., SAKISAKA, S., HIROSE, S., IKEHARA, Y. & ODA, K. 2015. Trans-Golgi protein p230/golgin-245 is involved in phagophore formation. *Biochem Biophys Res Commun,* 456**,** 275-81.

SONNICHSEN, B., LOWE, M., LEVINE, T., JAMSA, E., DIRAC-SVEJSTRUP, B. & WARREN, G. 1998. A role for giantin in docking COPI vesicles to Golgi membranes. *J Cell Biol,* 140**,** 1013-21.

STOLZ, A., ERNST, A. & DIKIC, I. 2014. Cargo recognition and trafficking in selective autophagy. *Nat Cell Biol,* 16**,** 495-501.

STRAPPAZZON, F., VIETRI-RUDAN, M., CAMPELLO, S., NAZIO, F., FLORENZANO, F., FIMIA, G. M., PIACENTINI, M., LEVINE, B. & CECCONI, F. 2011. Mitochondrial BCL-2 inhibits AMBRA1-induced autophagy. *EMBO J,* 30**,** 1195-208.

SUBRAMANI, S. & MALHOTRA, V. 2013. Non-autophagic roles of autophagy-related proteins. *EMBO Rep,* 14**,** 143-51.

SUN, Q., FAN, W., CHEN, K., DING, X., CHEN, S. & ZHONG, Q. 2008. Identification of Barkor as a mammalian autophagy-specific factor for Beclin 1 and class III phosphatidylinositol 3-kinase. *Proc Natl Acad Sci U S A,* 105**,** 19211-6.

SUNDARAMOORTHY, S., GOH, J. B., RAFEE, S. & MURATA-HORI, M. 2010. Mitotic Golgi vesiculation involves mechanisms independent of Ser25 phosphorylation of GM130. *Cell Cycle,* 9**,** 3100-5.

SVENNING, S. & JOHANSEN, T. 2013. Selective autophagy. *Essays Biochem,* 55**,** 79-92.

SZALAI, P., HAGEN, L. K., SAETRE, F., LUHR, M., SPONHEIM, M., OVERBYE, A., MILLS, I. G., SEGLEN, P. O. & ENGEDAL, N. 2015. Autophagic bulk sequestration of cytosolic cargo is independent of LC3, but requires GABARAPs. *Exp Cell Res,* 333**,** 21-38.

TAGUCHI-ATARASHI, N., HAMASAKI, M., MATSUNAGA, K., OMORI, H., KTISTAKIS, N. T., YOSHIMORI, T. & NODA, T. 2010. Modulation of local PtdIns3P levels by the PI phosphatase MTMR3 regulates constitutive autophagy. *Traffic,* 11**,** 468-78.

TAKAHASHI, Y., COPPOLA, D., MATSUSHITA, N., CUALING, H. D., SUN, M., SATO, Y., LIANG, C., JUNG, J. U., CHENG, J. Q., MULE, J. J., PLEDGER, W. J. & WANG, H. G. 2007. Bif-1 interacts with Beclin 1 through UVRAG and regulates autophagy and tumorigenesis. *Nat Cell Biol,* 9**,** 1142-51.

TAKAHASHI, Y., MEYERKORD, C. L., HORI, T., RUNKLE, K., FOX, T. E., KESTER, M., LOUGHRAN, T. P. & WANG, H. G. 2011. Bif-1 regulates Atg9 trafficking by mediating the fission of Golgi membranes during autophagy. *Autophagy,* 7**,** 61-73.

TAKAMURA, A., KOMATSU, M., HARA, T., SAKAMOTO, A., KISHI, C., WAGURI, S., EISHI, Y., HINO, O., TANAKA, K. & MIZUSHIMA, N. 2011. Autophagy-deficient mice develop multiple liver tumors. *Genes Dev,* 25**,** 795-800.

TANAKA, A., CLELAND, M. M., XU, S., NARENDRA, D. P., SUEN, D. F., KARBOWSKI, M. & YOULE, R. J. 2010. Proteasome and p97 mediate mitophagy and degradation of mitofusins induced by Parkin. *J Cell Biol,* 191**,** 1367-80.

TANAKA, M., KIM, Y. M., LEE, G., JUNN, E., IWATSUBO, T. & MOURADIAN, M. M. 2004. Aggresomes formed by alpha-synuclein and synphilin-1 are cytoprotective. *J Biol Chem,* 279**,** 4625-31.

TANG, H. W., WANG, Y. B., WANG, S. L., WU, M. H., LIN, S. Y. & CHEN, G. C. 2011. Atg1-mediated myosin II activation regulates autophagosome formation during starvation-induced autophagy. *EMBO J,* 30**,** 636-51.

TANG, Z., LIN, M. G., STOWE, T. R., CHEN, S., ZHU, M., STEARNS, T., FRANCO, B. & ZHONG, Q. 2013. Autophagy promotes primary ciliogenesis by removing OFD1 from centriolar satellites. *Nature,* 502**,** 254-7.

THOREEN, C. C., KANG, S. A., CHANG, J. W., LIU, Q., ZHANG, J., GAO, Y., REICHLING, L. J., SIM, T., SABATINI, D. M. & GRAY, N. S. 2009. An ATP-competitive mammalian target of rapamycin inhibitor reveals rapamycin-resistant functions of mTORC1. *J Biol Chem,* 284**,** 8023-32.

THUMM, M., EGNER, R., KOCH, B., SCHLUMPBERGER, M., STRAUB, M., VEENHUIS, M. & WOLF, D. H. 1994. Isolation of autophagocytosis mutants of Saccharomyces cerevisiae. *FEBS Lett,* 349**,** 275-80.

TOMAS, A., FUTTER, C. E. & EDEN, E. R. 2014. EGF receptor trafficking: consequences for signaling and cancer. *Trends Cell Biol,* 24**,** 26-34.

TOOZE, S. A. & RAZI, M. 2009. The essential role of early endosomes in autophagy is revealed by loss of COPI function. *Autophagy,* 5**,** 874-5.

TOTSUKAWA, G., KANEKO, Y., UCHIYAMA, K., TOH, H., TAMURA, K. & KONDO, H. 2011. VCIP135 deubiquitinase and its binding protein, WAC, in p97ATPase-mediated membrane fusion. *EMBO J,* 30**,** 3581-93.

TRESSE, E., SALOMONS, F. A., VESA, J., BOTT, L. C., KIMONIS, V., YAO, T. P., DANTUMA, N. P. & TAYLOR, J. P. 2010. VCP/p97 is essential for maturation of ubiquitin-containing autophagosomes and this function is impaired by mutations that cause IBMPFD. *Autophagy,* 6**,** 217-27.

TSUKADA, M. & OHSUMI, Y. 1993. Isolation and characterization of autophagy-defective mutants of Saccharomyces cerevisiae. *FEBS Lett,* 333**,** 169-74.

VALSDOTTIR, R., HASHIMOTO, H., ASHMAN, K., KODA, T., STORRIE, B. & NILSSON, T. 2001. Identification of rabaptin-5, rabex-5, and GM130 as putative effectors of rab33b, a regulator of retrograde traffic between the Golgi apparatus and ER. *FEBS Lett,* 508**,** 201-9.

VAN DER VAART, A., GRIFFITH, J. & REGGIORI, F. 2010. Exit from the Golgi is required for the expansion of the autophagosomal phagophore in yeast Saccharomyces cerevisiae. *Mol Biol Cell,* 21**,** 2270-84.

VASILE, E., PEREZ, T., NAKAMURA, N. & KRIEGER, M. 2003. Structural integrity of the Golgi is temperature sensitive in conditional-lethal mutants with no detectable GM130. *Traffic,* 4**,** 254-72.

VERGNE, I., ROBERTS, E., ELMAOUED, R. A., TOSCH, V., DELGADO, M. A., PROIKAS-CEZANNE, T., LAPORTE, J. & DERETIC, V. 2009. Control of autophagy initiation by phosphoinositide 3-phosphatase Jumpy. *EMBO J,* 28**,** 2244-58.

VON MUHLINEN, N., AKUTSU, M., RAVENHILL, B. J., FOEGLEIN, A., BLOOR, S., RUTHERFORD, T. J., FREUND, S. M., KOMANDER, D. & RANDOW, F. 2013. An essential role for the ATG8 ortholog LC3C in antibacterial autophagy. *Autophagy,* 9**,** 784-6.

WALENTA, J. H., DIDIER, A. J., LIU, X. & KRAMER, H. 2001. The Golgi-associated hook3 protein is a member of a novel family of microtubule-binding proteins. *J Cell Biol,* 152**,** 923-34.

WANG, H., BEDFORD, F. K., BRANDON, N. J., MOSS, S. J. & OLSEN, R. W. 1999. GABA(A)-receptor-associated protein links GABA(A) receptors and the cytoskeleton. *Nature,* 397**,** 69-72.

WANG, H. & OLSEN, R. W. 2000. Binding of the GABA(A) receptor-associated protein (GABARAP) to microtubules and microfilaments suggests involvement of the cytoskeleton in GABARAPGABA(A) receptor interaction. *J Neurochem,* 75**,** 644-55.

WANG, H., SUN, H. Q., ZHU, X., ZHANG, L., ALBANESI, J., LEVINE, B. & YIN, H. 2015. GABARAPs regulate PI4P-dependent autophagosome:lysosome fusion. *Proc Natl Acad Sci U S A,* 112**,** 7015-20.

WANG, X., CAMPBELL, L. E., MILLER, C. M. & PROUD, C. G. 1998. Amino acid availability regulates p70 S6 kinase and multiple translation factors. *Biochem J,* 334 (Pt 1)**,** 261-7.

WANG, Y., SEEMANN, J., PYPAERT, M., SHORTER, J. & WARREN, G. 2003. A direct role for GRASP65 as a mitotically regulated Golgi stacking factor. *EMBO J,* 22**,** 3279-90.

WARD, T. H., POLISHCHUK, R. S., CAPLAN, S., HIRSCHBERG, K. & LIPPINCOTT-SCHWARTZ, J. 2001. Maintenance of Golgi structure and function depends on the integrity of ER export. *J Cell Biol,* 155**,** 557-70.

WEBB, J. L., RAVIKUMAR, B., ATKINS, J., SKEPPER, J. N. & RUBINSZTEIN, D. C. 2003. Alpha-Synuclein is degraded by both autophagy and the proteasome. *J Biol Chem,* 278**,** 25009-13.

WEI, J. H., ZHANG, Z. C., WYNN, R. M. & SEEMANN, J. 2015. GM130 Regulates Golgi-Derived Spindle Assembly by Activating TPX2 and Capturing Microtubules. *Cell,* 162**,** 287-99.

WEIDBERG, H., SHPILKA, T., SHVETS, E., ABADA, A., SHIMRON, F. & ELAZAR, Z. 2011. LC3 and GATE-16 N termini mediate membrane fusion processes required for autophagosome biogenesis. *Dev Cell,* 20**,** 444-54.

WEIDBERG, H., SHVETS, E., SHPILKA, T., SHIMRON, F., SHINDER, V. & ELAZAR, Z. 2010. LC3 and GATE-16/GABARAP subfamilies are both essential yet act differently in autophagosome biogenesis. *Embo Journal,* 29**,** 1792-1802.

WEIDE, T., BAYER, M., KOSTER, M., SIEBRASSE, J. P., PETERS, R. & BARNEKOW, A. 2001. The Golgi matrix protein GM130: a specific interacting partner of the small GTPase rab1b. *EMBO Rep,* 2**,** 336-41.

WIEDENMANN, J., IVANCHENKO, S., OSWALD, F., SCHMITT, F., ROCKER, C., SALIH, A., SPINDLER, K. D. & NIENHAUS, G. U. 2004. EosFP, a fluorescent marker protein with UV-inducible green-to-red fluorescence conversion. *Proc Natl Acad Sci U S A,* 101**,** 15905-10.

WILD, P., MCEWAN, D. G. & DIKIC, I. 2014. The LC3 interactome at a glance. *J Cell Sci,* 127**,** 3-9.

WIRAWAN, E., LIPPENS, S., VANDEN BERGHE, T., ROMAGNOLI, A., FIMIA, G. M., PIACENTINI, M. & VANDENABEELE, P. 2012. Beclin1: a role in membrane dynamics and beyond. *Autophagy,* 8**,** 6-17.

WIRTH, M., JOACHIM, J. & TOOZE, S. A. 2013. Autophagosome formation--the role of ULK1 and Beclin1-PI3KC3 complexes in setting the stage. *Semin Cancer Biol,* 23**,** 301-9.

WOLFF, B., SANGLIER, J. & WANG, Y. 1997. Leptomycin B is an inhibitor of nuclear export: inhibition of nucleo-cytoplasmic translocation of the human immunodeficiency virus type 1 (HIV-1) Rev protein and Rev-dependent mRNA. *Chem Biol*.

WONG, M. & MUNRO, S. 2014. Membrane trafficking. The specificity of vesicle traffic to the Golgi is encoded in the golgin coiled-coil proteins. *Science,* 346**,** 1256898.

WONG, P. M., FENG, Y., WANG, J., SHI, R. & JIANG, X. 2015. Regulation of autophagy by coordinated action of mTORC1 and protein phosphatase 2A. *Nat Commun,* 6**,** 8048.

WONG, P. M., PUENTE, C., GANLEY, I. G. & JIANG, X. 2013. The ULK1 complex: sensing nutrient signals for autophagy activation. *Autophagy,* 9**,** 124-37.

WOODRUFF, J. B., WUESEKE, O. & HYMAN, A. A. 2014. Pericentriolar material structure and dynamics. *Philos Trans R Soc Lond B Biol Sci,* 369.

XIE, Y., KANG, R., SUN, X., ZHONG, M., HUANG, J., KLIONSKY, D. J. & TANG, D. 2015. Posttranslational modification of autophagy-related proteins in macroautophagy. *Autophagy,* 11**,** 28-45.

XU, G. M. & ARNAOUT, M. A. 2002. WAC, a novel WW domain-containing adapter with a coiled-coil region, is colocalized with splicing factor SC35. *Genomics,* 79**,** 87-94.

YAMAGUCHI, M., NODA, N. N., YAMAMOTO, H., SHIMA, T., KUMETA, H., KOBASHIGAWA, Y., AKADA, R., OHSUMI, Y. & INAGAKI, F. 2012. Structural insights into Atg10-mediated formation of the autophagy-essential Atg12-Atg5 conjugate. *Structure,* 20**,** 1244-54.

YAMAMOTO, A., MASAKI, R. & TASHIRO, Y. 1990. Characterization of the isolation membranes and the limiting membranes of autophagosomes in rat hepatocytes by lectin cytochemistry. *J Histochem Cytochem,* 38**,** 573-80.

YAMAMOTO, A., TAGAWA, Y., YOSHIMORI, T., MORIYAMA, Y., MASAKI, R. & TASHIRO, Y. 1998. Bafilomycin A1 prevents maturation of autophagic vacuoles by inhibiting fusion between autophagosomes and lysosomes in rat hepatoma cell line, H-4-II-E cells. *Cell Struct Funct,* 23**,** 33-42.

YAMAMOTO, H., KAKUTA, S., WATANABE, T. M., KITAMURA, A., SEKITO, T., KONDO-KAKUTA, C., ICHIKAWA, R., KINJO, M. & OHSUMI, Y. 2012. Atg9 vesicles are an important membrane source during early steps of autophagosome formation. *J Cell Biol,* 198**,** 219-33.

YAMANAKA, K., SASAGAWA, Y. & OGURA, T. 2012. Recent advances in p97/VCP/Cdc48 cellular functions. *Biochim Biophys Acta,* 1823**,** 130-7.

YANG, Y., FISKUS, W., YONG, B., ATADJA, P., TAKAHASHI, Y., PANDITA, T. K., WANG, H. G. & BHALLA, K. N. 2013. Acetylated hsp70 and KAP1-mediated Vps34 SUMOylation is required for autophagosome creation in autophagy. *Proc Natl Acad Sci U S A,* 110**,** 6841-6.

YLA-ANTTILA, P., VIHINEN, H., JOKITALO, E. & ESKELINEN, E. L. 2009. 3D tomography reveals connections between the phagophore and endoplasmic reticulum. *Autophagy,* 5**,** 1180-5.

YOUNG, A. R., CHAN, E. Y., HU, X. W., KOCHL, R., CRAWSHAW, S. G., HIGH, S., HAILEY, D. W., LIPPINCOTT-SCHWARTZ, J. & TOOZE, S. A. 2006. Starvation and ULK1-dependent cycling of mammalian Atg9 between the TGN and endosomes. *J Cell Sci,* 119**,** 3888-900.

YUE, Z., JIN, S., YANG, C., LEVINE, A. J. & HEINTZ, N. 2003. Beclin 1, an autophagy gene essential for early embryonic development, is a haploinsufficient tumor suppressor. *Proc Natl Acad Sci U S A,* 100**,** 15077-82.

ZHANG, C. H., WANG, Z. B., QUAN, S., HUANG, X., TONG, J. S., MA, J. Y., GUO, L., WEI, Y. C., OUYANG, Y. C., HOU, Y., XING, F. Q. & SUN, Q. Y. 2011. GM130, a cis-Golgi protein, regulates meiotic spindle assembly and asymmetric division in mouse oocyte. *Cell Cycle,* 10**,** 1861-70.

ZHANG, F. & YU, X. 2011. WAC, a functional partner of RNF20/40, regulates histone H2B ubiquitination and gene transcription. *Mol Cell,* 41**,** 384-97.

ZHAO, J., REN, Y., JIANG, Q. & FENG, J. 2003. Parkin is recruited to the centrosome in response to inhibition of proteasomes. *J Cell Sci,* 116**,** 4011-9.

ZHENG, J. Y., KODA, T., FUJIWARA, T., KISHI, M., IKEHARA, Y. & KAKINUMA, M. 1998. A novel Rab GTPase, Rab33B, is ubiquitously expressed and localized to the medial Golgi cisternae. *J Cell Sci,* 111 (Pt 8)**,** 1061-9.

ZHONG, Y., WANG, Q. J., LI, X., YAN, Y., BACKER, J. M., CHAIT, B. T., HEINTZ, N. & YUE, Z. 2009. Distinct regulation of autophagic activity by Atg14L and Rubicon associated with Beclin 1-phosphatidylinositol-3-kinase complex. *Nat Cell Biol,* 11**,** 468-76.

ZHOU, Z., SUN, X., ZOU, Z., SUN, L., ZHANG, T., GUO, S., WEN, Y., LIU, L., WANG, Y., QIN, J., LI, L., GONG, W. & BAO, S. 2010. PRMT5 regulates Golgi apparatus structure through methylation of the golgin GM130. *Cell Res,* 20**,** 1023-33.

ZOPPINO, F. C., MILITELLO, R. D., SLAVIN, I., ALVAREZ, C. & COLOMBO, M. I. 2010. Autophagosome formation depends on the small GTPase Rab1 and functional ER exit sites. *Traffic,* 11**,** 1246-61.